UNIVERSITAT POLITÈCNICA DE VALÈNCIA

Institut de Seguretat Industrial, Radiofísica i Mediambiental

A thesis submitted for the degree of Doctor of Philosophy

Uncertainty Quantification and Sensitivity Analysis for Cross Sections and Thermohydraulic Parameters in Lattice and Core Physics Codes. Methodology for Cross Section Library Generation and Application to PWR and BWR

Carles Mesado Melia

Supervisors:

Dr. Rafael Miró Herrero

Dr. Gumersindo Verdú Martín

Valencia, June 2017

"There are three certainties in life:
death, taxes and bugs in computer codes."

Modified quote of Benjamin Franklin

"Hi ha tres certeses en la vida:
la mort, impostos i errades en programes informàtics."

Modificació de la cita de Benjamin Franklin

"Hay tres certezas en la vida:
la muerte, impuestos y fallos en programas informáticos."

Modificación de la cita de Benjamin Franklin

Abstract

This PhD study, developed at Universitat Politècnica de València (UPV), aims to cover the first phase of the benchmark released by the expert group on Uncertainty Analysis in Modeling (UAM-LWR). The main contribution to the benchmark, made by the thesis' author, is the development of a MATLAB® program requested by the benchmark organizers. This is used to generate neutronic libraries to distribute among the benchmark participants. The UAM benchmark pretends to determine the uncertainty introduced by coupled multi-physics and multi-scale LWR analysis codes. The benchmark is subdivided into three phases:

1. Neutronic phase: obtain collapsed and homogenized problem-dependent cross sections and criticality analyses.
2. Core phase: standalone thermohydraulic and neutronic codes.
3. System phase: coupled thermohydraulic and neutronic code.

In this thesis the objectives of the first phase are covered. Specifically, a methodology is developed to propagate the uncertainty of cross sections and other neutronic parameters through a lattice physics code and core simulator. An Uncertainty and Sensitivity (U&S) analysis is performed over the cross sections contained in the ENDF/B-VII nuclear library. Their uncertainty is propagated through the lattice physics code SCALE6.2.1, including the collapse and homogenization phase, up to the generation of problem-dependent neutronic libraries. Afterward, the uncertainty contained in these libraries can be further propagated through a core simulator, in this study PARCSv3.2. The module SAMPLER -available in the latest release of SCALE- and DAKOTA 6.3 statistical tool are used for the U&S analysis. As a part of this process, a methodology to obtain neutronic libraries in NEMTAB format -to be used in a core simulator- is also developed. A code-to-code comparison with CASMO-4 is used as a verification. The whole methodology is tested using a Boiling Water Reactor (BWR) reactor type. Nevertheless, there is not any concern or limitation regarding its use in any other type of nuclear reactor.

The Gesellschaft für Anlagen und Reaktorsicherheit (GRS) stochastic methodology for uncertainty quantification is used. This methodology makes use of the high-fidelity model and nonparametric sampling to propagate the uncertainty. As a result, the number of samples (determined using the revised Wilk's formula) does not depend on the number of input parameters but only on the desired confidence and uncertainty of output parameters. Moreover, the output Probability Distribution Functions (PDFs) are not subject to normality. The main disadvantage is that each input parameter must have a pre-defined PDF. If possible, input PDFs are defined using information found in the related literature. Otherwise, the uncertainty definition is based on expert judgment.

A second scenario is used to propagate the uncertainty of different thermohydraulic parameters through the coupled code TRACE5.0p3/PARCSv3.0. In this case, a PWR reactor type is used and a transient control rod drop occurrence is simulated. As a new feature, the core is modeled chan-by-chan following a fully 3D discretization. No other study is found using a detailed 3D core. This U&S analysis also makes use of the GRS methodology and DAKOTA 6.3.

Resum

Aquest treball de doctorat, desenvolupat a la Universitat Politècnica de València (UPV), té com a objectiu cobrir la primera fase del *benchmark* presentat pel grup d'experts *Uncertainty Analysis in Modeling* (UAM-LWR). La principal contribució al *benchmark*, per part de l'autor d'aquesta tesi, es el desenvolupament d'un programa de MATLAB® solicitat pels organitzadors del *benchmark*, el qual s'utilitza per a generar lliberies neutròniques a distribuir entre els participants del *benchmark*. El *benchmark* del UAM pretén determinar la incertesa introduïda pels codis multifísics i multiescala acoblats d'anàlisi de reactors d'aigua lleugera. El citat *benchmark* es divideix en tres fases:

1. Fase neutrònica: obtenir els paràmetres neutrònics i seccions eficaces del problema específic, col·lapsats i homogeneïtzats, a més de la anàlisi de criticitat.

2. Fase de nucli: anàlisi termo-hidràulica i neutrònica per separat.

3. Fase de sistema: anàlisi termo-hidràulica i neutrònica acoblats.

En aquesta tesi es completen els principals objectius de la primera fase. Concretament, es desenvolupa una metodologia per propagar la incertesa de les seccions eficaces i altres paràmetres neutrònics a través d'un codi *lattice* i un simulador de nucli. Es porta a terme una anàlisi d'incertesa i sensibilitat per a les seccions eficaces contingudes en la llibreria neutrònica ENDF/B-VII. La seua incertesa es propaga a través del codi *lattice* SCALE6.2.1, incloent les fases per col·lapsar i homogeneïtzar, fins aplegar a la generació d'una llibreria neutrònica específica del problema. Després, la incertesa continguda en la esmentada llibreria pot continuar propagant-se a través d'un simulador de nucli, per a aquest estudi PARCSv3.2. Per a l'anàlisi d'incertesa i sensibilitat s'ha utilitzat el mòdul SAMPLER -disponible a l'última versió de SCALE- i la ferramenta estadística DAKOTA 6.3. Com a part d'aquest procés, també es desenvolupa una metodologia per a obtenir llibreries neutròniques en format NEMTAB per ser utilitzades en simuladors de nucli. S'ha realitzat una comparació amb el codi CASMO-4 per obtenir una verificació de la metodologia completa. Aquesta s'ha provat utilitzant un reactor d'aigua en ebullició del tipus BWR. Tanmateix, no hi ha cap preocupació o limitació respecte del seu ús amb un altre tipus de reactor nuclear.

Per a la quantificació de la incertesa s'utilitza la metodologia estocàstica *Gesellschaft für Anlagen und Reaktorsicherheit* (GRS). Aquesta metodologia fa ús del model d'alta fidelitat i un mostreig no paramètric per propagar la incertesa. Com a resultat, el nombre de mostres (determinat amb la fórmula revisada de Wilk's) no depèn del nombre de paràmetres d'entrada, sols depèn del nivell de confiança i incertesa desitjats dels paràmetres d'eixida. A més, las funcions de distribució de probabilitat no estan limitades a la normalitat. El principal inconvenient és que s'ha de disposar de les distribucions de probabilitat de cada paràmetre d'entrada. Si és possible, les distribucions de probabilitat d'entrada es defineixen utilitzant informació trobada a la literatura relacionada. En cas contrari, la incertesa es defineix en base a l'opinió d'un expert.

S'utilitza un segon escenari per propagar la incertesa de diferents paràmetres termo-hidràulics a través del codi acoblat TRACE5.0p3/PARCSv3.0. En aquest cas, s'utilitza un reactor tipus PWR per simular un transitori d'una caiguda de barra. Com a nova característica, cal assenyalar que el nucli es modela element a element seguint una discretització totalment 3D. No s'ha trobat cap altre estudi que utilitze un nucli tan detallat en 3D. També s'utilitza la metodologia GRS i el DAKOTA 6.3 per a aquesta anàlisi d'incertesa i sensibilitat.

Resumen

Este trabajo de doctorado, desarrollado en la Universitat Politècnica de València (UPV), tiene como objetivo cubrir la primera fase del *benchmark* presentado por el grupo de expertos *Uncertainty Analysis in Modeling* (UAM-LWR). La principal contribución al *benchmark*, por parte del autor de esta tesis, es el desarrollo de un programa de MATLAB® solicitado por los organizadores del *benchmark*, el cual se usa para generar liberías neutrónicas a distribuir entre los participantes del *benchmark*. El *benchmark* del UAM pretende determinar la incertidumbre introducida por los códigos multifísicos y multiescala acoplados de análisis de reactores de agua ligera. El citado *benchmark* se divide en tres fases:

1. Fase neutrónica: obtener los parámetros neutrónicos y secciones eficaces del problema específico colapsados y homogenizados, además del análisis de criticidad.
2. Fase de núcleo: análisis termo-hidráulico y neutrónico por separado.
3. Fase de sistema: análisis termo-hidráulico y neutrónico acoplados.

En esta tesis se completan los principales objetivos de la primera fase. Concretamente, se desarrolla una metodología para propagar la incertidumbre de secciones eficaces y otros parámetros neutrónicos a través de un código *lattice* y un simulador de núcleo. Se lleva a cabo un análisis de incertidumbre y sensibilidad para las secciones eficaces contenidas en la librería neutrónica ENDF/B-VII. Su incertidumbre se propaga a través del código *lattice* SCALE6.2.1, incluyendo las fases de colapsación y homogenización, hasta llegar a la generación de una librería neutrónica específica del problema. Luego, la incertidumbre contenida en dicha librería puede continuar propagándose a través de un simulador de núcleo, para este estudio PARCSv3.2. Para el análisis de incertidumbre y sensibilidad se ha usado el módulo SAMPLER -disponible en la última versión de SCALE- y la herramienta estadística DAKOTA 6.3. Como parte de este proceso, también se ha desarrollado una metodología para obtener librerías neutrónicas en formato NEMTAB para ser usadas en simuladores de núcleo. Se ha realizado una comparación con el código CASMO-4 para obtener una verificación de la metodología completa. Esta se ha probado usando un reactor de agua en ebullición del tipo BWR. Sin embargo, no hay ninguna preocupación o limitación respecto a su uso con otro tipo de reactor nuclear.

Para la cuantificación de la incertidumbre se usa la metodología estocástica *Gesellschaft für Anlagen und Reaktorsicherheit* (GRS). Esta metodología hace uso del modelo de alta fidelidad y un muestreo no paramétrico para propagar la incertidumbre. Como resultado, el número de muestras (determinado con la fórmula revisada de Wilk's) no depende del número de parámetros de entrada, sólo depende del nivel de confianza e incertidumbre deseados de los parámetros de salida. Además, las funciones de distribución de probabilidad no están limitadas a normalidad. El principal inconveniente es que se ha de disponer de las distribuciones de probabilidad de cada parámetro de entrada. Si es posible, las distribuciones de probabilidad de entrada se definen usando información encontrada en la literatura relacionada. En caso contrario, la incertidumbre se define en base a la opinión de un experto.

Se usa un segundo escenario para propagar la incertidumbre de diferentes parámetros termo-hidráulicos a través del código acoplado TRACE5.0p3/PARCSv3.0. En este caso, se utiliza un reactor tipo PWR para simular un transitorio de una caída de barra. Como nueva característica, el núcleo se modela elemento a elemento siguiendo una discretización totalmente en 3D. No se ha encontrado ningún otro estudio que use un núcleo tan detallado en 3D. También se usa la metodología GRS y el DAKOTA 6.3 para este análisis de incertidumbre y sensibilidad.

Contents

List of Figures

List of Tables

Chapter 1

Introduction

. . . what is this and what do we want?

Before current uncertainty tools, conservative approaches were performed for deterministic safety analysis. The objective of safety analysis is to ensure that enough margins exist between the real value and the threshold value at which the barrier against release of radioactivity fails. Currently, with the uncertainty tools available, the envelope for safe nuclear power plant operations can be predicted. For example, for most modern nuclear reactors, two of the most important limiting parameters are the peak cladding temperature and the enthalpy. These parameters are directly related with the possibility of clad and fuel damage and eventually, fission product release. Safety analysis requires, for normal and abnormal operations, proper safety margins to operate the nuclear plant under safe conditions. Uncertainty tools provide the uncertainty for phenomena related to these operations, and thus the safety margins can be established according to the regulatory body limitation.

Originally, very conservative modeling assumptions for nuclear power plant licensing were required in the USA. The purpose of this conservativeness, imposed by the *U. S. Nuclear Regulatory Commission* (NRC), was to assure the safety margins. However, it was well known that margins were excessive, large margins exist between the conservative calculations and the true value. One decade later, the NRC decided to revoke the conservative approaches in favor of *Best Estimate* (BE) calculations. Even though licensing analysis appears to be very conservative, key phenomena and uncertainty definitions seems to be more significant than originally estimated. Probabilistic and statistical methods should be used to determine the code uncertainty and fulfill licensing issues. The purpose is to provide enough evidence for postulated accidents that a given plant will not exceed the applicable licensing criteria with 95% probability and 95% confidence interval. The procedures and philosophy for safety in nuclear power plants are similar for different countries. However, licensing practice could vary. Some countries specify the uncertainty methodology, the code to be used and the acceptable criteria; whereas other countries are more flexible towards these decisions and allow the licensees to define this information. Although most of up-to-date *Uncertainty Quantification* (UQ) are concerned about *Large Break Loss Of Coolant Accident*, there is nothing that limits UQ to a particular type of plant scenario or reactor. For example, see Strydom 2013 for an UQ in a pebble bed high temperature gas reactor.

A graphical explanation of safety margins is shown in Fig. 1.1. It also shows the difference between BE and conservative calculations: while conservative calculations results are expressed as a set of conservative calculated values, BE results are expressed as an uncertainty range of possible values. Besides, Table 1.1 shows different options for uncertainty management. A full conservative approach is presented in option 1, it was introduced in the 1970s due to the lack of knowledge to model physical phenomena in a nuclear reactor. This option is no longer recommended, unreal predictions over the safety margins may be expected due to

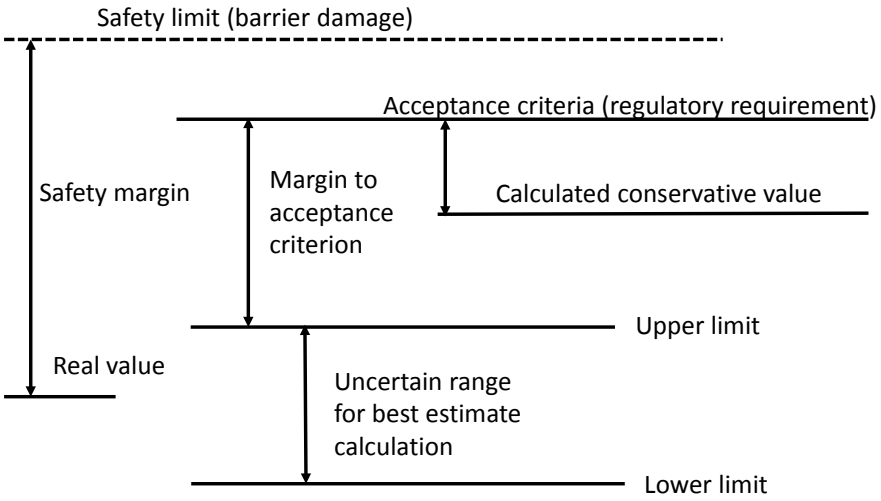

Fig. 1.1 – Concept of safety margin, extracted from D'Auria et al. 2008.

its conservative behavior. Option 3 is the most attractive option now and in the near future, it makes use of BE codes plus uncertainty evaluation to quantify safety margins. Currently, option 4 is still not common, thus there is still a big conservative contribution in present BE codes. All uncertainty methods have two limitations, (i) the needed resources may be prohibitive, and (ii) the results may change a lot among uncertainty methods. See Yankov et al. 2012, where two different UQ methods are used in a *Pressurized Water Reactor* (PWR) with some discrepancies in the relative power distribution.

In order to obtain real uncertainty for complex nuclear-related parameters, a big effort is done to build scaled experiments to understand different phenomena occurring in nuclear power plants. There are two types of experiments. On one hand, *Integral Test Facilities* (ITFs) are used if the phenomenon under study needs the interaction with other phenomena and it is not limited to a specific plant component. Thus, ITFs intends to reproduce a whole transient in a scaled nuclear power plant and it comprises all main components or zones in the real plant. On the other hand, *Separate Effects Test Facilities* (SETFs) are also scaled experiments where only one or few phenomena are under study. Thus, these phenomena are studied in isolation and they are not affected by third phenomena. Both, ITFs and SETFs, are designed according to proper scaling laws and always in relation with a built or designed reference plant. The measured phenomena, in both experiments, are expected to be as similar as in the reference plant.

Option	Computer code	Assumptions	Initial and boundary conditions
1	Conservative	Conservative	Conservative input data
2	BE	Conservative	Conservative input data
3	BE	Conservative	Realistic input data with uncertainties
4	BE	Based on prob. safety analysis	Realistic input data with uncertainties

Table 1.1 – Options for different uncertainty management, extracted from D'Auria et al. 2008.

1.1 Motivation and objectives

Following the uncertainty trend in current studies, the main motivation of this thesis is the study of the UQ and *Sensitivity Analysis* (SA) involved in a complete transient analysis. To achieve this purpose, the uncertainty of neutronic parameters is propagated at lattice and core levels. In that sense, this thesis covers the first phase of the benchmark released by the expert group on Uncertainty Analysis in Modeling (UAM-LWR), which the thesis' author participated. For example, in this thesis a MATLAB program is created on request of the benchmark organizers and is used to generate neutronic libraries to distribute among the benchmark participants.

It is desired to develop a methodology to propagate the uncertainty of cross sections and other neutronic parameters through a lattice physics code and core simulator. That is, the uncertainty contained in the problem-independent master library must be propagated up to the problem-dependent cross section library (collapsed and homogenized phases). The methodology must continue the propagation at core level, not only of neutronic parameters, but also for thermohydraulic parameters. The methodology must be valid for any type of reactor.

The thesis objectives can be summarized as follows.

1. Propagate neutronic parameter uncertainty through a lattice physics code.
   (a) Build a model for the reactor under study.
   (b) Propagate neutronic parameter uncertainties contained in the master library, that includes the collapse and homogenization phases.
   (c) Obtain the problem-dependent cross section library for the case under study.
2. Propagate neutronic parameter uncertainties through a core physics code.
   (a) Based on the output uncertainties obtained in the lattice physics code, propagate further the uncertainty of neutronic parameters contained in the problem-dependent cross section library.
   (b) Modify the source code of the core simulator to achieve the cross section perturbation.
   (c) Perform a SA, take the neutronic parameters contained in the problem-dependent library as input parameters and the main neutronic responses as the output parameters.
3. Propagate thermohydraulic parameter uncertainties through a thermohydraulic-neutronic coupled code in transient state.
   (a) Build the thermohydraulic model for the reactor under study fully discretized in 3D, valid for any transient analysis.
   (b) Propagate the uncertainty of selected thermohydraulic parameters through the thermohydraulic-neutronic coupled code.
   (c) Perform a SA, the analysis is performed following two approximations (i) analysis at the maximum response value, and (ii) analysis at each time step (index dependent).
4. Automatize all objectives presented before. Therefore, future studies can be implemented or updated with ease.

1.2 Thesis outline

The thesis is organized in seven chapters and six appendices. In the next chapter, the current state of the art is given for the *Uncertainty and Sensitivity* (U&S) methodologies and most important transport methods. Chapter 3 outlines the most used codes nowadays and focuses in the codes used in this thesis. It also explains, briefly, the basics for thermohydraulic and neutronic coupling and cross section library limitations. Chapter 4 explains, in detail, the models build to perform the simulations at two levels: lattice and core (neutronic and thermohydraulic). Chapter 5 and 6 contain the bulk of the thesis, the developed methodology for U&S analysis and then the results are given with extensive details. The last chapter, summarizes the conclusions and remarks of the thesis. This chapter contains important specifications for future projects and should be read to reach an up-to-day status in these matters.

The appendices contain information that it is though to be important but to extensive to be included in the bulk of the thesis. Appendix A gives a list of most common MT reactions, appendix B explain in detail the format of neutronic libraries in NEMTAB format (used in this thesis) and appendices C, D and E give extensive information for the uncertainty and sensitivity data obtained in this thesis. Finally, appendix F contains a list of publications, by the same author, achieved within the thesis framework.

Chapter 2

State of the art

. . . or how to dive in an ocean of information.

2.1 Uncertainty quantification and sensitivity analysis

In Chapter 1, it is explained the difference between conservative and uncertainty-based approaches for analysis. It is seen how uncertainty-based analysis are becoming more important and how uncertainty could be managed. Therefore, it is important to properly evaluate the uncertainty for a specific phenomenon of interest. It can be evaluated using two approaches. The first approach, **propagation of input uncertainty**, includes the identification of the most important input parameters whose uncertainty must be identified using a range and/or a *Probability Distribution Function* (PDF). In the second approach, **extrapolation of output uncertainty**, the uncertainty is deduced comparing the calculation results with experimental data obtained from ITFs or SETFs. Fig. 2.1 and Fig. 2.2 show a diagram for both approaches.

2.1.1 Propagation of input uncertainties

The input uncertainty (on input parameters) is propagated through the code or model in order to quantify the output uncertainty (on output parameters or model responses). The methods for propagation of input uncertainty can be classified as *probabilistic methods* (statistical) or *deterministic methods*.

According to D'Auria et al. 2008, statistical and deterministic methods have some common features,

- Input uncertainty is propagated through the model or code to determine the uncertainty on the model response.
- Uncertainties are identified. Dependencies between two or more uncertain input parameters must be identified and quantified provided that these dependencies are relevant.
- Besides input uncertainty, additional uncertainty is introduced by the model or code (simulation uncertainty).

and some differences.

- Statistical methods assign uncertainty only to a limited number of input parameters, whereas deterministic methods establish uncertainty for all input parameters.

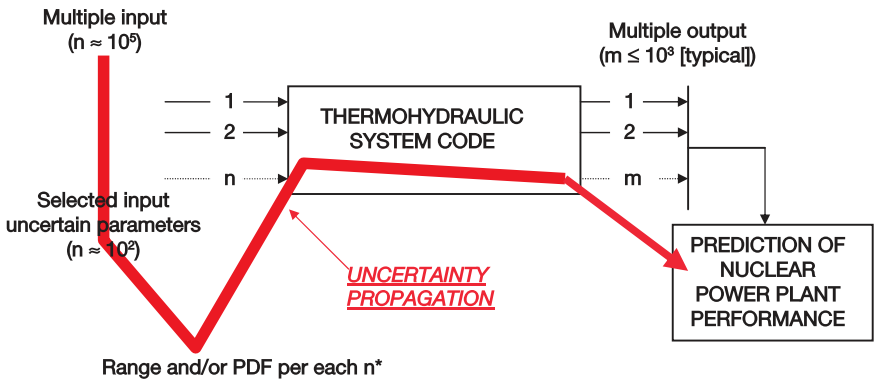

Fig. 2.1 – Diagram for input uncertainty propagation, extracted from D'Auria et al. 2008.

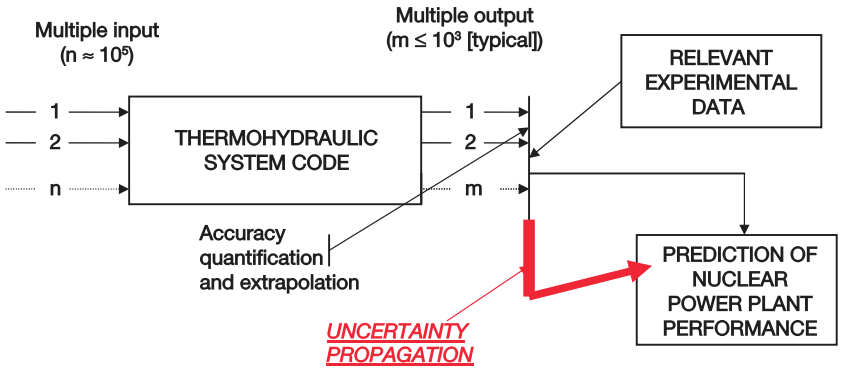

Fig. 2.2 – Diagram for output uncertainty extrapolation, extracted from D'Auria et al. 2008.

– Statistical methods are much easier to develop and use, but they require high number of model repetitions.

Before proceeding with the different UQ methods, it is important to understand the difference between uncertainty and sensitivity. On one hand, SA calculates the deviation on the output parameter variance apportioned by each input parameter (the user must choose which output and input parameters include into the SA). On the other hand, UQ obtains the range of possible output parameter values given a set of different input parameters. Input parameters have some uncertainty, thus UQ propagates this uncertainty through the code in order to obtain output uncertainties. Given these definitions, it is recommended to perform first a sensitivity analysis to isolate the most influencing input parameters, and then an UQ for the most influencing input parameters.

2.1.1.1 Probabilistic methods

Probabilistic methods estimate statistical quantities (such as the mean or variance) in order to characterize the uncertainty in the model response. The main framework behind statistical methods is explained within five steps.

1. First, a range and a PDFs for each uncertain input parameter must be identified. Ideally, the PDFs should be obtained using experimental data. However, in reality such data is commonly not available. In such cases, it is common to assign a uniform or normal distribution (Mesado et al. 2012), otherwise expert judgment is used to assign a range and PDFs. Nevertheless, the use of expert judgment is often unreal and should be used with precaution. It is also common to perform the UQ iteratively and change the ranges or PDFs on each iteration, however this affects greatly the results. Interdependencies among uncertain input parameters should be used, but it is often the case that dependencies are not available and input parameters are assumed to be independent.

2. The uncertain input parameters are sampled n times, there are several sampling techniques that can be used. The most important are explained next.

   Simple Random Sampling (SRS)**:** it is the simplest technique and most widely used. Each sample is generated independently for each uncertain input parameter according to its PDF. It is an expensive method since the number of samples must be quite large to obtain an acceptably small variance. This is an important drawback if the code or model is computationally expensive.

   Stratified sampling: each input parameter PDFs is divided into n subintervals with equal probability and one sample is draw from each subinterval. If a small number of samples is chosen and SRS is used, it is possible that most of the samples are taken around a specific point. This is prevented using stratified sampling because a better sampling over the whole uncertain range is performed. Thus, if the stratified sampling is used, the number of samples is generally smaller for a specified confidence level. However, this could introduce some bias on data.

   Latin Hypercube Sampling (LHS)**:** this is an improvement over the stratified sampling with additional computational cost to reduce the bias. After the stratified sampling is performed, the samples for each input parameter are permuted randomly. This assumes that the input parameters are uncorrelated. More accurate model response variance is obtained using LHS (Hernández-Solís 2012). More information can be found about LHS sampling method in Swiler and Wyss 2004.

   These sampling techniques are well studied, for example Hernández-Solís 2012, Strydom 2013 and Mesado et al. 2012 compare SRS and LHS sampling techniques. These studies show that LHS has a better domain coverage, however, significant differences are not found.

3. The number of samples or code runs, n, is an important parameter to consider. Parametric or non-parametric samplings are possible.

   Parametric sampling: the number of samples is dependent on the number of uncertain input parameters. Thus, if the number of uncertain input parameters is large, the number of samples could be computationally prohibitive. Moreover, it must be checked if the model response PDF follows a normal distribution. This can be done calculating statistical parameters, such as the skewness and kurtosis; or using a statistical test, such as the Lillefors test, Shapiro-Wilk test or the Kolmogorov-Smirnov test for normality.

   Nonparametric sampling: the number of samples could be greatly reduced using a non-parametric sampling because all uncertain parameters are sampled at the same time and the number of samples is not dependent on the number of uncertain input parameters. Moreover, any distribution could be assumed for input or output parameters.

The determination of the minimum sample runs, n, is important. For a nonparametric approach, the parameter n is such that when the code is run n times -or samples-, the response of interest will meet a certain tolerance limit (required a priori). The method to obtain n with a certain uncertainty, α, and a statistical confidence, β, was developed by Wilks (Wilks 1941 and Wilks 1942). The general formula, for one-sided tolerance region, is given by Eq 2.1 for order k. It can be simplified for first and second order according to Eq 2.2 and Eq 2.3 respectively. Numerical values can be seen in Table 2.1.

$$\sum_{j=0}^{n-k} \binom{n}{j} \alpha^j (1-\alpha)^{(n-j)} \geq \beta \tag{2.1}$$

$$1 - \alpha^n \geq \beta \tag{2.2}$$

$$1 - \alpha^n - n\,(1-\alpha)\,\alpha^{(n-1)} \geq \beta \tag{2.3}$$

If there are more than one dependent response (r), Eq 2.4 is used for one- or two-sided tolerance region (s), see Pal and Makai 2002 and Guba et al. 2003. This equation is remarkably similar to Eq 2.1 for one response. Numerical values can be seen in Table 2.2 for 1, 2 and 3 dependent responses.

$$\sum_{j=0}^{n-s\cdot r} \binom{n}{j} \alpha^j (1-\alpha)^{(n-j)} \geq \beta \tag{2.4}$$

Some studies (D'Auria et al. 2008 and Macián-Juan et al. 2012) suggest that Wilks formula for one-sided tolerance region and second order (Eq 2.3) can be used as two-sided first order. That leads to a minimum sample size of $n = 93$ for 95% of uncertainty and 95% of statistical confidence. Many studies use this sample size, for example Wieselquist et al. 2013, Vedovi et al. 2012 or Strydom 2013. However, in a recent study (Hong et al. 2013 and Hong and Connolly 2008), it has been shown that the recommended minimum number of samples can be obtained with Eq 2.5. For the same conditions, two-sided 95/95 and first order, the sample size increases to 146 (see Table 2.3).

$$1 + \alpha^n - 2\alpha^n \sum_{k=0}^{n} {}_nC_k \left(\frac{1-\alpha}{2\alpha}\right)^k \geq \beta \tag{2.5}$$

4. High-fidelity model vs surrogate model. For complex models, if the high fidelity model is used to propagate the uncertainty, the computational effort could be prohibitive. In this case, the high-fidelity or full model can be replaced by a surrogate model. The surrogate model represents the same physical scenarios but it runs simulations faster at expenses of accuracy and range of applicability. Several types of surrogate models are found:

   Simplified modeling: simpler assumptions are taken to build a new model.

   Response surface: the high-fidelity model is sampled over a specified range for each uncertain input parameter (input space). The model responses are used to generate a linear parametric expression which is an approximation of the full model. This approach assumes that the high-fidelity model responses behave smoothly over the input space chosen.

   Stochastic Finite Element Methods (SFEMs) this approach uses finite elements to build a response surface, thus it is more accurate and computational efficient than the linear parametric expression. However, the number of model responses is larger for the same input space.

   Neural networks: a self-learning set of surrogate models are used.

β	k	$\alpha_{\text{1-sided}}$				
		95.0	96.0	97.0	98.0	99.0
95.0	1	59	74	99	149	299
	2	**93**	117	157	236	473
96.0	1	63	79	106	160	321
	2	99	124	166	249	500
97.0	1	69	86	116	174	349
	2	105	132	177	266	534
98.0	1	77	96	129	194	390
	2	115	144	193	290	581
99.0	1	90	113	152	228	459
	2	130	164	219	330	662

Table 2.1 – Number of minimum samples for a first and second order one-sided tolerance region.

β	r	$\alpha_{\text{1-sided}}$			$\alpha_{\text{2-sided}}$		
		95.0	98.0	99.0	95.0	98.0	99.0
95.0	1	59	149	299	**93**	236	473
	2	93	236	473	153	386	773
	3	**124**	313	628	208	523	1049
98.0	1	77	194	390	115	290	581
	2	115	290	581	179	452	906
	3	148	374	749	237	598	1199
99.0	1	90	228	459	130	330	662
	2	130	330	662	198	499	1001
	3	165	418	838	259	652	1307

Table 2.2 – Number of minimum samples for a first order for one- and two-sided tolerance region and several dependent responses.

β	$\alpha_{\text{2-sided}}$				
	95.0	96.0	97.0	98.0	99.0
95.0	**146**	183	244	366	734
96.0	155	194	259	389	779
97.0	166	208	278	418	837
98.0	182	228	305	458	918
99.0	210	263	351	527	1057
99.5	237	297	397	597	1196
99.9	301	377	503	757	1517

Table 2.3 – Number of minimum samples for a first order two-sided tolerance region, extracted from Hong et al. 2013.

5. Apply UQ method. There are several UQ methodologies that falls into the probabilistic framework.

   Code Scaling, Applicability and Uncertainty (CSAU)**:** it was developed by the NRC for evaluating uncertainty in BE code calculations performed for design and safety analyses of *Light Water Reactor* (LWR). As an example, it is used in Vedovi et al. 2012 for *Boiling Water Reactor* (BWR) thermohydraulic instability analysis. CSAU comprise fourteen steps grouped into three main goals.

   (a) Requirements and code capabilities. Select a scenario, nuclear power plant and a specific version for the analysis code. Identify and rank the physical processes involved using a *Phenomena Identification and Ranking Table* (PIRT) to separate the most influence input parameters.

   (b) Assessment and ranging of parameters. Using experimental data, evaluate the code capabilities for the phenomena involving parameters isolated in the PIRT process. Generate an appropriate nodalization. Determine code and experiment accuracy. If some model is deficient, perhaps some bias must be introduced. Verify that the used BE code can scale up the experimental phenomena into the full-size plant (scale effects).

   (c) U&S analysis. Perform UQ to determine how input parameters affect the results. Then, SA to determine how the variability of input parameters affect the output parameters. Combine these information to obtain the total uncertainty for the code and for each phenomena studied. No particular method is specified for UQ, thus an appropriate method (or a surrogate model) must be chosen and justified.

   Gesellschaft für Anlagen und Reaktorsicherheit (GRS)**:** input parameters are sampled according to its predefined uncertain PDF. One system code run is needed per set of input sample. This method makes use of the high-fidelity model and nonparametric sampling. Therefore, the number of input parameters involved do not have any limitation. An important advantage is that the number of runs, n, depends only on the tolerance and confidence interval for the parameter of interest (output). Commonly, Wilks' formula is used to determine the number of runs (see Eq 2.1 and Eq 2.5). Based on the code results, statistics are applied to determine the sensitivity analysis. GRS is easy to implement, but the main disadvantage is that each input parameter must have a pre-defined PDF to quantify its uncertainty (normal and uniform PDF are commonly used). The GRS method is widely used in the literature. For example, Avramova et al. 2009 uses GRS methodology to evaluate the void distribution uncertainty in BWR bundle model.

   Empresa Nacional del Uranio, SA (ENUSA)**:** this method was developed in Spain and, as in GRS, both methods use the high-fidelity model and nonparametric sampling with Wilks' formula to determine the number of runs. However, it differs from GRS in that it selects the uncertain input parameters applying a PIRT.

   Generic Statistical Uncertainty Analysis Methodology (GSUAM)**:** it is similar to CSAU framework. It defines three sources of uncertainties: code, nuclear power plant conditions and fuel conditions. Among them, the code is the biggest source of uncertainty and must be evaluated comparing code results with experimental data.

   Best Estimate And Uncertainty (BEAU)**:** this method is similar to the CSAU framework. It uses a PIRT process and a surrogate model. It was developed in Canada for plant parameters uncertainty, mainly for *Canada Deuterium Uranium* (CANDU)[1] reactor licensing.

   Monte Carlo (MC)**:** this is the simplest technique to propagate uncertainty and is easy to implement. The high-fidelity model and parametric sampling is used, thus the number or code runs is relatively large.

[1] Nuclear reactors developed in Canada that use heavy water and natural uranium.

Dampster-Shafer: it is similar to MC approach but provides the lack of knowledge about the true distribution of an uncertain output parameter.

Variance-Based Methods: these methods use variance ratio to assess SA, for example the *Fourier Amplitude Sensitivity Test*. A linear relationship between input and output parameters is not assumed. However, they are computationally expensive and the information about the inverse cumulative distribution function is required for each uncertain input parameter.

First-Order and Second-Order Reliability Methods (FORM-SORM)**:** these methods estimate a probability of failure. They use optimization algorithms to find the most likely point of failure. Then, the probability of failure is fitted with a first or second order surface.

2.1.1.2 Deterministic methods

Deterministic methods compute sensitivities as local partial derivatives for a particular model response with respect to each uncertain input parameter. After the SA, an approach, such as the method of moments, is used to linearly combine the sensitivities and obtain the parameter uncertainty. The main difference between probabilistic and deterministic methods is related with the quantification of input uncertainties. PDF are not required, instead, uncertainty is quantified as a deterministic range or bound values. The range can be deduced from experimental data. These methods assume that the relationship between input and output parameters is linear.

Forward Sensitivity Analysis Procedure (FSAP)**:** it requires matrix inversion for each uncertain input parameter perturbation, thus great computational effort is needed. It is recommended only if the number of output parameters or model responses is bigger than the number of uncertain input parameters, which is rarely the case. Moreover, the method is only accurate for small perturbations of the input space.

Adjoint Sensitivity Analysis Procedure (ASAP)**:** it avoids to iteratively invert matrix for each uncertain input parameter perturbation. It is based on solving the adjoint sensitivity system, which is independent of the number of the uncertain input parameters. Some drawbacks include:

- For each model response of interest an adjoint sensitivity system must be solved.
- Implementation for an existing code is usually difficult and expensive.
- It produces a linear relationship for the model response uncertainty. This could be unreal for thermohydraulic systems.
- If the forward model is changed, the adjoint model must be consistently changed.

Atomic Energy Authority Winfrith (AEAW)**:** experts select the most important parameters and a reasonable uncertainty range is assigned to each of them (along with proper reasons). The uncertainty range is extracted using data, generally from SETFs. Several code runs are performed with a single or multiple input parameter variations in order to maximize or minimize the code result and thus, obtaining uncertainty range for the output parameter. The main implication is that the number of runs increases linearly with the number of input parameters.

Deterministic Realistic Method (DRM)**:** it is used in association with CATHARE (French BE thermohydraulic code). Quantification of the uncertainty is done using statistical methods. A realistic model calculates each output parameter uncertainty. However, later a penalization is applied and thus, the resulting confidence level is higher than the one obtained with just the statistical method. The main feature of this process is that the penalization is defined a priori.

2.1.2 Extrapolation of output uncertainty

These methods extrapolate the model response uncertainty comparing BE calculations again experimental data. They need an extensive set of data which is significant enough for the particular problem and also covers the range of interest. Thus, these methods are only appropriate for steady state scenarios and operational transients, they are not advisable for severe accident (because of the lack of significant data). The main advantage is that these methods do not require the identification of a subset of uncertain input parameters or their PDFs (or ranges).

Uncertainty Methodology based on Accuracy Extrapolation (UMAE)**:** calculates the output uncertainty by extrapolating the accuracy from experimental data (small scale facility) and ITFs to full scale nuclear power plants (big scale plant). Due to the difference in scaling criteria, some uncertainty is added to the model. The main advantage is that there is no limit for the number of input parameters. However, this method does not establish a correspondence between each input and output parameter (although it can be done with further statistical calculations). Furthermore, UMAE consistency depends on proving that the accuracy increases with the scale of the small scale facility.

Capability of Internal Assessment of Uncertainty (CIAU)**:** can be divided in two parts. First, select a nuclear power plant and its state. Each plant state is characterized by six relevant values (hypercube) as a function of time. For PWR, these are (i) upper plenum pressure, (ii) primary loop mass inventory, (iii) steam generator pressure, (iv) cladding surface temperature at 2/3 of core active height, (v) core power and (vi) downcomer collapsed liquid level. Second, each code calculation result is associated with one of the 6 relevant quantities for different transient times. Finally, each hypercube point is associated with an uncertainty extracted using uncertainty methods.

2.1.3 Recommendations for UQ method selection

Some considerations should be taken into account when choosing a particular UQ method.

1. Selection of input uncertainty parameters. With GRS no limitation is imposed on the number of uncertain input parameters, the number of code runs only depends on the uncertainty accuracy desired. A (PIRT) is performed following several steps. First an expert panel in the specific scenario is summoned. The scenario is subdivided into phases and all phenomena involved in each phase are listed. The phenomena are ranked, the phenomena that have a strong influence on the phase under study (controlling phenomena) should be included into the UQ as uncertain input parameter. An alternative for the expert panel is to use an *Analytical Hierarchical Process*. This process uses probabilities to assess the importance of each phenomena and thus, rank them without expert judgment.

2. Assign a range or PDF. These are assign to each input parameter to express quantitatively its state of knowledge. If the information for each uncertain input PDF is available (or assumptions are defined), then a probability method, such as GRS or ENUSA, can be used. However, if PDF are not reliable and the expert analysts can obtain maximum and minimum values for each uncertain input parameter, then AEAW method can be used. A PDF could be obtained using sample values and specifying a certain accuracy. Nevertheless, in thermohydraulics, it is common the case where the uncertainty distribution is unknown and the frequency data is not available. Thus, an assumed PDF is taken, for example uniform or normal distributions are the most used distributions. If later, new evidence sheds some light for a more realistic PDF, it is possible to update the PDF and proceed again with the methodology. Although, changing the PDF or its range have strong effects on the output uncertainty bounds.

3. Adding new information. More than 30 ITFs were build and operated to simulate the conditions for different normal and abnormal transient scenarios. More than 1000 experiments were performed and their data collected. If the selected system code has enough accuracy, regarding the experimental data, and the assumption of extrapolation is accepted, then the UMAE method is a good candidate. Nonetheless, if no data exists for a specific transient scenario, then the UMAE method is immediately discard.

4. Number of code calculations. According to Wilks' formula, for nonparametric samples, the number of code runs is independent of the number of uncertain input parameters and only depends on the tolerance limits and confidence level. CSAU methodology does not use Wilks' formula to determine the number of code runs. Therefore, for this method the number of code runs is dependent on the number of uncertain parameters, P. If only two levels for each uncertain input parameter are set (range maximum and minimum, in addition to the nominal state), the code runs, n, can be calculated as Eq 2.6. If a better space cover is desired, then all uncertain input parameters should be combined and n is expressed as Eq 2.7.

$$n = 2P + 1 \tag{2.6}$$

$$n = 3P \tag{2.7}$$

   If the computational resources or time exceed the available capacity, because there are too many input parameters and n results in a high number, several code runs can be used to create a response surface or surrogate method. The response surface can be used, instead of the BE code, to compute much cheaper responses and reduce dramatically the computational time. Response surfaces allow quantification of point values, however, they are not useful for time-dependent quantification.

5. Other recommendations. Full high-fidelity models are accurate but expensive in contrast to surrogate models. The difficulty for implementing the method and its flexibility should be examined. If the high-fidelity model is unlikely to change for a long period of time, ASAP method is recommended because even though it is difficult to implement, it is inexpensive to run. The assumption for linear approximation must be evaluated when using ASAP or other methods that use a surrogate model. When using deterministic methods, a SA should be preceded in order to identify the most influential uncertain input parameters.

According to Briggs et al. 2009, the predominant recommendation is to use the high-fidelity model with nonparametric sampling and the Wilks' formula to determine the sample size (GRS method). It gives good accuracy and it is easy to implement and use. This recommendation, using the revised Wilks' formula (Eq 2.5), is followed in this thesis. If computational time or effort is prohibitive, then a surrogate model should be considered. Several methods for UQ are presented so far, Table 2.4 and Table 2.5 summarize the main features for the statistical and deterministic methods.

2.1.4 Code adequacy for BEPU

Best Estimate Plus Uncertainty (BEPU) calculations have two main advantages, (i) more realistic plant safety margins for licensing and (ii) determine which input parameters have stronger impact on output uncertainty (SA). Whether a code is adequate to perform BEPU could be determined using either top-down or bottom-up evaluations. Both are divided in four parts.

Method	**Easy to implement**	**Number of code runs**	**Cost per run**	**Selection of uncertain input parameters**	**Flexible to add new model responses?**	**Flexible to model changes**	**Accuracy**
Monte Carlo	Yes	Parametric may be large	Full model - may be high	Data, experts	Yes	Yes	Accuracy of input uncertainty
GRS	Yes	Nonparametric (Wilks)	Full model - may be high	Data, experts	Yes	Yes	Accuracy of input uncertainty
ENUSA	Yes	Nonparametric (Wilks)	Full model - may be high	PIRT	Yes	Yes	Accuracy of input uncertainty
Simplified modeling	Additional model development	Can use nonparametric	Low	Data, experts	New simp. model		Less than full model
Response surfaces	Response surface development	Can use nonparametric	Low	Data, experts	New resp. surface		Less than full model, no discontinuity
SFEM	Additional model development	Can use nonparametric	Low for small number of inputs	Data, experts	New approx. model		Less than full model
Dumpster-Shafer	Yes	Parametric - may be large	Full model - may be high	Data, experts	Yes	Yes	Accuracy of input uncertainties
FAST	Fourier series expansion	Increase rapidly with no. of input parameters	May be high	Data, experts	Yes	Yes	Accuracy of input uncertainties
Original CSAU	Response surface development	Parametric - may be large	Low	PIRT	New resp. surface		Less than the full model
AREVA CSAU	Yes	Nonparametric (Wilks)	Full model - may be high	PIRT	Yes	Yes	Accuracy of input uncertainties

Table 2.4 – Main features comparison for statistical uncertainty methods, extracted from Briggs et al. 2009.

Method	Easy to implement	Number of code runs	Cost per run	Selection of uncertain input parameters	Flexible to add new model responses?	Flexible to model changes	Accuracy
FSAP	Yes	One per input parameter variation for each response	Full model - may be high	Data, experts	Yes	Yes	Assumes small input uncertainties, no discontinuities
ASAP	Adjoint development	One per input parameter for each response	Adjoint model < full model	None required	Developed adjoint		Assumes small input uncertainties, no discontinuities
UMAE-CIAU	Yes	One	Full model - may be high	None required	Possible extensive additional exp. data	Yes	Dependent on quality of experimental data

Table 2.5 – Main features comparison for deterministic uncertainty methods, extracted from Briggs et al. 2009.

2.1.4.1 Bottom-up evaluation

1. Pedigree: it is built up by knowledge about the particular code, experience must be gained (procedures, development, correlations...) and properly documented along with its uncertainty, limitations and assumptions.
2. Applicability: the range of use for each model or correlation must be known, documented and properly referenced. If the range of applicability is broadened, a proper justification should be provided.
3. Fidelity: ensure that the correlations used are correct, code validation against experimental data and benchmarking studies.
4. Scalability: experimental data for key phenomena are extracted from small-scale facilities. Thus, it must be demonstrated that this data also apply to simulate the full-scale plant.

2.1.4.2 Top-down evaluation

1. Numerics: solution evaluation for convergence (the range of possible numerical solutions is reduced with time), stability (system code does not fail for different transients, phenomena and models) and property conservation (a property may not be conserved if different algorithms or methods are used to calculate the property).
2. Fidelity: based on performing code assessments using ITFs or SETFs data for different transients and phenomena.
3. Applicability: the code should be able to simulate the key phenomena for different transients under study. Code validation or comparison between code results and data with known uncertainty is needed. The code adequacy can be classified according to experimental data uncertainty.
   (a) Excellent: results lie within or near the data uncertainty band at all times.
   (b) Reasonable: results do not always lie within the data uncertainty band, but have the same trend.
   (c) Minimal: Major trends and phenomena are not predicted. Wrong conclusions may be withdrawn.
   (d) Unacceptable: significant difference between results and experimental data. It may arise because the model is wrong, the wrong model is chosen or because the phenomenon is not well understood.
4. Scalability: scaling uncertainty due to inappropriate model developments derived from small-scale facilities when applied to full-scale plant. These uncertainty must be identified and evaluated.

Currently, it does not exist any standard procedure to qualify uncertainty methods. It is known that more data would be needed to improve or define new input uncertainty ranges. However, uncertainty methods that do not heavily relay on expert panels are preferred.

2.1.5 Source of uncertainty

BE code results could be greatly affected by uncertainty sources. These could arise due to code approximations or deficiencies, model limitations, material properties uncertainty, user error, compiler/platform error, numerical method approximations, lack of capabilities... they could be classified into four groups. A list of possible uncertainty sources is given hereafter.

1. Code or model approximations
   (a) Conservation equations are an approximation, thus they lead to some uncertainty or error. For example, not all interactions may be included.
   (b) Simplifications on the velocity field within the same or different phases. Slip ratio or velocity profile within the same phase (bubbles).
   (c) Energy and momentum balance not directly accounted into the equations. Natural convection may not be simulated properly using a system code.
   (d) Lack of code capabilities. Energy degradation or transformation from kinetic energy into heat may not be among the code options.
   (e) Commonly the system codes solve the problems using partial derivative equations. The numerical solution is approximate. Implicit, explicit, semi-implicit methods.
2. Plant uncertainty or representation
   (a) Geometry averaging or simplification either in 2D or 3D. Obviously, it is not possible to simulate the exact geometry with the current system codes. Channel or core simplifications, pump simplification... Due to increasing computational performance, new models are more realistic, for example Mesado et al. 2015 shows how to simulate a nuclear reactor core fully in 3D.
   (b) Uncertainty in boundary and/or initial conditions. Even though they are uncertain, the user must introduce some information into the code.
   (c) System discretization, the mesh used to solve the field equation plays an important role for uncertainty. In Canuti et al. 2012 the effect of four different grid meshes is studied over the multiplication factor in a PWR.
3. Empirical correlations
   (a) Experimental data is also uncertain. It should be provided and documented. Some codes provide covariance matrices for the experimental data, especially in nuclear codes with cross section libraries (Adetula and Bokov 2012).
   (b) Use of empirical correlations. Range of applicability specification, use of correlations outside the range, correlations implemented approximately.
   (c) Empirical correlations are obtained with steady state conditions and fully developed flow. However, this is not the case for most of the cells in a transient simulation.
   (d) Approximations in material properties.
   (e) Scaling effect. Empirical correlations are obtained in a facility usually much smaller than the real nuclear power plant (ITFs or SETFs). Therefore, the information into empirical correlations must be transferred into a model with different geometric dimensions. Empirical correlations ranges must be considered.
4. User effect
   (a) Code user effect. This is one of the greatest source of uncertainty, but sometimes it is not taken into account. Current system codes have big freedom for system representation. Changes in nodalization, interpretation or availability of information (such as code documentation or geometrical data). This source of uncertainty can be reduced with training of inexperienced users, well documented code guidelines, good code programming, large user community, good problem specifications and definitions... An example of good documentation including all details needed for simulation is included within the NEA benchmark (NEA 2004a).

(b) Computer, compiler and platform effect. A computer code is develop using a specific platform and the hardware available at the time. However, the code development time could extend up to a decade or more. Within this time, hardware can experience dramatic changes. The results must be reproducible across platforms. Round-off error, difference in arithmetic operations, different compilation procedures, and/or bad programming practices or techniques could play an important role.

2.1.6 Quantifying sensitivity

Sensitivity analysis quantifies the influence of the input parameters over the output parameters and its variability. Generally, two different levels of sensitivity analysis can be found.

Local level analysis focuses only over the neighborhood of a specific input space point -or nominal value. Using a local level analysis, sensitivity changes over the input space can be detected. The main limitation for this level is the computational cost, especially if the number of input parameters is relatively high.

Global level analysis considers the whole input domain space. A unique global level can be calculated, for example, using the integrated mean over the local sensitivity analysis. This level is usually less expensive than the local level, but it does not identify if an input sensitivity changes over the input domain space.

Generally, in order to measure the importance of a specific parameter (sensitivity), correlation coefficients or regression coefficients are used.

2.1.6.1 Correlation coefficients

For linear relation between two random variables the *Simple Correlation Coefficient* (SCC) -also called *Pearson Product Moment Correlation Coefficient*- or the *Partial Correlation Coefficient* (PCC) can be used. Both coefficients determine the relation between parameters and have their values bounded between -1 and 1. If the linear relation is strong, the coefficient is close to either +1, for positive correlations, or -1, for negative correlations. Values near 0 are obtained for random pairing between both parameters. Commonly, the strength of the correlation can be classified verbally.

$0.00 - 0.19$ very weak

$0.20 - 0.39$ weak

$0.40 - 0.59$ moderate

$0.60 - 0.79$ strong

$0.80 - 1.00$ very strong

If the input and output parameters are x and y respectively, and there are n samples (thus n code runs), the SCC (r_{xy}) is calculated as

$$r_{xy} = \frac{\sum_{i=1}^{n} x_i y_i - n\bar{x}\bar{y}}{\sqrt{\frac{1}{n}\sum_{i=1}^{n}(x_i - \bar{x})^2}\sqrt{\frac{1}{n}\sum_{i=1}^{n}(y_i - \bar{y})^2}} \tag{2.8}$$

where $\bar{x}$ and $\bar{y}$ are the input and output sample means respectively.

When there are several input and/or output parameters, the correlation coefficients can be calculated among them and arranged in a matrix fashion called *correlation matrix*. Thus, Eq 2.8 can be expressed as a matrix whose elements are given by Eq 2.9. Similarly, the correlation matrix can be expressed as *covariance matrix*, where the diagonal contains the variances, σ_i, and the off-diagonal elements are the covariance among parameters, σ_{ij}. As Eq 2.9 shows, the correlation value is a "scaled" covariance value.

$$SCC_{ij} = \frac{\sigma_{ij}}{\sigma_i \sigma_j} \tag{2.9}$$

However, the value of SCC could be influenced by other model parameters. Therefore a "corrected" correlation is provided by the PCC. This provides the correlation between two parameters (x and y) while holding all the other parameters constant (represented by z in Eq 2.10). Thus, the PCC value ($r_{xy|z}$) is only equal to the SCC value when the parameters x and y are uncorrelated with parameter z.

$$r_{xy|z} = \frac{r_{xy} - r_{xz} r_{yz}}{\sqrt{\left(1 - r_{xz}^2\right)\left(1 - r_{yz}^2\right)}} \tag{2.10}$$

If we define SCC^{-1} as the inverted matrix resulting from Eq 2.9, Eq 2.10 can be expressed using matrix notation whose elements are given by Eq 2.11.

$$PCC_{ij} = \frac{SCC_{ij}^{-1}}{\sqrt{SCC_{ii}^{-1} SCC_{jj}^{-1}}} \tag{2.11}$$

It is important to note that the sensitivity values obtained using these correlation coefficients depend strictly on the assumption of the model linearity. For nonlinear models, the same correlation coefficients can be used with ranks instead of the original values. Thus the *Simple Rank Correlation Coefficient* (SRCC) -also called *Spearman's Rank Correlation Coefficient*- or the *Partial Rank Correlation Coefficient* (PRCC) are used instead. Model linearity assumption can be verified if both coefficients, PCC and PRCC, give a similar result. SRCC and PRCC work with ranked values instead of the original values. The ranks are obtained arranging the original values in ascending order and then integer ranks are assigned. For ties (identical numbers on the original values), the average of ranks that would have been assigned if there had been no ties is assigned. More information can be found in Conover 1999.

The critical values for the Spearman's Rank Correlation Coefficient is calculated according to

$$r_s = \pm \frac{z}{\sqrt{n-1}} \tag{2.12}$$

where n is the number of samples and z represents the point on the standard normal PDF. This point is the probability, p, of observing a value greater than z, which is known as the upper critical value or quantile. The absolute value of r_s, between an input and output parameter, gives the minimum value for which the output parameter can be considered sensitive to the variation of the input parameter. For a confidence interval of 95%, $z = 1.96$, and if n is 146, then $r_s = 0.1628$.

2.1.6.2 Regression coefficients

In *regression analysis* or *response-surface analysis* a *response surface* or *regression function* is constructed to approximate the model. The regression function can be expressed as

$$\hat{y}(x) = \beta_0 + \beta_1 x_1 + \beta_2 x_2 + \cdots + \beta_n x_n \tag{2.13}$$

$$y = \hat{y}(x) + \Delta(x) \tag{2.14}$$

where $\Delta(x)$ is the error or difference between the regression function and the true model, The coefficients can be arranged in a vector $\boldsymbol{\beta}$, obtained by least squares and minimizing $\sum_{n=1}^{N}(y_n - \hat{y}(x_n))^2$.

It is useful to apply the next transformations -or "standardization"- to the input, x_n^*, and output, y_n^*, parameters before constructing the regression function.

$$x_n^* = \frac{x_n - \bar{x}}{\sigma_x} \tag{2.15}$$

$$y_n^* = y_n - \bar{y} \tag{2.16}$$

where σ_x is the standard deviation of sample x.

This standardization removes the impact of units of measurement and range differences among different parameters. Thus, a better comparison among parameters can be obtained with the standardized regression coefficients, $\boldsymbol{\beta}^*$. The only difference between $\boldsymbol{\beta}$ and $\boldsymbol{\beta}^*$ is found in β_0, which will be displaced $\Delta^*(x_n^*)$, all other terms are unchanged. The vector $\boldsymbol{\beta}^*$ provides estimates of the (scaled) partial derivatives of the output with respect to the selected inputs under the linear approximation of the model (McKay 1988). Because of the standardized transformation, the coefficients have the same units as the output and estimate the change in the output when the input is changed by one standard deviation unit.

There is a substantial difference between correlation coefficients and regression coefficients. On one hand, correlation coefficients measure the relation strength between parameters after its variability is normalized. On the other hand, regression coefficients measures the output change as a result of an input unit change. For example, for an output parameter function of time, the correlation coefficients could indicate constant strength and the regression coefficients could indicate variable intensity.

2.1.6.3 Variable reduction

For studies where the number of inputs is high (e.g., 50 or more), the computational -and sometimes the economical- cost can be prohibitive. Moreover, if the number of input parameters, k, is greater than the number of samples, n, the correlation matrix can be singular and thus, cannot be inverted. If n is greater than k, the correlation matrix can still be singular. Thus, in order to reduce collinearity -degree of linear dependence among the input vectors-, either n is increased or k is decreased. A screening process can be used to reduce the number of input parameters and thus, reduce the computational burden and collinearity.

The variable reduction or screening process follows two steps. Starting with the set of all input variables $I = x_1, x_2, \ldots x_k$, a subset of I is selected as sensitive parameters to form the subset of candidate variables $I^c(t)$ for time step t.

1. For each input parameter not in $I^c(t)$, compute the PRCC between it and the output holding constant all other input parameters in $I^c(t)$. For the first iteration, since $I^c(t)$ is empty, the SCC is used.

2. Include the input parameter with the largest absolute correlation coefficient in $I^c(t)$. Go back to step 1. The iterative process continues until one of the following conditions is reached.

   (a) The PRCC for the last selected input parameter is less than a minimum value, r_s.

   (b) The PRCC for the last selected input parameter is greater than a maximum value, r_f. This measures the linearity approach between $I^c(t)$ and the output.

The process is repeated independently for each time step. One subset of candidate variables is obtained per time step, $I^c(t_1)$, $I^c(t_2)$ ...

If r_s is too small, too many input parameters will be selected and the reduction in number of parameters is not effective. If it is too large, then too few input parameters will be selected, and the risk of missing important parameters is high. The choice of r_f is critical to avoid singular correlation matrices. The experience and expert judgment is usually used to select an appropriate value for r_s and r_f based on each particular case. A starting value of $r_f = 0.98$ is suggested (McKay 1988).

2.2 Reactor physics

2.2.1 Nuclear data

Nuclear data is essential to obtain accurate transport and core simulations. This data contains mainly cross sections, but also kinetic parameters. It is contained in several large cross section libraries that are maintained by different research institutes, national laboratories or governments. These are some of the most currently in use *Nuclear Data Libraries* (NDLs) available along with its newest version.

- BROND-2.2: Russian Evaluated Nuclear Data Library.
- CENDL-3.1: Chinese Evaluated Nuclear Data Library.
- ENDF/B-VII.1: United States Evaluated Nuclear Data File.
- ENDL-92: Evaluated Nuclear Data Library of the Lawrence Livermore National Laboratory.
- JEFF-3.2: Joint Evaluated Fission and Fusion File.
- JENDL-4.0: Japanese Evaluated Nuclear Data Library.
- RUSFOND-2010: Russian File of Evaluated Neutron Data.

Extensive information about cross section libraries can be found in Herman and Trkov 2005. Data in these libraries is usually classified according to the incident neutron energy and the nuclear interaction. A list for the most important nuclear interactions and the correspondent MT numbers is found in Appendix A.

2.2.2 Transport methods

The lattice physics codes solve the *Boltzmann transport equation* to obtain the neutron flux and the eigenvalue or multiplication factor. Boltzmann equation is expressed using cross sections and the angular neutron flux, the steady state equation is written as:

$$\Omega \cdot \nabla\psi(r,\Omega,E) + \Sigma_t(r,E)\psi(r,\Omega,E) = \int\int \Sigma_s(r,\Omega' \to \Omega, E' \to E)\psi(r,\Omega',E')dE'd\Omega' + \frac{1}{4\pi}S_f(r,E) \quad (2.17)$$

$$S_f(r,E) = \chi(E)/\mathrm{k_{eff}} \int \nu\Sigma_f(r,E')\phi(r,E')dE' \quad (2.18)$$

$$\phi(r,E) = \int \psi(r,\Omega,E)d\Omega \quad (2.19)$$

Where

r is the position vector,

E is the energy,

Ω is the angular direction,

$\psi(r, \Omega, E)$ is the angular neutron flux,

$\phi(r, E)$ is the scalar neutron flux,

$\Sigma_t(r, E)$ is the total cross section,

$\Sigma_s(r, \Omega' \rightarrow \Omega, E' \rightarrow E)$ is the scattering cross section,

$\nu\Sigma_f(r, E')$ is the fission cross section multiplied by the average neutrons produced per fission,

$\chi(E)$ is the spectrum for prompt and delayed neutrons, and

k_{eff} is the multiplication factor.

The Boltzmann equation is simply a balance of neutron flux in the system. The two terms on the left hand side of Eq 2.17 are (i) the neutrons in or out (leakage) of the system and (ii) the neutron disappearance due to nuclear interactions. The terms on the right hand side are (i) the neutrons changing energy due to scattering and (ii) neutrons produced by fission.

There are several methods to solve the Boltzmann equation for neutron transport. The most common methods are the *Method of Characteristics*, the P_N and the S_N. These methods solve the angular discretization of the Boltzmann equation. Next, a brief description of the P_N method and its simplification SP_N is developed. For a more detailed derivation of transport methods, the reader is referred to Stacey 2007.

2.2.2.1 P_N transport method

The *spherical harmonics method* or P_N makes use of the *associated Legendre polynomial*. This mathematical tool allows solving the angular dependence. For example, the angular neutron flux can be expressed without the angular dependence as

$$\psi(r, \Omega, E) = \sum_{n=0}^{\infty} \sum_{m=-n}^{n} \phi_n^m(r, E) Y_n^m(\Omega) \tag{2.20}$$

Where $Y_n^m(\Omega)$ is the *spherical harmonic function* with degree n and order m,

$$Y_n^m(\Omega) = \sqrt{\frac{(2n+1)(n-m)!}{(n+m)!}} P_n^m(\mu) e^{im\varphi} \tag{2.21}$$

and $P_n^m(\mu)$ is the *associated Legendre polynomial*.

Using the orthogonal property of the spherical harmonics, the coefficients of Eq 2.20 can be determined as

$$\phi_n^m(r, E) = \int Y_n^m(\Omega) \psi(r, \Omega, E) \tag{2.22}$$

and the scattering cross section

$$\Sigma_s(r, \Omega' \to \Omega, E' \to E) = \sum_{n=0}^{\infty} \frac{2n+1}{4\pi} \Sigma_s(r, E' \to E) P_n(\mu) \tag{2.23}$$

Introducing these relations into the Boltzmann equation, the Boltzmann equation can be transformed into a set of coupled partial differential equations with $\phi_n(r, E)$ as unknowns, being $n = 0, \ldots, N$. The multigroup energy approach can be used to eliminate the energy dependence. The energy domain of cross sections and neutronic parameters is discretized according to Section 2.2.4. In order to obtain more general multidimensional P_N equations, the simplified P_N approach must be applied (or the approximation SP_N). The resulting SP_N equations have significant improved computational efficiency and similar accuracy compared to the S_N or P_N equations.

The SP_N equations in matrix notation can be further developed into a set of linear equations that can be solved using any existing linear matrix solver library. The resulting equations are slightly more accurate for problems that are mainly diffusive. It is also acceptable for problems that have strong transport regions but the solution behaves almost one-dimensionally and has weak tangential derivatives at material interfaces. Therefore, SP_N equations are not accurate with high void regions, streaming regions, geometrical complex inhomogeneities, etc. The SP_N equations can be extended to transient state by adding the corresponding time derivative terms to each equation. The reader is referred to Stacey 2007 for more information.

2.2.2.2 Extended step characteristic approach

Traditional discrete ordinate methods are based on a finite difference approximation to solve the flux or leakage terms. However, with such difference schemes, it becomes difficult to represent a non-orthogonal complex geometry. For complex geometries, the *Extended Step Characteristic* (ESC) allows space discretization with non-orthogonal cells, instead, these are represented by arbitrary polygons.

The Boltzmann equation can be rewritten in a characteristic direction, s, as follows (energy dependence is omitted)

$$\frac{d\psi(s)}{ds} + \sigma_t(s)\psi(s) = Q(s) \tag{2.24}$$

integrating, the solution gives the angular flux for a specific direction.

$$\psi(s) = \psi_0 e^{-\sigma_t s} + e^{-\sigma_t s} \int_0^s Q e^{\sigma_t s} ds \tag{2.25}$$

where

s is the distance along the characteristic direction,

ψ is the angular neutron flux,

ψ_0 is the known angular neutron flux at $s = 0$,

$\phi(r, E)$ is the scalar neutron flux,

Σ_t is the total cross section and

Q is the source of angular neutron flux.

One of the simplest schemes to solve the neutron flux for a given mesh is the *Step Characteristic* (SC) method. This method has two assumptions (i) the source Q and total cross section σ_t are constant within a computational cell and (ii) the angular flux is constant on each cell boundary. In order to obtain the scalar flux, a set of characteristic directions is chosen from a quadrature set and the angular flux is numerically integrated. Eq 2.25 can be integrated along the length of unknown sides to determine its angular flux. Once the angular flux is known for all cell sides, a neutron balance in the cell determines the cell average angular flux. The extension of this scheme for any geometry is called ESC.

Again, the ESC method is based on two assumptions (i) the source Q and total cross section σ_t are uniform within a computational cell and (ii) the cell boundaries are defined by straight lines. Hence, in order to obtain an accurate solution, cells must be small and defined by polygons. In theory, there is not any limitation on the number sides for each cell. However, in reality, this is limited by the computational time. The relation flux-characteristic direction can be classified as (i) incoming, (ii) outgoing and (iii) parallel to the cell side. The incoming flux must be given by the specified boundary conditions or by the solution of adjacent cells. As in the SC, the outgoing flux is determined from the incoming flux, and then a cell neutron balance is used to obtain the cell average angular flux. The process is then repeated for all directions in the quadrature set. This sweeping process continues until all unknown fluxes are solved for all sides and directions. The predicted scalar flux is used to determine other quantities such as the fission, scattering reaction rates or the flux source Q. The process is repeated until all scalar fluxes are converged within a specified tolerance.

2.2.3 Diffusion equation

Boltzmann equation can be solved with methods seen before, nonetheless, it requires too many computational resources to solve a full nuclear reactor. In order to achieve faster calculations, the Boltzmann equation can be further simplified to obtain the *diffusion equation*. The diffusion equation is based in the diffusion theory and Fick's law Eq 2.26. This law expresses the net neutron current, $j(\boldsymbol{r}, t)$ as a function of the diffusion coefficient, D, and the flux $\phi(\boldsymbol{r}, t)$. This theory is derived with some assumptions and limitations, these are summarized next.

- Limitations exist within few mean free paths from the boundaries because of the leakage effect.
- It is assumed that the flux is mainly due to scattering collisions. However, near sources or sinks this is not true.
- In strong absorber media the flux variation is fast in space, but only slow flux variation in space are acceptable.
- Isotropic scattering is assumed, but it is not always true in a real reactor. It can be accounted for if a modified diffusion coefficient is used.
- Limitations in the proximity to interfaces with two different scatter properties. This can be partly solved with the use of ADFs, Section 2.2.4.1.
- Limitations exist for fast neutronic transients.

$$j(\boldsymbol{r}, t) = -D\nabla\phi(\boldsymbol{r}, t) \tag{2.26}$$

The diffusion equation, Eq 2.27, is solved coupled to Eq 2.28 which expresses the neutron precursor concentration as a function of time. For a complete derivation of both equations, the reader is referred to widely-known reactor physics books, such as Stacey 2007 or Duderstadt and Hamilton 1976. In these equations, the multigroup approximation is typically used to solve the energy dependence in the diffusion equation

because it reduces the computational burden. Usually, core physics codes use two different neutron energy groups (fast and thermal) to solve thermal reactors. However, it is also possible to use more neutron energy groups (especially for fast reactors). Therefore, cross sections and other neutronic parameters are discretized in G energy groups. See Section 2.2.4 for cross section energy discretization.

$$\begin{aligned}\frac{1}{v_g}\frac{\partial \phi_g}{\partial t}(\boldsymbol{r},t) = \nabla\cdot[D_g(\boldsymbol{r},t)\nabla\phi_g(\boldsymbol{r},t)] + \sum_{g'=1,g'\neq g}^{G}\Sigma_{s,g'\to g}(\boldsymbol{r},t)\phi_{g'}(\boldsymbol{r},t) + \\ (1-\boldsymbol{\beta})\,\chi_g^p\sum_{g'=1}^{G}\nu\Sigma_{f,g'}(\boldsymbol{r},t)\phi_{g'}(\boldsymbol{r},t) + \sum_{i=1}^{I}\lambda_i\chi_{i,g}^d C_i(\boldsymbol{r},t) - \Sigma_{t,g}(\boldsymbol{r},t)\phi_g(\boldsymbol{r},t)\end{aligned} \tag{2.27}$$

$$\frac{\partial C_i}{\partial t}(\boldsymbol{r},t) = \beta_i\sum_{g=1}^{G}\nu\Sigma_{f,g}(\boldsymbol{r},t)\phi_g(\boldsymbol{r},t) - \lambda_i C_i(\boldsymbol{r},t) \tag{2.28}$$

Where $\boldsymbol{r}$ is the position vector, t is time, g and g' are collapsed energy groups (out of G total energy groups) and i is the delayed neutron group (out of I total delayed neutron groups), usually there are 6 different delayed neutron groups. Other variables are

ϕ_g is the neutron flux,

D_g is the diffusion coefficient,

$\Sigma_{s,g'\to g}$ is the total scattering cross section from group g' to g,

$\nu\Sigma_{f,g}$ is the fission cross section multiplied by the average neutrons produced per fission,

$\Sigma_{t,g}$ is the total cross section,

$\boldsymbol{\beta}$ is the total delayed neutron fraction,

λ_i is the decay constant for neutron precursor group i,

χ_g^p is the spectrum for prompt neutrons,

χ_g^d is the spectrum for delayed neutrons,

v_g is the neutron velocity, and

C_i is the neutron precursor concentration group i.

The diffusion equation is simply a balance of neutron flux in the system. The terms on the right hand side of Eq 2.27 correspond to (i) neutrons in or out (leakage) of the system, (ii) neutrons changing energy due to scattering, (iii) prompt neutrons produced, (iv) delayed neutrons produced and (v) neutron disappearance due to other nuclear interactions. The sum of all this terms (left hand side), is just the accumulation of neutron flux in the system. The same can be done with Eq 2.28, which is a neutron precursor concentration balance, (i) neutron precursor creation due to fission and (ii) neutron precursor disappearance due to its decay. To solve the time-dependent diffusion equation, using two neutron energy groups, it is common to specify the following simplifications.

1. All neutrons produced by fission, prompt and delayed, belong to the fast group, thus $\chi_1^p = \chi_1^d = 1$ and $\chi_2^p = \chi_2^d = 0$.

2. The delayed neutron precursor yields do not depend on neutronic energy.

3. Up-scattering is negligible, $\Sigma_{2\to1} = 0$.

For sake of simplicity, the dependence on time and space is no longer shown. Furthermore, only one neutron precursor group and two neutron energy groups are defined. Index $g = 1$ for fast group (high energy) and index $g = 2$ for thermal group (low energy)[2].

$$\begin{aligned}\frac{1}{v_1}\frac{\partial\phi_1}{\partial t} &= \nabla\cdot[D_1\nabla\phi_1] - (\Sigma_{1\to2} + \Sigma_{a,1})\,\phi_1 + (1-\boldsymbol{\beta})\,(\nu\Sigma_{f,1}\phi_1 + \nu\Sigma_{f,2}\phi_2) + \lambda C \\ \frac{1}{v_2}\frac{\partial\phi_2}{\partial t} &= \nabla\cdot[D_2\nabla\phi_2] + \Sigma_{1\to2}\phi_1 - \Sigma_{a,2}\phi_2\end{aligned} \tag{2.29}$$

$$\frac{\partial C}{\partial t} = \beta\nu\Sigma_{f,1}\phi_1 + \beta\nu\Sigma_{f,2}\phi_2 - \lambda C \tag{2.30}$$

2.2.3.1 Coarse Mesh Finite Difference (CMFD) method

Coarsh Mesh Finite Difference (CMFD) is used for spatial discretization of the diffusion equation. In its formulation the balance equation for each node is coupled with the neighboring nodes through the leakage terms. The interface current in node m and u-direction, $J^{m\pm}_{g,u}$, between any two nodes can be expressed in terms of the node average fluxes of the two facing nodes.

$$J^{m\pm}_{g,u} = \mp\widetilde{D}^{m\pm}_{g,u}\left(\phi^{m\pm l_u}_g - \phi^m_g\right) - \widehat{D}^{m\pm}_{g,u}\left(\phi^{m\pm l_u}_g - \phi^m_g\right) \tag{2.31}$$

Where one side of the interface is represented by the "+" sign and the other side by "-" sign. The meaning of other variables are

$J^{m\pm}_{g,u}$ is the interface current between any two nodes,

$\widetilde{D}^{m\pm}_{g,u}$ is the nodal coupling coefficient,

$\widehat{D}^{m\pm}_{g,u}$ is the corrective nodal coupling coefficient,

ϕ^m_g is the node average flux, and

$\phi^{m\pm l_u}_g$ is the average flux at the positive or negative interface side in the u-direction.

In Eq 2.31, the first term on the right hand side is the interface current predicted by the finite difference approximation. It is based on $\widetilde{D}^{m\pm}_{g,u}$ (nodal coupling coefficient) which is estimated using a first order *Finite Difference Method* (FDM) approximation and is given by Eq 2.32.

$$\widetilde{D}^{m\pm}_{g,u} = \frac{2D^{m\pm l_u}_g D^m_g}{D^{m\pm l_u}_g \Delta u_m + D^m_g \Delta u_{m\pm l_u}} \tag{2.32}$$

However, some error is introduced in the interface current because the CMFD method uses a coarse mesh (compared to FDM). Therefore, a correction is achieved using $\widehat{D}^{m\pm}_{g,u}$ (corrective nodal coupling coefficient). This parameter can be calculated using a nodal method, see Section 2.2.3.2 and Section 2.2.3.3. The correction coefficient forces the interface current obtained with Eq 2.31 to be the same as that obtained with the nodal method used (higher order).

[2]It is common to establish the energy boundary at 0.625 eV

The leakage term in the diffusion equation can be expressed in terms of the interface current using Fick's Law,

$$D_{g,u}^{m}\nabla^2\phi_g^m = -\nabla J_{g,u}^m \approx \frac{J_{g,u}^{m+} - J_{g,u}^{m-}}{h_u^m} = L_{g,u}^m \tag{2.33}$$

and using Eq 2.31, the leakage term can be expressed as

$$L_{g,u}^m = a_{g,u}^{m-}\phi_g^{m-l_u} + a_{g,u}^m\phi_g^m + a_{g,u}^{m+}\phi_g^{m+l_u} \tag{2.34}$$

where the coefficients a are function of $\widetilde{D}_{g,u}^{m\pm}$ and $\widehat{D}_{g,u}^{m\pm}$.

The result of introducing Eq 2.34 into the diffusion equation can be expressed using matrix notation. The resulting linear system is known as CMFD fixed source problem. This problem can be solved by a Krylov subspace method (iterative linear system solver), usually preconditioned for speed enhancement. A direct method can be used if the condition number is large.

2.2.3.2 Analytical Nodal Method (ANM)

The *Analytic Nodal Method* (ANM) is presented for a two-node problem in one dimension (x) (Downar et al. 2010). For other directions, the derivation is similar. The steady state version of Eq 2.27 in 1D can be expressed as follows,

$$-D_g\frac{d^2\phi_g(\boldsymbol{r})}{dx^2} + \Sigma_{rg}\phi_g(\boldsymbol{r}) - Q_g(\boldsymbol{r}) = -L_g(\boldsymbol{r}) \tag{2.35}$$

where Q_g is the source term and L_g is the leakage term.

The analytical solution of Eq 2.35 can be expressed as the sum of the homogeneous and the particular solution. Hereafter, only the main equations are presented. If the homogeneous solution is defined as $\phi_g^H(\boldsymbol{r})$, the homogeneous equation is given as follows.

$$\begin{bmatrix} -D_1\frac{d^2}{dx^2} + (\Sigma_{r1} - \lambda\nu\Sigma_{f,1}) & -\lambda\nu\Sigma_{f,2} \\ -\Sigma_{g'\to g} & -D_2\frac{d^2}{dx^2} + \Sigma_{r2} \end{bmatrix} \begin{bmatrix} \phi_1^H(\boldsymbol{r}) \\ \phi_2^H(\boldsymbol{r}) \end{bmatrix} = \begin{bmatrix} 0 \\ 0 \end{bmatrix} \tag{2.36}$$

The eigenvalues of the homogeneous equation are B_0^2 and B_1^2. The first eigenvalue, B_0^2, is referred as the *fundamental buckling* and determines the asymptotic flux shape being realized away from the boundaries of a node. The second eigenvalue, B_1^2, is referred as the *first harmonic buckling* and governs the boundary effects near the boundary. The homogeneous solution is

$$\begin{bmatrix} \phi_1^H(\boldsymbol{r}) \\ \phi_2^H(\boldsymbol{r}) \end{bmatrix} = \begin{bmatrix} q & s \\ 1 & 1 \end{bmatrix} \begin{bmatrix} a_{21}sn(\kappa x) + a_{22}cn(\kappa x) \\ a_{23}sn(\mu x) + a_{24}cn(\mu x) \end{bmatrix} \tag{2.37}$$

The particular solution is represented by $\phi_g^P(\boldsymbol{r})$. Two different solutions can be found, depending on the value of $\lambda \mathrm{k}_\infty$. Where $\lambda = 1/\mathrm{k_e ff}$ and k_∞ is the multiplication factor for an infinite system (with no leakage). If $\lambda \mathrm{k}_\infty = 1$, which is the same as $\mathrm{k}_\infty = \mathrm{k_{eff}}$, a nontrivial solution is obtained. This solution is referred as the critical node case. However, this is rarely encountered. Therefore, only the case with $\mathrm{k}_\infty \neq \mathrm{k_{eff}}$ is considered here. The particular solution is expressed as

$$\phi_g^P(\boldsymbol{r}) = c_{g,0} + \sum_{p=1}^{4} c_{g,p}f_p(\xi) \tag{2.38}$$

The final solution is the sum of Eq 2.37 and Eq 2.38.

$$\begin{gathered}\begin{bmatrix} \phi_1(\boldsymbol{r}) \\ \phi_2(\boldsymbol{r}) \end{bmatrix} = \begin{bmatrix} \phi_1^H(\boldsymbol{r}) + \phi_1^P(\boldsymbol{r}) \\ \phi_2^H(\boldsymbol{r}) + \phi_2^P(\boldsymbol{r}) \end{bmatrix} = \\ \begin{bmatrix} q & s \\ 1 & 1 \end{bmatrix} \begin{bmatrix} a_{21} sn(\kappa x) + a_{22} cn(\kappa x) \\ a_{23} sn(\mu x) + a_{24} cn(\mu x) \end{bmatrix} + \begin{bmatrix} c_{10} + c_{11} f_1(\xi) + c_{12} f_2(\xi) \\ c_{20} + c_{21} f_1(\xi) + c_{22} f_2(\xi) \end{bmatrix}\end{gathered} \tag{2.39}$$

This solution is valid for the two nodes considered. Nevertheless, there are four coefficients per node that must be determined. Thus, yielding to eight unknowns in total, these can be solved providing the following eight constrains: average flux per node and energy group (4), flux continuity per energy group and interface (2) and current continuity per energy group and interface (2). Imposing these constrains, the coefficients can be calculated and then, using Eq 2.39 the neutron flux for each energy group known. Using the Fick's law and the fluxes, the net nodal current at the interface of the two nodes (J_g^{nodal}) can be obtained. With it, the corrective nodal coupling coefficient can be calculated using next equation.

$$\widehat{D}_{g,u}^{m\pm} = -\frac{J_g^{nodal} + \widetilde{D}_{g,u}^{m\pm}\left(\phi_g^+ - \phi_g^-\right)}{\phi_g^+ - \phi_g^-} \tag{2.40}$$

The corrective nodal coupling coefficient can be used in the subsequent CMFD calculations. $\widehat{D}_{g,u}^{m\pm}$ forces the interface current obtained with CMFD to be the same as that obtained with the ANM, which is higher order in accuracy. However, it must be said that the ANM is unstable for cases where $k_\infty \approx k_{\text{eff}}$. For this case, the *Nodal Expansion Method* (NEM) method is more stable and preferred.

2.2.3.3 Nodal Expansion Method (NEM)

The NEM is used to solve the neutron diffusion equation (Downar et al. 2010). Here, the NEM formulation for the three-dimensional, cartesian geometry and multigroup solution of the neutron diffusion equation is presented. The steady state version of Eq 2.27 can be expressed as follows.

$$\nabla \cdot D_g \nabla \phi_g(\boldsymbol{r}) + \Sigma_{t,g}\phi_g(\boldsymbol{r}) = \sum_{g'=1}^{G} \Sigma_{s,g\to g'}\phi_{g'}(\boldsymbol{r}) + \frac{\chi_g}{k_{\text{eff}}} \sum_{g'=1}^{G} \nu\Sigma_{f,g'}\phi_{g'}(\boldsymbol{r}) \tag{2.41}$$

Where

ϕ_g is the neutron flux,

D_g is the diffusion coefficient,

$\Sigma_{s,g\to g'}$ is the total scattering cross section from group g to g',

$\nu\Sigma_{f,g'}$ is the fission cross section multiplied by the average neutrons produced per fission,

$\Sigma_{t,g}$ is the total cross section,

k_{eff} is the multiplication factor, and

χ_g is the spectrum for prompt and delayed neutrons.

By integrating equation Eq 2.41 over the three dimensions in a node m with homogenized properties, the following equation is obtained,

$$D_g^m \frac{\partial^2}{\partial x^2}\phi_g^m(\boldsymbol{r}) - D_g^m \frac{\partial^2}{\partial y^2}\phi_g^m(\boldsymbol{r}) - D_g^m \frac{\partial^2}{\partial z^2}\phi_g^m(\boldsymbol{r}) + A_g^m \phi_g^m(\boldsymbol{r}) = Q_g^m(\boldsymbol{r}) \tag{2.42}$$

Besides, the net neutron current in a given direction, x, can be calculated using Fick's Law,

$$j_{g,x}^{m}(\boldsymbol{r}) = -D_g^m \frac{\partial}{\partial x}\phi_g^m(\boldsymbol{r}) \tag{2.43}$$

The process followed to solve the multigroup diffusion equation using NEM is as follows.

1. First, the standard FDM approximation is solved in a outer-inner iteration strategy. The "two-node problem" is solved for each node interface in each direction using NEM every certain number of outer iterations, ΔN_{out}[3].

2. NEM provides an improved estimate of the net surface current for each interface. The improved net surface currents are used to update the diffusion coupling coefficients obtained by the FDM. The FDM continues the calculations with the updated diffusion coupling coefficients for other ΔN_{out} outer iterations.

3. Finally, the whole process is repeated again until a convergence criterion is satisfied.

To correct the surface current in the FDM, $\overline{J}_{g,x+}^{m,FDM}$, the following approach is used in interface $x+$ between nodes m and $m+1$.

$$\overline{J}_{g,x+}^{m,FDM} = -\frac{D_{g,x+}^{m,FDM}}{\frac{\Delta x^m + \Delta x^{m+1}}{2}}\left(\overline{\phi}_g^{m+1} - \overline{\phi}_g^{m}\right) - \frac{\widetilde{D}_{g,x+}^{m,NEM}}{\frac{\Delta x^m + \Delta x^{m+1}}{2}}\left(\overline{\phi}_g^{m+1} + \overline{\phi}_g^{m}\right) \tag{2.44}$$

The first term on the right hand side of Eq 2.44 is the normal FDM approximation for the surface current and $D_{g,x+}^{m,FDM}$ is the actual FDM diffusion coupling coefficient. The second term on the right hand side represents the NEM correction applied to the FDM approximation. This procedure forces this approximation to yield the higher-order new surface current predicted by NEM while satisfying the node balance equation. By extension, the NEM predictions of average nodal flux, $\overline{\phi}_g^m(\boldsymbol{r})$, and fundamental eigenvalue, k_{eff}, are also forced in the FDM approximation.

2.2.4 Cross section collapse and homogenization

Discrete values of cross sections and other neutronic parameters must be obtained to apply the multigroup approximation seen previously in the energy discretization. The process to obtain discrete values from a continuous energy distribution is called *collapse*. A flux integration is used to obtain collapsed cross sections and other neutronic parameters in the so-called broad energy group.

$$\Sigma_{\alpha,g} = \frac{\int_{E_g}^{E_{g-1}} \Sigma_\alpha(E)\phi(E)dE}{\int_{E_g}^{E_{g-1}} \phi(E)dE} \tag{2.45}$$

$$\phi_g = \int_{E_g}^{E_{g-1}} \phi(E)dE \tag{2.46}$$

Where α is a generic nuclear interaction and E_g and E_{g-1} are the energy boundaries belonging to the broad-energy group g.

Eq 2.45 obtains the collapsed cross section when the continuous cross section energy distribution is available. Nonetheless, sometimes it is useful to compute collapsed cross sections based on other set of collapsed cross sections (being the energy structure of available cross sections further discretized than the computed cross

[3] ΔN_{out} can be specified and optimized case-to-case.

section structure). A flux-weighted average is used to obtain broad-group cross sections based on other set of fine-group cross sections.

$$\Sigma^i_{\alpha,G} = \frac{\sum_{g\in G} \Sigma^i_{\alpha,g}\phi^i_g}{\sum_{g\in G} \phi^i_g} \tag{2.47}$$

Where $\Sigma^i_{\alpha,G}$ is the collapsed cross section for a generic nuclear interaction α belonging to region i. The collapse is done from all fine energy groups g belonging to the broad energy group G.

Core physics codes solve the diffusion equation with the multigroup approximation for a relatively coarse mesh (typically cells in the order of several centimeters) with homogenized cells (one material per cell). Nevertheless, the core in a nuclear reactor is composed by different materials arranged in fuel assemblies. Each fuel assembly contains from several dozens to few hundred fuel rods inside cladding material. The fuel-clad gap is filled with gas, the space among fuel rods is filled with moderator and each fuel assembly may contain burnable poison and structure materials. Moreover, fuel composition and pin layout may change among different fuel assemblies. Thus, a full core can be discretized in thousands of heterogeneous regions. The mathematical process employed to mix several heterogeneous regions -with different material properties- and replace them by an equivalent homogeneous region is called *homogenization theory*. A proper procedure to obtain homogenized cross sections is still under discussion nowadays. However, a simplification based on the collapsed cross sections and a volume-weighted average is widely used.

$$\hat{\Sigma}_{\alpha,G} = \frac{\sum_{i\in I} \Sigma^i_{\alpha,g} V^i \phi^i_G}{\sum_{i\in I} V^i \phi^i_G} \tag{2.48}$$

Where V^i is the volume for region i contained in the homogenized region I, thus the sum all V^i is the total homogenized volume, V^I. $\hat{\Sigma}_{\alpha,G}$ is the collapsed and homogenized cross section for a generic nuclear interaction α.

2.2.4.1 Homogenization theory

Once the different unit cells or pin cells are homogenized, the fuel assembly is now composed by an array of homogenized regions embedded in a water gap and probably with burnable poison, structure material and other dissimilar fuel assemblies. The next step in the homogenization process is to perform a multigroup transport calculation to obtain the pin-cell homogenized cross section and average fluxes that will allow the homogenization of the entire fuel assembly.

The entire fuel assembly homogenization is usually performed using reflective boundary conditions over the water gap center line. Thus, an infinite lattice of identical fuel assemblies is assumed. However, this is not true if the surrounding fuel assemblies have different homogenized properties, there is a control rod nearby or there is a net leakage out of or into the assembly. This common situations in a nuclear reactor must be handled in the global core calculation. Large errors are found using the conventional homogenization methods (compared to exact solutions). The biggest source of error is found in the treatment of the diffusion coefficient at the interfaces between homogenized regions. This error arises from the fact that the homogenized diffusion equation, with flux and current continuity imposed at interfaces, lacks sufficient degrees of freedom to preserve both reaction rates and surface currents. Thus, the flux in the boundary -or interface- between two fuel assemblies may be different at both interface sides, see Fig. 2.3. It is still possible to preserve -in the homogenized problem- the volume-integrated reaction rates and surface-integrated currents found in the heterogeneous problem. In a mathematical formulation, this is expressed as Eq 2.49 and Eq 2.50. To accomplish these formulas, the flux continuity at the interface x_{i+1} (between homogenized regions i and $i+1$) must be changed according to the flux interface condition expressed in Eq 2.51.

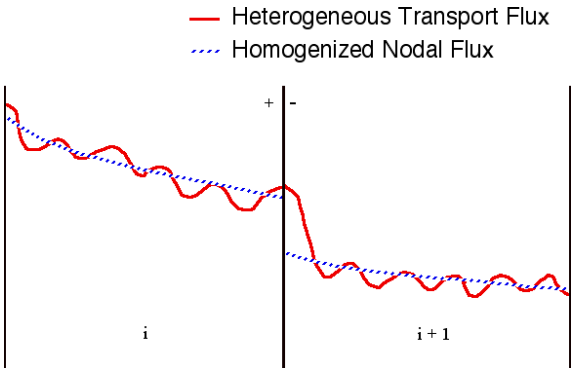

Fig. 2.3 – Homogeneous vs heterogeneous flux comparison in two adjacent fuel assemblies, extracted from DeHart 2005.

$$\int_{V_i} \hat{\Sigma}_{\alpha,g}(r)\hat{\phi}_g(r)dr = \int_{V_i} \Sigma_{\alpha,g}(r)\phi_g(r)dr \tag{2.49}$$

$$\int_{S_i^k} \hat{J}_g(r).dS = \int_{S_i^k} J_g(r).dS \tag{2.50}$$

Where the circumflex accent -or simply hat- over certain variable represents homogenized quantities. For example, homogenized cross section $\hat{\Sigma}_x^g$, homogenized flux $\hat{\phi}_g$ and homogenized current $\hat{J}_g$.

$$\hat{\phi}_i^+(r_{i+1})f_i^+(r_{i+1}) = \hat{\phi}_{i+1}^-(r_{i+1})f_{i+1}^-(r_{i+1}) \tag{2.51}$$

Where $\hat{\phi}_i^+(r_{i+1})$ and $\hat{\phi}_{i+1}^-(r_{i+1})$ are the homogenized flux within region i and $i+1$ respectively, but evaluated at the interface r_{i+1}. Similarly, $f_i^+(r_{i+1})$ and $f_{i+1}^-(r_{i+1})$ are the *flux discontinuity factors* within region i and $i+1$ respectively, but evaluated at the interface r_{i+1}. The flux discontinuity factors on each side of the interface can be expressed as the ratio of the heterogeneous to homogeneous flux at the interface.

$$f_i^+(r_{i+1}) = \frac{\phi_i^+(r_{i+1})}{\hat{\phi}_i^+(r_{i+1})} \quad f_{i+1}^-(r_{i+1}) = \frac{\phi_{i+1}^-(r_{i+1})}{\hat{\phi}_{i+1}^-(r_{i+1})} \tag{2.52}$$

One common definition for the homogenized diffusion coefficient is Eq 2.53. Its definition is not unique and other definitions are possible. The definition of the homogenized diffusion coefficient will modify the solution of the homogenized flux and, of course, the flux discontinuity factors.

$$\hat{D}_{ij}^g = \frac{\int_{r_i}^{r_{i+1}} \int_{y_i}^{y_{i+1}} D^g \phi^g dydx}{\int_{r_i}^{r_{i+1}} \int_{y_i}^{y_{i+1}} \phi^g dydx} \tag{2.53}$$

If the fuel assembly fulfills certain assumptions, the flux discontinuity factors can be calculated as the ratio of the surface integral of the heterogeneous assembly flux to the volume integral of the heterogeneous flux. The assumptions are 1) zero current symmetry boundary conditions and 2) uniform homogeneous flux distribution. Under these assumptions, the discontinuity factor is called *Assembly Discontinuity Factors* (ADFs) and is accurate only if the assembly net current is negligible over its boundaries. However, for scenarios where the leakage is significant, the calculated ADFs will be inaccurate.

One final comment over the homogenization process is needed. Once the heterogeneous transport calculation is done, both at pin-cell and fuel assembly level, the detailed flux distribution and homogenized cross sections are obtained. The homogenized cross sections can be used in a core physics code to solve the entire reactor core and obtain the global flux distribution (inter-assembly flux). However, at this point the flux detail at pin level (or intra-assembly flux) is lost due to fuel assembly region homogenization. Nonetheless, the intra-assembly flux can be recovered using the flux solution found in the heterogeneous transport calculation. This process is called *pin power reconstruction* or simply *flux reconstruction*.

2.2.5 Core depletion

While the reactor is in operation, the fuel is exposed to neutron flux. The subsequent nuclear interactions (such as fission or neutron absorption) change the fuel composition or isotopy, also known as transmutation or depletion. The fission products tend to be neutron-rich and decay by beta or neutron emission (they can also undergo neutron capture and be transmuted to heavier nuclides), the process is repeated until a stable isotope is formed. In general, while fuel is depleted the reactivity decreases because fissile nuclei are reduced and fission products are produced. However, at an early stage in the fuel cycle and depending on the initial composition, the transmutation-decay process produces more fissile nuclei than those that are consumed. These effect causes a positive reactivity effect and it is sustained until the concentration of transmuted fissile nuclei comes into equilibrium. The prediction of isotopic changes is importance in fuel managing and affects the reactor operation and its stability.

Fuel depletion depends only on spatial and temporal neutron flux distribution. Fortunately, neutron flux changes due to isotopic depletion occur relatively slow compared to other neutronic perturbations. Thus, the reactivity change introduced by depletion can be compensated with ease adjusting the control system. The depletion as a function of time for an homogeneous reactor fueled with a single isotope is easily obtained as follows. Eq 2.54 is simplified and the production term is not considered.

$$\frac{\partial N_F}{\partial t} = -N_F(\boldsymbol{r},t)\sigma_a^F\phi(\boldsymbol{r},t) \tag{2.54}$$

Where

N_F is the isotope concentration in fuel,

σ_a^F is the fuel absorption cross section, and

ϕ is the neutron flux.

If the neutron flux is known, the solution of above equation is

$$N_F(\boldsymbol{r},t) = N_F(\boldsymbol{r},0)\exp\left[-\sigma_a^F\int_o^t \phi(\boldsymbol{r},t')dt'\right] \tag{2.55}$$

where $N_F(\boldsymbol{r},0)$ is the isotopic concentration at initial time. Nonetheless, if the flux is not known, an approach must be taken to solve the flux integration. Two main approaches are used:

(a) Constant flux.

$$\phi(\boldsymbol{r},t) = \phi_0(\boldsymbol{r}) \tag{2.56}$$

Using this approach, Eq 2.55 can be expressed as

$$N_F(\boldsymbol{r},t) = N_F(\boldsymbol{r},0)e^{-\sigma_a^F\phi_0(\boldsymbol{r})t} \tag{2.57}$$

(b) Constant power.

$$P(\boldsymbol{r},t) = w_a N_F(\boldsymbol{r},t)\sigma_a^F \phi(\boldsymbol{r},t) = P_0(\boldsymbol{r}) \tag{2.58}$$

Where w_a is the energy released by neutron absorbed in fuel. Using constant power, Eq 2.55 can be expressed as

$$N_F(\boldsymbol{r},t) = N_F(\boldsymbol{r},0) - \frac{P_0(\boldsymbol{r})}{w_a}t \tag{2.59}$$

The predictions are different using flux or power constant approach. However, for relatively short depletion times, the predictions are in agreement and Eq 2.55 can be used on each depletion step to predict depletion changes.

Fuel depletion changes the reactivity and the multiplication factor in time. Thus, in order to keep the reactor with the desired power, the operator must adjust the control system to counteract the reactivity variation. This is accomplished via control rod movements and/or introducing a burnable poison. Different isotopes coexist in a real reactor (up to a few hundred) and the general depletion model can be expressed as a balance of nucleus A.

$$\frac{dN_A}{dt} = -\lambda_A N_A - \left[\sum_g \sigma_{a,g}^A \phi_g\right] N_A + \lambda_B N_B + \left[\sum_g \sigma_{\gamma,g}^C \phi_g\right] N_C \tag{2.60}$$

Where

$\lambda_A N_A$ is the loss of A due its radioactive decay,

$\left[\sum_g \sigma_{a,g}^A \phi_g\right] N_A$ is the loss of A due to neutron capture,

$\lambda_B N_B$ is the gain of A due to decay of B, and

$\left[\sum_g \sigma_{\gamma,g}^C \phi_g\right] N_C$ is the gain of A due to transmutation of C via neutron capture.

The above equation must be written for each isotope of interest in the reactor (heavy nuclides and fission products). In a real analysis with enough depletion accuracy, more than 200 nuclides must be taken into account. If isotopic accuracy is not essential, some simplifications can be introduced: (i) deplete only nuclides with high absorption cross section or high fission yield (especially fission products ^{135}Xe and ^{149}Sm, see Section 2.2.6.4), (ii) lump similar nuclides together, and (iii) omit nuclides with short half-lives. In addition, due to its fast depletion, burnable absorber poisons must be tracked accurately. All depletion equations (one per isotope) can be lumped in one expression using matrix notation,

$$\frac{dN}{dt} = A(\phi(t))N(t) + F(\phi(t)) \tag{2.61}$$

To solve the above equation it is common to decouple the depletion and neutron flux calculations. Suppose the isotopic concentration is known at initial reactor time. Thus, the macroscopic cross sections can be generated, and then, the neutron flux calculated solving the transport or diffusion equation. Using the predicted flux, the depletion equation, Eq 2.61, is solved for a short time (or depletion step) to obtain a new isotopic concentration. To solve the depletion equation, either constant flux or power must be assumed. The solution assuming constant flux is

$$N(t+\Delta t) = e^{A(t)\Delta t}N(t) + A(t)^{-1}\left[e^{A(t)\Delta t} - 1\right]F(t) \tag{2.62}$$

With it, the cross sections are updated using the isotopic concentration at the end of current depletion step. At this point, the control system must be adjusted to compensate the change in reactivity due to isotopic

variations. Then, the iterative process starts all over again and a new flux distribution is predicted to be used in the next depletion step.

2.2.6 Reactivity Control

When a nuclear reactor is loaded, the amount of fuel used initially is larger than the amount of fuel that would be required for just criticality. This excess reactivity allows the operator to overcome the multiplication factor drop that is produced during core operation due to fuel burn-up, fission product production and reactivity feedback produced by temperature or density changes. Obviously, to compensate the excess reactivity, it is necessary to introduce some form of negative reactivity that the operator is capable to control at will. This allows the operator to gradually control the excess reactivity, adjust the power level according to the load demands and/or shut down the reactor. In most modern nuclear reactors, the negative reactivity is inserted using a strong neutron absorber.

Before explaining the different mechanisms of reactivity control, some definitions are provided next.

- *Excess reactivity* (ρ_{ex}) is the core reactivity with all control elements removed. It is function of time (burn-up changes isotopy) and temperature (reactivity feedback).
- *Shutdown margin* (ρ_{sm}) is the negative core reactivity with all control elements inserted. It is function of time and temperature. The reactivity control system design is such that the shutdown margin is below criticality even if one control rod is stuck and is not inserted.
- *Total control element worth* ($\Delta\rho$) is the difference between excess reactivity and shutdown margin, $\Delta\rho = \rho_{ex} + \rho_{sm}$, where ρ_{sm} should be always negative.
- *Control element worth* ($\Delta\rho_i$) is the reactivity worth of an individual control element or the reactivity change when this element is fully inserted.

Three different mechanisms can be found in a nuclear reactor to modify the reactivity at will. It must be said that control rods -as well as soluble poisons- are used to overcome small changes in reactivity. For large reactivity excursions, burnable poisons (absorbers) are used.

2.2.6.1 Control rods

Control rods can be inserted or withdrawn according to the operator criterion. Control rods belonging to the same bank are moved together. In PWR most control rods are approximately made of 80% Ag, 15% In and 5% Cd, they are cylindrical in shape and are inserted through the upper plenum. Control rods are inserted through guide tubes (without fuel). For BWR the control rods are typically made of B_4C and the control rods are inserted through the lower plenum. They have cruciform shape and are inserted between fuel assemblies. Control rod position greatly affects the core power profile.

It must be ensured that the power density does not exceed its limits due to thermal considerations, radiation damage, uniform burn-up and isotopic distribution among others. Fuel lifetime can be extended if a uniform fuel depletion is provided. If the flux distribution or power shape are changed accordingly, it is possible to partially control the depletion

To compensate the initial excess reactivity in the core, when the reactor starts a new fuel cycle, a big extension of control rods must be inserted to achieve criticality. Imagine a PWR, where the control rods are inserted through the top region. The upper core region (with control material) will experience a reduction

in relative flux (and local power). As a result, the lower region will experience a power peak. As the reactor cycle proceeds, the fuel in the lower region (high relative power) will be depleted faster and the power peak will decrease. Then, the control rods will be slowly withdrawn and the peak will be shifted upwards to compensate the reduction in reactivity. The objective at the end of fuel lifetime is to obtain a uniform and complete depletion along the fuel assembly.

The same idea is applied to the BWR, however, due to the high coolant density in the lower core region -void is formed in the upper region- the control rods are inserted through the lower plenum. This compensates the power peak generated in the lower region as a result of the negative void reactivity coefficient. A more uniform flux profile is achieved.

2.2.6.2 Burnable poisons

When the core is loaded, some fuel pins are replaced by burnable absorber pins, such as gadolinium or boron. Mainly used in BWR, but also in PWR. Strong absorbers are chosen such that their absorption cross section is initially high but -because of material burn-up- decrease with time. They are depleted faster than the fuel material; thus, their negative reactivity contribution is negligible at the end of the assembly lifetime. This contributes to match the excess of fuel reactivity as it decreases with time. With the use of burnable poisons the fuel inventory can be greatly increased. Another advantage is that it does not have mechanical parts.

2.2.6.3 Chemical shim or soluble poisons

Small amounts of boric acid -up to 2500 ppm- are dissolved in the coolant and used as neutron poison. It provides a very uniform poison distribution over the whole reactor and its injection can be accurately adjusted. However, the disadvantage for this control mechanism is that the rate at witch it can be injected or removed is quite small. Thus, it is only used to compensate slow reactivity changes, such as fuel burn-up, fission product poisoning[4] and moderator temperature changes. The main advantage is that it reduced greatly the dependence on control rods. It is used mainly in PWR, although it is also used in modern BWR in emergency situations.

The chemical shim concentration is limited by the void coefficient. Typically, a LWR has a negative void coefficient (increase in void fraction leads to a reduction of moderation and power). However, when chemical shim is used, a decrease in coolant density will also lead to a decrease in poison concentration and therefore power could increase (positive reactivity effect). Thus, the concentration is limited to a negative void coefficient value, which provides a safe reactor behavior.

2.2.6.4 Fission product poisoning

Fission products and its decay products absorb neutrons that otherwise would produce more fissions, thus they are called *parasitic absorbers*. They reduce the reactivity and therefore the neutron multiplication factor. The most important parasitic absorbers for thermal reactors are ^{135}Xe and ^{149}Sm, being the effect of xenon poison much more significant than that of the samarium. Since their absorption cross sections decrease rapidly with increasing neutron energy (see Fig. 2.4), their effect is negligible for fast nuclear reactors.

The ^{135}Xe is the fission product with more significant influence on nuclear reactor operation. As seen in Fig. 2.5, the decay chain of ^{135}Te (Tellurium) is the main production form of ^{135}Xe (through the decay of ^{135}I). However, it can also be produced directly by fission. Almost 95% of ^{135}Xe produced in the reactor

[4]The main poison products produced by fission are ^{135}Xe and ^{149}Sm, see Section 2.2.6.4.

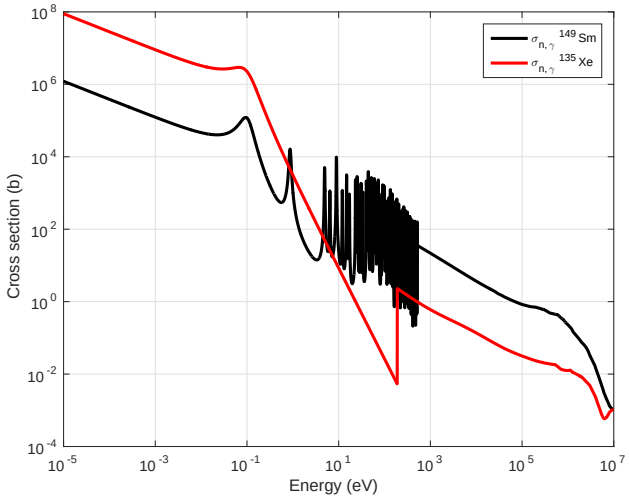

Fig. 2.4 – Microscopic radiative capture cross section for ^{149}Sm and ^{135}Xe.

$$\text{Fission} \Rightarrow {}^{135}_{51}\text{Sb} \xrightarrow[0.8\text{sec}]{\beta^-} {}^{135}_{52}\text{Te} \xrightarrow[19\text{sec}]{\beta^-} {}^{135}_{53}\text{I} \xrightarrow[6.57\text{h}]{\beta^-} {}^{135}_{54}\text{Xe} \xrightarrow[9.1\text{h}]{\beta^-} {}^{135}_{55}\text{Cs} \xrightarrow[2.3\times10^6\ \text{yr}]{\beta^-} {}^{135}_{56}\text{Ba (stable)}$$
$$\Uparrow \text{Fission} \qquad \Uparrow \text{Fission} \qquad \Uparrow \text{Fission}$$

Fig. 2.5 – Production and removal of ^{135}Xe, extracted from Jevremovic 2009.

$$\text{Fission} \Rightarrow {}^{149}_{60}\text{Nd} \xrightarrow[1.72\text{h}]{\beta^-} {}^{149}_{61}\text{Pm} \xrightarrow[53.1\text{h}]{\beta^-} {}^{149}_{62}\text{Sm (stable)}$$

Fig. 2.6 – Production of ^{149}Sm, extracted from Jevremovic 2009.

comes from decay of ^{135}I.

Reactivity decrease produced by ^{135}Xe is negligible for low flux levels. Then, with increasing flux, the reactivity decreases up to a certain flux level where isotopes concentration reach an equilibrium point and the reactivity does not decrease any more. When the reactor is shot down, the flux can be considered zero. Thus, ^{135}Xe is no longer produced by fission or removed by absorption, the only production and removal mechanism are the decay of ^{135}I and ^{135}Xe respectively. Xenon buildup can be minimized using gradual shutdown (instead of rapid SCRAM) to burn some xenon while shutting down.

The effect of ^{149}Sm poison is much different, see Fig. 2.6. It is produced by decay chain of ^{149}Nd (which is a fission fragment) and ^{149}Pm. However, ^{149}Sm is a stable isotope and is only removed by neutron radiative capture. After reactor shutdown, ^{149}Sm concentration increases and reaches an equilibrium in 20 days.

2.3 Transient and accident analysis

Before a nuclear power plant license is issued, the response of postulated disturbances to processes or equipment malfunction must be analyzed. These are called initiating events and are listed in US-NRC et al. 2007, chap. 15 by the NRC. In order to obtain the license, the designer must provide proves that the

plant will withstand these disturbances and malfunctions. A proper discussion for different transients and postulated accidents is required by the nuclear regulatory body. The discussion must consider a wide range of initiating events that must be categorized according to the type and frequency, additionally, an acceptance criteria must be provided. According to the frequency of occurrence, a particular initiating event can be classified as *Anticipated Operational Occurrence* (AOO), with small frequency, or accident. Some accidents receive the consideration of *Design Basis Accident* (DBA), these are of special interest for the license issue. For the sake of understanding, some descriptions follow.

Initiating event is an identified event that can lead to AOOs or accident conditions (either postulated or not) that challenges safety functions. Initiating events can be identified using deterministic or probabilistic analysis. Deterministic analysis are largely based on experience and assumptions, while probabilistic analysis are based on fault trees (top-down) and event trees (bottom-up).

Anticipated Operational Occurrences (AOOs). According to the NRC, the AOOs are conditions of normal operation that are expected to occur one or more times during the life of the nuclear reactor. They are also known as condition II (events expected to occur several times in the plant's lifetime) and condition III (events that may occur in the plant's lifetime). Some examples of AOOs are listed.

- Inadvertent control rod withdrawal.
- Inadvertent moderator cooldown.
- Inadvertent chemical shim dilution, only PWRs.
- Loss of normal feedwater.
- Control rod drop, only PWRs.
- Single failure of a control component.
- Minor reactor coolant system leak.
- Loss of off-site power
- Loss of feedwater heating.
- Trip of one or more recirculation pumps, only BWRs.

Postulated accidents. These are identified conditions that are not expected to occur during the life of the nuclear reactor. They are also known as condition IV events. Some examples of postulated accident are listed.

- Major rupture of a pipe containing reactor coolant, also known as *Lose Of Coolant Accident* (LOCA).
- Ejection of a control rod, only PWRs.
- Control rod drop accident, only BWRs.
- Major secondary system pipe break.
- Single reactor coolant pump rotor locked, only PWRs.
- Seizure of one recirculation pump, only BWRs.
- Anticipated Transients Without Scram (ATWS).
- Long-Term Station Blackout (LTSBO)

Design Basis Accident (DBA). According to the NRC, a DBA is a postulated accident that a nuclear facility must be designed and built to withstand without loss to the systems, structures, and components necessary to ensure public health and safety.

2.3.1 Design basis accidents

DBAs are classified according to the seven following categories, but additional categories can be considered if the designer needs to (e.g. new reactor designs). The forth type listed is of special interest for this thesis and is further developed in Section 2.3.3.

1. Increase in heat removal by the secondary system
2. Decrease in heat removal by the secondary system
3. Decrease in the *Reactor Coolant System* (RCS) flow rate
4. Reactivity and power distribution anomalies
5. Increase in reactor coolant inventory
6. Decrease in reactor coolant inventory
7. Radioactive release from a subsystem or component

An additional category is worth to mention, *Anticipated Transients Without Scram* (ATWS). This postulated accident is the combination of a frequent initiating event with the failure of the shutdown system. Even though ATWS are considered beyond-DBAs, the evolution of the plant in front of an ATWS (physic and thermohydraulic phenomena) must be evaluated. Thus, ATWS events must be analyzed as a category of postulated accidents. In addition, some DBAs are added even if they have a very low probability. These can be internal (operator error, sabotage...) or external (explosion nearby, terrorism...) and are site-dependent.

The plant designer must, first, prevent DBA, and then provide protection and mitigation (reduce its effects) against them. The nuclear regulatory body reviews all relevant DBAs for a specific nuclear plant before the license is issued. The designer must provide a description of the initiating events that can lead to each type of accident. The discussion includes the codes used for the safety analysis along with the models, simplifications, initial conditions and parameters... Conservative values must be used and the degree of conservatism must be discussed. If coupled codes are employed, then the discussion must include information of the coupling procedure. The results of most important variables (including the dose) must be included for each analysis along with the margins between the prediction and the established limits. For example, the following information must be tabulated for the DBAs consisting in a control rod ejection and control rod drop accident.

1. Percentage of fuel rods undergoing clad failure.
2. Radial peaking factors for rods undergoing clad failure.
3. Percent of fuel reaching or exceeding melting temperature.
4. Peaking factors for fuel reaching or exceeding melting temperature.
5. Percent of core fission products assumed released into reactor coolant.
6. Parameters used to determine activity release through the secondary system (PWRs only).
7. Parameters used to determine activity release through the containment.
8. Parameters used to determine activity release through the condenser leak paths (BWRs only).

2.3.2 Initiating events

According to the frequency of occurrence, initiating events can be classified as AOOs or as postulated accidents. Detailed information for AOOs and postulated accidents can be found in US-NRC et al. 2007 where specific acceptance criteria are presented. These are based on meeting specific *General Design Criterias* (GDCs) (Department of Energy 1983). A short list of some initiating events considered by the NRC is presented in Table 2.6.

For AOOs, three requirements are presented by the regulatory body (NRC) to meet the GDC. In relation to the third requirement, the NRC also recognizes that a condition II or III event, by itself, could not lead to a superior (more severe) condition event.

1. Pressure in the reactor coolant and main steam systems should be maintained below 110 percent of the design values in accordance with the American Society of Mechanical Engineers (ASME) Boiler and Pressure Vessel Code.

2. Fuel cladding integrity shall be maintained by ensuring that the minimum *Departure from Nucleate Boiling Ratio* (DNBR)[5] remains above the 95/95 DNBR limit for PWRs and that the *Critical Power Ratio* (CPR) remains above the *Minimum Critical Power Ratio* (MCPR)[6] safety limit for BWRs.

3. An AOO should not generate a postulated accident without other faults occurring independently or result in a consequential loss of function of the RCS or reactor containment barriers.

Regarding postulated accidents, four different requirements are presented to meet the GDC. Contrary to the AOOs, the postulated accidents could produce enough damage to shutdown the reactor and stop the power production.

1. Pressure in the RCS and main steam system should be maintained below acceptable design limits, considering potential brittle as well as ductile failures.

2. Fuel cladding integrity will be maintained if the minimum DNBR remains above the 95/95 DNBR limit for PWRs and the CPR remains above the MCPR safety limit for BWRs. If the minimum DNBR or MCPR does not meet these limits, then the fuel is assumed to have failed.

3. The release of radioactive material shall not result in off-site doses in excess of the guidelines of 10 CFR Part 100.

4. A postulated accident shall not, by itself, cause a consequential loss of required functions of systems needed to cope with the fault, including those of the RCS and the reactor containment system.

In Table 2.6, the required GDCs for some accidents are shown. Besides, a description list for these GDCs is presented hereafter.

– GDC 10: the reactor coolant system must be design with appropriate margins so specified acceptable fuel design limits are not exceeded during normal operations, including AOOs.

[5] The ratio of the heat flux needed to cause departure from nucleate boiling -or *Critical Heat Flux* (CHF)- to the actual local heat flux of a fuel rod. The nucleate boiling regime must be avoided in a nuclear reactor, it is characterized by big bubbles created on the clad surface. This phenomenon reduces considerably the clad-coolant heat transfer coefficient and challenge the fuel integrity.

[6] The smallest CPR that exists in the core. The CPR is the power in the assembly that will cause some point in the assembly to experience boiling transition, divided by the actual assembly operating power.

- GDC 13: availability of instrumentation to monitor variables and systems over their anticipated ranges to assure adequate safety plus appropriate controls to maintain these variables and systems within prescribed operating ranges.
- GDC 14: it ensures an extremely low probability of failure of the coolant pressure boundary.
- GDC 15: the design of the reactor coolant system and its auxiliaries with appropriate margin so the pressure boundary is not breached during normal operations, including AOOs.
- GDC 16: it ensures that containment design conditions important to safety are not exceeded as a result of postulated accidents.
- GDC 17: related with onsite and offsite electric power systems so safety-related structures, systems, and components function during normal operation, including AOOs.
- GDC 20: requires that the protection system initiate automatically appropriate systems to assure that specified acceptable fuel design limits are not exceeded as a result of AOOs.
- GDC 25: requires that the reactor protection system be designed to assure that specified acceptable fuel design limits are not exceeded for any single malfunction of the reactivity control systems, such as accidental withdrawal (not ejection or dropout) of control rods.
- GDC 26: the control of reactivity changes must provide acceptable fuel design limits that must not been exceeded during AOOs.
- GDC 27 and GDC 28: the reactor coolant system must be designed with appropriate margin to ensure that acceptable fuel design limits are not exceeded and that the capability to cool the core is maintained.
- GDC 31: the reactor coolant system must be designed with sufficient margin to ensure that the boundary behaves in a nonbrittle manner and that the probability of propagating fracture is minimized.
- GDC 35: it ensures that fuel and clad damage, should it occur, must not interfere with continued effective core cooling, and that clad metal-water reactor must be limited to negligible amounts.
- GDC 38: containment pressure and temperature must be maintained at acceptably low levels following any accident that deposits reactor coolant in the containment.
- GDC 50: the containment must not exceed the design leakage rate when subjected to the calculated pressure and temperature conditions resulting from any accident that deposits reactor coolant in the containment.
- GDC 60: the radioactive waste management systems must be designed to control releases of radioactive materials to the environment.

2.3.3 Reactivity initiated accident

A *Reactivity Initiated Accident* (RIA) is an accident in a nuclear reactor where the reactivity (and thus fission rate and power) is increased unintentionally. As a consequence some fuel rods may fail, or if the energy deposited -or enthalpy increase- on the core is high enough, it could lead (for severe accidents) to a core disruption. Some scenarios involving a RIA are classified as DBA. Thus, for licensing purposes, it must be proved that the reactor can withstand these scenarios without a significant fuel damage. The reactor is protected against RIA by means of the control safety system, but also by the negative feedback mechanism.

Section	Title	GDC															
		10	12	13	14	15	16	17	20	25	26	27	28	35	38	50	60
15.1.5	Steam System Piping Failures Inside and Outside of Containment (PWR)			✓				✓				✓	✓	✓			
15.2.1-5	Loss of External Load; Turbine Trip; Loss of Condenser Vacuum; Closure of Main Steam Isolation Valve (BWR); and Steam Pressure Regulator Failure (Closed)	✓		✓		✓		✓			✓						
15.2.6	Loss of Nonemergency AC Power to the Station Auxiliaries	✓		✓		✓					✓						
15.3.1-2	Loss of Forced Reactor Coolant Flow Including Trip of Pump Motor and Flow Controller Malfunctions	✓		✓		✓		✓	✓		✓						
15.4.1	Uncontrolled Control Rod Assembly Withdrawal From a Subcritical or Low Power Startup Condition	✓		✓				✓	✓	✓							
15.4.2	Uncontrolled Control Rod Assembly Withdrawal at Power	✓		✓				✓	✓	✓							
15.4.6	Inadvertent Decrease in Boron Concentration in the Reactor Coolant System (PWR)	✓		✓		✓					✓						
15.4.7	Inadvertent Loading and Operation of a Fuel Assembly in an Improper Position			✓													
15.6.1	Inadvertent Opening of a PWR Pressurizer Pressure Relief Valve or a BWR Pressure Relief Valve	✓		✓		✓					✓						
15.7.3	Postulated Radioactive Releases Due to Liquid-Containing Tank Failures																✓
15.8	Anticipated Transients without Scram		✓		✓		✓							✓	✓	✓	
15.9	Boiling Water Reactor Stability	✓	✓	✓					✓								

Table 2.6 – Acceptance criteria for transient and accident analyses.

The negative reactivity coefficients limit the power peak produced by the RIA and provide enough time to the control safety system to actuate and shutdown the reactor if needed.

If a fuel rod fails, fission products could be released to the coolant (into the vessel). If the failure is severe, a fuel pellet could be disrupted and some high-temperature fragments could come into contact with the coolant with the consequent steam generation and pressure pulse, this could damage other nearby rods, assemblies, or even the reactor vessel. The damage produced is proportional to the specific enthalpy increase, thus the regulatory acceptance criteria for a RIA are formulated in terms of this variable.

RIA scenarios could be broadly classified in four categories. An extensive classification of accidents and occurrences can be found in US-NRC et al. 2007, chap. 15.

(a) Control system failure is produced when a control rod is unintentionally withdrawn by a control system failure. However, the control system limits the worth for control rods and does not allow rod insertion beyond the *Reactivity Insertion Limit* (RIL). Thus, if a control rod is inadvertently withdrawn, the added positive reactivity will be manageable. This event is not classified as accident, but rather as transient.

(b) Control rod ejection can occur due to a failure of the control rod drive mechanism or its housing. In this case the rod is ejected in a fraction of a second and the addition of reactivity is much faster compared to the previous scenario. *Rod Ejection Accident* (REA) is considered a DBA in LWR[7] and therefore, it is classified as a postulated accident with low probability occurrence. Safety limits are placed for a proper reactor operation. REA are classified according to the reactor type. Lots of studies can be found related to REA accident analysis. For example, Barrachina et al. 2009 study the influence of different control rod configuration and Miró et al. 2006a study the REA accident using two different core physics codes in a PWR and BWR.

   – Control rod ejection (REA) for PWR. During normal operation conditions only one bank of control rods is inserted in the core (control rods are inserted through the upper plenum). Moreover, this bank is only partially inserted and therefore, the amount of reactivity added in a RIA is limited. However, with low-power operation conditions more banks are allowed to be inserted -also further inserted-. Thus, the worst possible scenario in a PWR, regarding reactivity insertion and fuel damage, is a *Hot Zero Power* (HZP)[8] condition. The rod could be ejected in 0.1 seconds in the worst scenario.

   – Control rod drop or *Rod Drop Accident* (RDA) for BWR. Control rods in BWR are inserted through the lower plenum. In a RDA the withdrawal is driven by gravity. The coolant pressure (in contrast to REA) does not influence the withdrawal rate[9] (which is slower compared to REA). Due to this fact, and due to a coarser core lattice in BWR, the power excursion is slower in RDAs. The power increase is compensated mainly by the negative fuel temperature (Doppler) reactivity coefficient. The negative void fraction coefficient (due to steam formation) also helps mitigating the power excursion. However, the moderator (void and temperature) feedback is slower than Doppler feedback. This is due to the fact that some time is needed to transfer the heat through the pellet (where it is generated), gap, clad and finally into the coolant. The worst scenario for

[7] In heavy water reactors, such as CANDU, REA are excluded from DBA. In CANDU reactors the control rods -called shutoff rods- are not used to control reactivity but for safe shutdown the reactor. Reactivity control is accomplished by means of on-power refueling and by water level controlled by the light water system

[8] This condition arise after a SCRAM (all control rods are suddenly inserted for an emergency shutdown). The reactor is working at nominal temperature and pressure, however, no fission rate and nearly no power is produced (only decay heat).

[9] Unless the pressure barrier is broken.

a RDA is in *Cold Zero Power* (CZP)[10] condition. Massih and Jernkvist 2010 study the power pulse characteristics for PWRs and BWRs for different operation conditions.

Control rod worth depends mainly on four variables (rod position in the reactor, insertion depth, core axial profile and burn-up distribution). A control rod ejection in a high-burn-up zone produces lower reactivity addition than a rod ejected in a low-burn-up zone. The maximum power obtained in the power peak and the local specific enthalpy is also dependent on the rod position and burn-up distribution (Massih and Jernkvist 2010).

(c) Moderator temperature or density (void) change. A drop in coolant temperature or void leads to a reactivity increase (for example with a loss of feedwater heating). The reactivity addition in these events is slow and thus, they are classified as transients rather than accidents.

(d) Dilution or removal of chemical shim. The negative feedback effect of borated coolant is lost if new unborated coolant is injected, for example after the *Emergency Core Cooling System* (ECCS) is activated. Moreover, a malfunction of the *Chemical Volume Control System* (CVCS) could also lead to an unintentional reactivity addition.

[10] This condition is characterized by a strongly subcooled coolant (perhaps due to a loss of feedwater heating) and nearly no power production (only decay heat).

Chapter 3

Tools

. . . the basis for this thesis.

Phenomena occurring in the core of a nuclear reactor are rather complicated. They involve two main fields in engineering: thermohydraulics and neutronics. It is often the case where phenomena interact with both fields (feedback), thus, they must be studied together. Historically, these fields are represented separately using different computational codes. However, the tendency in the last decade -and still growing today- is to couple computational codes and merge different fields. This tendency is not limited to thermohydraulic-neutronic codes, but also thermo-mechanical, radiation transport, computational fluid dynamics codes. . . and all kind of nuclear applications.

3.1 Codes

Due to its complexity, three main codes are needed to perform a complete 3D core simulation. A forth type of code can be added if *Uncertainty and Sensitivity* (U&S) analysis is desired.

1. Lattice physics codes. These codes have the capability for depletion and thus, it is possible to generate homogenized and collapsed cross sections and neutronic parameters. Lattice physics codes with depletion capabilities are used to simulate a small -but detailed- zone of the core, usually a fuel assembly either in 2D or 3D. These codes are based on Boltzmann equation.

2. Thermohydraulic system codes. They discretize the coupled balance equations, usually in 1D, to obtain the main thermohydraulic variables. One important limitation for most of the thermohydraulic codes is that they neglect turbulent phenomena.

3. Core physics codes. Also known as neutron kinetic codes or core simulators, they solve the diffusion equation with the multigroup approximation to speed up calculations and simulate the whole core. They use the homogenized and collapsed cross sections obtained by a lattice physics code.

4. Uncertainty propagation code. They perform *Uncertainty Quantification* (UQ), the uncertainty can be introduced either by cross section data, user uncertainty via input decks, numerical methods employed, empirical correlations, model approximations, geometry. . . Usually they also perform *Sensitivity Analysis* (SA).

Cross section generation codes can be used alone, but, as explained before, it is often the case that thermohydraulic and neutronic codes are coupled. Hereafter, the main available codes are discussed. Strong emphasis is made in the codes used in this thesis. The list, by no means, pretend to be exhaustive; more codes are available, but these are the most validated and intentionally known.

3.1.1 Lattice physics codes

Deterministic lattice physics codes use transport methods, such as the *Collision Probability*, *Method Of Characteristics* or the *Discrete Ordinates*, usually in 2D. These codes are often used to simulate a small reactor zone with varying degrees of detail. If available, the options for problem-dependent cross section generation are multiple. Cross sections can be represented either as tabulated data or as the sum of a base and partial cross section effect. The base cross section, takes into account the burn-up dependence or reactor history[1], while the partial cross section accounts for feedback parameters[2] -or instantaneous variables-, see Section 3.3. Cross sections are generated using the so-called branches calculations, where feedback parameters are changed one at a time. One important feature is the collapse and homogenization of problem-dependent cross sections for further use in a core physics code, see Section 2.2.4. In contrast of deterministic lattice physics codes, Monte Carlo lattice physics codes use stochastic methods to achieve the same purpose, usually in 3D. Examples of Monte Carlo codes with lattice capabilities include SERPENT or MCNP6.

3.1.1.1 CASMO

CASMO is a multigroup 2D deterministic lattice code with burn-up capability for PWR and BWR assemblies. It is developed at Studsvik Scandpower. It handles simple geometry of fuel pins of different composition, only in a square pitch array. Among the modeling capabilities, CASMO is able to simulate burnable absorber rods, cluster control rods (PWR), cruciform control rods (BWR), water gaps, in-core instrument channels...

Fig. 3.1 shows the main flow diagram for CASMO calculations. First, macroscopic cross sections (with 70 or 40 energy groups) are prepared for further calculations. Absorption and fission cross sections are corrected in the resonance regions to account for the fuel self-shielding. Then, the effective cross sections are used into collision probability calculations for micro group calculations. The micro group calculation is repeated for each pin type (including poison rods and water holes) and the obtained flux spectra is used for energy collapse. Next, a 2D macro group calculation is made (40 energy groups), the flux spectra obtained is used for cross section collapse (into 7 energy groups). The collapsed cross sections are used for the 2D transport calculation.

The master neutron data library is based on a *Evaluated Nuclear Data File* (ENDF). It contains cross sections for 108 materials, including individual nuclides, natural compositions and mixtures of elements. This library is tabulated in 70 energy groups -43 thermal groups (0.005 to 9.877 eV), 13 resonance groups (up to 15.03 eV), and 14 fast groups (up to 10 MeV)-. Its data is tabulated for different temperatures and contains absorption, fission, nu-fission, transport and scattering cross sections. An other cross section library can be used for PWR and BWR and it has 25 thermal groups, 7 resonance groups, and 8 fast groups (with the same energy boundaries).

CASMO is entirely written in FORTRAN-77. The main advantage is that it has a simple user oriented input and its computational time is affordable. An important drawback of CASMO is that it is not able to simulate pins with hexagonal geometry (that excludes VVER[3] calculations) or with triangular pitch. Moreover, the code is a black box. Thus, it does not give freedom to the user to define geometry or assign compositions. Another issue concerns the cross section library accuracy, it could be improved if a newer *Nuclear Data*

[1] It refers to the variations in thermohydraulic conditions, composition and exposure that experienced the reactor since the fresh fuel was introduced.

[2] These account for moderator temperature, moderator density, fuel temperature and boron concentration instantaneous change. Cross sections always change according to the reactor history.

[3] *Water-Water Energetic Reactor* (VVER) is a reactor originally developed in the Soviet Union, and now Russia, similar to PWR. Its main characteristic is that the bundles follow a hexagonal pattern.

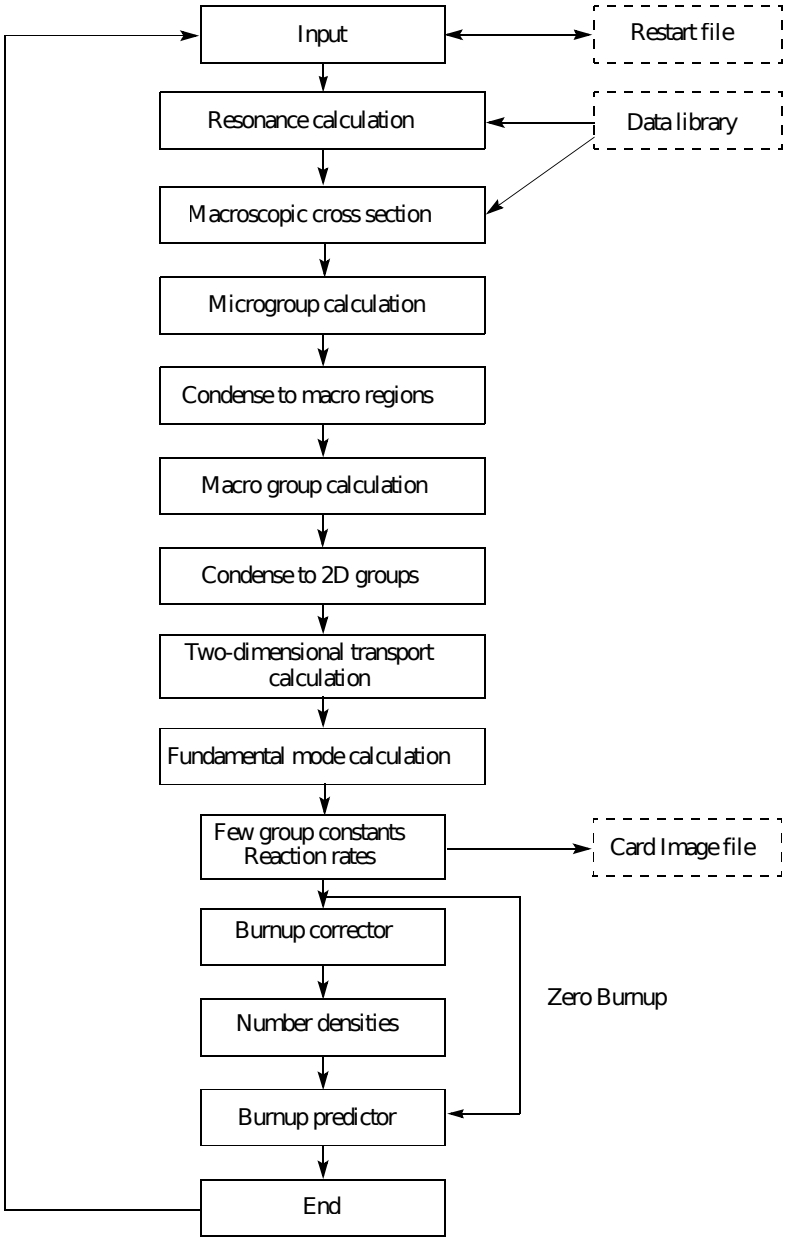

Fig. 3.1 – CASMO flow diagram, extracted from Edenius et al. 1995.

Library (NDL) were used (currently ENDF/B-IV is used). Extensive information of CASMO can be found in Edenius et al. 1995.

3.1.1.2 DOORS3.2/DORT & TORT

DOORS3.2 is a compilation of different codes with the main purpose of neutron/photon transport solver. Its development started in 1965 at Oak Ridge National Laboratory (ORNL). However, currently it is not further developed. Transport calculations are performed by DORT and TORT (deterministic codes) in 2D and 3D respectively. Nevertheless, it does not have the depletion capability and thus, problem-specific cross section generation is not possible. Therefore, strictly speaking, it is not a lattice code.

Directional domain is discretized using the method of discrete ordinates and solving the Boltzmann transport equation. Moreover, the spatial domain is discretized using the weighted difference method, the nodal method, or the method of characteristics. Energy dependence is solved with the multigroup approach. DORT and TORT does not treat the time dependence. Either cylindrical or cartesian geometries (in 2D or 3D) are allowed. Some of its main features are subcritical multiplication search, direct multiplication search, fixed-source and indirect criticality search. The main drawbacks are (i) transient simulations are not allowed (ii) cross section generation is not possible and iii) the code is outdated. More information about TORT and DORT can be found in its user's manual (Rhoades and Childs 1987).

3.1.1.3 HELIOS-2

HELIOS is a commercial deterministic lattice code with burn-up capability, also developed at Studsvik Scandpower. It solves the 2D transport equation based on unstructured mesh. The code consists in 3 sub-modules: AURORA, HELIOS and ZENITH. AURORA is in charge to pre-process the input deck, ZENITH gathers the output data and generates an appropriate output file and HELIOS is the main module that actually solve the transport equation and obtains the cross sections.

Since CASMO and HELIOS are developed for the same institution, the main solver and calculations for both codes are similar. The major difference is the degree of freedom HELIOS gives to the final user. With HELIOS the geometry and composition assignment to regions is entirely up to the user (much as with SCALE). Extensive studies using HELIOS lattice code can be found. For example, Ivanov et al. 2004 uses HELIOS for criticality calculation with different options within a Benchmark problem. Wemple et al. 2008 demonstrates the use of different transport methods with HELIOS-2. Núñez-Carrera et al. 2004 compares the obtained multiplication factor and isotopic distribution in a fuel pin with the reference code CASMO-4.

3.1.1.4 MCNP6.1.1

MCNP is not a lattice code -thus it does not generate cross sections-, but it is included in this section for its relevance in the nuclear reactor field. MCNP6 is a *Monte Carlo* (MC) radiation-transport code with continuous energy, it is developed at Los Alamos National Laboratory's (LANL). Its cross section library is based on ENDF/B-VI or ENDF/B-VII NDLs. It can track different particle types (electrons, neutrons, gamma...) over broad energy ranges. Current version 6.1.1 is in beta version and it contains MCNP5TM and MCNPXTM into a single code. More information can be found in MCNP user's manual (Denise et al. 2014).

Even though MCNP is not a lattice code, multiple studies can be found related to nuclear reactors. For example, Díez et al. 2013 performs a U&S analysis over the multiplication factor and cross section propagation within the OECD/NEA benchmark using MCNPX-2.7e and comparing with SCALE6.1. Jatuff et al. 2009

compares several lattice physics codes and different libraries for the full void range, the codes used are CASMO-4, HELIOS, PHOENIX, BOXER and MCNP4C.

3.1.1.5 SCALE6.2.1/TRITON-NEWT

SCALE is a software composed by multiple modules that can solve nuclear related problems. These modules are designed to cover a wide range of applications, safety analysis, radiation shielding, reactor design, spent fuel characterization and storage, criticality calculations... SCALE6.2.1 is developed in Oak Ridge National Laboratory (ORNL). Among its modules, TRITON is the driver that decides the main calculation flow and calls secondary modules according to the selected sequence. NEWT module is the deterministic 2D lattice code in SCALE toolkit. It uses the Step Characteristic approximation (one of the simplest schemes of the Method of Characteristics). SCALE version 6.2.1 with modules TRITON/NEWT with depletion sequence[4] are used in this thesis for cross section generation purposes.

TRITON is the control module in SCALE. With help of other modules, it produces cross section problem-dependent multigroup libraries and solves the transport equation in 1D, 2D or 3D -depending on the solver selected[5]- for the defined problem. Additionally, with ORIGENs calculations, depletion and isotopic concentration can be computed for transient simulations and its data used to update the cross section problem-dependent library. Moreover, this cross section library can be collapsed and homogenized according to the user specified materials and energy group structure.

SCALE provides a master cross section library that contains microscopic cross sections for a big range of nuclides and nuclear reactions. In order to correct these cross sections for spatial and energy self-shielding, SCALE provides several cell types.

- Infinite medium: the material specified is treated as an infinite homogeneous material. It is recommended for large masses of materials where the size of each material is larger than the average mean-free path of the material. It should not be used for materials made of heavy nuclides. This is the default cell type if no cross section treatment is specified for a certain material.
- Lattice of pins: this is the appropriate cross section treatment for large arrays of slabs, fuel pins or spherical pellets. Some limitations apply (i) only mirror boundary conditions, (ii) infinite array of 1D cells is assumed, (iii) for pin definition fuel must be the inner material and (iv) only several geometries are allowed. The most common geometries are the squared cell and the hexagonal cell, both depicted in Fig. 3.2.
- Multiregion: it is used when the geometry effects are not well represented by the lattice cell. There is more flexibility to define fuel regions, however, all geometries must have the same shape. Also limited to 1D geometries. Multiple outer boundary condition definitions.
- Double heterogeneous systems: this cell represents heterogeneous fuel spheres or grains coated with one or more materials.

Multiple cell calculations can be used, in fact it is recommended to define a different cell for each fuel rod type (Ade 2012). Not only in the geometrical sense, two fuel rods are considered different if they have different composition or if they are depleted differently (for example if one is in the assembly corner and the other in the center). This is an important factor, especially in BWR, where void fraction radial distribution is not flat and thus, fuel depletion depends on pin position. Problem-dependent cross sections are derived using the cells specified. There are five different **cross section processing options** supported by TRITON.

[4] ORIGENs module is used in SCALE6.2.1 for depletion and isotopic transmutation tracking.
[5] XSDRNPM module for 1D, NEWT for 2D and KENO-VI for 3D.

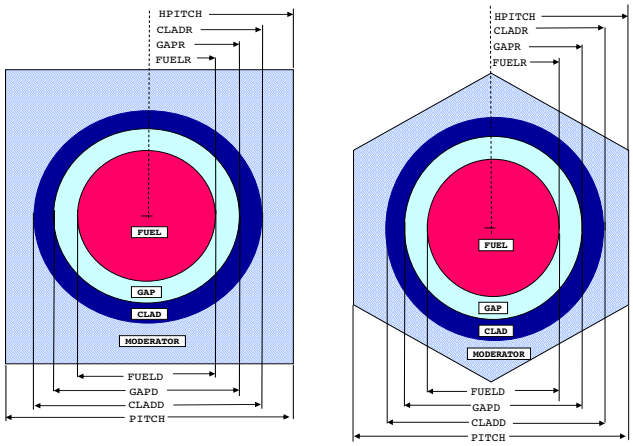

Fig. 3.2 – Lattice cell representation for square geometry (left) and hexagonal geometry (right), extracted from Goluoglu et al. 2011.

1. CENTRM with discrete ordinates (S_N) option. Problem-dependent multigroup cross sections are obtained with CENTRM for the resolved energy range, and BONAMI module -using the *Bondarenko self-shielding method*- in the unresolved resonance energy range. CENTRM also obtains the pointwise[6] flux using a discrete ordinate method. Then, PMC module is invoked to collapse pointwise cross sections using the -previously obtained- CENTRM pointwise flux solution. This provides the problem-dependent multigroup cross sections. CENTRM with S_N is the most accurate cross section processing option in SCALE and therefore, it is the default option.

2. CENTRM with two-region option. This option is identical to the previous option with the exception that CENTRM uses a two-region collision probability method to calculate the pointwise flux solution in the resolved resonance energy range. This processing option is faster than S_N option and can be used for most LWR. However, this option is not accurate for reactors using MOX[7] fuel pins or burnable poison rods (BWR). Moreover, it can only be used with cylindrical square-pitched pins and cylindrical triangle-pitched pins. TRITON allows using the S_N and the two-region options for different unit cells in the same model.

3. CENTRM with doubly heterogeneous option. Doubly heterogeneous fuel element analysis for problem-dependent cross section procedure is performed using CENTRM with S_N option. However, TRITON does not support this option for the U&S analysis sequence. More information is given in the MIPLIB (Material Information Processor library) manual (Goluoglu et al. 2011).

4. NITAWL. This option is no longer available in SCALE6.2. This option is similar to CENTRM two-region to solve the resonance energy range, but it is faster. It uses the *Nordheim Integral Treatment* method. However, it does not take into account the resonance overlap effects among multiple resonance-absorption isotopes. Due to this limitation, it can only be used with ENDF/B-V NDL, which is no longer available in SCALE6.2.

5. BONAMI. It uses the *Bondarenko self-shielding method* over the full energy range. This cross section processing option is fast, but may be not suited for some applications. Therefore, it is only recommended for preliminary results.

[6] This term is used when a fine energy structure is used, in the order of 10^5 energy groups
[7] Mixed oxide (MOX) fuel contains plutonium recovered from used reactor fuel enriched with ^{235}U.

Dancoff factors are important parameters for cross section self-shielding effect. Dancoff factors are defined as the free-flight transmission probability between fuel lumps of a heterogeneous system of fuel and moderator. They are computed by default by the MIPLIB library assuming an infinite lattice of equal fuel pins. However, this assumption may not hold for very heterogeneous fuel pin layouts, such as in BWR, and lead to inaccurate Dancoff factors. For heterogeneous assemblies, the MCDANCOFF module provides accurate Dancoff factors for further use in the depletion sequence. MCDANCOFF module is based on KENO 3D Monte Carlo module, more information is found in its manual (Petrie and Rearden 2011).

The **equation transport solver** uses the cross section problem-dependent multigroup library created using the cross sections processors cited before. In SCALE the transport equation solver is multidimensional, for 1D problems XSDRNPM module is used, NEWT for 2D and KENO-VI for 3D. It is a common approach to define the problem in 2D in order to generate problem-dependent cross section. Thus, **NEWT** is the (deterministic) 2D solver used in this thesis. Besides, KENO, even though more accurate for criticality calculations, requires bigger computational effort and it does not accept branch calculations in SCALE6.2.1 to generate homogenized and collapsed cross sections.

Traditional 2D discrete ordinates approach determines the particle average flux in a rectangular cell and the average flux in its four sides. Therefore, the geometry described in the problem is limited to simple geometries and rectangular (structured) grids. As an improvement, NEWT includes the *Extended Step Characteristic* (ESC) method for spatial discretization of an arbitrary mesh, see Section 2.2.2.2. Therefore, it provides freedom to define the geometry using any type of polygon. ESC provides average flux for all polygons and their sides. The process is repeated iteratively until convergence is achieved. Inner iteration is used to solve spatial fluxes for each energy group and outer iterations are used to converge all energy groups.

NEWT include different **capabilities**, including the following.

- Three solution types are provided, (i) eigenvalue (k_∞) calculation for criticality problems, (ii) k_∞ followed by a buckling correction (leakage in the third dimension) and (iii) source calculation with no k_∞ prediction.
- Forward and adjoint flux distribution.
- Collapsed and homogenized cross section for problem-dependent libraries. This is one of the main topics in this thesis.
- Diffusion coefficient and other neutronic parameters to include in the problem-dependent libraries.
- *Assembly Discontinuity Factors* (ADFs) (for internal and peripheral assemblies), used by the neutron kinetic code to take into account flux discrepancies with nearby fuel assemblies (also known as environmental effect).
- Pin power reconstruction, used by the neutron kinetic code to recover the flux at pin level (or intra-assembly flux) after the materials have been homogenized.
- Branch calculations to generate problem-dependent cross sections. Parallel capability is defined on Unix platforms for branch calculations.
- *Coarsh Mesh Finite Difference* (CMFD) acceleration, see Section 2.2.3.1. A coarse rectangular mesh is defined based on the original mesh, then these rectangular zones are homogenized to speed-up the ESC method convergence. A second level of CMFD acceleration is allowed, it alternates multigroup and two-group calculations. Although traditionally CMFD approach was only valid for square-pitched fuel bundles, now it also supports triangular-pitched fuel bundles.

Boundary conditions (BC) in NEWT can be defined using four options.

1. Reflective: a neutron leaving the system (through a boundary) in a particular direction will be returned to the system but at a mirrored angle.
2. White: provides isotropic flux return at the boundary.
3. Vacuum: any neutron across the boundary is lost and never returns to the system.
4. Periodic: neutrons leaving the system will be returned to the system with the same direction but through the opposite boundary.

The **depletion sequence** in TRITON build upon the transport sequence. ORIGENs module calculates the depletion/decay for each material defined to be depleted. The depletion capability can be subdivided into three steps.

1. Flux post-processing calculations. The transport flux solution is used to obtain region-averaged multigroup cross sections and multigroup flux for each depleted material.
2. COUPLE module uses the results of previous step to obtain three-group cross section library for each depleted material. This problem-dependent library is an updated version of the problem-independent cross section library.
3. ORIGENs depletes each material using the three-group problem-dependent library and the normalized power. Then the isotopic concentration is updated.

The depletion procedure is performed for specific time intervals or **depletion steps** where the power level is constant. However, this is a simplification and in a real reactor the power is continuously changing. The depletion changes the isotopy and flux distribution (and thus the problem-dependent cross sections). The user needs to specify the depletion steps used to compute the depletion. The shorter the depletion steps, the more accurate will be the isotopic concentration and problem-dependent cross sections. However, more computational time will be needed. The decision for depletion step length is up to the user. As starting point, according to Ade 2012, the following depletion steps are recommended. For reactors with burnable absorber pins, the burn-up between steps, must not be over 0.5 or 1.0 GWd/MTU before peak reactivity, after the peak it can be increased. For other reactors the depletion steps can be up to 2.0 or 3.0 GWd/MTU.

TRITON uses a **predictor-corrector approach** to advance in the depletion process. This approach performs transport and cross section calculations based on isotopic concentration obtained at *midpoint* of depletion intervals or cycles (predictor step). Then, the depletion process is performed over the full depletion step (corrector step) using the cross sections and flux distribution predicted at the midpoint. Depletion calculation is then extended to the next depletion interval midpoint and the process starts all over again, see Fig. 3.3 for a schematic view. In this figure, T means transport calculation (performed at interval midpoints, except at initial time) and D means depletion calculation (performed at beginning of each depletion step).

Branch calculations are available for depletion sequences. This option allows fast calculations for identical transport problems where only the feedback parameters are changed. Branch calculations are based on the "nominal" case. On each branch, TRITON rerun the cross section processing and the transport calculations with one or more of the feedback parameters modified. However, the key for speed up the calculations is that the depletion calculation is not repeated, but the depletion result of the "nominal" case is used. Therefore, the calculation using branches is much faster than performing a different transport problem for each feedback parameter combination. Branch calculations are performed at the same point in time as the depletion and cross section calculations, that is at initial time and at midpoint of each depletion interval. On each branch,

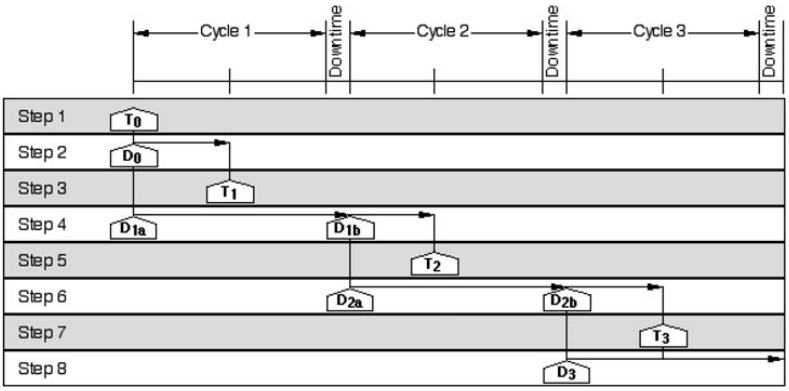

Fig. 3.3 – Algorithm of the predictor-corrector approach used by TRITON, extracted from DeHart 2005.

sets of problem-dependent cross sections as a function of the feedback parameters are obtained, possibly homogenized and collapsed. The process is repeated for all depletion intervals. Then, TRITON stores the responses in database files: `txtfile16` for ASCII data and `xfile016`[8] for binary data. Afterward, the user can transform this data into a specific cross section library format to be used later in a core physics code, see Section 3.3.1. In addition to feedback parameters, since SCALE version 6.1, it is also possible to specify different -user defined- Dancoff factors on each branch. The feedback parameters implemented in TRITON branches are:

- Fuel temperature.
- Moderator temperature.
- Moderator density.
- Boron concentration.
- Control rod position (in/out).

There are two **TRITON parameters** that are worth to be explained here (`addnux` and `weight`). TRITON has predefined group of nuclides that can be added as traces (10^{-20} at/b-cm) in order to accurately track the isotopy in the depletion process. Only isotopes defined in the model and those added as traces are accounted for depletion and isotopic calculations. With high values of `addnux` parameters, more nuclides will be added and, by extension, more accuracy will be reached. Big `addnux` values contain the nuclides in smaller `addnux` options. Thus, more computational effort is needed for bigger `addnux` values. The value of `addnux` ranges from 0 with no additional isotope (only the isotopes defined in the model are tracked) to 4 which contains 388 additional isotopes, being `addnux`=2 the default value. The value of the `addnux` option is a trade-off between accuracy and computational time. The second option, `weight`, is used to produce a collapsed problem-dependent cross section library. It runs a first transport sequence with NEWT and uses the predicted flux to weight the master library and produce a collapsed cross section library with 49 predefined energy groups. The problem-averaged flux is used for the weighting process. However, it is possible to specify the materials whose flux will be used for the weighting process. The main calculation flow and modules involved in the depletion sequence are depicted in Fig. 3.4. For more information about other TRITON parameters, the reader is referred to the TRITON user's manual (Jessee and DeHart 2011).

[8]The binary format of this file is described in TRITON user's manual Jessee and DeHart 2011 (appendix T1.A)

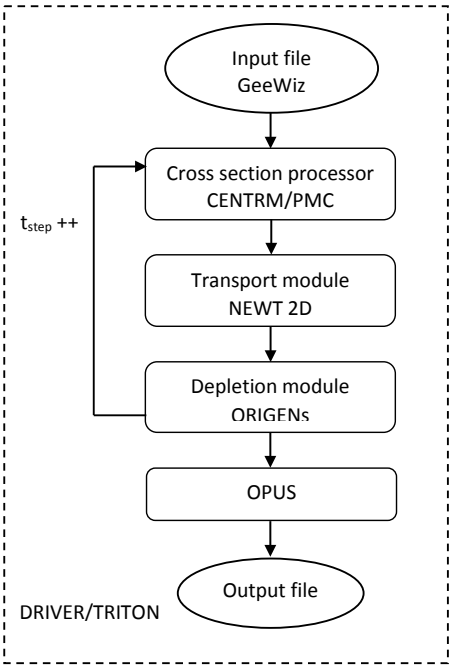

Fig. 3.4 – Simplified calculation flow for SCALE using a depletion sequence.

3.1.1.6 SCALE6.2.1/TRITON-KENO-VI

The 3D transport model option in SCALE is solved using KENO Monte Carlo module. KENO is also controlled by the driver module TRITON, thus some characteristics are already explained in Section 3.1.1.5. The main differences with NEWT are two, (i) the 3D representation in KENO -opposed to 2D NEWT- allows for a more realistic calculations, especially for axial perturbations (for example boundaries between top/bottom reflector with fuel assemblies) and (ii) the main solver in KENO is based in a Monte Carlo scheme, this produces more accurate results (if enough particles are tracked) but more computational effort is needed. KENO code is intended for criticality calculation (k_∞) and flux distribution prediction. The most important improvements in KENO-VI are the capability to perform calculations in the continuous energy mode -although the traditional multigroup approach is still possible- and the capability to calculate angular fluxes and flux moments for later use in sensitivity/uncertainty calculations. Additionally, a nice HTML output is provided by default. The boundary conditions are the same explained for NEWT, however now they are represented in 3D.

MC codes are based on stochastic techniques to solve a problem, in this case flux distribution and multiplication factor. KENO tracks NPG particles (neutrons) in one generation, from this generation KENO computes the average neutron properties. Therefore, the higher NPG, the lower the variability associated to the stochastic calculations. After the first generation is completed, a second generation with other NPG particles starts. The process is repeated up to GEN generations. The result, the running average, is updated each time a generation is completed. While computing the running average, the variability of first generations is higher (less samples are available), thus KENO allows the first NSK generations to be skipped from the final average result calculation.

In order to minimize the k_∞ variability, KENO employs *weighted tracking* rather than *analog tracking*. Particles are assigned a weight when they are born and they are tracked until they *die*, this is known as *particle*

history. In the weight tracking approach, when a particle experience absorption, its weight is reduced (opposite to analog tracking where the particle history is terminated). When a particle falls under a specified WTL weight, then *Russian roulette game* is played. If particle survived the game, it is assigned a new WTA weight, otherwise the particle is said to be dead and is no longer tracked.

For the reflector region, a particle becomes less important as it gets further from the fissile material and its energy is reduced. Thus, it is convenient to reduce its weight as the distance is increased. KENO provides the capability to define WTL and WTA as function of position and energy. Therefore, a particle can move form one region into another with WTL greater than the weight of the neutron. When this occurs, Russian roulette is played. On the contrary, if a particle moves to a region of higher importance and its weight is higher than WTH, the neutron is split into two neutrons, each with weight equal to one half of the original neutron weight. The procedure is repeated until the weight of the split neutron is below WTH. All this parameters can be customized, they are listed next along with its default value.

- GEN: number of generations to be run (default is 203).
- NPG: number of neutrons per generation (default is 1000).
- NSK: number of generations (1 through NSK) to be omitted when collecting results (default is 3).
- WTA: weight given to a particle that survives the Russian roulette game (default is 0.5).
- WTL: weight below which the Russian roulette is played (default is $WTA/3$). The default value (0.167) is shown to produce minimum k_∞-variance when WTA is 0.5.
- WTH: weight at which splitting occur (default is $WTA \times 3$).

The weight function for a given reflector or core material can be obtained solving the adjoint flux for a simplified problem. The adjoint flux gives the contribution of each neutron to the total fission rate as a function of its position and energy. Weight functions for several reflector types are predefined in KENO, the use of these functions minimize the k_∞-variance but it could increase the variance in other parameters, such as leakage or absorption.

SCALE is a well validated code. For example, Ilas et al. 2012, DeHart and Bowman 2011 and Gauld et al. 2011 validate the new capabilities of the depletion sequence with SCALE6.1. Some of the validated capabilities are isotopic concentration, burn-up procedures, decay heat, criticality calculations, ENDF/B-VII... They make use of TRITON/NEWT, TRITON/KENO and ORIGENs modules.

3.1.1.7 Serpent-2

Serpent is a MC 3D lattice physics code with continuous-energy and depletion capability. It is developed at VTT Technical Research Centre of Finland since 2004 and distributed by the OECD/NEA Data Bank and RSICC since 2009. It is written in standard ANSI-C language. The current version, Serpent-2, is under beta-testing phase, its main work is divided into two main works.

1. Advanced methods for spatial homogenization: such as implementation of diffusion solvers for homogeneous flux calculations.
2. Coupled multi-physics applications: the coupling scheme currently has two options: (i) built-in solvers for fuel behavior and thermohydraulics and (ii) external coupling via a universal multi-physics interface

More information about Serpent can be found in its user's manual (Leppänen 2015). An example of use is found in Rachamin et al. 2013, where HELIOS-2 and Serpent codes are used to obtain cross section library for a sodium cooled fast reactor. They are compared through the core physics code DYN3D.

3.1.2 Thermohydraulic system codes

3.1.2.1 RELAP5/MOD3.3 - U.S. NRC version

RELAP5 is a *Best Estimate* (BE) code, its first version started in 1966 developed by the *U. S. Nuclear Regulatory Commission* (NRC) for licensing purposes and analysis of any transient (*Anticipated Transients Without Scram* (ATWS), *Anticipated Operational Occurrences* (AOOs)) and postulated accidents in a LWR. It is based in a semi-implicit finite-difference technique in 1D with 3D fictitious nodalization (1D nodalization connected with cross junctions). It is able to simulate a wide range of thermohydraulic phenomena in both nuclear and nonnuclear systems including water, steam and mixture of both with or without solute. However, one important limitation (common in thermohydraulic codes for anticipated transients analysis purposes) is that temperature is not allowed to exceed the melting point of materials.

An important feature of this thermohydraulic code is the implementation of a point reactor kinetic model. This is a simplified neutronic model that accounts for prompt and decay power (with fission products and actinide decay). For the decay power two options are available, either *American Nuclear Society Proposed Standard* (ANS 5.1) or *American National Standard for Decay Heat Power in Light Water Reactors* (ANSI/ANS-5.1-1979). The following approach is used, the power distribution is calculated as separate space and time functions. This approach is valid when the power distribution do not substantially change in the space domain. Otherwise, this approximation can be applied when the neutronics do not play a big role or its accuracy is not important for the analyst. If a more accurate neutronic model is required, then RELAP5 can be coupled to a neutron kinetic code, for example PARCS2.7 (Barrachina et al. 2010a). Extensive information for RELAP5/PARCS can be found in Martínez-Murillo et al. 2011 and RELAP5 user's manual (Schultz 2003). The DOE version of RELAP5 has the capability for 3D thermohydraulic model, porous media model and it is already coupled (with a serial integration approach, see Section 3.2) with NESTLE 3D neutron kinetic code. See Section 3.2 for more information about thermohydraulic-neutronic coupled codes.

3.1.2.2 TRAC-BF1

TRAC-BF1, BE code, started its development in 1979 at Idaho National Engineering Laboratory (INEL) and is written in ANSI Standard FORTRAN 77. TRAC-BF1 uses a point kinetic neutronic model and can simulate BWR analysis (especially *Lose Of Coolant Accident* (LOCA) and ATWS), *Separate Effects Test Facilities* (SETFs) and experimental *Integral Test Facilities* (ITFs)... The base models in TRAC-BF1 were inherited from TRAC-PF1, it contains a two-fluid 1D and 3D thermohydraulic models. TRAC-PF1 presented some problems when BWR were simulated, these problems arose due to the bundles geometry differences between BWR and PWR. The bundle wall -or box- present in BWR channels leads to thermohydraulic phenomena (radiation, turbulence...) that are not present or are not important in a PWR. Currently, TRAC-BF1 is kept updated by Universitat Politècnica de València (UPV). More information can be found in its user's manual (Borkowski et al. 1992).

Some studies include Barrachina et al. 2013, where an improved boron transport model (second-order modified Godunov) is implemented in TRAC-BF1. Moreover, in Miró et al. 2015, a semi-automatic methodology to translate TRAC-BF1 models to TRACE is presented, it is also developed by the author of this thesis. This study is presented with a *Peach Bottom Turbine Trip* (PBTT) example.

3.1.2.3 TRACEv5.0p3

TRACE is the reference code for the NRC, it is intended to continue its uses in the future and its development is expected to grow. Therefore, aiming to obtain a model valid for future works, TRACE is the chosen thermohydraulic code used in this thesis. This code is the result of the NRC to unify its main thermohydraulic

codes (TRAC-PF1, TRAC-BF1, RELAP and RAMONA[9]) into one single code. TRACE is capable to perform BE analysis for *Loss Of Coolant Accident*, operational transients and other accident scenarios in PWR, BWR and experimental facilities. TRACE solves the two-phase flow differential equations (in 1D and 3D) describing thermohydraulic phenomena using finite volume numerical methods. Besides, the heat transfer equations are solved using a semi-implicit scheme and a time-differencing technique. Large time steps can be achieved as a result of the *Stability-Enhancing Two-Step* (SETS) method that allows the Courant limit[10] to be exceeded in hydraulic components for slow transients. Fast calculations are performed with SETS of slow-developing accidents and operational transients. SETS method was originally developed with TRAC-PF1. According to its user's manual (Bajorek et al. 2007) its main characteristics are:

- Multi-dimensional fluid dynamics: there are a large number of hydraulic 1D components in TRACE, but also cartesian (x,y,z) or cylindrical (r,θ,z) 3D vessels can be used. This component can be used to model reactor cores in PWR as explained in Section 4.2 with realistic cross-flow calculations and other 3D phenomena, for a detailed explanation the reader is referred to Mesado et al. 2015.
- Non-homogeneous, non-equilibrium modeling: TRACE considers two-phase flow (with six-equations), thus a variety of thermohydraulic phenomena are considered: counter-current flow, stratified flow, *Departure from Nucleate Boiling Ratio* (DNBR) calculations, dissolved solution tracking, non-condensable gases...
- Flow-regime-dependent constitutive equation package: flow regimes can be calculated accurately with a build-in package incorporated into the code.
- Comprehensive heat transfer capability: heat transfer is treated either in 1D or 2D (r,z) for user defined heat structures representing slabs, rods or spheres. Heat transfer is calculated using flow-regime-dependent heat transfer coefficients, besides a dynamic fine-mesh for heat transfer is used during reflood.
- User's possibilities: the code is composed by numerous components. How they are connected and used is up to the user. There is not any limitation in the number of components or connections used.
- Component and functional modularity: different phenomena are modeled using separate subroutines. It is modular by functions, meaning that all components have access to these subroutines. This allows the code to be upgraded with minimum effort.
- Neutronic calculations: PARCSv3.0 neutron kinetic code is already included in TRACEv5.0, providing a professional tool for accurate thermohydraulic-neutronic phenomena calculations.
- Kinetic model: One-dimensional (default) or three-dimensional reactor kinetic capabilities are possible when coupled when PARCS.
- Restart capability is included.

Moreover, there are some limitation in TRACE use.

- Strictly speaking, TRACE can only be used inside the specified ranks of each variable.
- TRACE does not accurately calculate transfer of moments, for example in plenum components.
- Not appropriate for transients with strong change in core power, unless it is coupled with PARCS.

[9] Thermohydraulic code for BWR analysis.
[10] See footnote 23.

- The code does not calculate thermal stratification in the liquid phase in 1D components. However, it does in 3D components.
- It should not be used in models where the viscous stresses are greater or equal than the wall (or interfacial) shear stresses.
- TRACE does not allow fuel rod failure in the simulation. However, it calculates other important values that can be used to determine a rod failure (such as enthalpy or the DNBR).
- The fluid heating due to viscous heating is generally ignored. Nonetheless, a model is implemented to account for the direct heating due to pump rotor.

In previous versions, TRACE and PARCS were coupled following a parallel processing approach. However, in the last version, the neutron kinetic code PARCSv3.0 is coupled with TRACE following a serial integration approach. Therefore, a powerful tool is provided with TRACE for accurate thermohydraulic-neutronic transient analysis. For example, Gajev 2012 use TRACE/PARCS coupled code for an U&S analysis for instabilities in Ringhals-1 BWR. Extensive information for TRACE/PARCS can be found in PARCS (Downar et al. 2010). See Section 3.2.1 for more information about TRACE/PARCS coupled code.

Hereafter, a brief description of some TRACE models and correlations is developed. For a complete description of the numerous TRACE models and correlations, the reader is referred to TRACE user's and theory manual, Bajorek et al. 2007 and Bajorek et al. 2011. Here, only the most relevant correlations and models related to the work developed in this thesis are presented.

Pressure losses

In order to calculate the pressure losses in the system, TRACE accounts for the wall drag and the pressure loss due to geometry changes (form drag).

- Wall drag: models the fluid-wall shear using a friction factor approach.
- Form drag: models geometry specific pressure loses using user specified additive loss coefficients. For example abrupt flow area expansions or contractions.

The additive loss (form drag) can be specified in TRACE as friction coefficients, $FRIC$, or K-factors, K, the latter specification is recommended by TRACE developers. Internally, TRACE converts the K-factors into friction coefficients using the following equation.

$$FRIC_{j+1/2} = K_{j+1/2} \frac{D_{h,j+1/2}}{D_{x,j} + D_{x,j+1}} \tag{3.1}$$

Where D_x is the cell length and the hydraulic diameter, D_h, is mainly used (but not exclusively) in TRACE for the evaluation of pressure losses resulting from wall friction. It can be expressed using the flow area, A_f, and the wetted perimeter, P_w.

$$D_h = \frac{4 \cdot A_f}{P_w} \tag{3.2}$$

TRACE can calculate a K-factor for abrupt expansions, Eq 3.3, and abrupt contractions, Eq 3.4, in cell face $j + 1/2$. These values are added to the loss coefficients input specified. The user can introduce K-factors for cell edges in 1D and 3D components (vessels).

$$K = \left(1 - \frac{A_j}{A_{j+1}}\right)^2 \left(\frac{A_{j+1/2}}{A_j}\right)^2 \tag{3.3}$$

$$K = \left[0.5 - 0.7\frac{A_{j+1}}{A_j} + 0.2\left(\frac{A_{j+1}}{A_j}\right)^2\right] \left(\frac{A_{j+1/2}}{A_{j+1}}\right)^2 \tag{3.4}$$

Therefore, the irreversible loses due to an area change can be predicted using Eq 3.5.

$$\Delta P_{j\to j+1} = \rho\left(\frac{V_{j+1}^2}{2} - \frac{V_j^2}{2}\right) + \rho K \frac{V_{j+1/2}^2}{2} \tag{3.5}$$

Regarding the wall drag model, TRACE calculates the pressure gradient due to wall friction using Eq 3.6.

$$\left.\frac{dP}{dz}\right|_f = -C_{wl}|V_l|V_l - C_{wg}|V_g|V_g \tag{3.6}$$

Where

$\left.\frac{dP}{dz}\right|_f$ is the pressure gradient due to wall friction,

C_{wl} and C_{wg} are the wall drag coefficient for wall-liquid and wall-gas shear respectively, and

V_l and V_g are the liquid and gas phase velocity.

In order to calculate the wall drag coefficient, C_w, different correlations are implemented in TRACE. These have different valid conditions according to the heat and flow regime: single-phase flow, Pre-CHF, horizontal stratified flow and Post-CHF. These are briefly explained hereafter.

– Single-phase flow: the wall drag coefficient is defined as

$$C_w = f_w \frac{2\rho}{D_h} \tag{3.7}$$

where

f_w is the Fanning friction factor[11],

ρ is the fluid density, and

D_h is the hydraulic diameter.

– Pre-CHF flow regimes: all wall drag is only applied to the liquid phase. Different correlations are summarized according to the flow regime in Table 3.1. If void fraction is greater than 90%, then the annular flow regime correlation is used. Whereas, if it is less than 80%, the bubbly/slug flow regime correlation is used. Otherwise, the transition correlation is used.

Where

$Re_{2\Phi,l}$ is the two-phase Reynolds number,

f_{film} is the friction factor for the annular flow,

f_{lam} is the laminar component of friction factor,

[11] In TRACE, this is obtained using Churchill formula because it applies to all flow regimes.

Annular/Mist	Transition	Bubbly/Slug
$C_{wl} = f_{film}\frac{2\rho_l}{D_h}$ $f_{film} = \left(f_{lam}^3 + f_{turb}^3\right)^{1/3}$ $f_{lam} = \begin{cases} \frac{24}{Re_{2\Phi,l}}, & \alpha > 99 \\ \frac{16}{Re_{2\Phi,l}}, & \alpha < 95 \\ \frac{16+8\left(\frac{\alpha-0.95}{0.99-0.95}\right)}{Re_{2\Phi,l}}, & \text{otherwise} \end{cases}$ $f_{turb} = \frac{1}{\left[3.6\log_{10}\left(\frac{6.9}{Re_{2\Phi,l}}+\left(\frac{\epsilon/D}{3.7}\right)^{1.11}\right)\right]^2}$	$C_{wl} = wf_{BS}C_{wl}^{BS} + (1-wf_{BS})\,C_{wl}^{AM}$ $wf_{BS} = \frac{0.9-\alpha}{0.9-0.8}$	$C_{wl} = f_{wl}\frac{2\rho_l}{D_h}(1+C_{NB})^2$ $C_{NB} = \text{Min}\left(2, 155\frac{d_B}{D_h}\left[\alpha(1-\alpha)\right]^{0.62}\right)$

Table 3.1 – Wall drag coefficient for Pre-CHF flow regimes.

f_{turb} is the turbulent component of friction factor,

C_{wl}^{BS} is the wall drag coefficient for the bubbly/slug flow regime,

C_{wl}^{AM} is the wall drag coefficient for the annular/mist flow regime,

α is the void fraction,

d_B is the bubble departure diameter, and

C_{NB} is the correction factor accounting for nucleate boiling.

– Horizontal stratified flow: both the liquid and gas are in contact with the pipe wall, consequently the wall drag coefficient must be specified for both phases, Eq 3.8. The friction factor is evaluated with Eq 3.9 and Eq 3.10 for turbulent and laminar flow respectively. The Reynolds number is calculated for each phase with a modified diameter.

$$C_{wk} = f_{wk}\frac{P_k S_k}{2A} \tag{3.8}$$

$$f_{wk} = \frac{0.046}{Re_k^{0.2}} \tag{3.9}$$

$$f_{wk} = \frac{16}{Re_k} \tag{3.10}$$

– Post-CHF flow regimes: the wall temperature is above the minimum stable film boiling temperature. Different correlations are summarized according to the flow regime in Table 3.2. If void fraction is greater than 90%, then the disperse flow regime correlation is used. Whereas, if void is less than 60%, the inverted annular flow regime correlation is used. Otherwise, the transition correlation is used.

Where

$f_{2\Phi,g}$ is the Fanning friction factor for the gas phase,

$Re_{2\Phi,g}$ is the two-phase Reynolds number for the gas phase,

f_{pg} is the effective friction factor,

Inverted annular	Transition	Dispersed
$C_{wg} = f_{2\Phi,g}\frac{2\rho_g}{D_h}$	$C_{wg} = (1 - wf_{DF})\, C_{wg}^{IA} + wf_{DF} C_{wg}^{DF}$	$C_{wg} = f_{pg}\frac{2\rho_g}{D_h}$
$Re_{2\Phi,g} = \frac{\alpha\rho_g \lvert V_g \rvert D_h}{\mu_g}$	$wf_{DF} = \frac{\alpha - 0.6}{0.9 - 0.6}$	$f_{pg} = f_{wg}\left[1 + \mathrm{Min}\left(12, LF\right)\right]^{0.3}$
		$LF = \dot{m}_p / \dot{m}_g$

Table 3.2 – Wall drag coefficient for Post-CHF flow regimes.

LF is the loading factor,
C_{wl}^{IA} is the wall drag coefficient for the bubbly/slug flow regime, and
C_{wl}^{DF} is the wall drag coefficient for the annular/mist flow regime,

Critical heat flux

The determination of the heat flux regime is very important to predict an accurate *Critical Heat Flux* (CHF). This condition is encountered when the cooler cannot absorb more heat flux and transient boiling starts on the walls, the big bubbles created reduce the heat transfer efficiency dramatically. The CHF point is defined by the heat flux and the wall temperature (q_{CHF}, T_{CHF}). This point separates the Pre-CHF regimes, where the liquid phase wets the wall (nucleate boiling), from the Post-CHF regimes, where the liquid-wall contact is either transition boiling or non-existing (film boiling).

The CHF model identifies the heat flux where the Pre-CHF and Post-CHF regimes converge. In TRACE, a three-dimensional linear interpolation is used to obtain the CHF based on the *AECL-IPPE CHF Table*. This look-up table was obtained with experimental data for 8 mm tubes as a function of three parameters: pressure, mass flux and dryout quality. The AECL-IPPE table covers a wide range of conditions:

$3 \leq D \leq 40$ (mm)

$0.1 \leq P \leq 20$ (MPa)

$6 \leq G \leq 8000$ (kg/m^{2}s)

$-0.5 \leq x \leq 1$

$80 \leq L/D \leq 2485$

The following formula is used to predict the CHF,

$$q_{CHF} = K_1 K_2 K_8 \cdot fn\{P, G, x\} \tag{3.11}$$

where

q_{CHF} is the CHF,

K_1 is the correction factor for the tube diameter,

$$K_1 = \mathrm{Max}\left(0.6, \sqrt{0.008/D_h}\right) \tag{3.12}$$

K_2 is the correction factor for the rod bundle geometry (pitch to diameter, P/D_R),

$$K_2 = \left[2\frac{P}{D_R} - 1.5\right] e^{-x^{1/3}/2} \tag{3.13}$$

K_8 is the correction factor for low flow conditions, it is implemented using an interpolation procedure, and

$fn\{P, G, x\}$ is the look-up table value.

In order to predict the location of film dryout and hence the point of boiling transition. Two approaches[12] are implemented in TRACE, CISE-GE correlation (Eq 3.14) and Biasi CHF correlation (Eq 3.15) to calculate the *critical quality-boiling length*, x_{crit}. This is the axial distance from the location where the bulk fluid enthalpy reaches saturation to the dryout point. This feature is not available in the AECL-IPPE lookup table. $x_{crit,1}$ and $x_{crit,1}$ can be obtained with Eq 3.16, where k subindex can be 1 or 2.

$$x_{crit} = \frac{A \cdot L_B}{B + L_B} \frac{1.24}{R_f} \tag{3.14}$$

$$x_{crit} = \text{Max}\left(x_{crit,1}, x_{crit,2}\right) \tag{3.15}$$

$$x_{crit,k} = \frac{A_k \cdot L_B}{B_k + L_B} \frac{P_h}{P_w} \left(\frac{1}{R_f}\right)^{1/2} \tag{3.16}$$

Where

A and B are a functions of mass flux and pressure,

L_B is the boiling length,

R_f is the radial peaking factor,

P_h is the heated perimeter, and

P_w is the wetted perimeter.

Material properties

Another important issue for heat transfer is the determination of physical material properties (density, specific heat and thermal conductivity). In a reactor, this is especially important for fuel and clad materials. The fuel density is expressed using correlation Eq 3.17 and clad density with correlation Eq 3.18.

$$\rho = \frac{f_{TD}\left[\left(1 - f_{PuO_2}\right)\rho_{UO_2} + f_{PuO_2}\rho_{PuO_2}\right]}{1 + 3\frac{\Delta L}{L_0}} \tag{3.17}$$

Where

ρ is the fuel density (kg/m^3),

f_{TD} is the fraction of theoretical fuel density,

f_{PuO_2} is the weight fraction of PuO_2 in the fuel,

$\rho_{UO_2} = 10980$ kg/m^3,

[12] Both approaches extracted from TRAC-BF1 code.

T (K)	c_p J/kg-K
300	281
400	302
640	381
1090	375
1093	502
1113	590
1133	615
1153	719
1173	816
1193	770
1213	619
1233	469
1248	356

Table 3.3 – Zircaloy specific head as a function of temperature, experimental data by Brooks & Stansbury and Deem & Eldridge.

$\rho_{PuO_2} = 11460$ kg/m^3,

$\frac{\Delta L}{L_0}$ is the strain caused by thermal expansion, function of temperature.

$$\rho = \frac{6551.4}{1 + 2\left(\frac{\Delta L}{L}\right)_r + \left(\frac{\Delta L}{L}\right)_z} \tag{3.18}$$

Eq 3.18 takes into account the thermal expansion in the radial and axial directions.

The fuel and clad specific heat are function of the temperature. To obtain the specific heat for a fuel material, Eq 3.19 is used. Whereas for the clad material (Zircaloy), a linear interpolation is used based on experimental data shown in Table 3.3. For temperatures greater than 1248 K, the specific heat of Zircaloy is taken as a constant value of 356 J/kg-K.

$$c_p = 15.496\left[\frac{b_1 b_4^2 e^{b_4/T}}{T^2[e^{b_4/T} - 1]^2} + 2b_2 T + \frac{b_3 b_5}{b_6 T^2} e^{-b_5/b_6 T}\right] \tag{3.19}$$

Where b_i are constants depending on the fuel composition. In Bajorek et al. 2011 values of b_i for uranium dioxide and mixed oxides are presented.

The thermal conductivity for fuel material with theoretical density of 95% is calculated with Eq 3.20, and corrected according to Lucuta for the porosity in Eq 3.21. Whereas, the clad thermal conductivity is calculated using correlation Eq 3.22 for Zircaloy and Eq 3.23 for zirconium dioxide.

$$k_{95} = \frac{1}{A + a \cdot g_c + BT + f(bu) + (1 - 0.9e^{-0.04bu})g(bu)h(T)} + \frac{E}{T^2} e^{-F/T} \tag{3.20}$$

$$k = 1.0789 k_{95} \cdot \frac{f_{TD}}{1 + 0.5\,(1 - f_{TD})} \tag{3.21}$$

Where A, B, C, D, E, F, a and Q are constants given in Bajorek et al. 2011 and

k is the fuel thermal conductivity (W/m-K),

k_{95} is the thermal conductivity with theoretical density of 95%,

$f(bu)$ and $g(bu)$ are functions of burn-up,

$h(T)$ is a function of temperature,

f_{TD} is the fraction of theoretical fuel density, and

g_c is the gadolinium concentration.

$$k_{Zr} = 7.51 + 2.09 \cdot 10^{-2}T - 1.45 \cdot 10^{-5}T^2 + 7.67 \cdot 10^{-9}T^3 \tag{3.22}$$

$$k_{ZrO_2} = 1.96 - 2.41 \cdot 10^{-4}T + 6.43 \cdot 10^{-7}T^2 - 1.95 \cdot 10^{-10}T^3 \tag{3.23}$$

3.1.3 Core physics codes

3.1.3.1 PARCSv3.0 - U.S. NRC version

PARCS is the neutronic reference code for the NRC and therefore, it is the chosen neutron kinetic code used in this thesis. The same reasons to chose TRACE code, apply here. PARCS is a 3D neutronic reactor core simulator developed at Purdue University (PU), its first version was released in 1998, and perhaps it is one of the most neutronic codes used worldwide. It solves the transport equation with the diffusion approximation in steady and transient states for PWR and BWR. Either cartesian (two energy group) or hexagonal (any energy structure) fuel assemblies are defined. More information about PARCS can be found in its user's manual (Downar et al. 2010).

PARCS is coupled with TRACE5.0 (serial integration approach) and RELAP5 (parallel processing approach). Thus, accurate predictions for thermohydraulic and neutronic transients are simulated, see Section 3.2.1. If it is run alone, the user must introduce the initial conditions using 3D mappings in several files (fuel temperature, moderator temperature and moderator density). PARCS accept two types of cross section library formats: NEMTAB[13] (tabular approach) and PMAXS (polynomial fitting approach), see Section 3.3.1. In the NEMTAB format, PARCS interpolates (linearly or quadratically) the cross sections according to the feedback parameters for each node. Previously, cross sections must be homogenized and collapsed to a given energy structure, see Section 2.2.4. A brief summary of the **numerical methods** implemented in PARCS is given hereafter.

PARCS can solve spatial kinetic calculations involving the *eigenvalue problem* and the time-dependent neutron transport calculation. The transport equation must be discretized in space and time. For the temporal discretization, the theta-method and a second order analytic precursor integration technique are employed. This temporal discretization allows relative large time steps. For the spatial discretization, the nonlinear nodal method is employed along with the CMFD (see Section 2.2.3.1) and the local two-node problem are respectively solved. The temporal and spatial differencing of the spatial kinetic equation results in a fixed source type problem at every time step.

As it is shown before, the **eigenvalue problem** introduces k_{eff} into the diffusion equation to determine how far the system is from steady conditions (criticality). This is necessary to handle transient problems that do not start from a critical state. All transient problems require an initial steady state calculation to initialize the core conditions. If the k_{eff} were not introduced into the diffusion equation the initial core conditions

[13] See Appendix B for a detailed NEMTAB format explanation.

would not be steady and a poor convergence solution would be obtained.

For a cell m, the eigenvalue problem can be expressed as follows.

$$\begin{aligned}\frac{1}{\mathrm{k_{eff}}}\left(1-\boldsymbol{\beta}^m\right)\chi_g^p\sum_{g'=1}^{G}\nu\Sigma_{f,g}^m\phi_g^m+\chi_g^d\sum_{i=1}^{I}\lambda_i C_i^m+\\ \sum_{g'=1}^{G}\Sigma_{g'\to g}^m\phi_{g'}^m-\sum_{u=x,y,z}\frac{1}{h_u^m}\left(J_{g,u}^{m+}-J_{g,u}^{m-}\right)-\Sigma_{t,g}^m\phi_g^m=0\end{aligned} \tag{3.24}$$

$$\frac{1}{\mathrm{k_{eff}}}\beta_i^m\sum_{g'=1}^{G}\nu\Sigma_{f,g}^m\phi_g^m-\lambda_i C_i^m=0 \tag{3.25}$$

Where

m is the cell index,

g and g' are the collapsed energy group index, out of G total energy groups,

i is the number of delayed neutron group index, out of I total delayed neutron groups,

x, y and z are the cartesian directions,

h_u is the cell length in u-direction,

$J_{g,u}^{m+}$ and $J_{g,u}^{m-}$ are the surface average current on both sides of the interface,

$\mathrm{k_{eff}}$ is the effective multiplication factor or eigenvalue.

ϕ_g is the neutron flux,

$\Sigma_{g'\to g}$ is the total scattering cross section from group g' to g,

$\nu\Sigma_{f,g'}$ is the fission cross section multiplied by the average neutrons produced per fission,

$\Sigma_{t,g}$ is the total cross section,

$\boldsymbol{\beta}$ is the total delayed neutron fraction,

λ_i is the decay constant for neutron precursor group i,

χ_g^p is the spectrum for prompt neutrons,

χ_g^d is the spectrum for delayed neutrons,

v_g is the neutron velocity, and

C_i is the neutron precursor concentration group i.

Usually PARCS takes two neutron energy groups and 6 neutron precursor groups. However, it is also possible to use more groups (especially for fast reactors where 6 energy groups are usually used). Moreover, PARCS can apply ADFs for a better flux distribution approximation[14]. In a steady state calculation, the partial derivative with respect to time becomes zero and the prompt and delayed neutron effects are merged. If we define $\lambda = \frac{1}{k_{eff}}$, then, Eq 3.24 can be expressed using matrix notation.

$$M\phi = \lambda F\phi \tag{3.26}$$

Where M is termed *migration matrix* and contains all non-fission terms in Eq 3.24, F is termed *fission matrix* and contains the fission terms. Eq 3.26 can be solved using the *fission source iteration method*. The *Wielandt eigenvalue shift method* is used in PARCS to accelerate the convergence[15]. The Wielandt convergence depends on the eigenvalue step, δk. In general, fewer outer iterations are needed for small δk. However, the matrix to be solved becomes less diagonally dominant and the number of inner iterations increases. According to Downar et al. 2004, a value of $\delta k = 0.04$ is recommended.

For the **fixed source problem**, a *theta time discretization method* and a second order precursor integration technique are applied. If we define $R_g^{m,n}$ as the right hand side of equation Eq 3.24, then the theta time discretization method can be expressed as follows.

$$\frac{\phi_g^{m,n} - \phi_g^{m,n-1}}{\nu_g^m \Delta t} = \theta R_g^{m,n} + (1-\theta) R_g^{m,n-1} \tag{3.27}$$

Where m is the cell index, n is the iteration index and θ is a weighting factor ($0 \leq \theta \leq 1$). The *Crank-Nicholson* scheme assumes $\theta = 0.5$, it is second order accurate and allows relative large time steps for most transient calculations.

The solution of the *fixed source problem* consist in the simultaneous solution of the CMFD and local two-node problem. PARCS solves the CMFD penta-diagonal matrix using a Krylov subspace method and the *Bi-Conjugate Gradient Stabilized* (BiCGSTAB)[16] algorithm preconditioned[17] with BILU3D[18]. The local two-node problem is used to correct the discretization errors in the nodal interface currents resulting from the finite difference approximation in a coarse mesh. This can be solved using any nodal diffusion method. In PARCS, the *Nodal Expansion Method* (NEM) (see Section 2.2.3.3) and *Analytic Nodal Method* (ANM) (see Section 2.2.3.2) are implemented. On one hand, the ANM is unstable for cases where k_∞ and k_{eff} are close. On the other hand, NEM kernel does not involve a particular solution, thus it is numerically stable under all conditions. Besides, the local two-node problem solved with NEM uses an analytic solution (obtained with symbolic manipulation). Thus, the process is computationally more efficient than using a direct or iterative matrix solver. However, this limits the number of groups to that introduced to solve the symbolic equations. A third option is available to solve the local two-node problem, the hybrid ANM/NEM scheme. In this scheme a criterion is specified for a given ϵ, Eq 3.28. Any node satisfying this criterion is labeled as near-critical node and therefore, the NEM solution is calculated. For nodes that do not satisfy the criterion, the ANM method is applied.

$$\delta = \left| \frac{k_\infty}{k_{eff}} - 1 \right| < \epsilon \tag{3.28}$$

[14] The diffusion equation is not accurate near interfaces or boundaries, see Section 2.2.3.

[15] Wielandt method is used in PARCS because the Krylov CMFD solver developed for the solution of the transient fixed source problem can then be used with only minor corrections for the eigenvalue calculations (Downar et al. 2004). Other possible method to accelerate the convergence, but not implemented in PARCS, is the *Chebyshev polynomial method*.

[16] The *Conjugate Gradient* method can be used to construct the Krylov subspace. However, this method is only valid for symmetric positive defined matrices. BiCGSTAB extends this method and suppresses this limitation.

[17] A preconditioned matrix transforms the linear system into a new system that converges faster.

[18] It takes advantage of the diagonal dominance associated with the CMFD matrix.

For high accuracy applications in which the diffusion theory is not valid, PARCS can solve the transport equation using the P_N transport method using the SP_N kernel[19], see Section 2.2.2.1. The SP_N kernel implemented in PARCS is truncated for $N > 3$. The SP_3 uses a *Fine-Mesh Finite Difference* (FMFD) method (pin by pin). However, under certain circumstances, this method can be inefficient in terms of accuracy and time. Therefore, the *Nodal Expansion Method* (NEM) is also implemented to solve the SP_N approach. This method is more computationally efficient than FMFD. Moreover, in PARCS the SP_3 NEM equations are defined to resemble the NEM equations for the diffusion equation. Thus, the same subroutines can be used with only minor modifications.

In order to solve reactors with hexagonal assemblies (VVER), PARCS has an **hexagonal nodal method**. The *Triangle-based Polynomial Expansion Method* (TPEN) method is used with a CMFD acceleration scheme. The TPEN method solves two transverse-integrated neutron diffusion equations for a hex-octahedron node. One is the radial equation defined for a hexagon and the other is the axial equation defined for the z-direction. The radial problem is solved by splitting the hexagon into six triangles and then by employing a polynomial expansion of flux within each triangle.

PARCS also allows **pin power reconstruction**. The nodal methods are based on homogenized nodal cross sections and therefore, the resulting neutron flux does not reflect any intranodal heterogeneity. The process to recuperate the intranodal flux from the homogenized nodal flux is termed pin power reconstruction or "dehomogenization" process. This process is based on the assumption than the intranodal flux can be estimated by the product of the nodal homogenized flux and a local heterogeneous function. The heterogeneous functions accounts for heterogeneities caused by water holes, burnable absorber pins, enriched fuel, etc. Therefore, the heterogeneous function is different for each fuel assembly type and must be generated by a lattice physics code as nodal cross sections are generated. The intranodal flux distribution is given as 1D flux shape for each spatial dimension. This limitation arise from the fact that most nodal methods employ integration procedures in one dimension, such as presented in Eq 2.35. Pin power reconstruction methods assume that the axial and radial flux dependences of the intranodal flux are separable and thus, these methods are based on 2D geometries. Two main approaches are available, one based on polynomial expansions and the other using analytic functions.

The first approach approximates the radial intranodal flux dependence using 2D *polynomials expansions* and some exponential functions applied only to the thermal energy group. In modern derivations of this method, 13 different terms are used in the expansion. Therefore, 13 constrains must be used: the node average flux, four surface average fluxes, four currents and four flux values at each corners. The node average flux, the surface average fluxes and the currents are obtained with the lattice physics code. However, the corner flux values must be approximated using a polynomial. The second approach uses *analytic functions* for the expansion, each analytic function is the solution of the 2D diffusion equation. In contrast to the polynomial expansion approach, the analytic function approach involves coupling between the flux expansion on both energy groups, thus it is more accurate. Because of this enhanced accuracy, PARCS uses the analytic expansion approach for pin power reconstruction calculations. However, the boundary conditions are changed with respect to the original approach. The surface average current is used instead of the surface average flux. The change is made due to two reasons (i) if the surface average flux is used, the nodal neutron balance is not ensured with the resulting 2D intranodal flux and (ii) surface average current is easily obtained based on the converged CMFD solution, while the surface average flux requires additional calculations.

[19] Nonetheless, the SP_N is not valid for hexagonal geometries.

Other models for a complete neutronic analysis are available in PARCS, these include:

- Critical boron concentration search. It is the boron concentration corresponding to $k_{eff} = 1$ and is obtained by a linear interpolation. Two points must be known in advance (ppm_1, k_{eff1}) and (ppm_2, k_{eff2}). PARCS proceeds iteratively based on the two most updated points.

$$ppm = ppm_2 + \frac{1 - k_{eff2}}{k_{eff1} - k_{eff2}}(ppm_1 - ppm_2) \tag{3.29}$$

- Fuel depletion analysis. Cross sections in PMAXS format could include the burn-up as additional fitting parameter. PARCS can use this feature to advance the cross section dependence on the burn-up for each time step. Therefore, the analyst is able to (i) deplete the core to find a typical "equilibrium" condition and (ii) obtain burn-up distribution and the associated cross sections. This capability was implemented in version 2.5. See Section 3.3.1 for PMAXS library format.

- Rod cusping correction. Rod cusping effects are observed when the k_{eff} varies in a wavy shape. The intranodal flux distribution can be largely distorted in nodes where the control rod is partially inserted due to the presence of the strong thermal absorber. In this case, the volume weighted scheme to predict homogenized nodal cross sections can lead to significant errors during the core calculation. This effect is typically seen when the control rod insertion depth is changed. PARCS corrects this effect solving a three-node problem by the FMFD scheme for partially rodded nodes.

- Adjoint calculation. The adjoint solution of the initial eigenvalue problem is necessary to compute the dynamic reactivity during the transient calculation. The adjoint problem within the nonlinear nodal method can be easily calculated by the transpose of the CMFD coefficient matrix for the forward solution. The adjoint CMFD coefficient matrix is solved using the same Wielandt shift method used to obtain the forward solution.

- Decay heat. After a reactor is shut down, important amounts of heat are continuously being released due to radioactive decay of fission products and transuranic elements. The amount of heat released depends on the concentration of fission products and the reactor history. The total volumetric heat density for the decay heat is given using next equation.

$$q_t(\boldsymbol{r}, t) = (1 - \alpha_T) \sum_{g=1}^{G} \kappa_g \Sigma_{f,g}(\boldsymbol{r}, t)\phi_g(\boldsymbol{r}, t) + \sum_{i=1}^{I} \zeta_i D_i(\boldsymbol{r}, t) \tag{3.30}$$

  Where

  $q_t(\boldsymbol{r}, t)$ is the total volumetric decay heat density,
  $D_i(\boldsymbol{r}, t)$ is the concentration of decay heat precursors in decay heat group i,
  ζ_i is the decay constant in decay heat group i,
  $\Sigma_{f,g}(\boldsymbol{r}, t)$ is the fission cross section,
  $\phi_g(\boldsymbol{r}, t)$ is the nodal average flux,
  α_T is the total fraction of the fission energy appearing as decay heat, $\alpha_T = \sum_{i=1}^{I} \alpha_i$, and
  κ_g is the energy released by fission.

- Xenon/Samarium treatment. Xenon and Samarium produced during the reactor lifetime affect the reactor power, see Section 2.2.6.4. PARCS is able to track their concentration and update the absorption macroscopic cross section accordingly.

3.1.3.2 SIMULATE-3

SIMULATE-3 has capabilities for steady state coupled thermohydraulic-neutronic and core-follow calculations. It performs calculations only in steady state and at core level (chan to chan). According to its user's manual (DiGiovine et al. 1995) it uses two energy groups for the analysis of both PWRs and BWRs and employs fourth-order polynomial representations of the intranodal flux distribution in both groups. The types of calculations performed by the code are:

- Depletion in 2D or 3D.
- Symmetry options are: 1/8, 1/4, 1/2 or full core.
- Reload shuffling.
- Reactivity coefficient calculation.
- Rod worth calculation (REA).
- Xenon transient.
- Criticality searches.

SIMULATE uses cross sections from CASMO results through the linkage code TABLES-3. TABLES-3 can be used to add or delete data from the binary library. In SIMULATE, cross sections are expressed as a summation of partial cross sections, as in Eq 3.31. TABLES-3 tabulates partial cross sections as a function of up to three parameters a, b and c, see Eq 3.32. Then, this data is used to fit the cross sections as a function of many variables. The general form of the fitting equation follows Eq 3.33, where $\Sigma(A_0, B_0, \ldots, Z_0)$ defines the cross section at the base conditions.

$$\Sigma_i = \sum_{\alpha} \Delta\Sigma_{i\alpha} \tag{3.31}$$

$$\Delta\Sigma_{i\alpha} = F_{i\alpha}(a, b, c) \tag{3.32}$$

$$\begin{aligned}\Sigma(A, B, \ldots, Z) = \Sigma(A_0, B_0, \ldots, Z_0) &+ \int_{A_0}^{A} \frac{\partial}{\partial A}\Sigma(A, B_0, \ldots, Z_0)dA \\ &+ \int_{B_0}^{B} \frac{\partial}{\partial B}\Sigma(A, B, \ldots, Z_0)dB + \ldots \\ &+ \int_{Z_0}^{Z} \frac{\partial}{\partial Z}\Sigma(A, B, \ldots, Z)dZ\end{aligned} \tag{3.33}$$

Pin reconstruction and kinetic data in SIMULATE are obtained with a similar expression, Eq 3.34. However, the exposure, Exp, is explicitly taken into account because it has a major effect over these parameters.

$$\begin{aligned}P(A, B, \ldots, Z) = P(Exp, B_0, \ldots, Z_0) &+ \int_{B_0}^{B} \frac{\partial}{\partial B}P(Exp, B, \ldots, Z_0)dB + \ldots \\ &+ \int_{Z_0}^{Z} \frac{\partial}{\partial Z}P(Exp, B_0, \ldots, Z)dZ\end{aligned} \tag{3.34}$$

3.1.4 Uncertainty propagation codes

3.1.4.1 SCALE6.2.1/TSUNAMI

TSUNAMI (**T**ools for **S**ensitivity and **Un**certainty **A**nalysis **M**ethodology **I**mplementation in **One** **D**imension) is the SCALE module for deterministic U&S analysis, except the first response -which is always k_{eff}- other system responses are expressed as ratios. Responses are based on cross sections, nuclear reactions and flux distribution. To achieve the U&S analysis, TSUNAMI propagates the uncertainty in the nuclear data -contained in the master cross section library- to obtain the uncertainty in the defined system responses. TSUNAMI makes use of the covariance library, *COVLIB*, predefined in SCALE. This library contains uncertainty data for 2587 nuclide-reaction pairs and sensitivity coefficients (in matrix format) for 2546 nuclide-reaction pairs, both discretized in 44 energy groups. TSUNAMI expresses the sensitivity data either as a function of energy (sensitivity profiles) or as a sensitivity energy-integrated coefficients (integration over the sensitivity profile).

TSUNAMI obtains the sensitivity decomposed in two components, implicit and explicit data. The difference can be explained if we divide the sensitivity calculation into two steps, (1) sensitivity of the system response due to the resonance self-shielded cross-section data and (2) sensitivity of the resonance self-shielded cross-section data to the data input to the resonance self-shielding calculations. The former process is the explicit component of sensitivity, the latter is the implicit component. Total sensitivity is the sum of both components. SAMS (**S**ensitivity **A**nalysis **M**odule for **S**CALE) module calculates the implicit and explicit sensitivity data based on the results of the direct and adjoint transport problem and the covariance library, see Eq 3.40. It is also possible to exclude the implicit sensitivity from the calculations. Some cross section covariance or uncertainty data are too large or are not specified for all nuclides-reaction pairs. SAMS also allows the customization of some parameters in order to cope with this problem. The user can introduce the standard deviation for cross section nuclide-reaction pairs whose covariance data is too large or does not exist in the covariance library. The new standard deviation value can be specified for thermal, intermediate and fast energy regions. A correction when the uncertainty or the implicit sensitivity are too large or the option for a user-defined covariance library are also available.

First, TSUNAMI runs one direct transport solution and one generalized adjoint solution. Then, the sensitivity (implicit/explicit) and uncertainty calculations for the first response, k_{eff}, are performed by SAMS module using the *Generalized Perturbation Theory* (GPT). If more than one system response is defined, one adjoint transport solution per each system response is run (there is no need to run the forward solution again). The transport module used is defined by the user according to the model dimensions -1D (XSDRNPM), 2D (NEWT) or 3D (KENO)-. Fig. 3.5 shows the general flow diagram for a TSUNAMI calculation using XSDRNPM 1D transport solver.

Sensitivity coefficients are obtained by SAMS module. These coefficients are defined in a way that when multiplied by the variation of the correspondent input parameter (e.g. cross section), they quantify the sensitivity in the output parameter whose sensitivity is referred to (e.g. k_{eff}). This is termed *uncertainty propagation* and can be expressed as

$$S\left(k_{eff}, \sigma^i_{x,g}\right) = \frac{\delta k_{eff}/k_{eff}}{\delta\sigma^i_{x,g}/\sigma^i_{x,g}} \tag{3.35}$$

where the subscript i denotes nuclide, x denotes the nuclear reaction and g the energy group. Using the *Conventional Perturbation Theory* (CPT) the total variation of k_{eff} (or other integral parameter) is defined as the sum of all individual variations for each input parameter.

$$\frac{\delta k_{eff}}{k_{eff}} = \sum_i S\left(k_{eff}, \sigma^i_{x,g}\right)\frac{\delta\sigma^i_{x,g}}{\sigma^i_{x,g}} \tag{3.36}$$

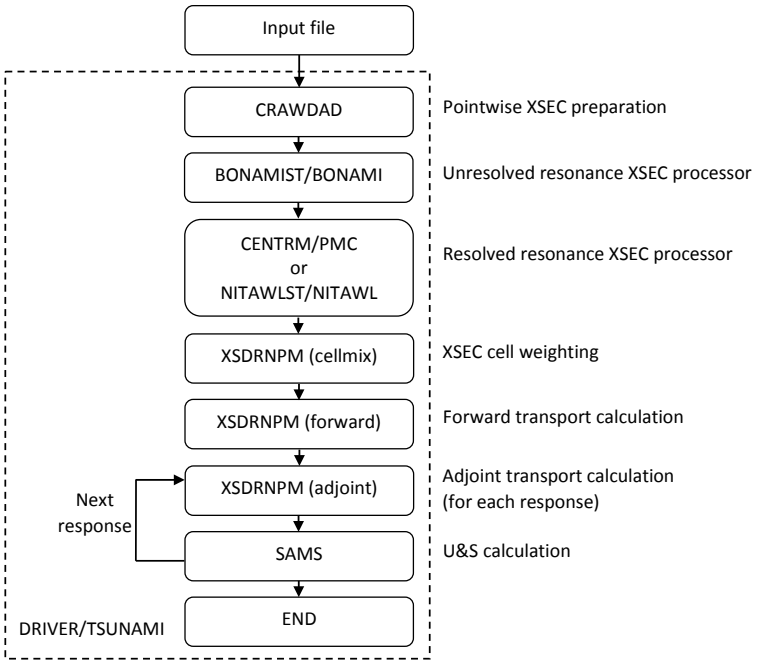

Fig. 3.5 – TSUNAMI flow diagram using XSDRNPM 1D transport solver, extracted from Edenius et al. 1995.

The GPT, which is an extension of CPT, makes use of the solution of both the direct and the adjoint -or inverse- problem. GPT defines the sensitivity coefficient of a given output parameter, R, to a specified cross section $\sigma^i_{x,g}$ as

$$S(R,\sigma^i_{x,g}) = \frac{\sigma^i_{x,g}}{R}\frac{dR}{d\sigma^i_{x,g}} = \frac{\sigma^i_{x,g}}{R}\left\{\frac{\partial R}{\partial \sigma^i_{x,g}} - \left\langle \Psi^*, \left(\frac{\partial A}{\partial \sigma^i_{x,g}} - \frac{1}{\mathrm{k_{eff}}}\frac{\partial F}{\sigma^i_{x,g}}\right)\Phi\right\rangle - \left\langle \Psi, \left(\frac{\partial A^*}{\partial \sigma^i_{x,g}} - \frac{1}{\mathrm{k_{eff}}}\frac{\partial F^*}{\sigma^i_{x,g}}\right)\Phi^*\right\rangle\right\} \tag{3.37}$$

where

R is the integral response whose sensitivity is evaluated,

$\sigma^i_{x,g}$ is the cross section (i nuclide, x reaction and g group) whose uncertainty is being propagated,

$\mathrm{k_{eff}}$ is the multiplication factor,

Ψ and Ψ^* are the importance function for the direct and adjoint problem,

Φ and Φ^* are the flux distribution for the direct and adjoint problem,

A and A^* are the absorption operators for the direct and adjoint problem and

F and F^* are the fission operators for the direct and adjoint problem.

This sensitivity coefficient can be divided into two different effects, direct and indirect.

$$S_{DIR}(R,\sigma^i_{x,g}) = \frac{\sigma^i_{x,g}}{R}\frac{\partial R}{\partial \sigma^i_{x,g}} \tag{3.38}$$

$$S_{IND}(R,\sigma^i_{x,g}) = \frac{\sigma^i_{x,g}}{R}\left\{ -\left\langle \Psi^*, \left(\frac{\partial A}{\partial \sigma^i_{x,g}} - \frac{1}{\mathrm{k_{eff}}}\frac{\partial F}{\sigma^i_{x,g}}\right)\Phi\right\rangle - \left\langle \Psi, \left(\frac{\partial A^*}{\partial \sigma^i_{x,g}} - \frac{1}{\mathrm{k_{eff}}}\frac{\partial F^*}{\sigma^i_{x,g}}\right)\Phi^*\right\rangle \right\} \tag{3.39}$$

On one hand, the direct effect accounts for the uncertainty variation of R due to the cross section that are *directly* related with R. On the other hand, the inverse effect accounts for the uncertainty variation of R due to the cross section that are *implicitly* related with R.

If we define a vector S_R, whose elements are the individual sensitivity for all available $\sigma^i_{x,g}$ (Eq 3.35 for CPT or Eq 3.37 for GPT), the total variance for the system response, σ^2_R, is defined by the so-called "sandwich formula"

$$\sigma^2_R = S_R C S^T_R \tag{3.40}$$

where C is the covariance matrix for the individual cross sections contained in vector S_R (S^T_R denotes the transposed vector). Moreover, the covariance for the system response R due to two particular reactions, x and y, and two different nuclides, i and j, can be computed as

$$\sigma^2_{R^{i,j}_{x,y}} = S_{R,\sigma^i_x} C_{\sigma^i_x,\sigma^j_y} S^T_{R,\sigma^j_y} \tag{3.41}$$

The $C_{\sigma^i_x,\sigma^j_y}$ matrix is simply read from the covariance library, where covariance matrices for different reactions and nuclides are stored. Vectors S_{R,σ^i_x} and S_{R,σ^j_y} must be computed by the U&S analysis code.

Unfortunately, TSUNAMI does not allow branch calculations and depletion calculations are not straightforward. Therefore, it is not possible to propagate the homogenized and/or collapsed cross section uncertainty and cannot be used for the purpose of this thesis. As an example in the literature, Díez et al. 2013 compares TSUNAMI and MCNPX-2.7 $\mathrm{k_{eff}}$ uncertainty for the *Three Mile Island* (TMI) model in the OECD/NEA benchmark framework. Extensive information can be found in TSUNAMI user's manual for 1D models, Rearden et al. 2011, and Rearden 2011 for 3D models.

3.1.4.2 SCALE6.2.1/SAMPLER

SAMPLER is the new module in SCALE6.2 for stochastic UQ, unfortunately SA is still not available in SCALE6.2.1. SAMPLER provides UQ for nuclear data and input parameters (such as geometry or physical quantities). The uncertainty propagation is achieved applying (stochastic) perturbation factors to the parameters whose uncertainty is being propagated. The process is repeated for a defined number of sampled perturbations. SAMPLER can be used not only for transport sequence in SCALE, but also for other modules such as Monaco[20]. However, nuclear data cannot still be sampled for *Continuous Energy* (CE) MC calculations (CE-KENO and CE-Monaco). SAMPLER also provides parametric capability to determine the system response over a range of a user defined input parameter, e.g. geometrical distances, densities,

[20] Monaco is a general-purpose, fixed-source, multigroup Monte Carlo shielding code for SCALE

temperatures, isotope concentrations...

The module TSUNAMI utilize a different approach for U&S analysis based on GPT. Both modules, deterministic TSUNAMI and MC SAMPLER, have their advantages and disadvantages. Nevertheless, the recommendation is to use SAMPLER in any of these situations.

- Studies with a high number of system responses. TSUNAMI realizes an adjoint calculation for each response. This increases exponentially the computational time as the number of responses increases. On the contrary, with SAMPLER, the number of simulations is independent of the number of system responses.
- If the code in use does not have adjoint calculation capability. The implementation of such capability requires an important effort.
- If depletion capability is required, TSUNAMI is not able to perform burn-up calculations.
- Cases for which first order perturbation theory is not valid.

The Medusa module, provided by XSUSA program, was used to generate a set of 1000 perturbation factors for the multigroup cross section libraries. The perturbations were generated assuming normal *Probability Distribution Functions* (PDFs) and random sampling (Williams et al. 2013b) and covariances given by the covariance library provided by SCALE. The perturbation are defined as multiplicative factors for each nuclide i, nuclear reaction x and energy group g.

$$Q^i_{x,g} = 1 + \frac{\Delta\sigma^i_{x,g}}{\sigma^i_{x,g}} \tag{3.42}$$

Where

$Q^i_{x,g}$ is the perturbation factor for a specific isotope, reaction and energy group, and

$\frac{\Delta\sigma^i_{x,g}}{\sigma^i_{x,g}}$ is the relative covariance obtained from the covariance library.

Thousand different perturbations are defined and are stored in a perturbation library provided by SCALE developers. The perturbation library contains perturbation factors for 406 isotopes with different nuclear reactions, they are discretized in 44 energy groups. The immediate advantage is that perturbations do not need to be recomputed for each SAMPLER case. Nonetheless, the user does not have the option to modify uncertainty information for each cross section.

In this thesis, instead of using the default perturbation library, it is decided to proceed with an in-house perturbation library. Therefore, the user is free to choose any PDF and/or the sampling method to generate the new perturbations -using DAKOTA statistical tool-. As indicated in Williams et al. 2013b, perturbations in the original perturbation library are randomly generated and follow a normal PDF with mean one and covariance given by the covariance library. These specifications are used to generate the new perturbations. Although the new library follow the same specifications as the default SCALE library, the generation of a new library is intended as an added feature for future uncertainty studies –in which individual PDFs or the sampling method can be changed-.

SAMPLER can perturb (1D) cross sections and Bondarenko self-shielding factors. Nonetheless, (2D) scattering distributions (also included into the master library) cannot be perturbed because their covariance data is not provided in the covariance library. Bondarenko factors and problem-independent cross sections

are obtained from the same master library. Thus, perturbations used for self-shielding calculations (Bondarenko factors and continuous energy cross sections) must be consistent with perturbations made to the problem-independent cross sections. This can be achieved using the same perturbation, $Q^i_{x,g}$, to obtain the infinite diluted multigroup cross sections, $\sigma^i_{x,g}$, Bondarenko factors, $f^i_{x,g}(\sigma_0, T)$, and continuous energy cross sections, $\sigma^i_x(E)$.

$$\sigma'^i_{x,g} = Q^i_{x,g}\sigma^i_{x,g} \tag{3.43}$$

$$f'^i_{x,g}(\sigma_0, T) = f^i_{x,g}\left(\frac{\sigma_0}{Q^i_{x,g}}, T\right) \tag{3.44}$$

$$\sigma'^i_x(E) = Q^i_{x,g}\sigma^i_x(E) \quad \text{for} \quad E \in g \tag{3.45}$$

After all perturbations are applied and a used specified number of runs are completed, SAMPLER computes some useful statistical data. For example: variance (uncertainty), covariance matrices, correlation matrices, histograms, scatter plots... The main drawback in SAMPLER in SCALE6.2.1 is that it does not calculate sensitivity coefficients, while TSUNAMI code has this capability. Extensive information can be found in SAMPLER user's manual (Williams et al. 2013a). Lot of studies related with UQ can be found in the literature. This is partly possible due to the UAM-OECD benchmark for U&S analysis in LWR. Yankov et al. 2012 performs a UQ comparing TSUNAMI and SAMPLER for the TMI model in the OECD/NEA benchmark framework. SCALE6.2.1 version and its module SAMPLER with TRITON/NEWT 2D lattice code are used in this thesis for nuclear data uncertainty propagation purposes.

3.2 Coupling of thermohydraulic and 3D neutronic codes

The physics behind the phenomena occurring in a nuclear reactor can be represented by thermohydraulic or neutronic codes. However, for some phenomena, both physics are strongly tight and a single code is not enough to represent the real problem. In these cases, thermohydraulic and neutronic codes must be run in coupled mode. This means that they exchange information iteratively at specific points in the calculation. A coupled code should provide solution for a specific problem with a reasonable time while keeping the accuracy at specified levels. Several characteristics are defined for a coupling methodology, the next list is specific for thermohydraulic and neutronic codes.

- Coupling approach. Two different approaches. On one hand, *serial integration* requires harder modification of both codes. Usually the neutronic code is included in the thermohydraulic code as a subroutine, this gives the final code more versatility and stability. On the other hand, with *parallel processing* both codes are run independently and they exchange data using PVM[21] environment or MPI[22] protocol. One advantage of the latter approach is that the codes are isolated and can be maintained independently. One example of parallel processing coupling is RELAP5/PARCS, more information about this coupling can be found in Martínez-Murillo et al. 2011.
- Spatial mesh overlays. A mapping for thermohydraulic and neutronic cells must be provided, a node-to-node mapping is more intuitive but other options are available. If different meshes are used, a weighting factor representing the power fraction for each thermohydraulic cell must be included. Mapping for BWR stability studies are shown to be more harsh (Miró et al. 2002) since modal analysis methods -especially in regional instabilities- are needed. Another factor affecting the mesh mapping is related with the thermohydraulic channel collapse. Computational effort could be high if the core is

[21] *Parallel Virtual Machine* (PVM) is a software package.
[22] *Message Passing Interface* (MPI) is a library.

modeled channel by channel (especially in BWR). A node optimization could be performed to alleviate computational resources, similar fuel assemblies could be collapsed into one thermohydraulic channel while maintaining accuracy (for example with the SIMTAB methodology). The criteria to collapse *similar* channels are based on different variables: burn-up, fuel type, initial fuel composition, reactor history... Nonetheless, collapse has the effect to smooth the reactivity and power distribution. Barrachina et al. 2010b shows this effect on different collapsed models and compares them to a non-collapse model using RELAP5/PARCS coupled code.

- Coupled time-step algorithms. One possible approach is to perform thermohydraulic and neutronic calculations at each time step. However, this is not computationally efficient since thermohydraulic phenomena occur at a much slower time-scale than neutronic phenomena. Thus, one of the codes is defined as the master (normally the thermohydraulic code), and the slave code is run at a specified logic: (i) every n time steps in the master code, or (ii) when a previously specified change is detected in an important variable (fuel temperature, power, moderator density, etc.).

- Coupling numerics. On one hand, *implicit schemes* are more difficult to implement and more computational effort is needed. However, they allow larger time steps and are unconditionally stable (but not necessarily accurate). On the other hand, *explicit schemes* are easier to program but its time step must be limited according to the *Courant limitation*[23]. Otherwise, the solution could be physically unrealistic[24] and problems of numerical instability arise. A third scheme could be used, a *semi-implicit scheme* makes use of previous schemes, takes advantage of their properties and obtains better accuracy.

- Coupled convergence schemes. Convergence is achieved when the main variables change less than a user prefixed value. Usually these variables are thermohydraulic variables, such as temperature, pressure, void fraction...

3.2.1 TRACEv5.0/PARCSv3.0 coupled code

The effort made to couple TRACE thermohydraulic code and PARCS neutron kinetic code provides a professional tool for thermohydraulic-neutronic analyses with great accuracy. TRACE5.0P3/PARCSv3.0 coupled code is used in this thesis for transient analysis and uncertainty propagation purposes. PARCS code is integrated into TRACE as a subroutine, thus the couple follows a serial integration approach. This gives the final code more stability compared to previous versions (where the use of an interface, such as PVM, was required). Both codes exchange information at certain points in the calculation flow. The process is shown in Fig. 3.6. First, TRACE starts the calculation and obtains the main thermohydraulic variables, among them the fuel and moderator temperatures and moderator density. Then, TRACE sends this data to PARCS, which is now able to calculate the power distribution. Finally, this data is send back to TRACE and a new iteration starts for a new time step. The process followed by RELAP/PARCS coupled code is very similar to the process described hereafter.

The power calculated by PARCS is distributed among the thermohydraulic cells according to the mapping correspondence between the thermohydraulic and neutronic meshes. This information is given in the *MAPTAB* file. The mapping information in this file can be written as a table or as a matrix. Table format is valid for all components, whereas matrix format is only valid for cores defined using chan 1D components (only BWR) or using only one 3D vessel. Each format is divided into the hydraulic-neutronic mapping and

[23] Courant number is defined as $C = \frac{vdt}{dx}$. The Courant limitation ($C \leq 1$) restricts the fluid to flow more than one computational cell per time step.

[24] Explicit schemes define thermohydraulic variables in one cell as function of the same variable in the neighbor cells. Thus, unrealistic results are obtained if the Courant limitation is violated. As an exception, SETS method is provided in TRACE thermohydraulic code, see Section 3.1.2.3

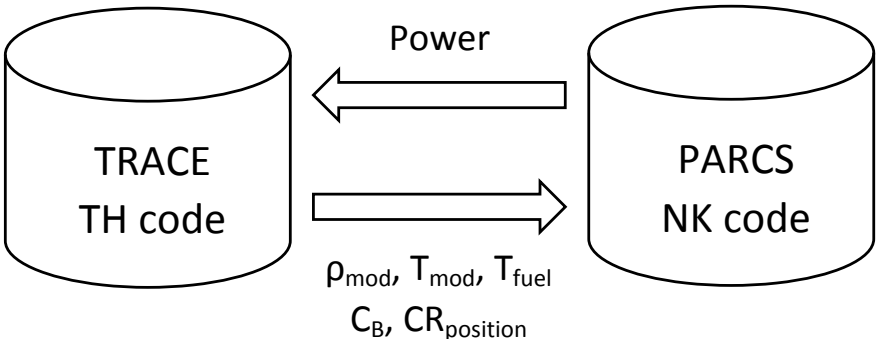

Fig. 3.6 – Information exchanged by TRACE/PARCS coupled code.

Column	Type	Meaning
1	integer	PARCS cell number. Cells are numbered first increasing the x-axis, then the y-axis, and finally the z-axis. Cells outside the reflector zone (not coupled to TRACE) are not numbered.
2	integer	Hydraulic ID component in TRACE model.
3	integer	Axial cell for 1D components or axial plane for vessel 3D components.
4	integer	For 1D components this should be 0. For vessel 3D component, this is the radial cell into the axial plane specified in the third column. For cartesian vessels, cells are numbered first increasing the y-axis and then the x-axis. For cylindrical vessel, first the θ-axis is increased and then the r-axis. TRACE cells that are not coupled to PARCS are numbered.
5	real	Weighting volume fraction if one PARCS cell is coupled with several TRACE cells. All weighting factors assigned to the same PARCS cell must sum either one or zero. If the sum is equal to 0, then this neutronic cell is not connected to any thermohydraulic cell.

Table 3.4 – MAPTAB `TABLE1` card: hydraulic-neutronic mapping.

the thermo-neutronic mapping. Tabular format for both mappings are explained in detail in Table 3.4 and Table 3.5.

Mapping file with matrix format is easier, but with the component limitation stated before. Three main cards are used in the MAPTAB matrix format, these are explained hereafter.

- `VOLRMAP1` card: it indicates only if the hydraulic components used are 1D chans or a 3D vessel. The word `chan` or `vessel` is used.
- `VOLRMAP2` card: contains a matrix of integers with the hydraulic ID components as elements. However, one extra row (top) and column (left) are added showing the row or column index in the neutronic plane. PARCS cells that are not coupled are filled with any character besides 0-9, usually an asterisk (*).
- `VOLRMAP3` card: contains a matrix of real numbers with the radial weighting factor for each hydraulic cell specified in `VOLRMAP2` card. One extra row (top) and column (left) are added showing the row or column index in the neutronic plane. PARCS cells that are not coupled are filled with any character besides 0-9, usually an asterisk (*).

Column	Type	Meaning
1	integer	PARCS cell number. Cells are numbered first increasing the x-axis, then the y-axis, and finally the z-axis. Cells outside the reflector zone (not coupled to TRACE) are not numbered.
2	integer	Thermal (heat structure) ID component in TRACE model.
3	integer	Rod group number for the heat structure specified in the first column.
4	integer	Axial cell for the rod specified before.
5	real	Weighting volume fraction if one PARCS cell is coupled with several TRACE cells. All weighting factors assigned to the same PARCS cell must sum either one or zero. If the sum is equal to 0, then this neutronic cell is not connected to any thermohydraulic cell.

Table 3.5 – MAPTAB `TABLE2` card: thermo-neutronic mapping.

A couple of extra cards complete the MAPTAB file (both formats). The first card is the `DOPL` (optional) card to calculate the Doppler fuel temperature feedback. It contains only one real number, ω, representing the weighting of fuel centerline, T_f^0, and fuel surface, T_f^c, to obtain the Doppler temperature, $T_{Doppler}$.

$$T_{Doppler} = (1-\omega)T_f^0 + \omega T_f^c \tag{3.46}$$

The second card `REFLPROP` indicates the initial conditions for the reflector zone, in this order: coolant temperature (K), fuel temperature in (K), coolant density (kg/m^3), void fraction and soluble born concentration (ppm).

One more feature is worth to mention here. PARCS has the capability to generate an automatic MAPTAB file under specific TRACE models.

- Cylindrical TH volumes with the 3D vessel component when no mapping information is specified.
- Cylindrical TH volumes with the 3D vessel component when a radial mapping specified.
- Multiple BWR chan 1D components to a 3D neutronic core. Radial mapping is required.
- BWR chan 1D component(s) to a 1D neutronic core.

More information about the MAPTAB file and PARCS coupling can be found in PARCS user's manual (Downar et al. 2010).

A schematic procedure for a TRACE/PARCS simulation can be seen in Fig. 3.7. As seen in this figure, three different steps are run to perform a transient simulation. These are *Steady State Alone* (SSA), *Coupled Steady State* (CSS) and *Coupled Transient* (CTR). The first step (SSA) makes use only of the thermohydraulic code, whereas the intermediate (CSS) and later steps (CTR) are coupled with the neutronic code. Both, the CSS and CTR, start using the thermohydraulic solution of the previous steps (restart). However, only the CTR uses the restart for the neutronic model in the CSS. PARCS can also be coupled with RELAP5 thermohydraulic code, the methodology is similar, but it makes use of a parallel interface (PVM). Other examples of thermohydraulic-neutronic coupled codes are TRAC-BF1/VALKIN (Miró et al. 2006b) or SIMTRAN with SIMULA/COBRA (Aragonés 2008).

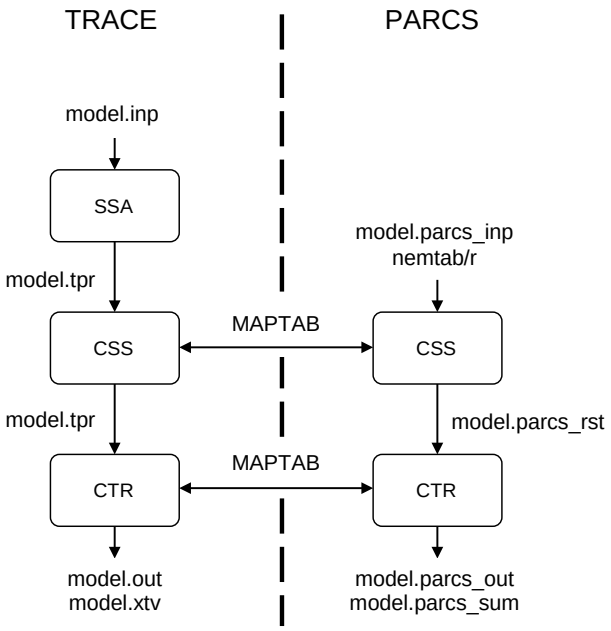

Fig. 3.7 – Diagram for TRACE/PARCS coupled code.

3.3 Cross section library generation for neutron diffusion codes

The main concern in cross section library generation is related with the feedback parameters. How to efficiently represent their effect in the generated cross sections is currently a topic under study. This is accomplished using branch calculations where the feedback parameters are "instantaneously" changed. There are three important features that the user needs to specify. Extensive information about these concerns and others can be found in Wang et al. 2013.

- Feedback parameters to be included. Fuel temperature and moderator density -or void fraction- are necessary (besides control rod condition). However, moderator temperature is not generally included as a library dependence. It is argued that this dependence is included in the moderator density, provided constant pressure and a single phase (Sánchez-Cervera et al. 2014b). Another possible dependence is the boron concentration (Martínez-Murillo et al. 2011), but it can be omitted for normal operations and in PWR if boron is not diluted. The burn-up can also be included, but its effect is not significant unless the transient simulation in the core physics code is extremely large or the reactor power is very high.
- Number of points for each feedback parameter. The core physics code interpolates (NEMTAB) -or use the polynomial approximation (PMAXS)- the cross sections based on the feedback parameters for each node. Therefore, with increasing number of points, more accuracy is obtained with the interpolation or polynomial fitting process. The drawback is that computational time in the cross section generation code is increased exponentially. As a general rule, more points are needed for the tabulated libraries for a given accuracy (Hueso et al. 2011).
- The range for the feedback parameters. The range must be enough to simulate all desired transient using the core physics code. If some feedback parameter exceeds its range, an unacceptable error is produced and the neutronic library should be generated again with an increased range for the extrapolated feedback parameter.

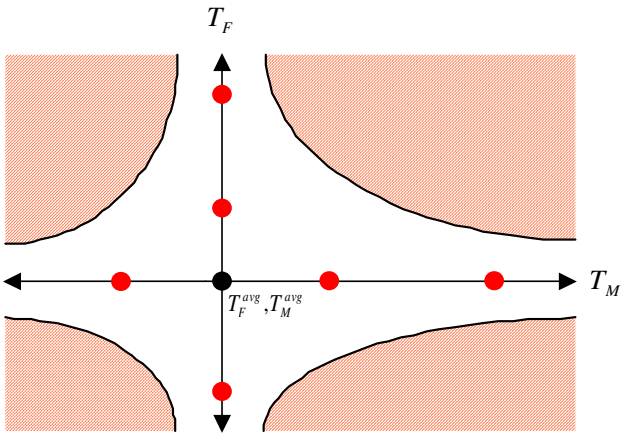

Fig. 3.8 – Diagram for cross sections without cross-term dependency, extracted from D'Auria et al. 2004.

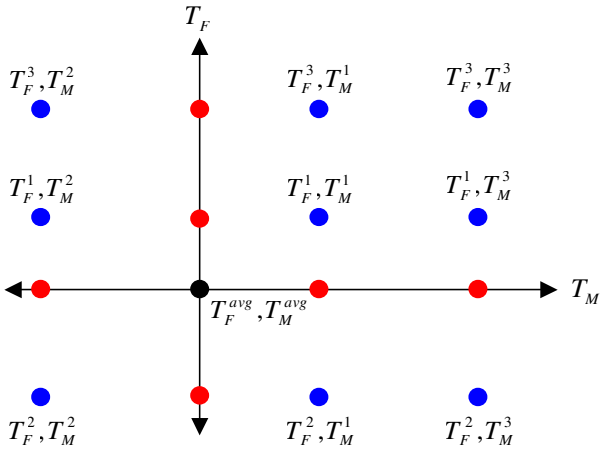

Fig. 3.9 – Diagram for cross sections accounting for cross-term dependency, extracted from D'Auria et al. 2004.

The branch calculation has one important drawback. Cross sections are not dependent on one feedback parameter, but on several parameters. Thus, changing feedback parameters, one at a time, only defines one dependence. The standard methods for cross section generation do not take into account the cross-term cross sections. Therefore, they are inaccurate for transients with large variations from nominal conditions. This effect can be seen in Fig. 3.8 where, for sake of simplicity, only two feedback parameters are considered (fuel and moderator temperature). The nominal condition is represented as a black dot and feedback perturbation conditions are represented as red dots. As the thermohydraulic conditions get further from calculated conditions (shaded areas) the error due to cross-term effect increases.

To reduce this error, the cross-term cross sections must be included in the branch calculations. The *Adaptive High-order Table Loop-up Method* was developed at Pennsylvania State University to compute cross sections which contains the cross-term dependence. This methods varies two or more feedback parameters at the same time (see Fig. 3.9). Thus, accounting for non-linear effects on thermohydraulic feedback parameters. Because of the cross-term dependency, these cross sections are more accurate.

It is also possible to increase the accuracy using higher-order interpolation (instead of linear interpolation). Studies show that cross section dependence on feedback parameters is not necessarily linear (D'Auria et al. 2004). In fact, a quintic spline is found to have the greatest accuracy and stability. With higher-order interpolation procedures, the same accuracy can be obtained with less points, thus less library size and less lattice calculations. Of course, the computational time needed to use quintic spline in a core physics code makes the process prohibitive.

The dependence of microscopic cross section for fission products need to be included in cross section libraries, especially the Xe and Sm, see Section 2.2.6.4. Other data that should be stored in cross section libraries include corner discontinuity factors, pin power peaking factors, ADFs, effective delayed neutron fractions (β_{eff}), decay constants (λ), etc. Use of ADFs improves the leakage prediction among different zones. In the axial direction, ADFs are not defined because usually the fuel is uniform and the flux does not experience big changes (with the exception of the assembly and top/bottom reflector interfaces). However, for some advanced reactors, fuel rods can change composition axially or partial fuel rods can be inserted. In this cases, the use of ADFs could improve the transport solution (flux and power distribution) and, by extension, the weighted cross sections.

The kinetic parameters β_{eff} and λ are usually not included in deterministic U&S analysis because little or no information about sensitivity coefficients for kinetic parameters is found in current NDLs. It is known that the kinetic parameters play an important role in output parameter variance. Their importances depend, among others, on fuel depletion. When fuel is depleted the content of Pu is buildup -due to transmutation- and the β_{eff} is reduced since β_{eff} for Pu is lower than that for U. This effect produces higher fluctuations -especially in BWR-. Therefore, towards the end of the cycle, the influence of kinetic parameters increases. Methods to calculate the β_{eff} uncertainty are given in Ivanov et al. 2013 and Kodeli 2013.

Several methodologies for cross section generation are available. For example, the SIMTAB methodology -developed at Universitat Politècnica de València (UPV) (Roselló 2004)- is based on CASMO and SIMULATE results. It performs a neutronic composition collapse (to reduce computational time and library size) and generates the appropriate cross section library in NEMTAB format. The composition reduction is based on the assumption that different compositions with close burn-up -for example $\Delta B \leq 0.1$ GWd/TU (Martínez-Murillo et al. 2011)- can be treated as only one neutronic composition. Moreover, guidelines for cross section generation can be found in Wang et al. 2013. This study compares the cross section generated using CASMO, HELIOS and TRITON lattice codes. Then, the generated libraries are tested with TRACE/PARCS coupled code.

3.3.1 Cross section library formats

Two main cross section library formats are used currently: (i) NEMTAB where the cross sections are tabulated according to several feedback parameters and (ii) PMAXS where the cross sections are fitted with a n-degree polynomial as a function of feedback parameters and reactor history parameters. The main advantage of PMAXS libraries is that its size is smaller than NEMTAB libraries. Thus, they can be read faster and less memory is needed. However, as available computational resources increase, this is not a problem if NEMTAB format is used. Another advantage for PMAXS is that it is easy to add a new feedback parameter -let's say burn-up-. It is just a matter of adding a new variable in the polynomial fitting procedure (burn-up is included by default in PMAXS). Whereas in NEMTAB libraries, more effort is needed since a new library must be generated for each burn-up condition and the size increases exponentially. The PMAXS libraries can be directly generated from the macroscopic cross section libraries of lattice codes such as HELIOS, TRITON, and CASMO with the GenPMAXS program (Generation of the Purdue Macroscopic XS set). The main advantage of NEMTAB library is that it is easier to obtain the library and understandable for novel

users. See Appendix B for a detailed NEMTAB format explanation.

In both cases, the cross sections are expressed as a combination of feedback parameters. NEMTAB libraries take into account the fuel temperature and moderator density. Moreover, rodded cross section effect is accounted generating a second library NEMTABR. However, recent studies are developed to include the boron concentration as separate NEMTAB libraries (Martínez-Murillo et al. 2011). For PMAXS libraries, according the GenPMAXS manual (Xu and Downar 2005), there are 12 acceptable feedback parameters, where only the first five of them are mandatory.

1. Control rod fraction
2. Density of coolant
3. Soluble poison concentration in coolant
4. Temperature of fuel
5. Temperature of coolant
6. Impurity of coolant
7. Density of moderator
8. Soluble poison concentration in moderator
9. Temperature of moderator
10. Impurity of moderator
11. Density difference between neighbor and current assembly
12. Burn-up difference between neighbor and current assembly

For this thesis, the NEMTAB format is used. There are two reasons to use this format: (i) the research group already gained experience using this format in the past and (ii) it is easier to use and understandable for novel users.

3.3.2 Covariance libraries

Available covariance data in the NDLs is currently being updated and increased. However, nuclear data covariance libraries for cross section reaction pairs and resonance parameters are being developed. Some methods are used to approximate the nuclide uncertainties not available in the NDLs, thus called "low-fidelity" covariance data. Therefore, they are not generally included in the official NDLs, but distributed with the main U&S analysis codes -such as SCALE-. The most extensive NDL is ENDF/B-VII.0 with data for 393 nuclides discretized into 238 energy groups. It contains "low-fidelity" covariance data for the number of neutrons per fission, resonance parameters and reaction cross sections at different temperatures. Other covariance data, such as angular distribution, energy distribution or production yields are still not available.

Uncertainties into broad-group cross section are included inevitably due to approximations during the energy collapse process. This uncertainty is mainly apportioned by the energy weighting function used to average the pointwise data to obtain the broad-group cross sections. Besides, zero uncertainty is assumed if the covariance data for an isotope is not included in the NDL, this will underestimate the uncertainty for core calculations. Some modules are available to process multigroup covariance data, these include ERRORR/COVR, ERRORJ or ANGELO/LAMBDA. There are two main covariance library formats, COVFILES and COVERX.

3.4 Thesis overview

A methodology is devised to propagate cross sections and other nuclear data through SCALE and PARCS. The propagation is performed at assembly level -with SCALE6.2.1- and core level -PARCSv3.2-. The first level takes into account the cross section uncertainties contained in the master library ENDF/B-VII (default library provided with SCALE6.2.1). The default perturbation library provided with the module SAMPLER is used. However, a procedure to create an in-house perturbation library is also devised and explained in this thesis to be used in future works. The propagation process adds the uncertainty incorporated due to the collapse and homogenization cross section phase. Then, using SCALE results, a NDL with mean cross sections and a second NDL with their standard deviations are generated -both libraries are NEMTAB formatted-. In the second level, the NDLs of standard deviations is used to perturb the mean cross sections and run several perturbed PARCS simulation in steady state alone. In this PhD thesis PARCS source code is modified for this purpose. Each simulation is perturbed using the standard deviations and a perturbation factor obtained with DAKOTA 6.3 statistical tool, these factors follow a normal distribution and are randomly sampled. Finally, the uncertainty propagated is reflected in PARCS output parameters (multiplication factor, axial power peak and peak node location). Even though in this thesis the methodology to propagate the cross section uncertainty is shown without thermohydraulic coupling, there is not any limitation in this methodology that prevents the core physics code to be coupled with a thermohydraulic code, as it was proved by the same thesis' author in Mesado et al. 2012. The UQ is performed with SAMPLER module, while the SA is performed with DAKOTA. The reactor type used is the BWR. See Fig. 3.10 for a flow diagram that shows the information exchanged in the whole process, Table 3.6 complements the information given.

Moreover, a similar methodology is used to propagate the thermohydraulic uncertainty through TRACE-PARCS coupled code. A total of 43 thermohydraulic parameters are selected to be propagated. Their PDF definitions are found in related literature or, if not found, defined based on expert judgment. These uncertainties are finally reflected on the enthalpy, power and reactivity predicted by PARCS. The U&S analysis is performed with DAKOTA 6.3 statistical tool and the reactor type used is a PWR. See Fig. 3.11 for a flow diagram that shows the information exchanged in the whole process, Table 3.7 complements the information given.

Finally, it must be said that MATLAB scripts have been created, within the thesis framework, to automatically perform both propagation methodologies. On one hand, USAS-XL is a MATLAB collection of scripts that automatically propagate cross section uncertainty through SCALE and PARCS. Among other features, it translates CASMO input decks into SCALE format and propagates the cross section uncertainty in the master library using SAMPLER module. As a byproduct of USAS-XL, the TXT2NTAB program is created (Mesado et al. 2017). It is a MATLAB program developed to generate NEMTAB libraries out of SCALE results (txtfile16). This program has been created on request of the expert group on Uncertainty Analysis in Modelling (UAM-LWR) and is used to generate NEMTAB libraries to distribute among the benchmark participants. On the other hand, RESTING is also a collection of MATLAB scripts that automatically generate TRACE input models at core level either in 1D or 3D. Among other features, it performs U&S analysis for user defined thermohydraulic parameters or automatically adjust the bypass flow. RESTING provides a user-friendly input system to use its different modules with ease.

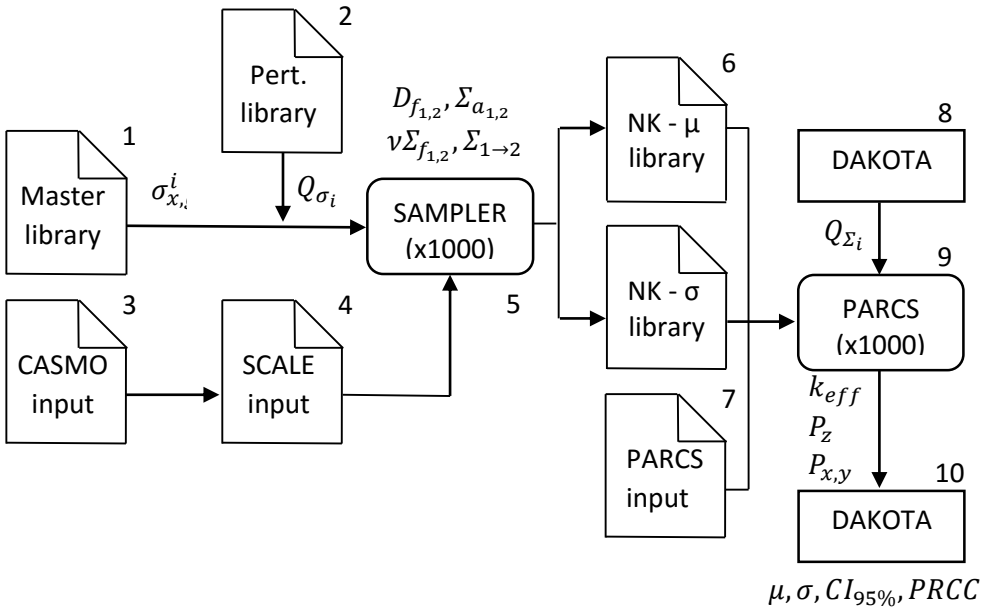

Fig. 3.10 – Thesis summary: flow diagram for neutronic parameter propagation.

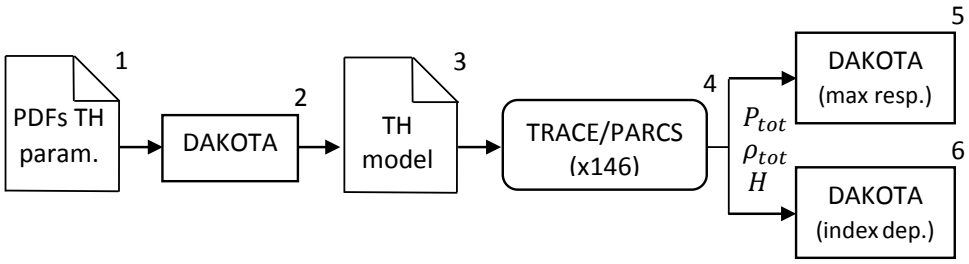

Fig. 3.11 – Thesis summary: flow diagram for thermohydraulic parameter propagation.

Item	Description	Section
1	Input parameters are the problem-independent cross sections contained in the master library, ENDF/B-VII in this case. $\sigma^i_{x,g}$ is the cross section for nuclear interaction x, energy group g and isotope i.	5.1.1
2	A perturbation library is provided with SCALE6.2.1. It contains perturbation factors for each isotope, energy group and nuclear interaction. Moreover, a procedure to create an in-house perturbation library is also devised and explained in this thesis to be used in future works.	
3	CASMO input decks are provided for each segment.	4.1
4	A MATLAB script is written to translate CASMO input deck to its SCALE homologous.	
5	SAMPLER module is run using 1000 perturbations for all feedback parameter combinations and all segments. The output parameters are the main homogenized cross sections.	5.1.2.1
6	Two neutronic libraries are generated using SAMPLER results, both in NEMTAB format. One contains the mean cross sections, the other their standard deviations.	4.1.1
7	PARCS input is build for a BWR core.	4.3
8	DAKOTA tool is used to generate 1000 perturbation sets for each neutronic composition and main homogenized cross sections contained in the neutronic library.	5.1.2.2
9	PARCS is run 1000 times, each with a different perturbation set.	
10	A U&S analysis is performed using DAKOTA for the multiplication factor, axial power peak and peak node location.	

Table 3.6 – Information description for cross section propagation.

Item	Description	Section
1	Selection of input parameters and definition of its uncertainty information (PDF). This is accomplished based on a bibliography review, PIRT process or expert judgment.	5.2.1
2	DAKOTA is used to sample the input parameters (according to its PDF) and generate appropriate perturbations.	
3	Thermohydraulic model for a PWR core is built for TRACE code. Its major feature is that the core is fully discretized in 3D.	4.2
4	TRACEv5.0P3/PARCS3.0 couple code is used to run all perturbations. As output parameters, the total power, total reactivity and the enthalpy are chosen.	4.3
5	Two different U&S analysis are done with DAKOTA. One for the most unfavorable situation (maximum response).	5.2.2
6	The second U&S analysis is done for each time step.	

Table 3.7 – Information description for thermohydraulic parameter propagation.

A list of codes and models used within this thesis is given hereafter.

- SCALE6.2.1. SCALE is used due to its flexibility to solve nuclear related problems. It has a wide range of modules, it is highly validated and used worldwide.

- SAMPLER. The stochastic sampling methodology is chosen due to the high number of input parameters. It gives U&S, unfortunately SA is not available in SCALE6.2.1 but will be incorporated in future versions.

- TRITON-NEWT. The 2D deterministic and depletion sequence is chosen because its ability to generate problem-dependent cross sections and its easiness to define -almost- any geometry.

- PARCSv3.2. It is the neutronic reference code for the NRC and it is continuously being developed and tested. PARCS source code is modified to perturb cross sections read from the problem-dependent neutronic library.

- TRACE5.0P3. It is the thermohydraulic reference code for the NRC and it is also continuously being developed and tested.

- TRACE5.0P3/PARCSv3.0. The effort made to couple TRACE thermohydraulic code and PARCS neutron kinetic code provides a professional tool for thermohydraulic-neutronic analyses with great accuracy. In this version PARCS code is integrated into TRACE as a subroutine, this gives the final code more stability. Even though, two different versions of PARCS are used in this thesis (3.0 and 3.2), for precaution, it is checked that same solvers are used and that they do not contain significant modifications.

- DAKOTA 6.3. It provides a big range of statistical applications. Here, it is used to obtain UQ and SA at core level with PARCS.

- NEMTAB. It is used because the research group already gained experience using this format in the past and also, it is easier to use and understandable for novel users. This limitation is not strict, if the correspondent script is changed, other formats could be used -for example PMAXS-.
- ENDF/B-VII. It is the most modern NDL and provides a wider range of information. SCALE6.2 provides new cross section libraries with 56 and 252 energy groups based on ENDF/B-VII.
- MATLAB. It is easy to develop scripts with MATLAB. Besides, it is optimum for pre- and post-processing tools.
- TXT2NTAB. It is a MATLAB program developed to generate NEMTAB libraries out of SCALE results (txtfile16).
- USAS-XL. -Uncertainty & Sensitivity Analysis for Scale Xsec Libraries- is a MATLAB program developed to automatically propagate cross section uncertainty through SCALE and PARCS.
- RESTING. -REactor Simulation Trace INput Generator- is a MATLAB program developed to generate TRACE input models -either in 1D or 3D- that are accurately tested to reproduce a transient. It also propagates user defined thermohydraulic parameters. It provides a user-friendly interface.

Chapter 4

Models

. . . the only way: a brick-over-brick process.

In this chapter, the models built to propagate the uncertainty are explained. Different codes are used to achieve this goal. The neutronic parameters are propagated using the lattice physics code SCALE6.2.1 and the core physics code PARCSv3.2 (without thermohydraulic feedback). The thermohydraulic parameters are propagated using the thermohydraulic-neutronic coupled code TRACE5.0p3/PARCSv3.0. In the subsequent sections, these models are explained along with a code-to-code verification. It must be said that scripts are programmed to automatically generate these models using MATLAB. These scripts are programmed to allow modification to the main model characteristics and features. Therefore, it is easy to produce input decks with the confidence that they are already tested.

4.1 Lattice physics model

Inputs and results for the reactor under study -a BWR- are provided using the lattice physics code CASMO-4. The information is divided into segments, each segment represents one region of the core (in this case there are 9 different segments). Thus, the collection of all segments contains the information for the whole core. In order to obtain an equivalent model, a MATLAB program is developed to translate the CASMO input decks to its homologous SCALE input decks. Table 4.1 shows a summary for the most important CASMO cards along their variables and a short description. Fig. 4.1 contain a sketch for the main geometric distances used in CASMO for an assembly and its cruciform control rod. SCALE model is built to resemble the CASMO model, examples can be seen from Fig. 4.2 to 4.5. The detail of a cruciform control rod is seen in Fig. 4.4.

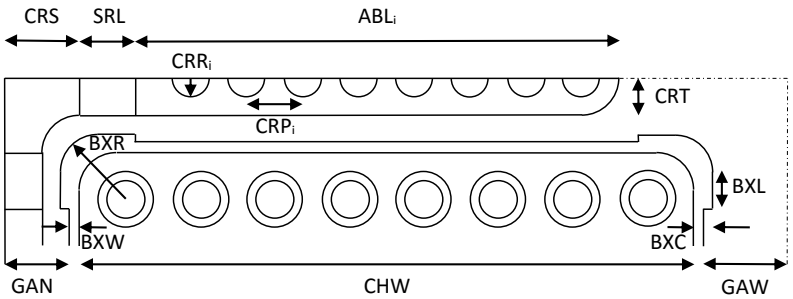

Fig. 4.1 – Main geometric distances in CASMO for an assembly and its cruciform control rod.

Card	Variable	Description
TMO	`tmo`	History for moderator temperature.
TFU	`tfu`	History for fuel temperature.
BWR	`npst`	Number of pins along one side of the assembly.
	`s`	Pin pitch.
	`chw`	Inner distance between the box walls.
	`bxw`	The thickness of the box wall.
	`gaw`	The thickness of half of the wide water gap.
	`gan`	The thickness of half of the narrow water gap.
	`bxr`	The outer radius of the rounded box corners.
	`isym`	Symmetry in assembly.
	`bxc`	Thickness of the box wall at corners.
	`bxl`	Length of extra thick box corners.
MIX	id=302	Default mixture Zircaloy.
	id=347	Default mixture Stainless Steel.
	id=750	Default mixture Inconel.
	id=72000	Default mixture Hafnium.
PIN	`c`	Pin occupies `c` pin cells.
	`rad`	Radius.
	`comp`	Composition.
LPI	`lpi`	Pin layout.
FUE	`id`	Fuel type id.
	`den`	Fuel density.
	`comp`	Composition: $w_{234} = 0.008 \cdot w_{235}$, w_{235} and $w_{238} = 100 - w_{234} - w_{235}$.
	`wGd`	Fraction of Gadolinium.
LFU	`lfu`	Fuel type layout.
HOX	`hox`	Homogeneous mixture.
CRD	`crt`	Thickness of the half of the control rod.
	`crs`	Starting point for the cruciform control rod.
	`srl`	Length of the central steel region.
	`abl`	Length of zone i.
	`crr`	Radius of the absorbing cylinder in zone i.
	`crp`	Pitch between absorbing cylinders in zone i.
	`comp`	Composition in zone i.
DEP	`dep`	Exposure in MWd/kgU.
REF	`t`	Reflector area thickness.
	`com`	Reflector area composition.

Table 4.1 – Summary of CASMO input cards.

The BWR contains burnable absorber pins, these pins provide an effective mean to control the core power as they insert negative reactivity while they are burning, see Section 2.2.6.2. According to Ade 2012, four different recommendations are followed to model burnable absorber pins.

1. Due to the fast burn-up behavior of these pins, they are modeled using different concentric rings, see central pin in Fig. 4.3. The use of different geometrical bodies helps to obtain an improved flux and isotopic radial distribution.

2. The cell treatment is performed specifying the multiregion cell option. This option is preferred when the default cell treatment (lattice) is not appropriate. With multiregion, several concentric rings can be specified. This feature match the geometry in previous recommendation.

3. Burnable absorber pins are depleted using constant flux instead of constant power. Again, due to its fast depletion, this helps to obtain a better isotopic prediction, see Section 2.2.5.

4. The depletion steps for assemblies with burnable absorber pins are limited to 0.5 or 1.0 GWd/MTU before peak reactivity, after the peak the step can be increased. For other assemblies, the depletion steps can be up to 2.0 or 3.0 GWd/MTU.

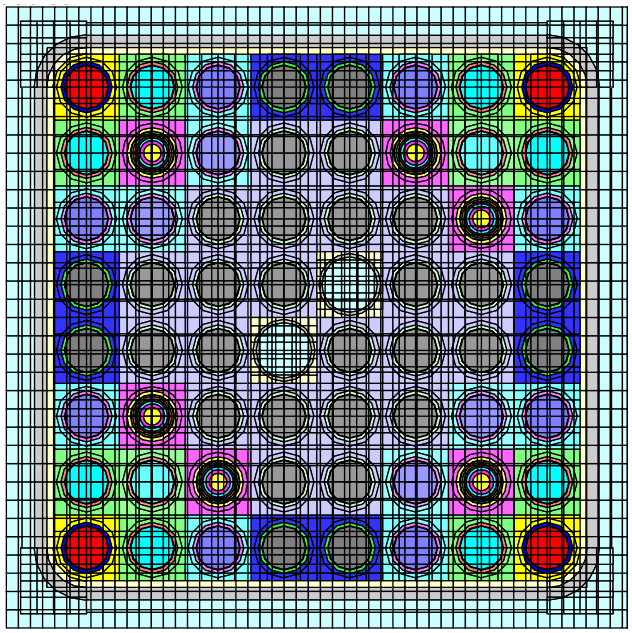

Fig. 4.2 – Fuel assembly for BWR without control blade, build with SCALE.

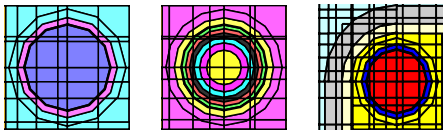

Fig. 4.3 – From left to right, details for a fuel pin, burnable absorber pin and fuel assembly corner.

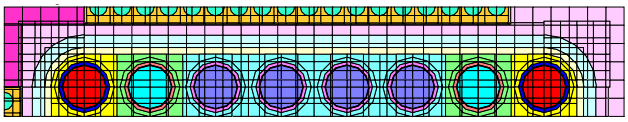

Fig. 4.4 – Detail of the cruciform control rod.

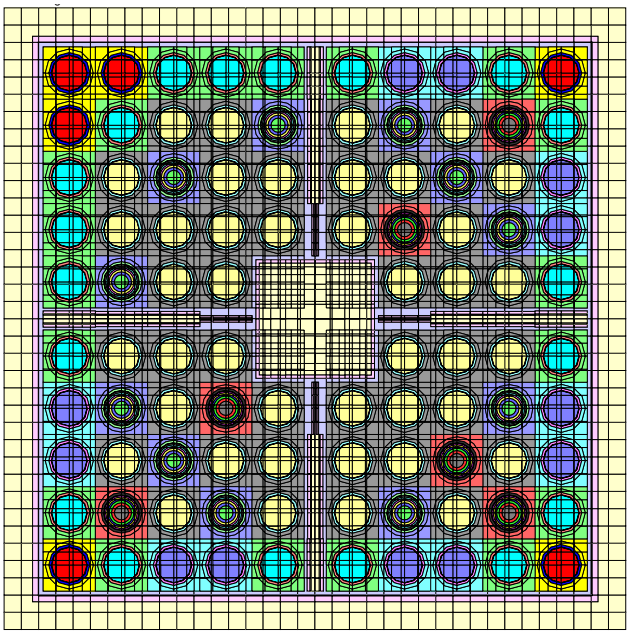

Fig. 4.5 – Another fuel assembly for BWR, build with SCALE.

One more recommendation is followed regarding Dancoff factors. These factors are directly related with the cross section self-shielding calculation. SCALE provides an automatic Dancoff factor calculation assuming an infinite lattice of equal fuel pins. However, default factors could be erroneous for very heterogeneous models. In BWR, due to the void formation, the moderator density can experience a strong variation, not only over the axial direction, but also over the cross section of a fuel bundle. Therefore, MCDancoff module, provided by SCALE, is used to calculate accurate Dancoff factors for a user-specified model. More information is found in Section 4.1.2.

The main features for the model built in SCALE are summarized in Table 4.2. In order to demonstrate some of the features shown in this table, a simple model is constructed. It is based on the fuel assembly shown in Fig. 4.2. It is depleted with three cycles of one year each, 30 days of decay time after the first and second cycle and 1500 days of decay time for the last cycle. The fuel and moderator temperature is set to 879.5 K and 561.4 K respectively, the moderator density is 0.45632 g/cm^3. The burnable absorber pins treatment and geometry are specified according to the recommendations explained before in this section. This model is run with SCALE and the results are obtained as a function of burn-up. Even though in this thesis the propagation methodology is performed in fresh fuel conditions (no burn-up), this test (with burn-up dependence) is seen as a starting point for future works, where the methodology will be performed with depletion. Fig. 4.6 shows the flux predicted for the collapsed groups: fast (left) and thermal (right). Blue-colored areas represent low flux and dark red-colored areas represent high flux. Fast flux is concentrated in fuel regions, while thermal flux is high in big moderator areas. Thermal flux is almost negligible in burnable absorber pins.

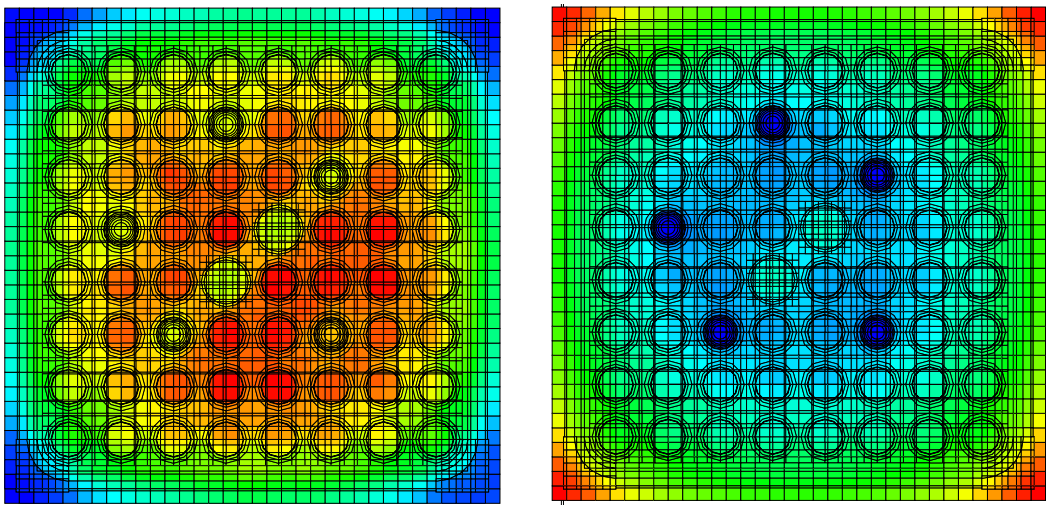

Fig. 4.6 – Predicted fast flux (left) and thermal flux (right), depicted by SCALE.

In Fig. 4.7 the k_∞ evolution is plotted as a function of burn-up (left). Each data set represents the model with a different number of rings modeling the burnable absorber pins. Only burn-up up to 15 GWd/MTU is shown, after that the results of all data sets converge. The k_∞ difference for each data set experienced around the reactivity peak (9 GWd/MTU) is shown on the right figure. In Fig. 4.8 each data set is obtained with an increasing number of depletion steps within each cycle. The k_∞ difference for each data set experienced around the reactivity peak (12 GWd/MTU) is shown on the right figure.

As the number of rings modeling a burnable absorber pin gets higher, the different data sets converge. Nevertheless, the computational time increases. As it is expected, the same trend is seen as the number of depletion steps within a cycle increases. Both effects are particularly important in a broad range centered in the peak of reactivity. In the reactivity peak, the absolute difference between the extreme cases (case with more rings/steps and case with less rings/steps) is 3900 pcm for Fig. 4.7 and 8600 pcm for Fig. 4.8.

Fig. 4.9 shows the k_∞ evolution using the default Dancoff factors -assuming an infinite lattice fuel pins- (solid black line), or using more accurate Dancoff factors obtained with the MCDancoff module (solid red line). The absolute difference is plotted in the secondary y-axis (dashed-blue line). For fresh fuel conditions both predictions differ almost 700 pcm. As the fuel is burned, this difference decreases to a burn-up point (around 22 GWd/MTU) where the predictions cross and the difference starts to develop again. At the end of the bundle life (long decay time), the difference experiences a sudden drop.

Fig. 4.10 shows the k_∞ evolution using different *Evaluated Nuclear Data File* (ENDF) cross section libraries, either in SCALE6.2 beta 4 or the previous version SCALE6.1.1. In SCALE6.2 beta version only library ENDF/B-VII.0 v7-238 (with 238 energy groups) is available. Moreover, old libraries ENDF/B-V and ENDF/B-VI are removed. Additionally, using the `weight`[1] TRITON parameter, the problem-dependent flux solution can be used to collapse the v7-238 library to a new problem-dependent library with 49 energy groups (represented in Fig. 4.10 as data set "S62b4 v7-49"). Additional libraries with 238 energy groups but different ENDF versions in SCALE6.1.1 are also used. The range spanning the higher and lower predictions (dashed-blue line) is shown in the secondary y-axis. The bar plot (right) shows the k_∞ difference for fresh fuel conditions, the difference in pcm -with respect to the v7-238 prediction- is shown on the top of each bar.

[1] See Section 3.1.1.5

Feature	Value	Comment
SCALE version	SCALE6.2.1	The newest version of SCALE at this time.
Reactor type	BWR	Reactor specifications.
Control rods	Cruciform	
Number of segments	9 (3 reflectors)	
Cross section library	v7-56	ENDF/B-VII with 56 and 252 groups are the new cross section libraries distributed with SCALE6.2. ENDF/B-VII is the most modern and complete NDL.
Cross section processor	CENTRM	Default and recommended option in SCALE6.2.1. More accurate than NITAWL (see Fig. 4.11), which is removed in SCALE6.2.
TRITON parameter `addnux`	4	This provides the highest accuracy during depletion calculations, see Fig. 4.12.
Energy group collapse	Fast: 40 Thermal: 16	Using the new 56-group NDL distributed with SCALE6.2.
Collapsed energy boundary	0.625 eV	Same boundary used by PARCS for thermal reactors.
Homogenization	Assembly or Reflector	For fuel segments, all materials in the assembly are homogenized. For reflector segments, all materials in the reflector zone are homogenized.
Acceleration *Coarsh Mesh Finite Difference* (CMFD)	Activated	To reduce computational resources.
Acceleration CMFD 2nd level	Activated	To reduce computational resources.
Pin cell discretization	4x4	Even numbers produce better results than odd numbers, see Ade 2012.
Fuel pin treatment	Latticecell	Most common treatment, infinite array of 1D cells is assumed.
Burnable absorber pin treatment	Multiregion	Recommended treatment in Ade 2012 for burnable absorber pins.
Operation conditions	Beginning of cycle (fresh fuel)	To reduce computational resources.
Fuel pin burn-up	Constant power	Default burn-up option.
Burnable absorber pin burn-up	Constant flux	Recommended burn-up option in Ade 2012 for burnable absorber pins.
Rings modeling Gd-pins	6	For a better depletion and isotopic prediction of fast burnable absorbers (see Fig. 4.7), recommended in Ade 2012.
Dancoff factors	Default factors	The use of MCDancoff module to calculate accurate factors is recommended in Ade 2012, see also Fig. 4.9). However, due to an important increase of memory, default factors are used.
Feedback fuel temperature points	7	See Section 4.1.1
Feedback moderator density points	7	
Feedback control rods	In/Out	

Table 4.2 – Main features for the lattice physics model (BWR fuel assembly).

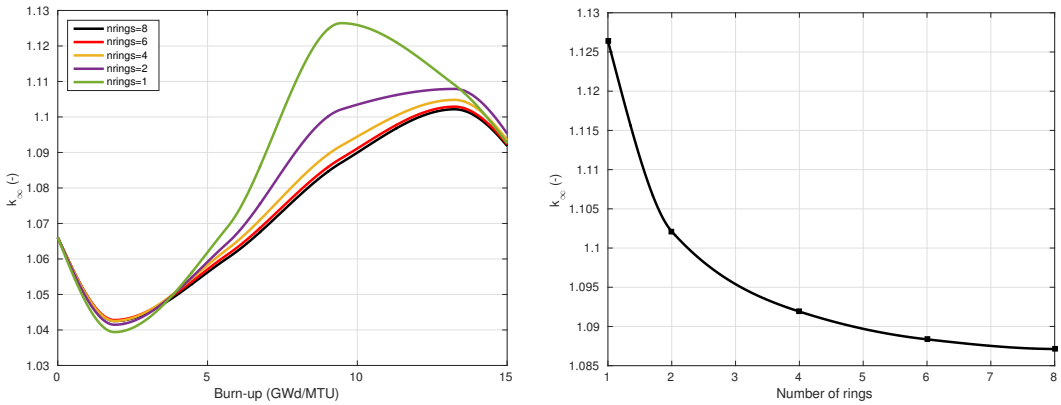

Fig. 4.7 – k_∞ evolution as a function of the rings modeling the burnable absorber pins. Evolution with burn-up (left) and evolution for the reactivity peak (right).

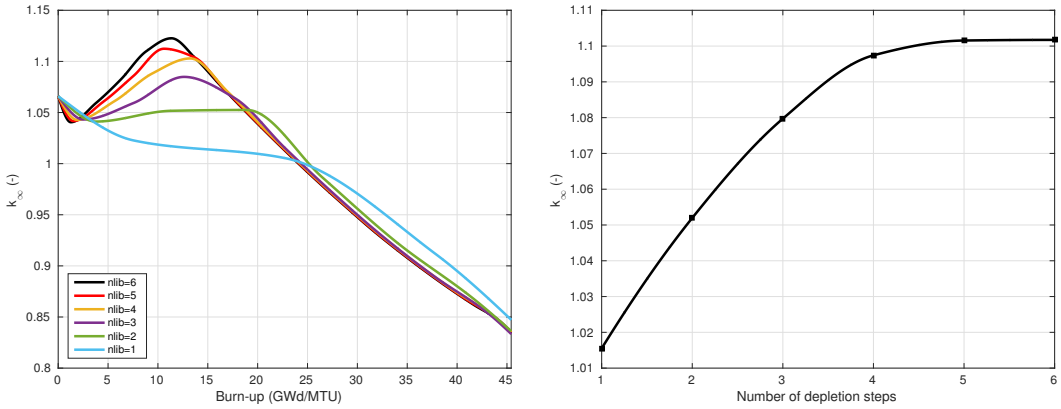

Fig. 4.8 – k_∞ evolution as a function of the depletion step number. Evolution with burn-up (left) and evolution for the reactivity peak (right).

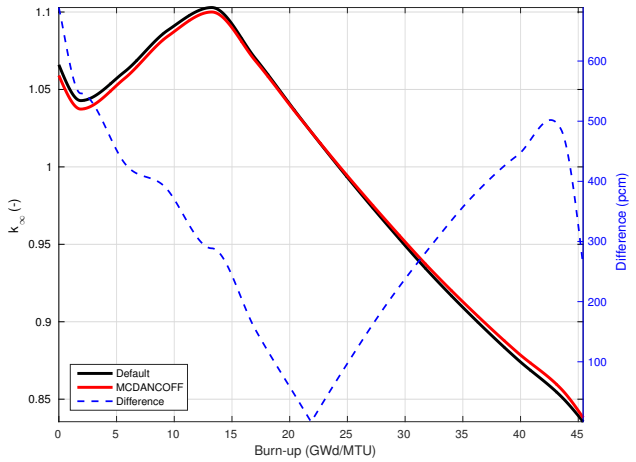

Fig. 4.9 – k_∞ evolution using the default Dancoff factors (black line) and the improved Dancoff factors with MCDancoff module (red line), the absolute difference is shown in the secondary y-axis (dashed-blue line).

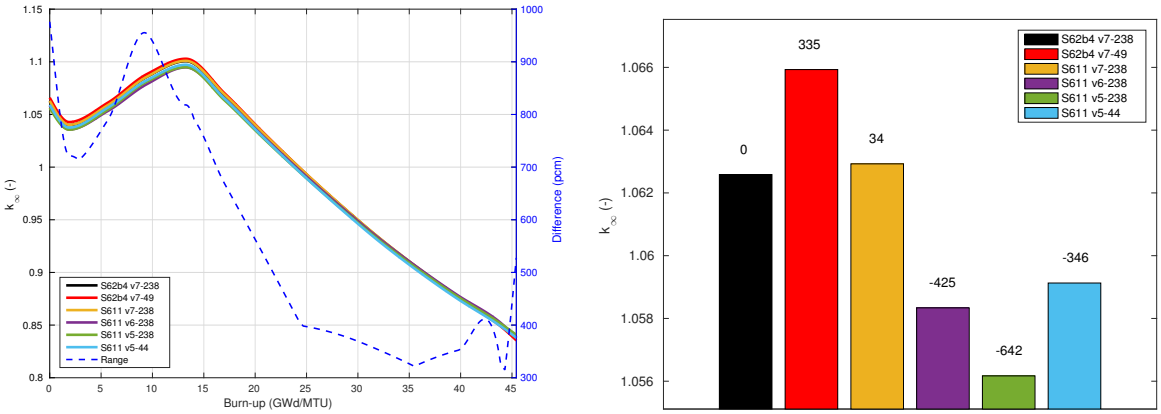

Fig. 4.10 – k_∞ evolution using several ENDF cross section libraries. Evolution with burn-up (left) and prediction values for fresh fuel conditions (right).

The predicted range fluctuates around 700-1000 pcm before the 15 GWd/MTU and, just before the reactivity peak, it experiences a strong decrease. It decreases to 300-400 pcm and increases again to 500 pcm at the end of the bundle life (long decay time). Predictions using ENDF/B-VII for both SCALE versions are almost identical ("S62b4 v7-238" and "S611 v7-238"). However, the flux-weighted library in SCALE6.2 beta 4 seems to overpredict the k_∞, respect to the other library versions. Other ENDF versions in SCALE6.1.1 underpredict the k_∞, being "S611 v5-44" the closest prediction with respect to the results obtained with "S611 v7-238". The maximum and minimum predictions correspond to "S62b4 v7-49" and "S611 v5-238" respectively. Same trends are observed with the results for fresh fuel conditions (bar plot).

Fig. 4.11 shows the k_∞ evolution using two different cross section processing options, CENTRM (the default option) and NITAWL. Because of compatibility issues, NITAWL processing option must be used only with ENDF/B-V (either 238 or 44 energy structure) and has been removed in the new SCALE version. Therefore, the comparison is made using SCALE6.1.1 and v5-44 library. The absolute difference is plotted in the secondary y-axis (dashed-blue line). Both predictions for fresh fuel conditions differ around 900 pcm. This difference experience a maximum of 1000 pcm at maximum reactivity. As the fuel is burned the difference decreases to a burn-up point (around 31 GWd/MTU) where the predictions cross. Then, the difference starts to develop again up to 800 pcm. The large disagreement observed justifies why NITAWL is obsolete.

Fig. 4.12 and Fig. 4.13 show the k_∞ evolution and ^{235}U density evolution as a function of burn-up and time respectively. Each data set uses a different values for the `addnux`[2] TRITON parameter. As the `addnux` value gets higher the predictions converge. The results show that `addnux` values of 0 or 1 should not be used for real predictions (only for approximation purposes), higher `addnux` values converge. A zoom plot is added to distinguish the lines for the higher `addnux` values. The left plot in Fig. 4.13 shows the ^{235}U density evolution after 1100 days.

[2]See Section 3.1.1.5

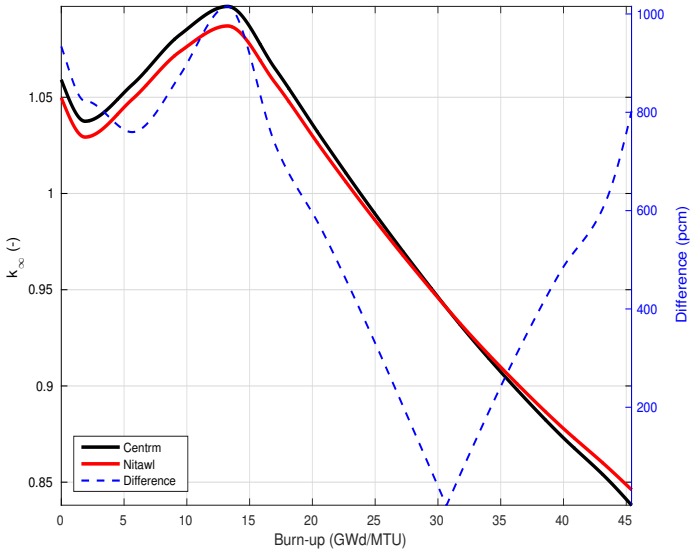

Fig. 4.11 – k_∞ evolution using CENTRM (black line) and NITAWL (red line) cross section processing options within SCALE6.1.1, the absolute difference is shown in the secondary y-axis (dashed-blue line).

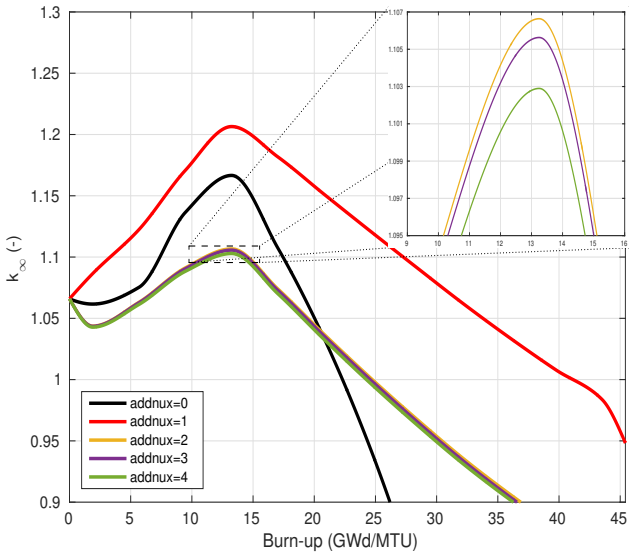

Fig. 4.12 – k_∞ evolution using different `addnux` values, zoom for the reactivity peak and higher `addnux` values.

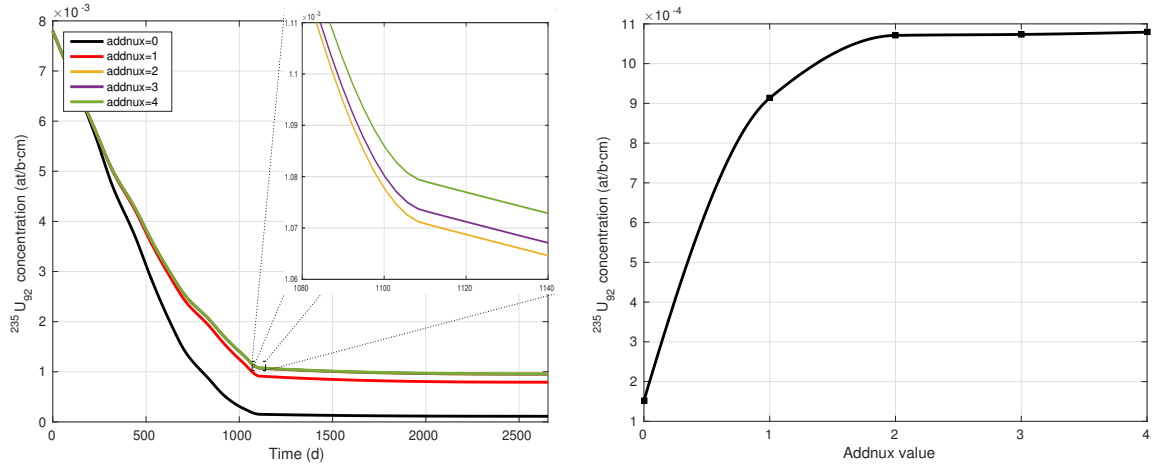

Fig. 4.13 – ^{235}U concentration evolution using different `addnux` values, zoom for higher `addnux` values. Evolution with burn-up (left) and concentration at 1100 s (right).

4.1.1 NEMTAB library generation

An expert user must decide the feedback state points for each feedback parameter. This decision has strong implications in the neutronic code results, see Section 3.3. In this thesis, 62 different feedback combinations are studied for each segment: 7 moderator densities -or a combination of void fractions and moderator temperature-, 7 fuel temperatures and 2 control rod states (in and out). Feedback state points selected for this thesis can be seen in Table 4.3 and Table 4.4 for the fuel temperature and moderator density respectively. The reactor history points are constant and can be seen in the same tables, except the control rod history which is always out. Nonetheless, some of this feedback combinations are not realistic, i.e. when both, moderator density and fuel temperature, are either very high or very low. Feedback combinations chosen in this thesis can be seen in Fig. 4.14. The segments representing the reflector do not require simulations with control rods, thus they have half of the feedback state points (31).

Some comments related to the chosen feedback state points are needed here. The fuel temperature range (293 to 2132.2 K) is broad enough to cover almost all possible *Design Basis Accidents* (DBAs) (see Section 2.3.1) and beyond DBAs (these accidents can be analyzed by coupled system codes[3]). Higher temperatures could lead to fuel damage or even melting (UO_2 melting point is around 2800 K). However, these phenomena are not included as capabilities in system codes. Regarding the moderator, its density is a function of void fraction and its temperature. Therefore, for each combination of two of them in Table 4.4, the third is known. The selected feedback parameters in the moderator range from pure liquid -at several temperatures- and up to 100% steam, several intermediate points where both phases coexist -at saturated temperature- are also included. In a real problem, more intermediate points could be needed, especially inside the zone of normal operation for a *Boiling Water Reactor* (BWR), i.e. moderator density 400 - 800 kg/m^3 and fuel temperature between 400 and 1400 K. If a real problem is known to develop with high voids, then the void fraction points should be focused in the region greater than 80%. Two reasons apply here: (i) predictions in this region are known to be less accurate and (ii) neutronic parameters have a stronger variation in this range. Both reasons are reassured in Wang et al. 2013. However, the points and ranges defined in Table 4.4 are enough for the purpose of this thesis: develop and test the methodology in an arbitrary case.

[3]Such as TRACE/PARCS and RELAP5/PARCS

	$\mathbf{T_{fuel}}$ **(K)**
1	293.0
2	660.8
3	879.5
4	1028.6
5	1396.5
6	1764.3
7	2132.2
Hist.	879.5

Table 4.3 – Fuel temperature feedback and history points.

	$\mathbf{D_{moderator}}$ **(kg/m^3)**	**Void (%)**	$\mathbf{T_{moderator}}$ **(K)**
1	38.14	100	561.4
2	177.53	80	561.4
3	456.32	40	561.4
4	735.11	0	561.4
5	840.34	0	493.0
6	942.81	0	393.0
7	998.29	0	293.0
Hist.	456.32	40	561.4

Table 4.4 – Moderator feedback and history points.

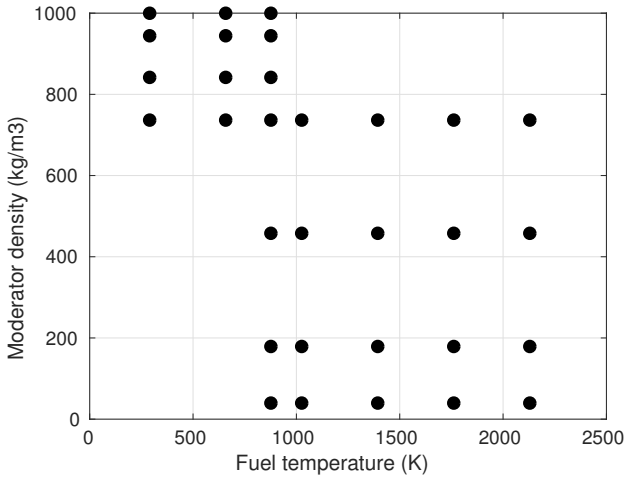

Fig. 4.14 – Feedback parameter combinations for SCALE.

Energy Group No.	Energy Boundaries (eV)	Broad Group No.	Energy Group No.	Energy Boundaries (eV)	Broad Group No.
1	2.000E+7	1	30	2.175E+1	
2	6.434E+6		31	2.120E+1	
3	4.304E+6		32	2.050E+1	
4	3.000E+6		33	7.000E+0	
5	1.850E+6		34	6.875E+0	
6	1.500E+6		35	6.500E+0	
7	1.200E+6		36	6.250E+0	
8	8.611E+5		37	5.000E+0	
9	7.500E+5		38	1.130E+0	
10	6.000E+5		39	1.080E+0	
11	4.700E+5		40	1.010E+0	
12	3.300E+5		41	6.250E-1	2
13	2.700E+5		42	4.500E-1	
14	2.000E+5		43	3.750E-1	
15	5.000E+4		44	3.500E-1	
16	2.000E+4		45	3.250E-1	
17	1.700E+4		46	2.500E-1	
18	3.740E+3		47	2.000E-1	
19	2.250E+3		48	1.500E-1	
20	1.915E+2		49	1.000E-1	
21	1.877E+2		50	8.000E-2	
22	1.175E+2		51	6.000E-2	
23	1.160E+2		52	5.000E-2	
24	1.050E+2		53	4.000E-2	
25	1.012E+2		54	2.530E-2	
26	6.750E+1		55	1.000E-2	
27	6.500E+1		56	4.000E-3	
28	3.713E+1		57	1.000E-5	
29	3.600E+1				

Table 4.5 – Energy group structure, collapse from 56 to 2 groups.

One more comment on CASMO results is needed. For reflector segments, CASMO gives the cross sections and neutronic parameters with and without correction of the flux discontinuity factor. Differences are small if neutronic libraries are generated using CASMO results -with and without correction- and used in a diffusion code, see Section 4.4.2.

The resulting cross sections for each feedback state, defined in SCALE branches, are homogenized and collapsed. The homogenization is performed for all materials in the assembly (including the control rod if present). For reflector segments, only the materials representing the reflector are homogenized. Then, the cross sections are collapsed into two energy groups with 0.625 eV as energy boundary. Table 4.5 shows the energy structure collapse from 56 fine groups to 2 broad groups. The fast and thermal broad groups are composed by the first 40 and last 16 fine groups respectively. These two groups are then required by PARCS code, which uses the same energy boundary for thermal reactors.

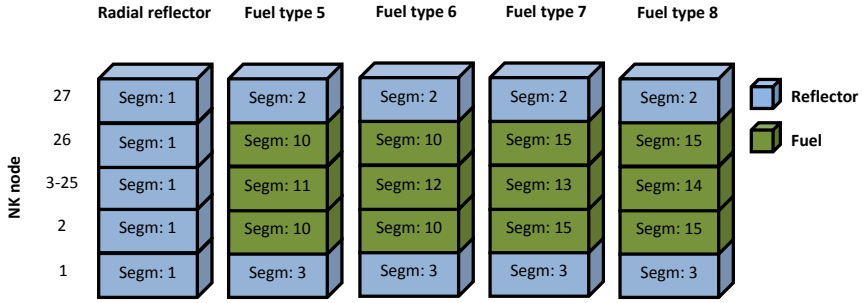

Fig. 4.15 – Segment composition for each fuel type.

Unfortunately, not all combination points shown in Fig. 4.14 are available on the provided CASMO results. Some of them do not exist or are incomplete -meaning that cross sections and neutronic parameters for some of the feedback parameter combinations do not exist-. Most of the uncompleted points lie on the normal operation zone (below saturation density for a BWR) and therefore, cannot be used for the purpose of this thesis. There is only one point in CASMO inside the normal operation zone and information completeness, that is 879.5 K and 456.32 kg/m^3.

Generated NEMTAB libraries contain tabulated cross sections for three different feedback parameters, i.e. fuel temperature, moderator density and control rod state (boron concentration is not considered in this thesis). Where each moderator density is a combination of moderator temperature and void fraction. Control rod dependence is handled creating two different NEMTAB libraries, one for rodded conditions (nemtabr) and one for unrodded conditions (nemtab). The problem-dependent cross section library generated is only valid for this particular BWR and for a specific operation conditions (matching the reactor history and burn-up), in this case beginning of cycle. Since it is assumed that neutronic compositions for reflector segments are not significantly affected by control rods, the data for reflector compositions is invariable for both libraries.

Due to high computational resources needed, the generated NEMTAB libraries are limited to fresh fuel conditions (beginning of cycle). This is accomplished setting a low burn-up level and only one short cycle in the SCALE model. However, the methodology is not limited to fresh fuel conditions and any burn-up can be used. To obtain neutronic libraries for a specific burn-up, the neutronic parameters are the result of an interpolation of the predicted neutronic parameters as a function of burn-up. The correspondent burn-up for each neutronic cell, the operation conditions and the information related to the segments (core configuration) is given by the nuclear power plant. The neutronic compositions in the generated NEMTAB library are filled according to this information. For a case with burn-up, all neutronic compositions belonging to the same segment are possibly different and are determined, as explained before, using an interpolation according to the specific burn-up. However, in this thesis, because the operational point corresponds to the beginning of cycle (fresh fuel conditions), all neutronic compositions belonging to the same segment are identical. According to the core configuration, there are 4 fuel assembly types and 9 segments (3 of them are reflector zones), see Fig. 4.15.

The reactor height is divided into 27 different axial levels, where the upper and lower cells represent the upper/lower reflector (non-active cells). There are three possible approaches to determine the total number of neutronic compositions.

1. One neutronic composition per neutronic cell. This results in large neutronic libraries, but is required for non-fresh conditions. Due to the large library generated, this option can lead to insufficient virtual memory errors during core physics code execution. Assuming 3 neutronic compositions to represent

the reflector zones (bottom, top and radial), the total number of neutronic compositions is determined by:

$$\mathrm{NK}_{comp} = n_{chan}(n_z - 2) + 3 \tag{4.1}$$

2. One neutronic composition per axial level for each fuel assembly type. This results in smaller neutronic libraries, but can only be used for fresh conditions or low burn-up levels. The total number of neutronic compositions is:

$$\mathrm{NK}_{comp} = n_{type}(n_z - 2) + 3 \tag{4.2}$$

3. One neutronic composition per segment. This results in even smaller neutronic libraries, but can only be used strictly for fresh conditions. The total number of neutronic compositions is:

$$\mathrm{NK}_{comp} = n_{segm} \tag{4.3}$$

Where

NK_{comp} is the number of neutronic compositions,

n_{chan} is the number of fuel assemblies in the reactor,

n_z is the number of axial levels,

n_{type} is the number of different fuel assembly types, and

n_{segm} is the number of different segments.

Even tough the studied case represents a reactor with fresh fuel conditions, to achieve a balance between computational resources and accuracy, the second approach to obtain the number of neutronic compositions is chosen. Thus, following Eq 4.2, 103 different neutronic compositions are defined.

$$\mathrm{NK}_{comp} = n_{type}(n_z - 2) + 3 = 4(27 - 2) + 3 = 103 \tag{4.4}$$

4.1.2 MCDancoff module

By default SCALE computes generic Dancoff factors using the MIPLIB library and assuming an infinite lattice of equal fuel pins. However, this assumption may not hold for very heterogeneous fuel pin layouts, such as in BWR, and lead to inaccurate Dancoff factors. Due to void formation in BWR, the moderator density can experience strong variations, not only over the axial direction, but also over the cross section of a fuel bundle. For example, a Dancoff factor differs substantially between a central pin and an edge or corner pin. This effect can be seen in Fig. 4.17, where the Dancoff factors calculated with MCDancoff module are represented for a bundle with two central water rods. MCDancoff module is used to generate accurate Dancoff factors, it is based on *Monte Carlo* (MC) calculations and the geometry is defined as in KENO-VI (3D). The statistical parameters are set following the recommendations in MCDancoff data guide (Petrie and Rearden 2011) or being more conservative. The number of particles per generation is set to 300, the number of generations is increased from 100 (recommended) to 300. Since Dancoff calculation is a fixed source integration, there is no need to skip generations and therefore, the number of generations to skip is set to 0. All boundary conditions are set to mirror. In Fig. 4.16, the model geometry can be seen as represented by Keno3D tool, some materials are removed on purpose for an enhanced view of the inner assembly.

The Dancoff factors are calculated for each fuel pin, each void fraction feedback point and each segment. Then, according to each pin position, they are grouped into three groups: central pins, edge pins and corner

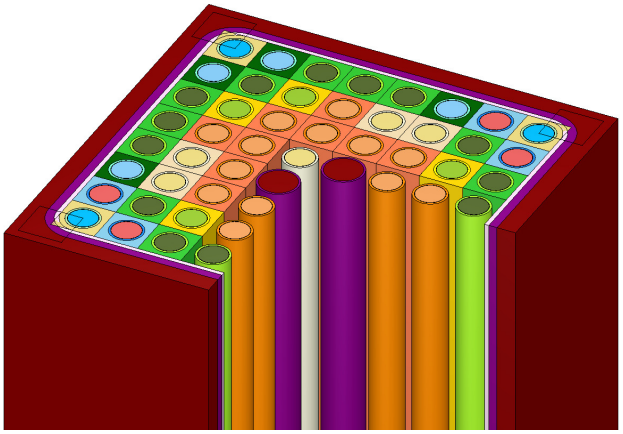

Fig. 4.16 – MCDancoff geometry representation by Keno3D.

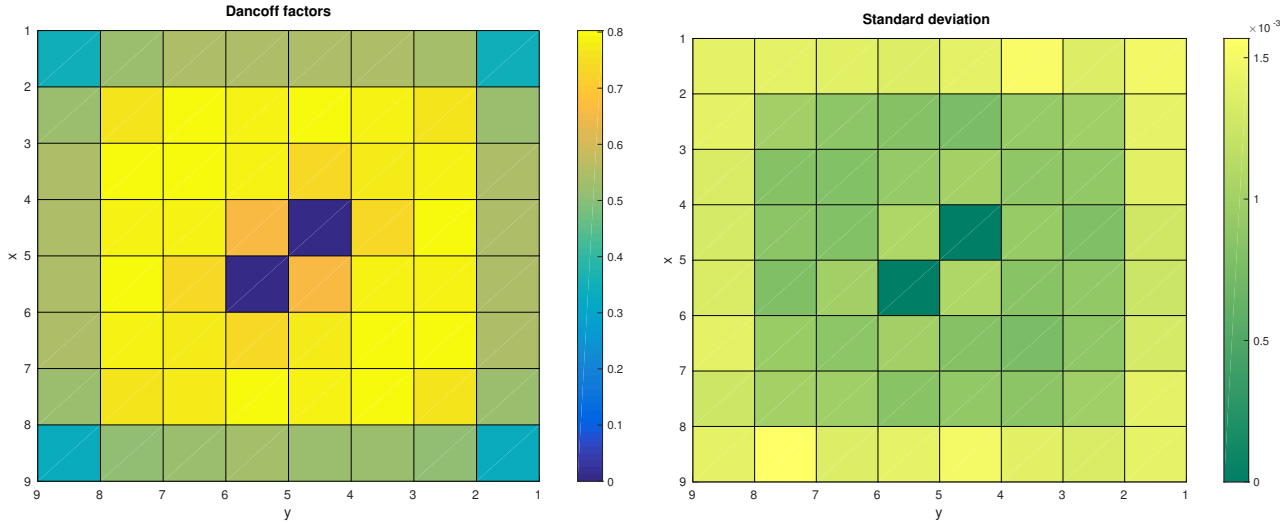

Fig. 4.17 – Dancoff factors predicted by MCDancoff module (left) and its standard deviation (right).

pins. The resulting average Dancoff factor is assigned to each pin group. Afterward, extra cell definitions are added to the lattice physics model if needed. For example, if two pins can be represented by one cell, but one of them is a central pin and the other is a corner pin, an extra cell is defined with a different Dancoff factor. Moreover, resulting Dancoff factors are also specified in SCALE branches according to the void fraction feedback parameter and cell definitions.

4.2 Thermohydraulic model for system codes

This time the nuclear reactor type is a PWR and the thermohydraulic code chosen to built the model is TRACE5.0p3. The model built has the main advantage that the reactor core is fully modeled in 3D. TRACE components discretized in three dimensions are used to achieve this goal. Therefore, in comparison to traditional models, asymmetric phenomena are better represented using this new feature. Hereafter, the model used in this thesis is presented, a 3D model using one cartesian and a cylindrical vessel. Nevertheless, two

additional 3D models are created using TRACE, for more information the reader is referred to Mesado et al. 2015. Due to the large number of variables and subscripts used to present the thermohydraulic model, a nomenclature section is presented in Section 4.2.2.

The main characteristics for the 3D model used are as follows.

- There is one cartesian vessel that represents all fuel assemblies. In the same axial level, each cell corresponds to one fuel assembly. Thus, there is not any fuel assembly collapse.
- There is one cylindrical vessel with two radial nodes. The innermost node represents the core bypass and the outermost simulates the downcomer, see Fig. 4.18 (left).
- The cylindrical vessel has $n_z + 2$ axial levels, n_z levels equally distributed as the cartesian vessel plus two additional axial levels representing the upper and lower plenum.
- The cylindrical vessel could be discretized in the theta direction to model different theta sectors. See Fig. 4.18 for a vessel discretized into 3 different theta cells.
- To establish the theta connection, a mapping assigning fuel element and its theta sector is needed, see Fig. 4.18 (right).
- Two mappings are established, one for the inlet connections and another for the outlet connections. They could be different, i.e. one bundle could be connected to different theta sectors at inlet and outlet levels.
- One break component is connected to each theta sector in the downcomer (outer radial node in the cylindrical vessel). The connection is at axial level, z_{break}.
- One fill component is connected to each theta sector in the downcomer (outer radial node in the cylindrical vessel). The connection is at axial level, z_{fill}, being $z_{fill} < z_{break}$.
- One heat structure is coupled with each cell representing a fuel assembly (cartesian vessel). Besides, one heat structure is associated with each bypass theta sector (cylindrical vessel).
- The heat transfer between bypass and downcomer (reactor barrel) is modeled through a heat structure. It does not have fuel rods, but is coupled to the inner/outer radial cell of the cylindrical vessel (convection boundary condition at both sides).
- One power component heats all heat structures but the heat structures simulating the reactor barrel.
- It is not possible to connect the fill or break component directly to the cylindrical vessel, thus one-cell big pipes are used between them.
- In order to connect both vessels, single junctions are used in the axial connections. See Table 4.8 for axial connection information.
- Both vessels are also connected sideways at all levels, one-cell pipes are used. See Table 4.9 for radial connection information. Single junctions cannot be used as sideways junctions for the thermohydraulic model.
- Forward and backward friction factors for all 1D components are required (parameter `nfrc1=2`). Although they are set identically in both directions, this could be useful for future studies.

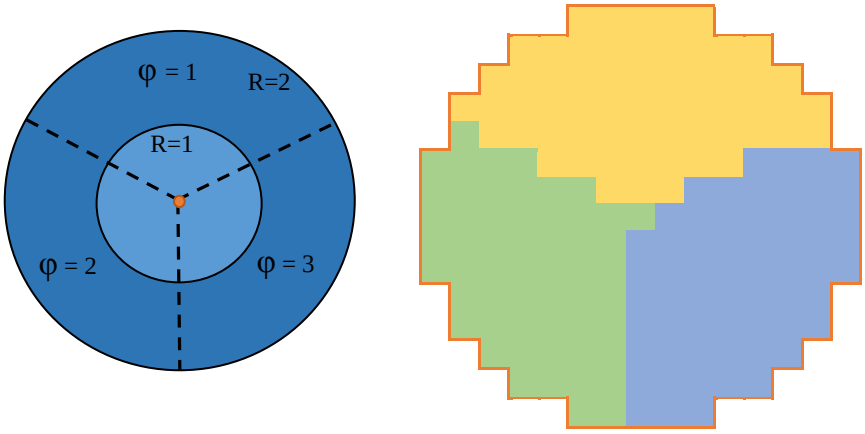

Fig. 4.18 – Cylindrical vessel discretized into 3 theta cells and 2 radial cells (left). Mapping between cartesian vessel cells and cylindrical theta cells (right).

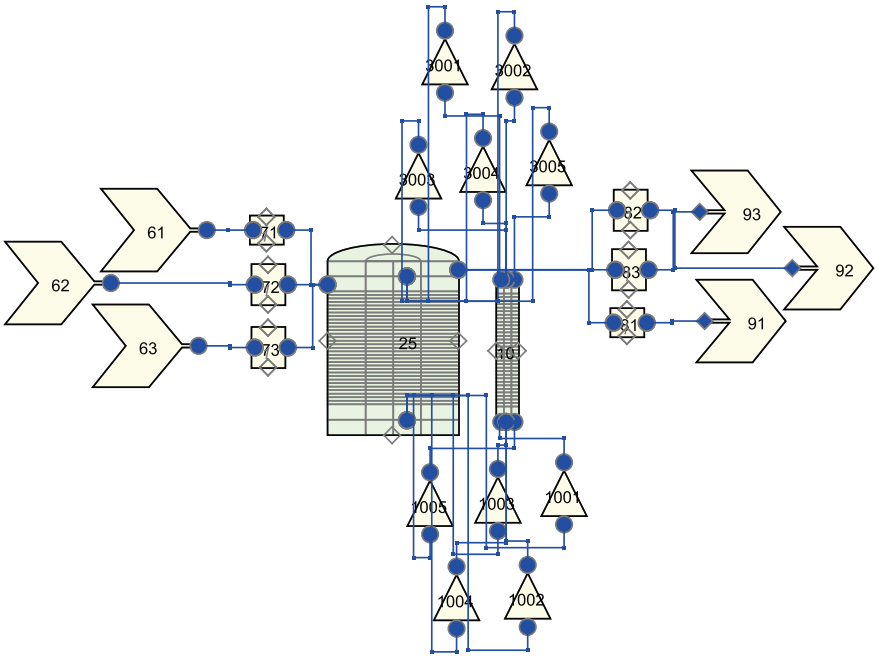

Fig. 4.19 – Thermohydraulic model sketch, simplified 5x5 cartesian vessel and three theta sectors.

See Fig. 4.19 for a simplified model (5x5 vessel without lateral junctions) and three theta sectors in the cylindrical vessel. Sketch using SNAP tool. As it can be seen, there is not any independent component representing the plenums because they are included in the cylindrical vessel. The inlet and outlet flow area for the cylindrical vessel are defined by next equations.

$$A_{in} = 2\pi Z(z_{fill})\sqrt{\frac{fa_{dc} + fa_{by}}{\pi}} \tag{4.5}$$

$$A_{out} = 2\pi Z(z_{break})\sqrt{\frac{fa_{dc} + fa_{by}}{\pi}} \tag{4.6}$$

Where

fa_{dc} is the downcomer flow area,

fa_{by} is the bypass flow area,

z_{fill} is the axial level where the fill components are connected to,

z_{break} is the axial level where the break components are connected to, and

$Z(k)$ is the cell height for a given axial level (k).

If n_{chan} is the total number of fuel assemblies and n^t_{chan} is the number of fuel assemblies in the t^{th} theta sector, the theta fraction, φ_t, is defined in Eq 4.7. Since there are several fills and breaks, the flow area for each fill or break component, fa^t_{fill} and fa^t_{break}, is the inlet/outlet flow area times the theta fraction, see Eq 4.8 and Eq 4.9. Similarly, the flow through each fill, $Flow^t_{fill}$, can be obtained with Eq 4.10.

$$\varphi_t = \frac{n^t_{chan}}{n_{chan}} \tag{4.7}$$

$$fa^t_{fill} = A_{in} \times \varphi_t \tag{4.8}$$

$$fa^t_{break} = A_{out} \times \varphi_t \tag{4.9}$$

$$Flow^t_{fill} = Flow_{tot} \times \varphi_t \tag{4.10}$$

The inlet/outlet flow area (fa^t_{fill} and fa^t_{break}) is applied to the fill/break flow area and its attached one-cell big pipe. These pipes are set horizontally and their friction factors are zero. Moreover, they are connected to the cylindrical vessel at inlet and outlet levels (z_{fill} and z_{break}), one to each theta sector and to the outer radial cell ($+R$).

The heat structures are defined with zero flux as the center boundary condition. The outer surface of heat structures associated to fuel assemblies (cartesian vessel) are coupled to the corresponding hydraulic cells. While the outer surface of heat structures heating the bypass are connected to each theta sector (innermost radial cell at cylindrical vessel). The characteristics of fuel assemblies, such as the number of fuel rods, are given by the manufacturer. This is introduced in TRACE using the surface multiplier variable (rdx). The bypass cells are heated by means of a heat structure per theta sector. Heat structures coupled to bypass cells are not modeled as fuel rods (TRACE variable $nofuelrod$ equal 1). The surface multiplier for each heat structure in a bypass cell, rdx^t_{by}, is given by the following equation.

$$rdx^t_{by} = \varphi_t \sum_{f=1}^{n^t_{chan}} rdx_f \tag{4.11}$$

Property	x**-direction**	y**-direction**	z**-direction**
Flow Area Fraction (FAF)	1	1	faf_z
Hydraulic Diameter (HD)	$Y_{cell}Z$	$X_{cell}Z$	hd_z
Friction Factor ($KFAC$)	$0.5(kfac_{x1} + kfac_{x2})$	$0.5(kfac_{y1} + kfac_{y2})$	$kfac_z$

Table 4.6 – Face cell physical properties for cartesian vessel.

All heat structures -except the heat structures representing the barrel- are powered by a single power component. The total reactor power, prompt heat and 3D nodal power distribution ($P(x, y, z)$) are provided by the power plant (or SIMULATE output files). With this data, the power fraction for each cell representing a fuel assembly, $\chi(x, y, z)$, can be obtained with Eq 4.12. Similarly, the power fraction for each cell representing the bypass, χ^t_{by} can be calculated with Eq 4.13.

$$\chi(x, y, z) = P(x, y, z)\frac{1 - H_{by}}{n_{cells}} \tag{4.12}$$

$$\chi^t_{by} = \frac{H_{by}}{n_{cells}}\varphi_t n_t \tag{4.13}$$

Where

n_{cells} is the number of cells heated by heat structures,

$$n_{cells} = n_{chans} + n_t \tag{4.14}$$

H_{by} is the power fraction that heats directly the bypass,

φ_t, is the theta fraction defined in Eq 4.7, and

n_t is the number of theta sectors.

The heat structure modeling the barrel between the downcomer and the core bypass has no power associated. Its thickness is set equal to the barrel thickness and the chosen material is stainless steel 304.

All cells in the vessel component have the same dimensions. Since each cell represents a fuel assembly, its dimensions, X_{cell} and Y_{cell}, are given by the manufacturer. Its flow area fraction can be calculated as shown in Eq 4.15. Note that the quantity $X_{cell}Y_{cell}$ (assembly total area) is bigger than the fuel assembly flow area, fa, because the structural components inside the assembly block a fraction of the total area. Thus, the flow area fraction for a fuel assembly cell must be smaller than one.

$$faf_z = \frac{fa}{X_{cell}Y_{cell}} \tag{4.15}$$

The physical properties for the cartesian vessel cell face in the x-direction, y-direction and z-direction can be seen in Table 4.6. The friction factors in all three dimensions, if not given by the manufacturer, must be defined by the expert analyzer.

Eq 4.16 shows that the volume fraction is the same as the flow area fraction in z-direction. However, the volume fraction must be calculated at the cell center (whereas the flow area fraction is obtained at cell faces), thus a linear interpolation is applied. See Eq 4.17 for fuel assembly volume fraction, and Eq 4.18 for bypass volume fraction. Index k represents the axial cell index.

Property	Bypass ($r = 1$)	Downcomer ($r = 2$)
Flow Area Fraction Radial (FAF_r)	see below	0
Flow Area Fraction Theta (FAF_t)	1	1
Flow Area Fraction Axial (FAF_a)	1	see below
Volume Fraction ($FVOL$)	1	1
Friction Factor Radial ($KFAC_r$)	0	0
Friction Factor Theta ($KFAC_t$)	0	0
Friction Factor Axial ($KFAC_a$)	$kfac_{z,by}$	$kfac_{z,dc}$

Table 4.7 – Face cell physical properties for cylindrical vessel.

$$fvol = \frac{faZ}{X_{cell}Y_{cell}Z} = \frac{fa}{X_{cell}Y_{cell}} = faf_z \tag{4.16}$$

$$fvol^k = \frac{1}{2}\left(faf_z^k + faf_z^{k+1}\right) \tag{4.17}$$

$$fvol_{by}^k = \frac{1}{2}\left(faf_{z,by}^k + faf_{z,by}^{k+1}\right) \tag{4.18}$$

Regarding the cylindrical vessel, as mentioned, it has two additional axial levels to simulate the lower/upper plenum. The height of this additional levels is the same as the first/last axial level height in the cartesian vessel. Spatial discretization for the cylindrical vessel, a-direction (axial), r-direction (radial) and t-direction (theta) is done with the following equations.

$$Z_a = [Z(1), Z(1), Z(2), \ldots, Z(n_z), Z(n_z)] \tag{4.19}$$

$$X_r = \left[\sqrt{\frac{fa_{by}}{\pi}}, \sqrt{\frac{fa_{by} + fa_{dc}}{\pi}}\right] \tag{4.20}$$

$$Y_t = 360\frac{n_{chan}^t}{n_{chan}} \tag{4.21}$$

Other physical properties, such as flow area fractions and friction factors, can be seen in Table 4.7.

Where $kfac_{z,by}$ and $kfac_{z,dc}$ are the friction factors, in the z-direction, for bypass and downcomer respectively. An iterative method to obtain appropriate values for the friction factors in the bypass is presented in Section 4.2.1. Values for the friction factors in the downcomer must be set by the expert analyzer (if not given by the plant).

The flow area fraction in radial direction for the first and last axial levels, Eq 4.22, is set to 1. Therefore, the fluid is able to flow from the bypass to the downcomer and vice versa. These cells simulate the lower and upper plenum.

$$FAF_r^{z,r=1} = \begin{cases} 1, & z = 1 \text{ or } n_z \\ 0, & \text{otherwise} \end{cases} \tag{4.22}$$

The flow area fraction in axial direction for the downcomer (outer radial cell in the cylindrical vessel) between the z_{fill} and z_{break} is set to zero. However, the expert analyst could set this value to a certain area fraction,

	Cylindrical vessel		Cartesian vessel	
Plenum	Axial level	Direction	Axial level	Direction
Lower	1	$+Z$	1	$-Z$
Upper	$n_z + 2$	$-Z$	n_z	$+Z$

Table 4.8 – Axial connections between both vessels.

$faf_{fill2break}$, thus the inlet fluid could flow directly upwards through the downcomer and directly to the outlet without cooling the core, Eq 4.23. This behavior is more realistic, nonetheless, studies have shown that $faf_{fill2break}$ near 10^{-3} leads to convergence and stability problems.

$$FAF_a^{z,r=2} = \begin{cases} faf_{fill2break}, & z_{fill} < z < z_{break} \\ 1, & \text{otherwise} \end{cases} \tag{4.23}$$

The hydraulic diameter for both radial cells can be expressed as follows.

$$HD_a^{r=1} = hd_{by} \tag{4.24}$$

$$HD_a^{r=2} = hd_{dc} \tag{4.25}$$

$$HD_r^{r=1} = 2\pi Z\sqrt{\frac{fa_{by}}{\pi}}\varphi^t \tag{4.26}$$

$$HD_r^{r=2} = 2\pi Z\sqrt{\frac{fa_{by} + fa_{dc}}{\pi}} \tag{4.27}$$

$$HD_t^{r=1} = Z\sqrt{\frac{fa_{by}}{\pi}} \tag{4.28}$$

$$HD_t^{r=2} = Z\sqrt{\frac{fa_{by} + fa_{dc}}{\pi}} \tag{4.29}$$

In order to connect both vessels, single junctions are used in the axial connections. All single junctions are set vertically. Their friction factors and hydraulic diameters are set equal to the first/last fuel assembly cell associated. The axial connections between both vessels must be set according to Table 4.8, otherwise the fluid does not flow correctly. Bear in mind that the axial level in the cylindrical vessel is referred to a maximum level of $n_z + 2$ because of the two additional levels (upper and lower plenums). To establish the theta connection a mapping assigning fuel element and its theta sector is needed, see Fig. 4.18 (right). The mapping for the upper and lower connections could be different.

For sideways connections -between cartesian and cylindrical vessel- one-cell pipes are used. Single junctions cannot be used as sideways junctions because TRACE does not allow more than one single junction to be connected to the same target cell and the same direction. The error thrown by TRACE is displayed hereafter.

```
*****************
**   warning   **
*****************

Connections in the same plane in one vessel are not in the same plane
of the other vessel

*****************
**   warning   **
*****************

Vessel 10, junction 3070201 is inconsistent with Vessel 10, junction
```

Sidewards pipes are set horizontally and their lengths are set to 0.1 m. Connections are set for every axial level and every single cell between the outermost cartesian vessel cells and the inner radial cell in the cylindrical vessel -i.e. between all orange faces in Fig. 4.18 (right) and the center orange point in Fig. 4.18 (left)-. Again, the theta connections are determined by the theta sector mapping, Fig. 4.18 (right). Connections between both vessels are summarized in Table 4.9 and its physical properties in Table 4.10. In this table, variables $kfac_{x,by}$ and $kfac_{y,by}$ are the friction factor for the bypass in the x and y-direction respectively. An iterative method to obtain their appropriate values is presented in Section 4.2.1.

The total number of components is detailed in Table 4.11, and expressed in Eq 4.30.

$$n_{comp} = 3 + 6n_t + 3n_{chan} + 2n_z(n_x - 2 + n_y - 2) \tag{4.30}$$

Where n_x and n_y are the number of cells in the cartesian vessel in x and y-directions respectively. The same can be done with the total number of junctions in the thermohydraulic model, Table 4.12 and Eq 4.31.

$$n_{junc} = 4[n_t + n_{chan} + n_z(n_x - 2 + n_y - 2)] \tag{4.31}$$

Finally, it is advisable to use some of the parameters available for TRACE regarding its inner numerical methods, these are specified in the namelist data cards. These parameters could increase the accuracy of the model and are summarized in Table 4.13.

Cylindrical vessel			**Cartesian vessel**	
Axial level	Radial cell	Direction	Axial level	Direction
$2, 3, \ldots, n_z + 1$	1	$-R$	$1, 2, \ldots, n_z$	$\pm X$ or $\pm Y$

Table 4.9 – Sidewards connections between both vessels.

Property	**x-direction**	**y-direction**
Flow Area Fraction	$x_{cell} \times Z$	$y_{cell} \times Z$
Hydraulic Diameter	$x_{cell} \times Z$	$y_{cell} \times Z$
Friction Factor	$kfac_{x,by}$	$kfac_{y,by}$

Table 4.10 – Sidewards connection physical properties.

Component	Quantity
Fill	n_t
Break	n_t
Big pipe	$2n_t$
Power	1
Cartesian vessel	1
Cylindrical vessel	1
Heat structure bypass	n_t
Heat structure barrel	n_t
Heat structure bundle	n_{chans}
Lower single junction	n_{chans}
Upper single junction	n_{chans}
One-cell pipe	$2n_z(n_x - 2 + n_y - 2)$

Table 4.11 – Component list in the thermohydraulic model.

Junction from	Junction to	Quantity
Fill	Inlet big pipe	n_t
Inlet big pipe	Cylindrical vessel	n_t
Cylindrical vessel	Outlet big pipe	n_t
Outlet big pipe	Break	n_t
Cylindrical vessel	Lower single junction	n_{chan}
Lower single junction	Cartesian vessel	n_{chan}
Cartesian vessel	Upper single junction	n_{chan}
Upper single junction	Cylindrical vessel	n_{chan}
Cartesian vessel	Sidewards one-cell pipe	$2n_z(n_x - 2 + n_y - 2)$
Sidewards one-cell pipe	Cylindrical vessel	$2n_z(n_x - 2 + n_y - 2)$

Table 4.12 – Junction list in the thermohydraulic model.

Parameter	Value	Description
`nosets`	1	Set the Semi-Implict numerical methods to solve the two-phase flow equations (instead of SETS). This option enforces a material Courant time step limit.
`nrslv`	1	Axial-direction conduction heat-transfer calculation in all heat structures.
`nsolver`	1	Enables the use of the SuperLU direct sparse matrix solver for all linear systems associated with flow equations. With this option, it is possible to create 1D flow loops connecting different directions in a vessel (e.g. one end of a loop connected to a vessel axial face and the other to a radial face).

Table 4.13 – Main TRACE parameters for numerical method options.

4.2.1 Bypass flow adjustment

An iterative process to adjust the bypass flow is developed in Mesado et al. 2015. The process modifies the bypass friction factor until the specified theoretical flow value is reached. In Fig. 4.20 a flow chart for the friction factor iterative process is presented.

Where

i: iteration count.

z: axial node.

$Flow^{*}_{by}$: theoretical bypass flow.

$Flow_{by}(i,z)$: simulation bypass flow for a given iteration and axial level.

$Flow_{error}$: maximum acceptable error.

$K^{Z}_{by}(i,z)$: bypass friction factor (axial) for a given iteration and axial level.

$K^{R}_{by}(i,z)$: bypass friction factor (radial) for a given iteration and axial level.

The iteration process starts generating the input deck and running the simulation. The resulting bypass flow, $Flow_{by}$, is read and compared with the theoretical bypass flow, $Flow^{*}_{by}$. If the difference is small enough (smaller than $Flow_{error}$), the iterative process ends. Otherwise it applies a correction for the axial bypass friction factor, K^{Z}_{by}, for each axial level (1D and 3D models). Only for 3D models, it is also possible to apply a correction for the radial bypass friction factor, K^{R}_{by}, for each axial level.

The correction for the axial bypass friction factor is proportional to the square ratio of the last obtained bypass flow and the theoretical flow (for each axial level). However, imagine that a certain bypass friction factor is small (say less than 1) and the resulting bypass flow is less than the theoretical bypass flow. In this case, the desired increase in bypass flow cannot be archived decreasing the friction factor anymore. Thus, the radial bypass friction factor at the immediate inferior level is increased by a factor of four. As a result, less flow will escape the bypass radially in the immediate inferior level and it will flow axially upwards.

The iteration process is carried out until the absolute error is satisfied. The error, $Flow_{error}$, is obtained comparing the bypass flow, for the last iteration step, with the theoretical bypass flow. For each new iteration step, a restart file is created. Thus, a restart is run with the considerable decrease in the simulation time. Once the friction factors are adjusted for the steady state simulation (SSA), the process is repeated for the coupled (with PARCS) steady state simulation (CSS). By default the initial guess for the CSS simulation is the converged value for the SSA. However, if the expert analyzer requests it, a new guess for the CSS simulation could be introduced. Once the CSS simulation is converged, the coupled transient simulation is run (CSS converged friction factors are used). See the diagram in Fig. 4.21.

Traditional 1D models do not have cross flow, thus the bypass flow is constant with height. Nevertheless, 3D vessel models simulate the cross flow for the whole core. The cross flow exists between reflector zones and fuel assemblies, and also among fuel assemblies. Therefore, in 3D models, because of the cross flow, the bypass flow strongly fluctuates along the axial axis. This is especially relevant in the 3D thermohydraulic model. Due to its theta sectors, friction factors could vary from one theta sector to another. The iterative process described above is successfully used to adjust the bypass flow for the 3D model presented here and others in Mesado et al. 2015. As an example, in Fig. 4.22, the bypass flow for a 3D model with three theta sectors (dashed lines) is compared with the homologous 1D model (straight lines). The x-axis represents

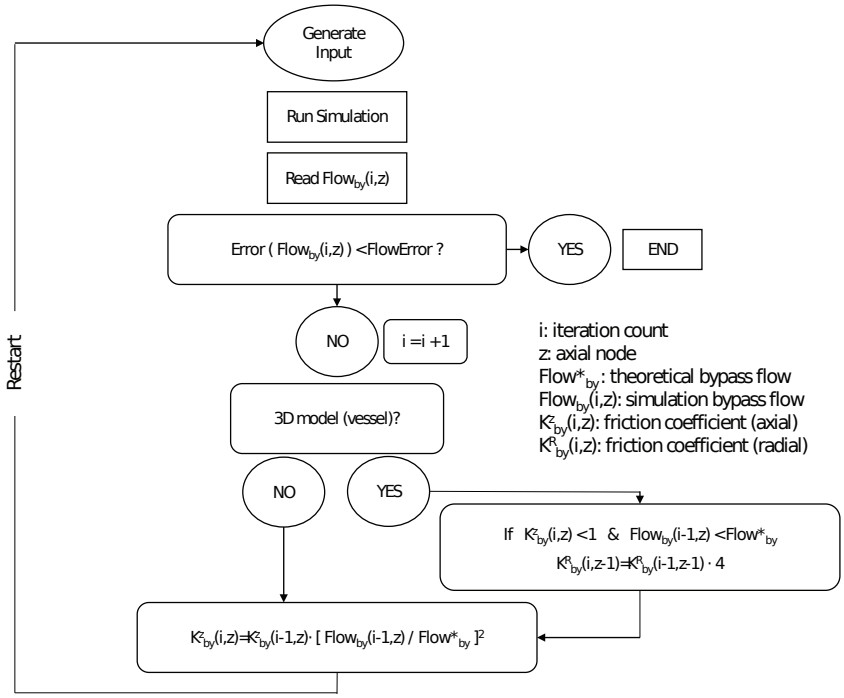

Fig. 4.20 – Bypass friction factor adjustment iteration process.

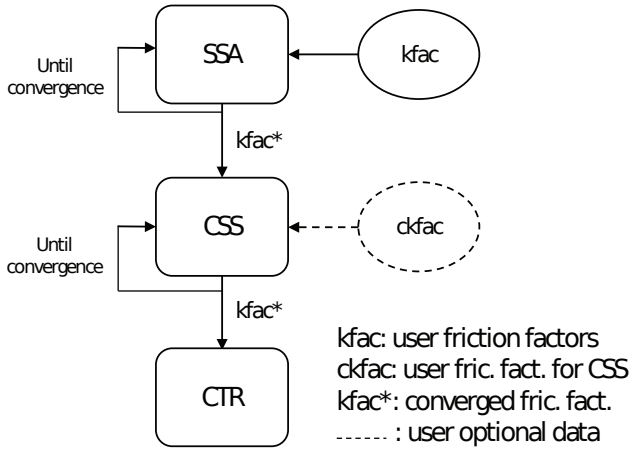

Fig. 4.21 – Friction factor input value for different simulation states.

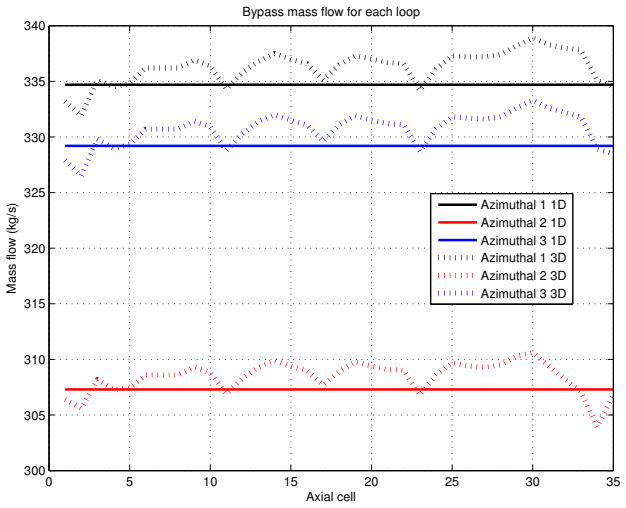

Fig. 4.22 – Bypass flow (axial direction) comparison between 1D and 3D models.

the axial cells (z-direction). The 1D model is built using pipes in RELAP code. In this case a maximum absolute error of 5 kg/s is set.

4.2.2 Nomenclature

Due to the large number of variables and subscripts used to present the thermohydraulic model, a summary for all variables is shown in this section. Along with the variable, a description and its source are also presented. The source can be an equation, a table, data provided by the nuclear plant or expert judgment.

Variable	Description	Source
φ^t	Assembly fraction for each theta sector	Eq 4.7
$\chi(x,y,z)$	Power fraction for each cell representing a fuel assembly	Eq 4.12
χ^t_{by}	Power fraction for each cell representing the bypass	Eq 4.13
A_{in}	System inlet area	Eq 4.5
A_{out}	System outlet area	Eq 4.6
fa	Assembly flow area	Plant
fa_{by}	Bypass flow area	Plant
fa_{dc}	Downcomer flow area	Plant
fa^t_{break}	Break flow area for each theta sector	Eq 4.9
fa^t_{fill}	Fill flow area for each theta sector	Eq 4.8
FAF_a	Flow area fraction in a-direction for cylindrical vessel	Table 4.7
FAF_r	Flow area fraction in r-direction for cylindrical vessel	Table 4.7
FAF_t	Flow area fraction in t-direction for cylindrical vessel	Table 4.7
FAF_x	Flow area fraction in x-direction for cartesian vessel	Table 4.6
FAF_y	Flow area fraction in y-direction for cartesian vessel	Table 4.6
FAF_z	Flow area fraction in z-direction for cartesian vessel	Table 4.6
faf_z	Flow area fraction in z-direction for assembly cells	Eq 4.15
$Flow_{by}$	Bypass mass flow	Sim
$Flow^*_{by}$	Theoretical bypass mass flow	Plant
$Flow_{error}$	Bypass mass flow maximum error accepted	Expert

$Flow^{t}_{fill}$	Inlet mass flow for each theta sector	Eq 4.10
$Flow_{tot}$	Total inlet mass flow	Plant
$FVOL$	Volume fraction for cylindrical vessel	Table 4.7
$fvol$	Volume fraction	Eq 4.16
$fvol^{k}$	Volume fraction for each axial level for assembly cells	Eq 4.17
$fvol^{k}_{by}$	Volume fraction for each axial level for bypass cells	Eq 4.18
H_{by}	Power fraction that heats directly the bypass	Expert
$HD^{r=1}_{a}$	Hydraulic diameter in a-direction for cylindrical vessel (bypass)	Eq 4.24
$HD^{r=2}_{a}$	Hydraulic diameter in a-direction for cylindrical vessel (downcomer)	Eq 4.25
$HD^{r=1}_{r}$	Hydraulic diameter in r-direction for cylindrical vessel (bypass)	Eq 4.26
$HD^{r=2}_{r}$	Hydraulic diameter in r-direction for cylindrical vessel (downcomer)	Eq 4.27
$HD^{r=1}_{t}$	Hydraulic diameter in t-direction for cylindrical vessel (bypass)	Eq 4.28
$HD^{r=2}_{t}$	Hydraulic diameter in t-direction for cylindrical vessel (downcomer)	Eq 4.29
HD_{x}	Hydraulic diameter in x-direction for cartesian vessel	Table 4.6
HD_{y}	Hydraulic diameter in y-direction for cartesian vessel	Table 4.6
HD_{z}	Hydraulic diameter in z-direction for cartesian vessel	Table 4.6
hd_{z}	Hydraulic diameter in z-direction for assembly cells	Plant
$hd_{z,by}$	Hydraulic diameter in z-direction for bypass cells	Plant
K^{by}_{R}	Bypass friction factor r-direction	Expert
K^{by}_{Z}	Bypass friction factor z-direction	Expert
$KFAC_{a}$	Friction factor in a-direction for cylindrical vessel	Table 4.7
$KFAC_{r}$	Friction factor in r-direction for cylindrical vessel	Table 4.7
$KFAC_{t}$	Friction factor in t-direction for cylindrical vessel	Table 4.7
$KFAC_{x}$	Friction factor in x-direction for cartesian vessel	Table 4.6
$kfac_{x}$	Friction factor in x-direction	Expert
$KFAC_{y}$	Friction factor in y-direction for cartesian vessel	Table 4.6
$kfac_{y}$	Friction factor in y-direction	Expert
$KFAC_{z}$	Friction factor in z-direction for cartesian vessel	Table 4.6
$kfac_{z}$	Friction factor in z-direction in assembly cells	Expert
$kfac_{z,by}$	Friction factor in z-direction in bypass cells	Expert
$kfac_{z,dc}$	Friction factor in z-direction in downcomer cells	Expert
n_{cells}	Number of cells	Eq 4.14
n_{chan}	Number of fuel assemblies	Plant
n^{t}_{chan}	Number of fuel assemblies for each theta sector	Expert
n_{comp}	Number of components in the system	Eq 4.30
n_{junc}	Number of junctions in the system	Eq 4.31
n_{t}	Number of theta sectors in cylindrical vessel	Expert
n_{x}	Number of cells in x-direction for cartesian vessel (typically one cell per bundle)	Plant
n_{y}	Number of cells in y-direction for cartesian vessel (typically one cell per bundle)	Plant
n_{z}	Number of cells in z-direction for cartesian vessel (axial levels)	Expert
$P(x,y,z)$	3D power distribution	Plant
rdx	Number of fuel rods per heat structure in assembly cell	Plant
rdx^{t}_{by}	Number of fuel rods per heat structure in bypass cell for each theta sector	Eq 4.11
X_{cell}	Length in x-direction for assembly cell (bundle x-length)	Plant
X_{r}	Radial discretization for cylindrical vessel	Eq 4.20
Y_{cell}	Length in y-direction for assembly cell (bundle y-length)	Plant

Y_t	Theta discretization for the cylindrical vessel	Eq 4.21
Z	Axial discretization for the cartesian vessel	Expert
Z_a	Axial discretization for the cylindrical vessel	Eq 4.19
z_{break}	Axial level for break connection	Expert
z_{fill}	Axial level for fill connection	Expert

Table 4.14 – Nomenclature for the thermohydraulic model.

4.3 Core neutronic physics model

Two different models at core level are built with the core physics code PARCS. One for the PWR and another for the BWR. The main characteristics for both models are summarized in Table 4.15. Both models contain 2 prompt neutron groups and 6 delayed neutron groups. All boundary conditions are set to zero flux, thus all neutrons traveling outside the reflector are lost. The decay heat model is activated and the diffusion equation solver is HYBRID -recommended in PARCS manual (Downar et al. 2010)-, see Section 3.1.3.1. The association between fuel assemblies and neutronic nodes is one to one, thus the models are not collapsed. The thermohydraulic 3D boundary conditions used for the BWR are between 600 and 1200 K for the fuel temperature, and moderator density between 100 and 800 kg/m^3. These are given to PARCS as 3D radial maps. The fuel type mapping and the control rod bank distribution are seen in Fig. 4.24 and Fig. 4.25 respectively, for PWR (left) and BWR (right).

For the PWR model, a control rod insertion -considered an *Anticipated Operational Occurrence* (AOO)- is simulated. The neutronic model in PARCSv3.0 is coupled with the 3D model explained in Section 4.2 (TRACE 5.0p3). Hence, the themohydraulic conditions are given by TRACE and are not explicitly set in PARCS. The rod insertion data corresponds to an experiment performed in a real nuclear reactor (test), the rod position can be seen in Fig. 4.23. The test is performed releasing a control rod -with maximum worth- from its lock and allowing its free fall, the reactor is operating at 100% of its nominal power. The insertion (fall) lasts 2.1 seconds, it begins at 50.0 seconds. The whole simulation lasts 100.0 seconds, the purpose of the initial 50.0 seconds is to ensure that the initial conditions are converged (transient simulation). The control rod inserted is shown in Fig. 4.25 (left) as bank 14, initially the control rod is fully withdrawn at notch 340.

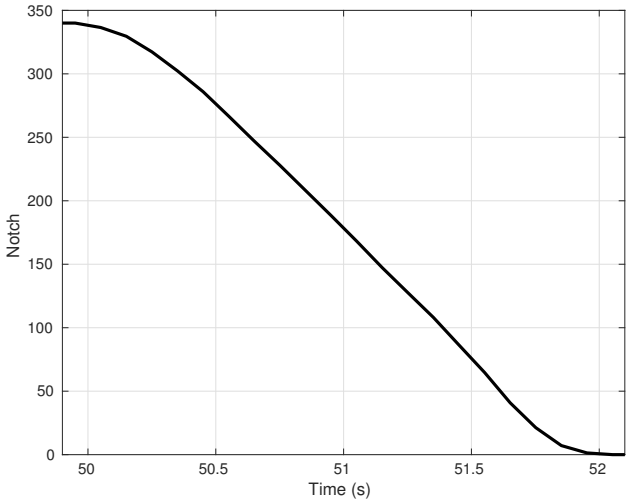

Fig. 4.23 – Control rod insertion for the PWR.

Property	PWR	BWR
Type	PWR	BWR
Power level	100%	92%
Fuel assemblies	177	624
Assembly layout	16x16	8x8
Control rod banks	14	4
Radial cells	17x17	30x30
Axial cells	34 (2 reflectors)	27 (2 reflectors)
Cell dimensions	23x23 cm	15.24x15.24 cm
Cell height	10.625 cm	15.24 cm
Fuel assembly cells	177	624
Reflector zone cells	64	116
Fuel types	3	4
Neutronic compositions	1379 (3 reflectors)	103 (3 reflectors)

Table 4.15 – Main features for the neutron kinetic model (PWR and BWR cores).

4.4 Verification

4.4.1 Lattice physics model

A code-to-code comparison between SCALE (red lines) predictions and CASMO (black lines) -as reference code- is shown in this section. Cross sections and neutronic parameters are presented in Fig. 4.26 and Fig. 4.27. Differences using v7-56 or v7-252 and with default or more accurate Dancoff factors are very small in most of the cross sections to be seen in these charts. The results are presented for segment number 14 with control rods withdrawn. Group 1 is the high-energy group (fast) and group 2 is the low-energy group (thermal). The comparison is made for the whole void range and a fuel temperature equal to 879.5 K.

In comparison with Wang et al. 2013, the same trends can be seen for all cross sections represented in Fig. 4.26. The mentioned study does not show results for parameters shown in Fig. 4.27. It can be concluded that SCALE predictions are in agreement with CASMO for all void range. The following conclusions can be extracted comparing the results in the mentioned study and data in Fig. 4.26.

- k_{eff}: SCALE and CASMO values cross each other as the void fraction increases. SCALE prediction is slightly overestimated (respect to CASMO).
- Σ_{12}: this cross section behaves almost linearly with the void. SCALE values are overestimated with respect to CASMO.
- D_{f1}: discrepancies are lower for high void fraction level. SCALE overestimates these values.
- D_{f2}: the match is almost perfect over the void fraction.
- Σ_{a1}: the match is almost perfect over the void fraction.
- Σ_{a2}: almost linear behavior as a function of void fraction, SCALE overestimate this cross section.
- $\nu\Sigma_{f1}$: SCALE underestimate this cross section.
- $\nu\Sigma_{f2}$: SCALE overestimate this cross section.

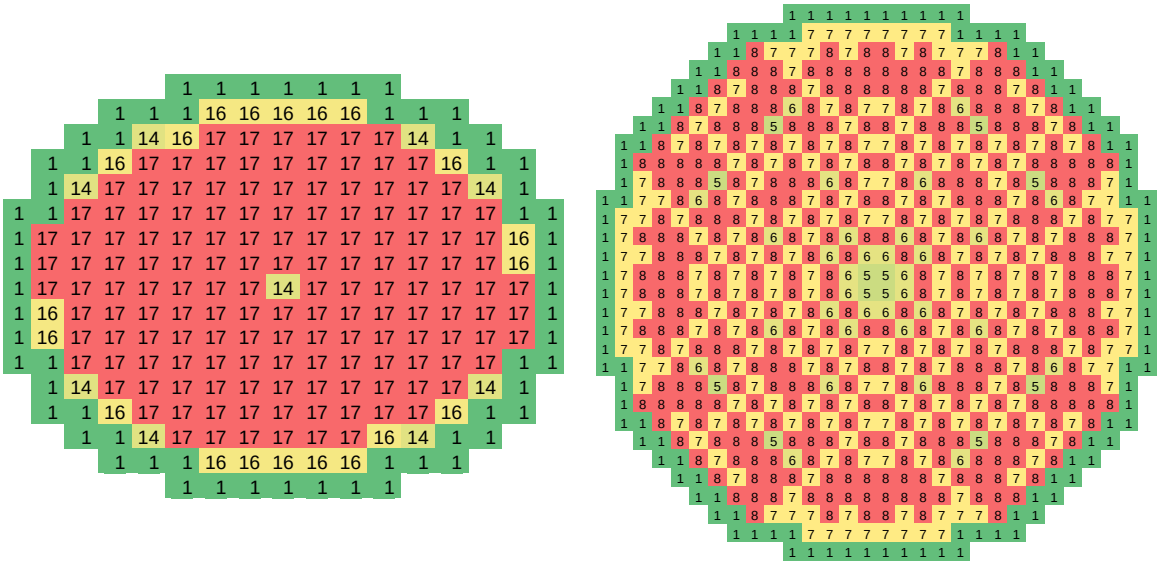

Fig. 4.24 – Fuel type radial mapping, PWR (left) and BWR (right).

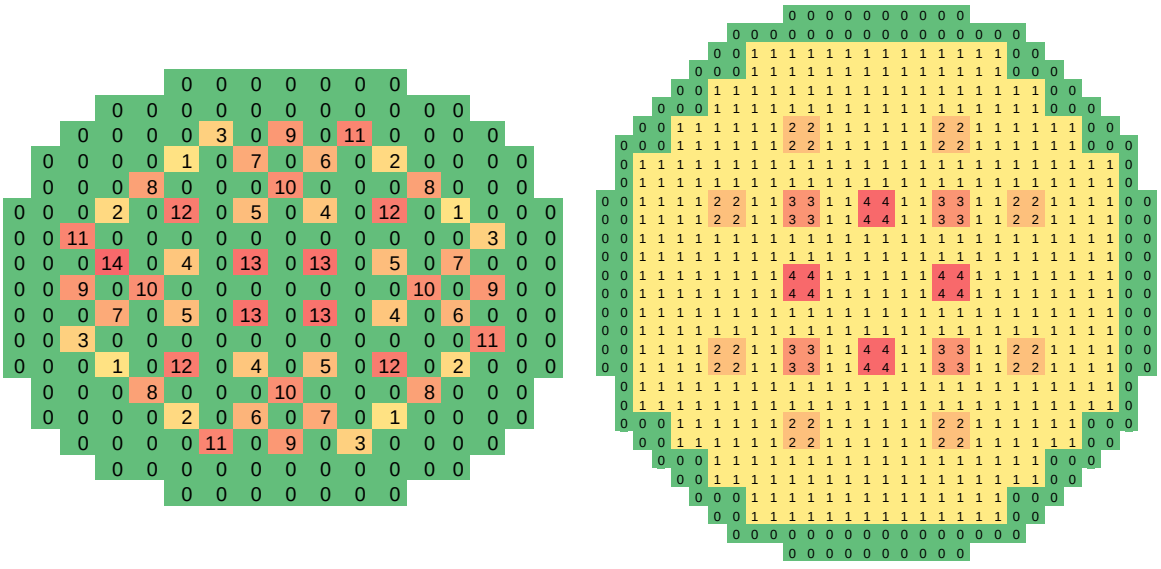

Fig. 4.25 – Control rod bank distribution, PWR (left) and BWR (right).

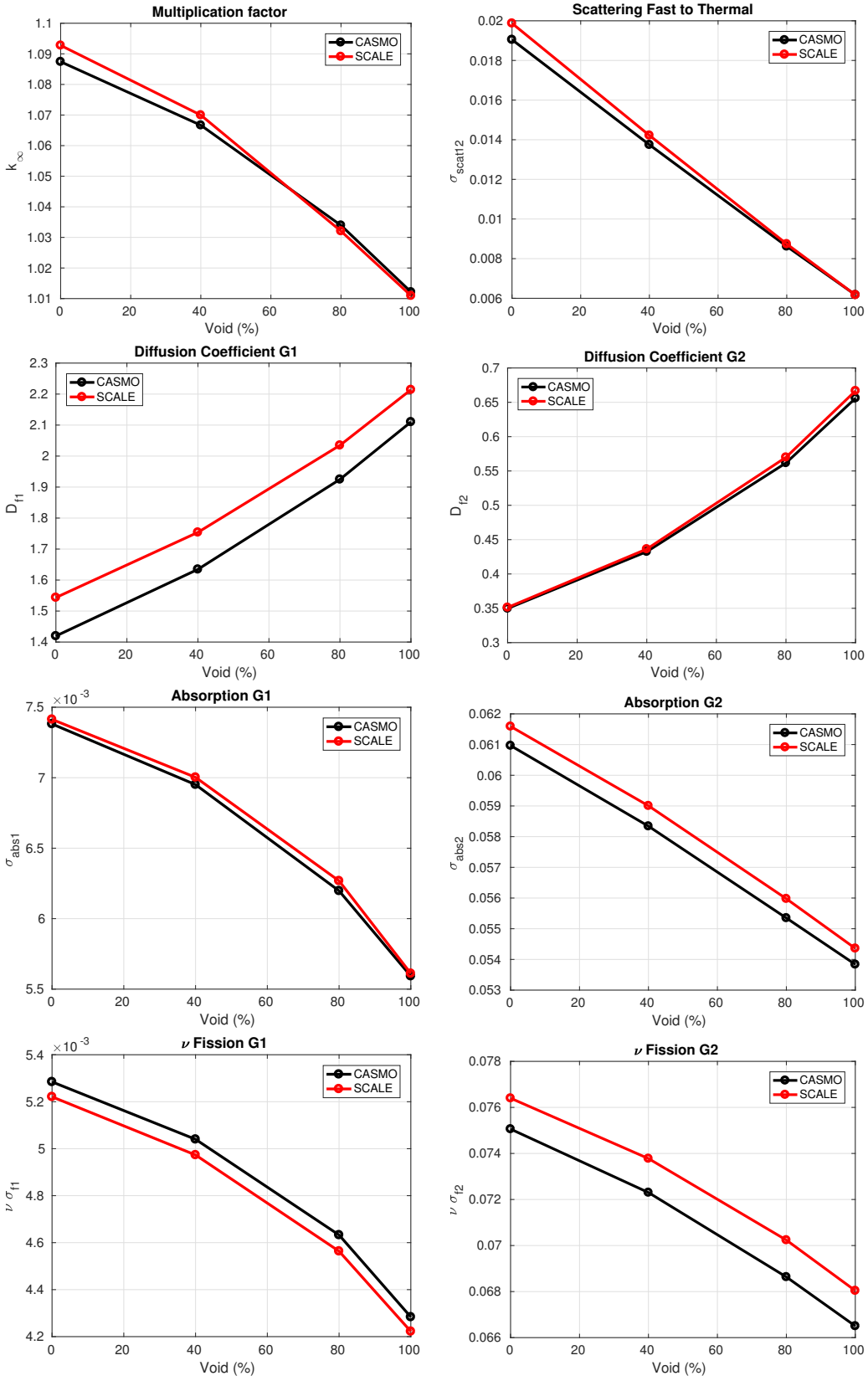

Fig. 4.26 – Code-to-code comparison between CASMO (black lines) and SCALE (red lines) - neutronic parameters.

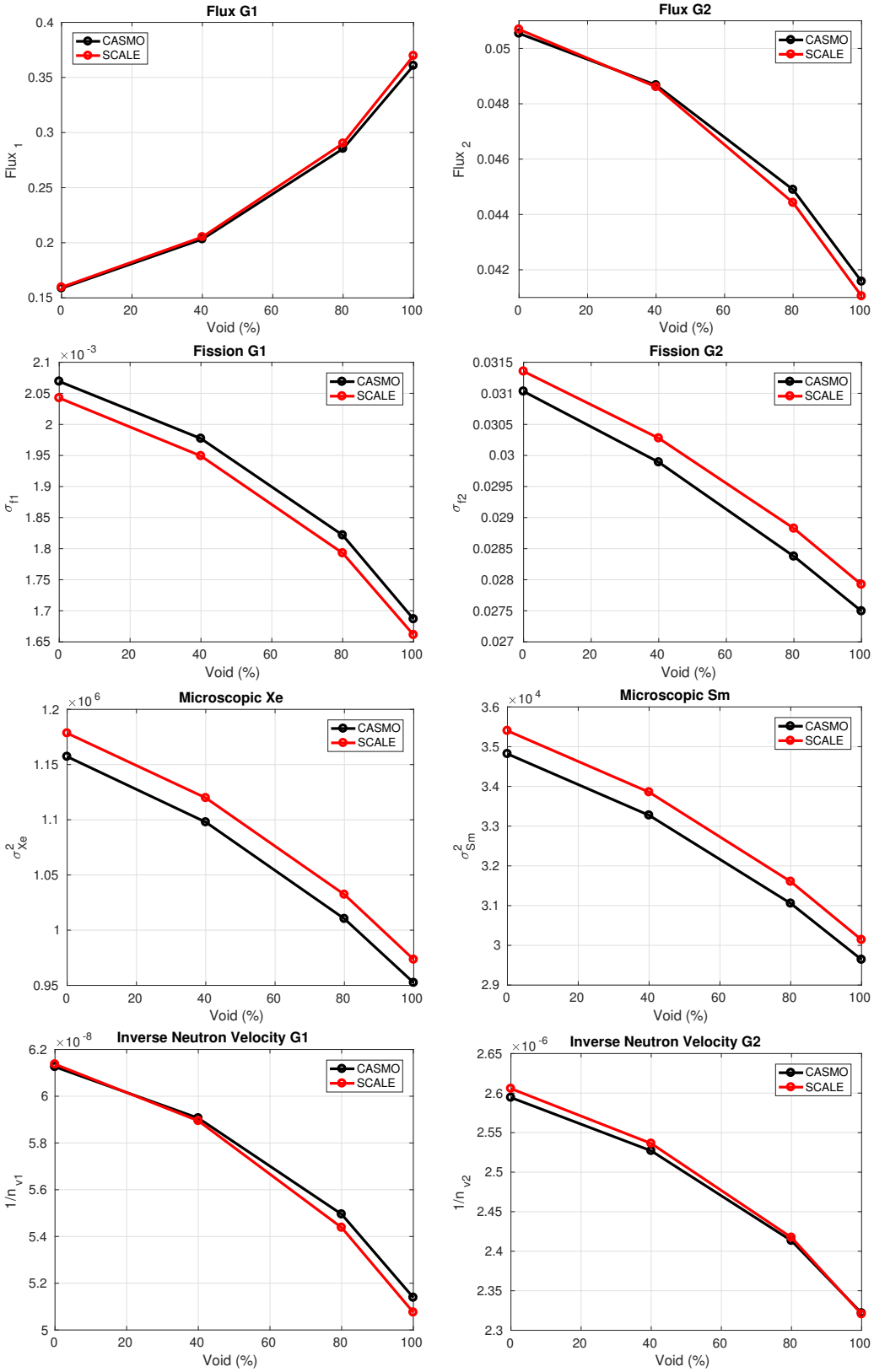

Fig. 4.27 – Code-to-code comparison between CASMO (black lines) and SCALE (red lines) - neutronic parameters.

4.4.2 NEMTAB generation

In order to verify the NEMTAB generation, steady state simulations with PARCSv3.2 alone and the BWR core are used. NEMTAB libraries can be obtained following CASMO or SCALE predictions as explained in Section 4.1.1. The PARCS model used is explained in Section 4.3 (BWR reactor). However, due to the limitations shown in Section 4.1.1 regarding the feedback parameter points available in CASMO, constant 3D maps as thermohydraulic boundary conditions are generated with fuel temperature of 879.5 K and 456.32 kg/m^3 as moderator density.

SCALE and CASMO results are compared to verify the NEMTAB library generation. CASMO is used as the reference code in all cases. Fig. 4.28 compares the normalized axial power profiles and Fig. 4.29 compares the radial power profile. Two cases are shown, the left plot is an ARO case (all rods out), and the right plot is an ARI case (all rods in). Results for SCALE are obtained with the use of accurate Dancoff factors (MCDANCOFF module) and the v7-252 library. Results for CASMO are obtained with the use of the flux discontinuity factor (FDF) in the reflector zones. Results for other computational parameters are very similar and differences are almost imperceptible in a chart. These can only be seen numerically and are discussed in the following paragraphs.

The multiplication factor obtained is shown in Table 4.16 for all combinations of computational parameters (FDF, Dancoff and library) and both cases ARO and ARI. Table 4.17 and Table 4.18 shows the errors for the k_{eff} and axial/radial power profiles, also with all computational parameter combinations. The root mean square (RMS) error is used to express profile errors, while the difference in the k_{eff} is expressed with pcm units.

A better axial/radial power profiles are obtained for the ARO case with a RMS error of 0.2% and 0.6% respectively and about 12.0% and 1.9% for the ARI case. The axial power profile error increases in the power peak zone -especially in the ARI case- and the radial power profile error increases in the reflector zone. Regarding the k_{eff} difference, the trend changes and the smallest difference is 174 pcm for the ARI case and 244 pcm for the ARO case. Comparing both libraries (v7-56 and v7-252) it is seen that axial and radial differences are very similar for both cases. Reduction in about 0.4% are found in the axial difference for the ARI case when the v7-252 library is used. The k_{eff} difference is slightly reduced when the v7-252 library is used with default Dancoff factors (k_{eff} difference is reduced 12 pcm), but it is better to use the v7-56 library when accurate Dancoff factors are used (k_{eff} difference is reduced 32 pcm). The k_{eff} difference, for the ARO case, is also reduced when the v7-252 library and the default Dancoff factors are used (about 70 pcm), but the difference is negligible when accurate Dancoff factors are used. The use of the default/MCDANCOFF Dancoff factors does not have almost any effect on the axial or radial power profiles. However, it can reduce the k_{eff} difference about 40% when the v7-56 library is used and about 30% when the v7-252 library is used. The use of the flux discontinuity factor in CASMO increases the k_{eff} difference with SCALE -especially for the ARI case (+17 pcm)- but slightly reduces the axial and radial power profile differences in the ARI case.

After the brief sensitivity study explained above, the v7-56 library and the accurate Dancoff factors (MCDANCOFF) are recommended for criticality studies with SCALE6.2.1. These parameters lead to a more balanced results on the different errors, see boldface values on Table 4.17 and Table 4.18. Nevertheless, due to the computational resources and time required when perturbations are applied, the default[4] Dancoff factors -with v7-56 library- are used for the *Uncertainty and Sensitivity* (U&S) in this thesis.

[4] An increase in computational resource when accurate Dancoff factors are used is expected. However, a huge increase in memory used by SCALE is observed, the reason for such a dramatic increase is unknown. Therefore, default Dancoff factors are used to propagate neutronic parameters with SAMPLER (1000 perturbations).

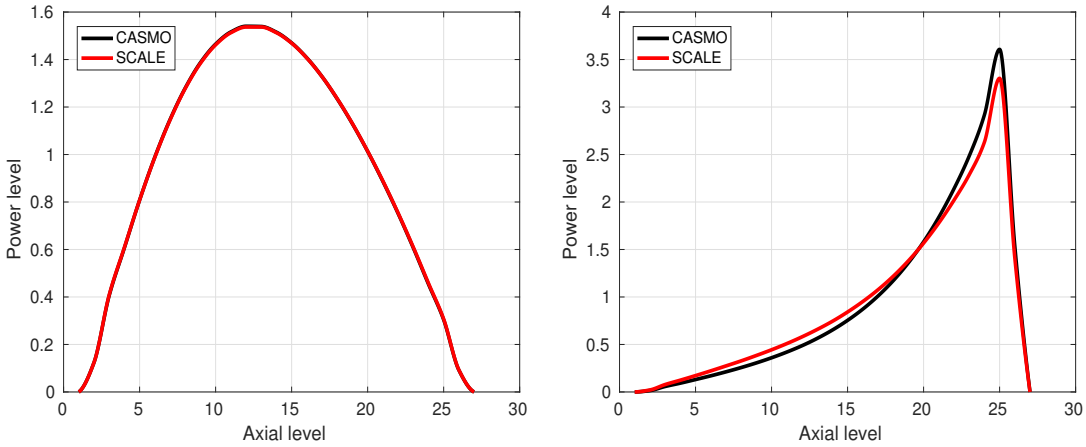

Fig. 4.28 – Axial power profile predicted by PARCSv3.2, ARO (left) and ARI (right).

	CASMO		**SCALE v7-56**		**SCALE v7-252**	
	With FDF	Without FDF	Default	MCDANCOFF	Default	MCDANCOFF
ARO	**1.03171**	1.03172	1.03601	**1.03417**	1.03533	1.03416
ARI	**0.79702**	0.79719	0.80023	**0.79893**	0.80011	0.79925

Table 4.16 – k_{eff} predicted by PARCSv3.2.

Parameter		k_{eff} **(pcm)**		**RMS$_{axial}$ (%)**		**RMS$_{radial}$ (%)**	
FDF	Dancoff	v7-56	v7-252	v7-56	v7-252	v7-56	v7-252
Yes	Default	429.5	362.1	0.24	0.21	0.53	0.53
No	Default	428.4	361.0	0.24	0.21	0.63	0.63
Yes	MCDANCOFF	**246.0**	244.9	**0.24**	0.21	**0.53**	0.53
No	MCDANCOFF	244.9	243.8	0.23	0.21	0.63	0.63

Table 4.17 – Errors predicted by PARCSv3.2, ARO case.

Parameter		k_{eff} **(pcm)**		**RMS$_{axial}$ (%)**		**RMS$_{radial}$ (%)**	
FDF	Dancoff	v7-56	v7-252	v7-56	v7-252	v7-56	v7-252
Yes	Default	321.1	308.9	11.98	11.53	1.75	1.73
No	Default	303.7	291.5	12.83	12.39	2.03	2.01
Yes	MCDANCOFF	**191.5**	223.3	**12.09**	11.56	**1.74**	1.72
No	MCDANCOFF	174.1	205.9	12.95	12.42	2.02	2.00

Table 4.18 – Errors predicted by PARCSv3.2, ARI case.

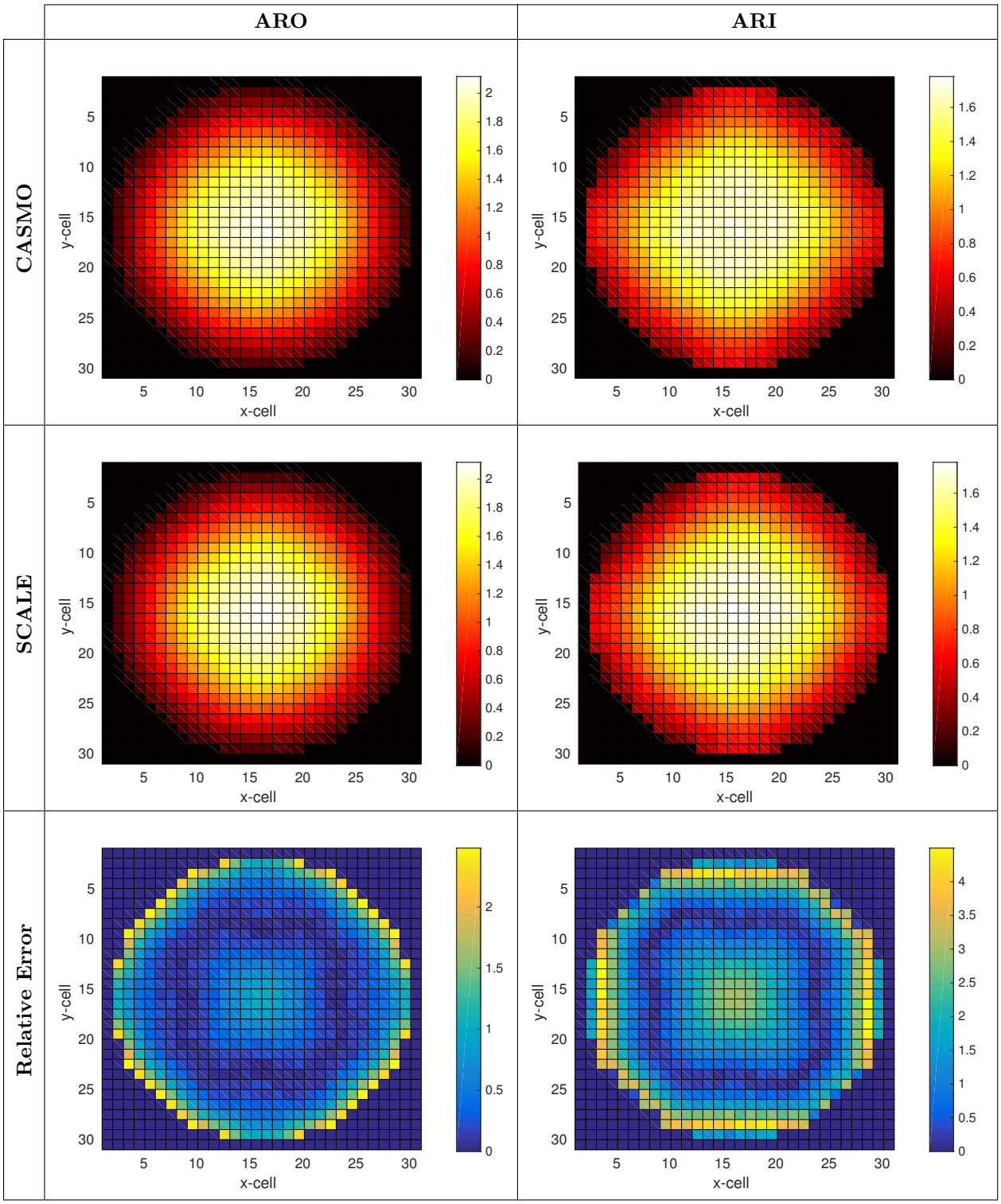

Fig. 4.29 – Radial power profile predicted by PARCSv3.2, ARO (left) and ARI (right).

4.4.3 Thermohydraulic model

In order to verify the 3D model, a traditional 1D model is created in TRACE. It has one pipe per fuel assembly (no collapsed model) and its heat structure associated. The bypass is modeled using a big pipe, also with a heat structure component. All pipes are connected to an upper and lower plenum. The boundary conditions in the fill and break components are the same as in the 3D model. See Fig. 4.30 for a simplified traditional model (collapsed), sketch using SNAP tool. Moreover, a collection of plots is presented comparing the traditional 1D model and the 3D model developed in this chapter. Table 4.19 summarizes the information of this comparison (figure number, variable and source).

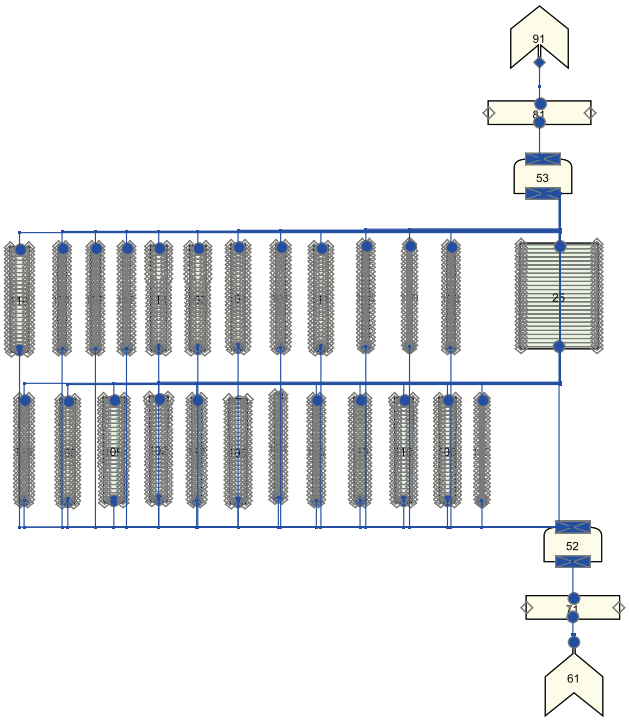

Fig. 4.30 – Traditional model sketch, simplified collapsed model.

Figure	Variable	Source
Fig. 4.31	Mass flow	TRACE (SSA)
Fig. 4.32	Liquid density	TRACE (SSA)
Fig. 4.33	Liquid temperature	TRACE (SSA)
Fig. 4.34	Centerline fuel temperature	TRACE (SSA)
Fig. 4.35	Surface fuel temperature	TRACE (SSA)
Fig. 4.36	Nomalized 2D power	TRACE-PARCS (CSS)
Fig. 4.37	Total power and k_{eff}	TRACE-PARCS (CTR)
Fig. 4.38	Reactivity components	TRACE-PARCS (CTR)
Fig. 4.39	Enthalpy and minimum DNBR	TRACE-PARCS (CTR)
Fig. 4.40	Average Doppler and moderator temperature	TRACE-PARCS (CTR)

Table 4.19 – Figures comparison summary.

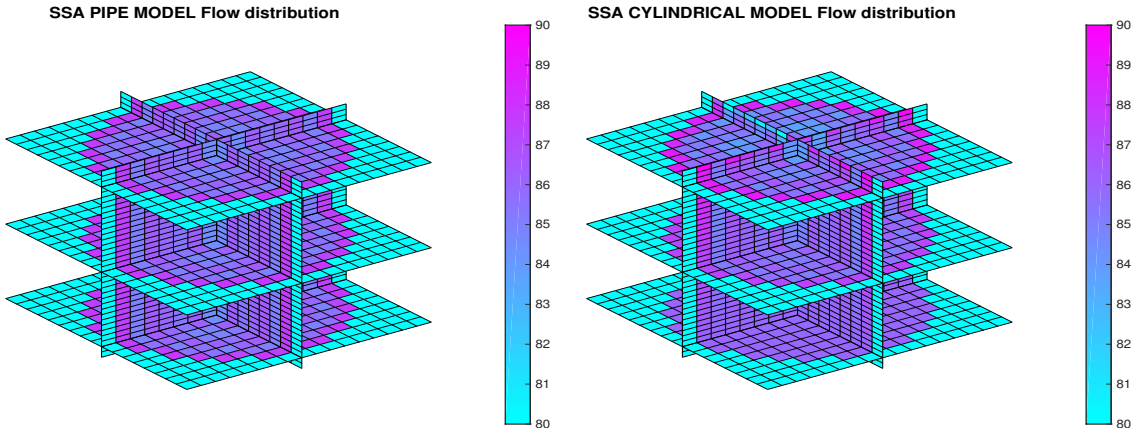

Fig. 4.31 – Mass flow 3D distribution (kg/s).

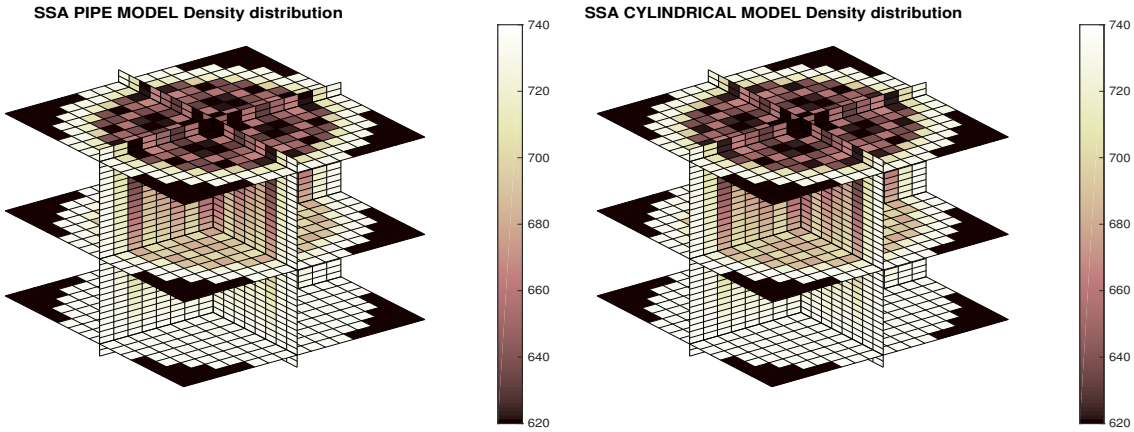

Fig. 4.32 – Liquid density 3D distribution (kg/m^3).

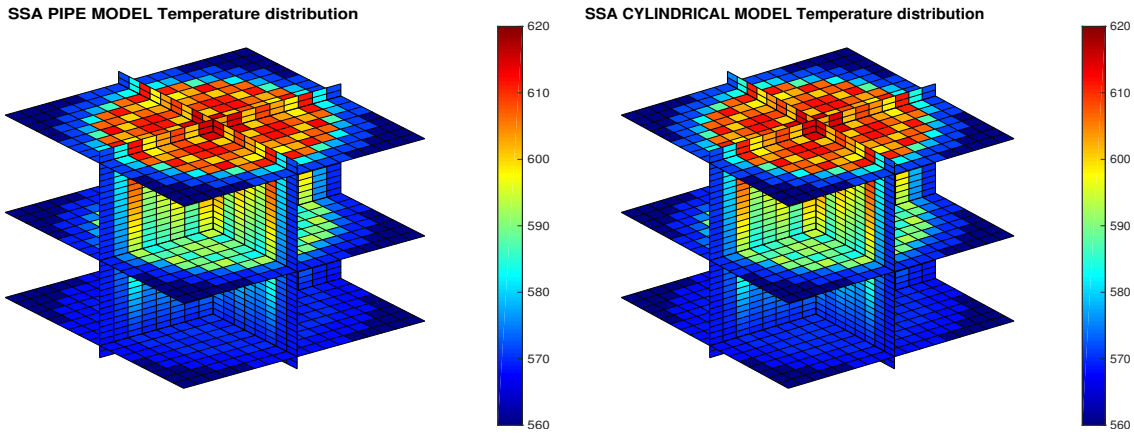

Fig. 4.33 – Liquid temperature 3D distribution (K).

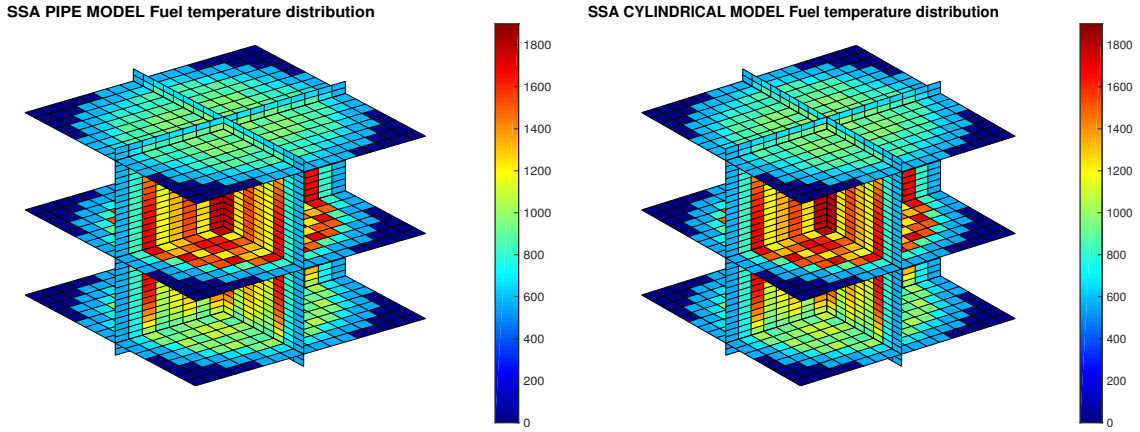

Fig. 4.34 – Centerline fuel temperature 3D distribution (K).

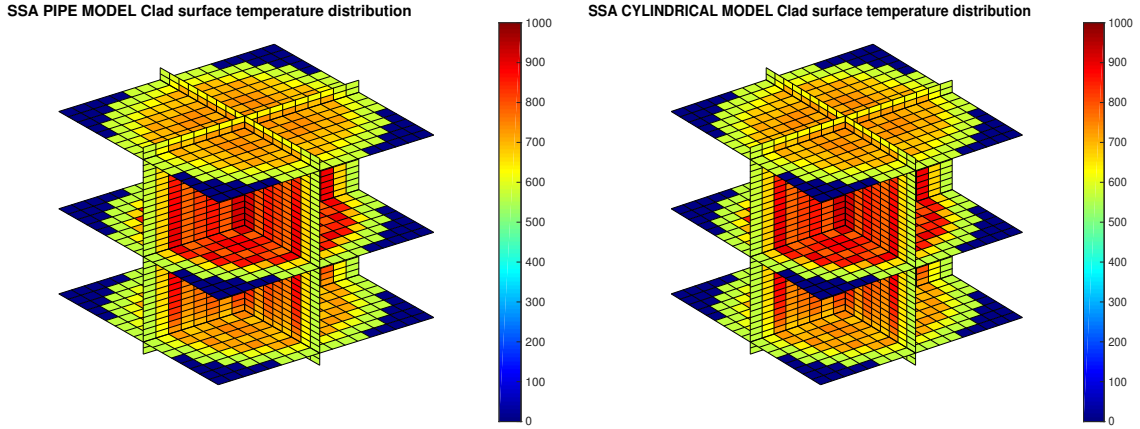

Fig. 4.35 – Surface fuel temperature 3D distribution (K).

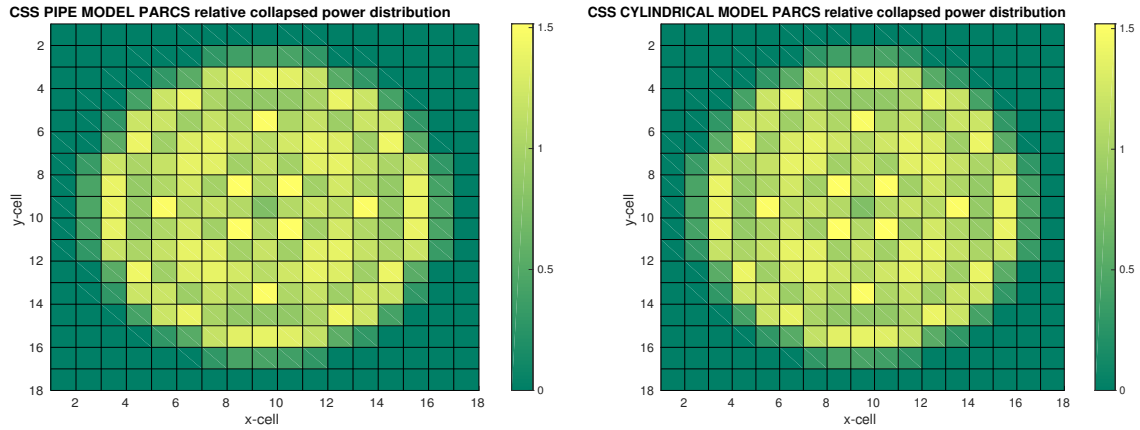

Fig. 4.36 – Normalized power 2D distribution (TRACE-PARCS coupled steady state).

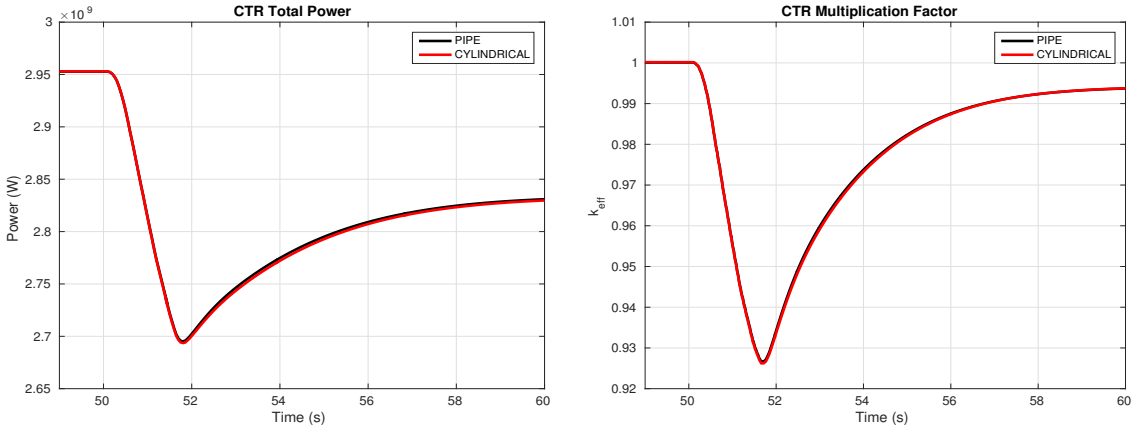

Fig. 4.37 – Total reactor power (left) and multiplication factor (right).

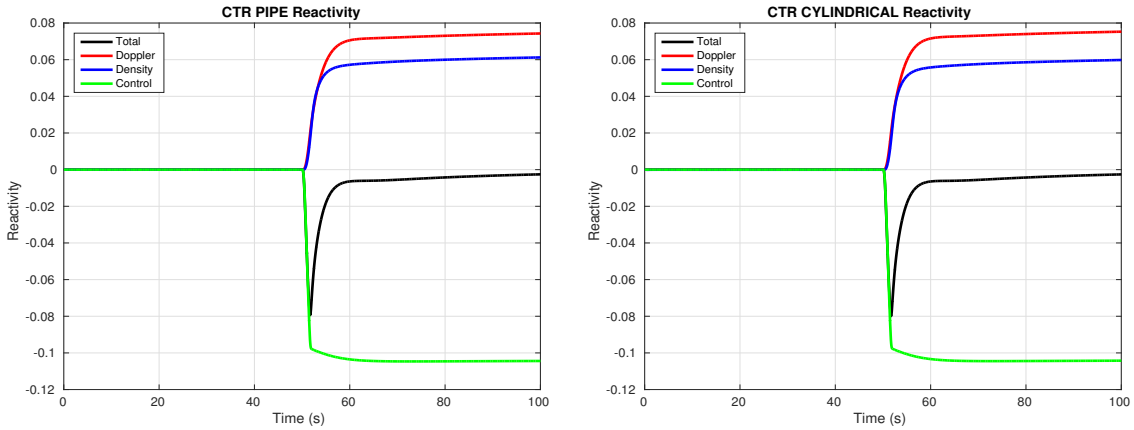

Fig. 4.38 – Reactivity components from PARCS ($).

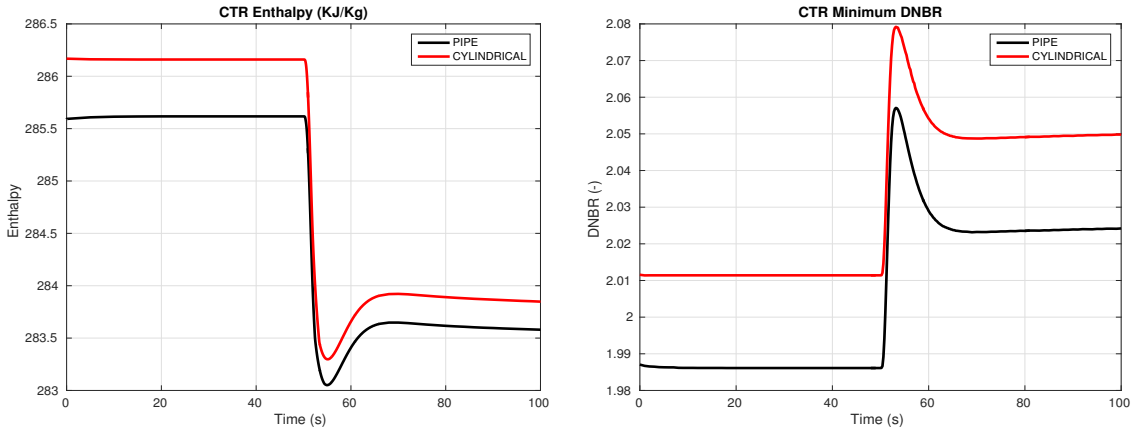

Fig. 4.39 – Enthalpy (left) from PARCS and minimum DNBR from TRACE (right).

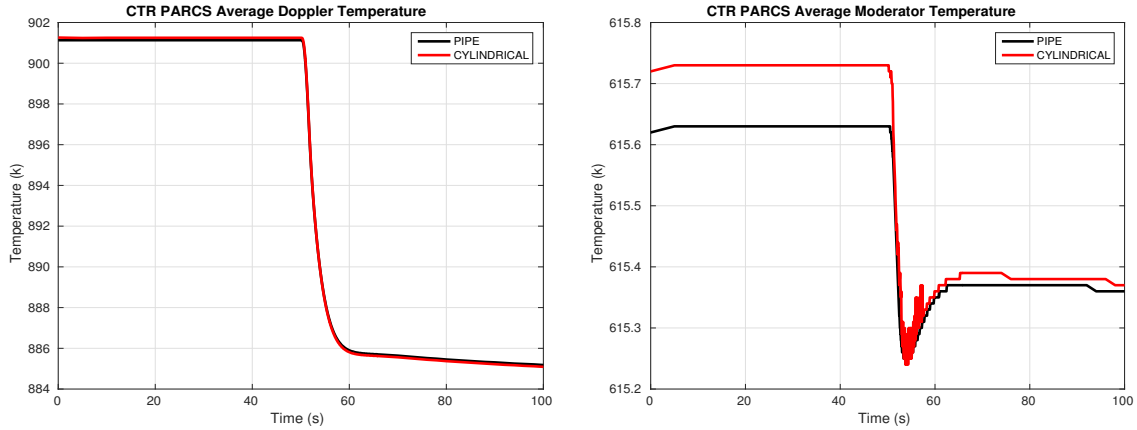

Fig. 4.40 – Average Doppler temperature (left) and average moderator temperature (right), from PARCS.

In this thesis, the recent tendency to extend codes or models into a 3D discretization is followed. All comparisons show, almost, a perfect agreement between the 1D and the 3D models. It is true that the 3D model uses considerably more computational time, but the main advantage of the 3D model, in comparison of the traditional 1D model, is that it can represent asymmetric phenomena realistically -especially the cross-flow among fuel elements and phenomena occurring in the bypass-. In this thesis, a control rod insertion was simulated. Even though the control rod inserted was not in the core center, the results with both models were basically identical. The explanation for this is in the physics scale controlling this phenomenon. A control rod insertion affects the moderator only locally, but not a big scale of it. Thus, the 3D model is suitable for asymmetric phenomena that change the moderator conditions in a relatively big scale. For example, significant coolant temperature variation in a cold leg or a pump trip in one of the loops. Besides, a difference in the DNBR calculated is shown in Fig. 4.39 (right plot). In this case, experimental data is not available to perform a validation, but it is suspected that the 3D model provides the best estimate data.

Chapter 5

Methodology

. . . make your life less uncertain but more repetitive.

A methodology is devised to propagate cross sections and other nuclear data through SCALE6.2.1 and PARCSv3.2. The propagation process can be divided into two steps. The first step performs the propagation at assembly level with SCALE, while the second step is at core level with PARCS. The first step takes into account the cross section uncertainties contained in the master library ENDF/B-VII (default library provided with SCALE6.2.1). The propagation process adds the uncertainty incorporated due to the collapse and homogenization cross section phase. In the second step, the *Nuclear Data Library* (NDL) generated is used to run a steady state alone with PARCS. PARCS source code is modified to perturb the main cross sections with perturbation factors generated with DAKOTA 6.3 statistical tool. Perturbation factors follow a normal distribution and are sampled using a random sampling method. Finally, the uncertainty propagated is reflected in PARCS output parameters (multiplication factor -k_{eff}-, axial power peak -P_z- and peak node location -N_z-). Even though in this thesis the methodology to propagate the cross section uncertainty is shown without thermohydraulic coupling, there is not any limitation in the methodology that prevents the core physics code to be coupled with a thermohydraulic code, as it was proved by the same thesis' author in Mesado et al. 2012. The default perturbation library provided with the module SAMPLER is used to propagate the uncertainty through SCALE. Nonetheless, a procedure to create an in-house perturbation library is developed and is shown here to be used in future works. The perturbations -for the perturbation library and PARCS- are generated with DAKOTA statistical tool following a normal distribution and using a random sampling method. SAMPLER module is used to perform the *Uncertainty Quantification* (UQ) in SCALE, while DAKOTA tool is used to perform the *Uncertainty and Sensitivity* (U&S) in PARCS. The BWR core is used.

Moreover, a similar methodology is used with the PWR core to propagate the thermohydraulic uncertainty through TRACE-PARCS coupled code. A total of 43 thermohydraulic parameters are selected to be propagated. Their *Probability Distribution Function* (PDF) definitions are found in the related literature or, if not found, defined based on expert judgment. These uncertainties are finally reflected on the enthalpy, power and reactivity predicted by PARCS. The U&S analysis is performed with DAKOTA 6.3 statistical tool and the PWR core is used.

The methodology for uncertainty propagation of cross sections is explained in Section 5.1 and the methodology for thermohydraulic uncertainty propagation is explained in Section 5.2. The most important data for both methodologies is summarized in Table 5.1. Before going into details on the developed methodology, a comment regarding the chosen sample size must be made.

– Lattice level (first step). The uncertainty through SCALE is propagated using the covariance library included with SAMPLER. Therefore, the accuracy of results increases with the number of samples. The maximum number of samples allowed in SAMPLER is chosen, 1000 samples or perturbations.

– Core level (second step). There are 3 dependent output parameters (k_{eff}, P_z and N_z). For these responses, it is only of interest the upper tolerance region. Thus, using Eq 2.4 for a 95/95 case with one-sided tolerance region and 3 partially dependent responses, the minimum sample size is 124 (Table 2.2). Nevertheless, 1000 samples are run again.

– Thermohydraulic parameters. In this case, there are also 3 dependent output parameters for TRACE-PARCS (power, reactivity and enthalpy). Again, it is only of interest the upper tolerance region and the minimum sample size is 124, but 146 samples are run.

Property	**Nuclear data propagation**		**TH parameter prop.**
Reactor	BWR	BWR	PWR
Code	SCALE6.2.1	PARCSv3.2	TRACE5.0p3 & PARCSv3.0
U&S code	SAMPLER	DAKOTA 6.3	DAKOTA 6.3
Model scale	Lattice	Core	Core
Model description	Section 4.1	Section 4.3	Section 4.2 & Section 4.3
Simulation state	SSA (BOC)	SSA	SSA, CSS & CTR
Input parameters	Problem-independent cross sections in ENDF/B-VII.	Problem-dependent homogenized and collapsed cross sections for the whole core and all feedback parameter combinations.	Thermohydraulic parameters for TRACE model.
Number of input parameters	99232	715	43
Output parameters	Problem-dependent homogenized and collapsed cross sections for one segment and specific feedback parameter set.	Multiplication factor, axial power peak and peak node location.	Power, enthalpy and reactivity.
Number of output parameters	7	3	3
Sampling method	SRS	SRS	SRS & LHS
PDF	Normal	Normal	Normal & Uniform

Table 5.1 – Data summary for cross section and thermohydraulic parameter uncertainty propagation.

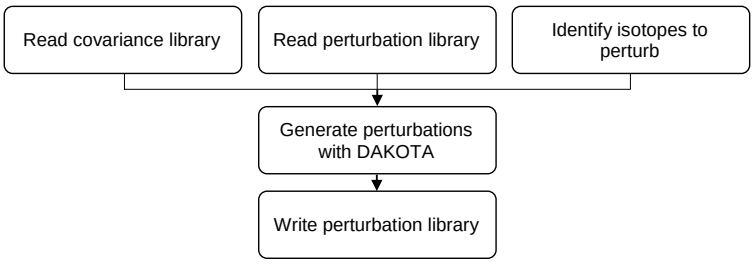

Fig. 5.1 – Flow diagram to generate a perturbation library.

5.1 Cross section propagation

The methodology developed to propagate the uncertainty of cross sections is developed in this section. The uncertainty is propagated through a lattice physics code and then through a core physics code, the process is schematically depicted in Fig. 3.10.

5.1.1 Perturbation library generation

Even though the default perturbation library provided in SCALE6.2.1 is used in this thesis, a procedure to create an in-house perturbation library is developed. It is thought that can be used in future works. The advantage for a in-house perturbation library is that the user is free to choose any PDF and/or sampling method to generate the perturbations. The flow diagram to generate the perturbation library is presented in Fig. 5.1.

First, the original perturbed library (MG_Perturbations[1]) and the covariance library (56groupcov and 252groupcov[2]) -both provided in SCALE6.2.1- are read.

- The covariance library contains data for 2587 different cross sections and 2546 covariance matrices. This library is based on several different uncertainty approximations with varying degrees of "fidelity". It includes evaluated covariances obtained from ENDF/B-VII, ENDF/B-VI, and JENDL3.3. Fig. 5.2 shows the covariance matrix for the ^{235}U between elastic scattering and fission nuclear interactions, the upper and side plots show the relative standard deviation as a function of energy.
- The perturbation library has 1000 sets of perturbations for 1772 different isotope-reaction pairs. This library is obtained using Medusa module in XSUSA program assuming multivariate normal PDF and covariance given by the covariance library.

If each isotope-reaction pair (1772) and energy group (56 provided the v7-56 library is used) is considered a different parameter. The total number of input parameters is 99232, this could consume much of the available computational resources. SAMPLER module is programmed to withstand this number of input parameters, however, computational resources needed by DAKOTA could be huge. To reduce the computational burden, only the isotopes found in the SCALE model are perturbed. As explained in Section 3.1.1.5, the user can control the isotopes that SCALE is tracking in the depletion module by means of the `addnux` TRITON parameter. In this thesis a value of four -highest- is chosen for `addnux` parameter. The process to decide if cross section for isotope i, reaction x and energy group g is included as input parameter to propagate is explained hereafter. The process is also schematically depicted in Fig. 5.3.

1. Isotope n^i is searched in the perturbation and covariance libraries. If n^i is found in both libraries, proceed with step 2, otherwise discard n^i.

[1] Library in binary format.
[2] Libraries in binary format, but ASCII versions are available if asked to the *U. S. Nuclear Regulatory Commission* (NRC).

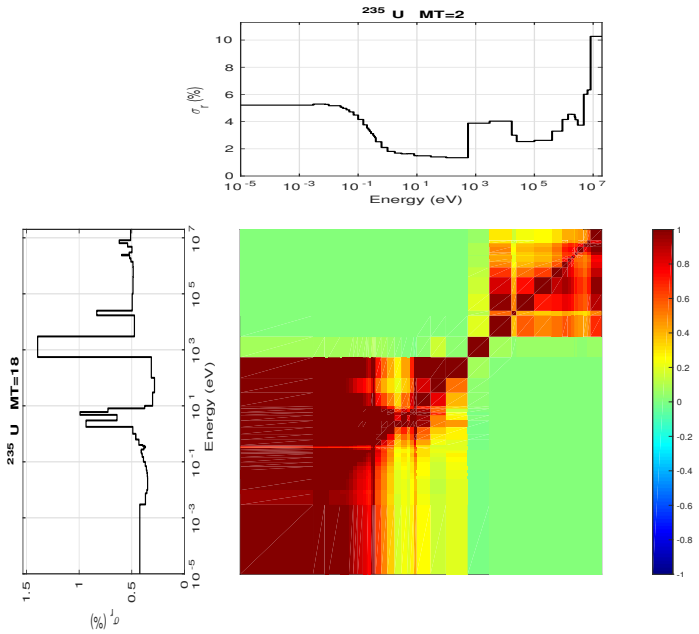

Fig. 5.2 – Covariance matrix for ^{235}U between elastic scattering (MT=2) and fission (MT=18).

2. For reaction x, if n_x^i is found in both libraries, proceed with step 3, otherwise discard n_x^i. Loop over all reactions.

3. If standard deviation of $n_{x,g}^i$ is greater than zero, then include $n_{x,g}^i$ as input parameter, otherwise discard $n_{x,g}^i$. Loop over all energy groups (g). Then, proceed to step 1 with next isotope.

After the input parameters are isolated, new perturbation factors must be created using DAKOTA statistical tool. As indicated in Williams et al. 2013b, perturbations in the original perturbation library are randomly generated and follow a normal PDF with average one and covariance given by the covariance library. Here, the user is free to keep or change the distribution for each isotope-reaction pair and/or the sampling method. Then, the perturbations are arranged following the AMPX format to generate the new perturbation library.

Three final comments related to the generation of perturbations must be included.

– Perturbations in SAMPLER are multiplicative factors, as shown in Eq 3.43. Therefore, their PDF average must be set equal to one.

– To avoid nonphysical negative perturbations, lower and upper limits must be set (for example 0 and 2 respectively). This seems in agreement with the default perturbations in MG_Perturbations library. However, other limits could be used, for example $\pm\sigma$ or $\pm 2\sigma$. In this case, results must be checked for any negative perturbation.

– Parameters found in the original perturbation library, but excluded following the process in Fig. 5.3, must be set as non-perturbed factors. Since perturbations in SAMPLER are multiplicative factors, this is accomplished setting its perturbation equals to one.

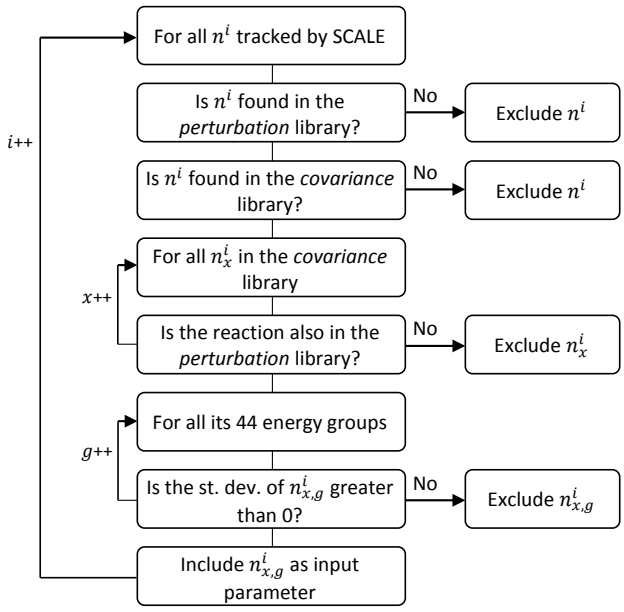

Fig. 5.3 – Flow diagram to exclude cross sections as input parameters.

5.1.2 Propagate cross section uncertainty

Two steps are followed to propagate the cross section uncertainty through all the process. The first step propagates the uncertainty through the lattice physics code (SCALE6.2.1) using SAMPLER module. Unfortunately, SAMPLER module lacks capability for *Sensitivity Analysis* (SA) in SCALE6.2.1. The second step propagates the uncertainties through PARCSv3.2 core physics code and DAKOTA is used to perform this U&S analysis. These two steps are further explained hereafter.

5.1.2.1 Uncertainty propagation through SCALE6.2.1

The model explained in Section 4.1 is used in SAMPLER to propagate the uncertainty, the v7-56 library and default[3] Dancoff factors are used. SAMPLER applies the perturbations found in the perturbation library to the cross sections found in the master library ENDF/B-VII. In this thesis, fission yields and decay data are not perturbed. The uncertainty information for these parameters is still under study and is not accurate and therefore, it is left for a future study. According to the core configuration, the whole core is composed by 9 different types of segments (3 of which represent the reflector zone), see Fig. 4.15. Each segment must be run 1001 times (one per perturbation set plus one non-perturbed case). Moreover, each segment has 62[4] different feedback parameter combinations, see Table 4.3 and Table 4.4. Due to the high number of simulations ($9 \cdot 1001 = 9009$) and computational resources, only fresh fuel is considered at this point. USAS-XL[5]

[3] Although accurate Dancoff factors are recommended, a huge increase in memory used by SCALE is observed when accurate Dancoff factors are used. Therefore, default Dancoff factors are used instead.

[4] Since reflector segments do not have the control rod variation, these segments only have half of the feedback parameter combinations, 31.

[5] Uncertainty & Sensitivity Analysis for Scale Xsec Libraries (USAS-XL) is a MATLAB program created within the context of this thesis to automatically propagate cross section uncertainty through SCALE and PARCS. Among other features, it translates CASMO input decks into SCALE format and propagates the cross section uncertainty in the master library using SAMPLER.

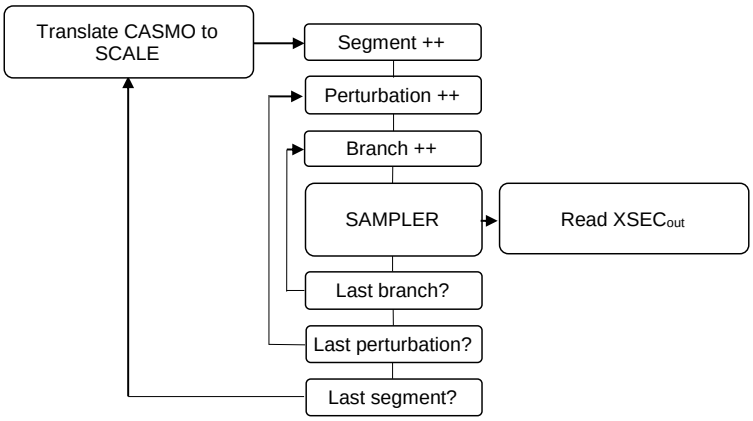

Fig. 5.4 – Flow diagram to generate homogenized and collapsed cross sections.

and TXT2NTAB [6] MATLAB programs are developed to automatically propagate cross section uncertainty through SCALE and PARCS. See Section 4.1 for more information about the SCALE model. The whole process can be seen in Fig. 5.4.

The output parameters are seven problem-dependent homogenized and collapsed cross sections. These are obtained for each branch defined in SCALE (feedback parameter combination) and for each segment. The seven output parameters are listed next.

1. Diffusion coefficient for fast group, D_{f1}.
2. Diffusion coefficient for thermal group, D_{f2}.
3. Absorption cross section for fast group, Σ_{a1}.
4. Absorption cross section for thermal group, Σ_{a2}.
5. Average neutrons per fission times the fission cross section for fast group, $\nu\Sigma_{f1}$.
6. Average neutrons per fission times the fission cross section for thermal group, $\nu\Sigma_{f2}$.
7. Scattering cross section from fast to thermal group, Σ_{12} (down-scattering).

SAMPLER is currently under development and has some bugs that prevents successful statistical calculations in two special situations. These bugs have been reported and are expected to be solved in a future version. These situations are (i) branches are used and (ii) more than one homogenized region is defined. Both features are used in this thesis, branches are used to define different feedback parameter sets and two homogenized regions are defined for reflector segments. To cope with this problem, a workaround method is devised. The main idea behind this workaround is explained in four steps.

1. Run all simulations with SAMPLER. The simulations will finish but afterward an error is thrown and the statistical calculation fails. The error is shown hereafter. Keep the cross section results (either `txtfile16` or `xfile016`).

[6] TXT2NTAB is a program developed to generate NEMTAB libraries out of SCALE results (Mesado et al. 2017). This program has been created on request of the Expert Group on Uncertainty Analysis in Modelling (UAM-LWR) and is used to generate NEMTAB libraries to distribute among the benchmark participants.

```
Calculations are done.
Gathering response data..*
Responses gathered, performing evaluations.terminate called after throwing an instance
    of 'Standard::assertion'
what(): Insist: data1.size() == data2.size(), failed in
    /tmp/regression/workspace/Jupiter-Scale-Dev/source/packages/
    ScaleUtils/Math/Stats.cpp, line 110.
The following message was provided:
"Data size for correlation must match."
sh: line 1: 14178 Aborted                 /home/cmesado/scale6.2b2/bin/sampler < input
```

2. The results are rearranged so there are as many finished simulations as branches. Fig. 5.5 shows the hierarchical file structure, names inside a rectangle represent directories. Index i goes from zero (unperturbed simulation) to the total number of perturbations, in this thesis 1000.

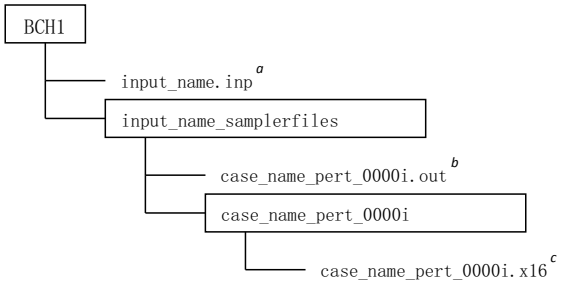

Fig. 5.5 – File structure for SAMPLER module.

   - File `input_name.inp` is the SAMPLER input file, it contains the response definitions (homogenized and collapsed cross sections). The sequence block could be empty since simulations will not be run (see next step).
   - Output file `case_name_pert_0000i.out` only contains the sentence *SCALE is finished.*
   - File `case_name_pert_0000i.x16` contains the cross section data obtained by SCALE in step 1. However, only data for the first feedback parameter combination (or branch) and the interested homogenized region (reflector, if it exists) is introduced. This means that the file format must be changed accordingly, the file is written as if it were a simulation without branches or multiple homogenized regions. File `case_name_pert_0000i.x16` must be in binary format. Its ASCII[7] counterpart file, `txtfile16`, is described in TRITON user's manual (Jessee and DeHart 2011, appendix T1.A).

3. SAMPLER is run again. However, this time SAMPLER thinks all simulations are finished and proceed with the statistical calculations (only for the first branch and the interested homogenized region). Statistical calculations are completed because, for SAMPLER, there is not any branch or more than one homogenized region.

4. Go back to step 2, now write file `case_name_pert_0000i.x16` containing cross section information for the next branch. Proceed iteratively until statistical calculations for all branches are completed.

Two more comments about this workaround are needed. First, SAMPLER does not include the scattering cross section among groups as a default response. Therefore, when writing file `case_name_pert_0000i.x16`, it is easy to swap desired scattering data (from fast to thermal group) with any other undesired data, for

[7] SCALE provides the executable `x16convert` to convert `xfile016` binary file to ASCII format `txtfile16`

example, transport cross section[8]. Second, this workaround is presented for homogenized and collapsed cross section responses, but it could be used for any other response. To achieve the desired results, only file `case_name_pert_0000i.x16` in step 2 needs to be changed accordingly.

The information given by SAMPLER includes covariance and correlation matrices, average responses and standard deviations, histograms, response tables, scatter plots...

5.1.2.2 Uncertainty propagation through PARCSv3.2

Three main steps are followed to propagate the uncertainty through PARCS. Its model is detailed in Section 4.3 and the BWR core is used. The thermohydraulic 3D boundary conditions used for the BWR are between 600 and 1200 K for the fuel temperature, and moderator density between 100 and 800 kg/m^3. These are given to PARCS as 3D radial maps.

1. The results of SAMPLER calculations, as a function of burn-up, are gathered for each segment (see Section 5.1.2.1). Especially important are the average responses and the average standard deviation of parameters -averaged over all samples or perturbations-.

2. Two problem-dependent NEMTAB libraries (rodded and unrodded) are generated according to Section 4.1.1. One containing the average cross sections and the other their standard deviations. The average and standard deviations for the seven main cross sections are obtained in the previous step, all other cross sections and kinetic parameters are obtained from the unperturbed simulation.

3. Using DAKOTA, 1000 sets of perturbations are generated for the seven main cross sections for each neutronic composition. According to Eq 4.4, there are 103 neutronic compositions, each with seven main cross sections. However, there are 3 neutronic compositions representing the reflectors, where the fission cross section for both energy groups is zero and thus, reflectors have only five main cross sections. Therefore, the number of input parameters is $100 \cdot 7 + 3 \cdot 5 = 715$. Note that perturbation factors are not defined for each feedback parameter (fuel temperature, moderator density and control rod) or collapsed energy group. All perturbations are generated with the following properties: normal PDFs, random sampling method, 0 as average value and an upper/lower limit of ± 1.

4. Then, 1000 steady state simulations with PARCS (without thermohydraulic coupling) are run, each simulation with a different set of perturbations. PARCS source code is modified to read the perturbations generated by DAKOTA and the NEMTAB library of standard deviations. Then, PARCS perturbs the main cross sections, it obtains the perturbed cross sections with the following formula:

$$XS_i^p = \bar{XS}_i + \sigma_{XS_i} Q_i \tag{5.1}$$

Where

i is the perturbation index (up to 1000),

XS_i^p is a vector containing all 715 perturbed cross sections,

$\bar{XS}_i$ is a vector containing all averaged cross sections, these are read by default by PARCS from the NEMTAB library of average values,

σ_{XS_i} is a vector containing all cross section standard deviations, these are read by PARCS from the NEMTAB library of standard deviation values, and

[8] Transport cross section value is repeated in "sigtr (ousc)" place. Thus, no information is lost.

Q_i is a vector containing all perturbation factors generated with DAKOTA.

NEMTAB libraries are divided in sections for different neutronic compositions. Each neutronic composition contains its cross section data tabulated as a function of feedback parameters (fuel temperature, moderator density and control rod) and the collapsed energy group (see Appendix B). Since perturbation factors, Q_i, are defined for the seven main cross sections and different neutronic compositions (see previous step), the same Q_i is applied to the entire table (which defines the cross sections as a function of feedback parameters and collapsed energy groups).

5. Finally, the U&S analysis is performed, again, with DAKOTA. The output parameters are the multiplication factor -k_{eff}-, the axial power peak -P_z- and peak node location -N_z- predicted by PARCS. These output parameters are chosen because they are inherent to the reactor safety. These responses are obtained and introduced in a file along with the perturbations generated by DAKOTA. With this information, DAKOTA is able to perform a complete U&S analysis. DAKOTA output results for the U&S analysis include average responses and standard deviation, lower and upper limits for averages and standard deviations, normality parameters (such as skewness and kurtosis) and sensitivity coefficients assuming linear (PCC and SCC) and non-linear relations (PRCC and SRCC).

5.2 Thermohydraulic parameter propagation

The thermohydraulic uncertainty propagation through the thermohydraulic-neutronic coupled code TRACE-PARCS is done using DAKOTA statistical tool. In total, 43 different input parameters are considered and two sampling methods (*Simple Random Sampling* (SRS) and *Latin Hypercube Sampling* (LHS)) are compared. As output parameters, PARCS predictions for the enthalpy, power and reactivity are set. These neutronic parameters are chosen because they represent the neutronic reactor state. Moreover, as seen in Section 2.3.2, the enthalpy and reactivity (along with other parameters) define the safety limits for *Anticipated Operational Occurrences* (AOOs) or postulated accidents (US-NRC et al. 2007). The thermohydraulic model uses a fully 3D core and is explained in detail in Section 4.2. The neutronic model is explained in Section 4.3 (PWR core).

5.2.1 Input parameters

An extensive research in the literature is made in order to select the input parameters and characterize their uncertainty distributions. A list of thermohydraulic parameters is presented in Table 5.2 and Table 5.3[9] for normal and uniform distributions respectively. They are shown along with the parameters defining their PDFs and the reference where the information is found. If PDF information is not found for a given parameter, expert judgment is applied[10]. The same thermohydraulic parameter for different fuel types is considered as different input parameters (but its PDF definition is not changed among fuel type). As shown in Table 4.15, the PWR has three different fuel types plus a bypass. In total, 43 different thermohydraulic parameters are propagated. In Section 3.1.2.3, a brief review of how most of these thermohydraulic parameters affect TRACE internal models is given.

It must be said that uncertainty information for parameters representing boundary conditions (such as output pressure or inlet liquid temperature) must be chosen with caution. Thermohydraulic-neutronic coupled codes are very sensitive to boundary conditions. Even if all simulations finish successfully with a defined input uncertainty, some simulations may crash if the sampling method is changed (keeping the same uncertainty

[9] In this table, uncertainties are expressed either as multiplication factors (centered in 1) or as adding factors (centered around 0).

[10] Even though it is preferred not to use expert judgment, sometimes it must be use due to the lack of uncertainty information.

#	Definition	Fuel type	Variable	Mean	Standard deviation	Reference
1	Output pressure	-	P_{out}	1.0	0.002	Expert Opinion
2	Reactor power	-	q_{tot}	1.0	0.005	Expert Opinion
3	Inlet mass flow	-	m_{in}	1.0	0.001	Expert Opinion
4	Wall roughness	1	ϵ_1	1.0	0.25	Expert Opinion
5		2	ϵ_2			
6		3	ϵ_3			
7		Byp	ϵ_b			
8	Pitch to diameter ratio	1	p/d_1	1.0	0.05	Expert Opinion
9		2	p/d_2			
10		3	p/d_3			
11		Byp	p/d_b			
12	Assembly flow area	1	A_{flow1}	1.0	0.01	Petruzzi and D'Auria 2008 page 13
13		2	A_{flow2}			
14		3	A_{flow3}			
15		Byp	A_{flowb}			
16	Radial fuel peaking factor	1	RFPF_1	1.0	0.01	Petruzzi and D'Auria 2008 page 13
17		2	RFPF_2			
18		3	RFPF_3			
19		Byp	RFPF_b			

Table 5.2 – Thermohydraulic parameters to propagate through TRACE following a normal distribution.

definitions). Therefore, uncertainty definitions must suit all sampling methods (in this case SRS and LHS). Normally, this is achieved performing an iterative process. In this thesis, it is found that if SRS is used, the uncertainty for boundary parameters must be decreased (respect to LHS) to successfully finish all simulations.

5.2.2 Uncertainty propagation through TRACE5.0P3-PARCSv3.0

The process to perform U&S analysis with DAKOTA is similar to the process explained before for the cross section uncertainty propagation. It can be summarized in four steps.

1. Using the uncertainty distributions (PDFs) defined before, 146 sets of perturbations are created with DAKOTA tool.
2. Using RESTING[11] MATLAB program, 146 input decks for TRACE are created. A different perturbation set is applied to each input deck. An unperturbed case is also defined.
3. Run TRACE-PARCS coupled code for each input deck. Simulation process shown in Fig. 3.7 is followed to obtain a satisfactory convergence.
4. Results for the different responses are gathered for the 146 transient simulations. Then, DAKOTA tool is used to perform U&S analysis. This is already explained in the last paragraph of Section 5.1.2.2.

[11] REactor Simulation Trace INput Generator (RESTING) is a MATLAB program created within the context of this thesis to automatically generate TRACE input models at core level either in 1D or 3D. Among other features, it performs U&S analysis for user defined thermohydraulic parameters or automatically adjust the bypass flow. RESTING provides a user-friendly input system to use its different modules with ease.

#	Definition	Fuel type	Variable	Lower limit	Upper limit	Reference
20	Fuel heat capacity	-	Cp_{fuel}	0.99	1.01	Boyack et al. 1989, page 60
21	Clad heat capacity	-	Cp_{clad}	0.97	1.03	Boyack et al. 1989, page 60
22	Fuel thermal conductivity	-	K_{fuel}	0.954	1.046	Boyack et al. 1989, page 60
23	Clad thermal conductivity	-	K_{clad}	0.94	1.06	Boyack et al. 1989, page 60
24	Inlet flow temperature	-	T_{in}	-0.1	+0.1	Petruzzi and D'Auria 2008 page 13/Expert
25	Critical heat flux multiplier	-	CHFM	-0.4	+0.3	Wickett et al. 1998 page 3.24
26	Heat fraction to bypass	-	$q_{\text{byp}}/q_{\text{tot}}$	-2.375E-5	+2.375E-5	Expert Opinion
27	Heat fraction to moderator	-	$q_{\text{mod}}/q_{\text{tot}}$	-9.263E-4	+9.263E-4	Expert Opinion
28 29 30 31	Gap size	1 2 3 Byp	z_{gap1} z_{gap2} z_{gap3} z_{gapb}	-7.4E-6	+7.4E-6	Expert Opinion
32 33 34 35	Gap heat transfer coefficient	1 2 3 Byp	h_{gap1} h_{gap2} h_{gap3} h_{gapb}	0.65	1.35	Gajev 2012 page 50
36 37 38 39	Grid friction factor	1 2 3 Byp	k_{fac1} k_{fac2} k_{fac3} k_{facb}	0.95	1.05	Gajev 2012 page 50
40 41 42 43	Hydraulic diameter	1 2 3 Byp	D_{hyd1} D_{hyd2} D_{hyd3} D_{hydb}	0.995	1.005	Gajev 2012 page 50

Table 5.3 – Thermohydraulic parameters to propagate through TRACE following a uniform distribution.

As explained in Mesado et al. 2012, two different approximations are used. First approximation, or *maximum response approach*, calculates the U&S analysis only at time step where the maximum absolute response is found. Thus, only one U&S analysis is run per output parameter. This approximation gives sensitivity information for the most critical transient time step. The second approximation, or *index dependent approach*, calculates the U&S analysis for each time step (whole simulation) and for all responses. This approximation gives sensitivity information for the whole transient simulation, thus, a wider sensitivity view for the analyst is obtained.

Neither approach is mentioned in the cross section propagation process. Regarding the lattice physics code, the reason is that the nuclear data simulations are performed using fresh fuel conditions and thus, only one depletion step is possible. The same applies to the core physics code using steady state conditions. The U&S analysis is performed over the converged results. Nevertheless, if the U&S analysis were performed as a function of exposure (lattice code) and/or using transient conditions (core code), both approaches could be used.

One last comment applies here, the neutronic library used to run the neutronic code PARCS was given and therefore, was not obtained by the thesis' author. The same methodology applied to obtain the neutronic library for the BWR core could be used here. However, due to the lack of the PWR segment information, it was obtained with SIMULATE3 and following the SIMTAB methodology.

Chapter 6

Results

. . . or how to show a million data in a bunch of plots.

In this chapter, the results produced in this PhD work are presented. As explained in Chapter 5, the uncertainty propagation is performed over two different scenarios. A summary table with the most important features of both scenarios is given in Table 5.1. The first scenario (steady state and BWR core) is subdivided into two levels. In the first level (lattice), cross sections are propagated starting from the master nuclear data library ENDF/B-VII using SAMPLER module with SCALE6.2.1. Then, a proper formatted neutronic library (with collapsed and homogenized neutronic parameters) is generated, Section 5.1.2.1. In the second level (core), these libraries are used in PARCSv3.2 (steady state conditions) to obtain the uncertainty on the multiplication factor -k_{eff}-, axial power peak -P_z- and peak node location -N_z-, Section 5.1.2.2. DAKOTA statistical tool is used for this purpose. The second scenario (transient state and PWR core) propagates several thermohydraulic parameters through the thermohydraulic-neutronic coupled code TRACEv5.0P3-PARCSv3.0. A real control rod insertion is simulated using transient conditions (data obtained in a test performed in a real nuclear reactor). The uncertainty over the predicted power, reactivity and enthalpy is obtained, Section 5.2.

6.1 Cross section propagation

6.1.1 Propagation through SCALE6.2

The *Uncertainty and Sensitivity* (U&S) analysis is repeated for each segment and each feedback parameter combination. Thus, there are a lot of data to process. For sake of brevity, only the results corresponding to a representative segment (segment 14) and a certain combination of feedback parameters (456.32 kg/m^3, 879.5 K and control rod withdrawn) are presented here. Results for intermediate fuel segments (11, 12, 13 and 14, see Fig. 4.15) are very similar, the same is true for fuel segments on the core extremes (10 and 15). Reflector segments (1, 2 and 3) are more dissimilar because they use different homogenized materials.

Fig. 6.1 shows the correlation matrix between output parameters (homogenized and collapsed cross sections) for fuel segments with (right) and without (left) control rods. For fuel segments, the most correlated output parameters are 1) $D_{f1} - \Sigma_{12}$ with a very strong negative correlation ($|\sigma_{xy}| \geqslant 0.8$), 2) $D_{f1} - \Sigma_{a1}$ with a very strong negative correlation and 3) $\Sigma_{a1} - \Sigma_{12}$ with a strong positive correlation ($0.6 \leqslant |\sigma_{xy}| < 0.8$). The correlation matrix for reflector segment 2 is shown in Fig. 6.2. For reflector segments the correlation matrix is smaller because cross section $\nu\Sigma_f$ -for both energy groups- is always zero and is not represented. For this segment, the most correlated output variables are 1) $D_{f1} - \Sigma_{12}$ with a very strong negative correlation and 2) $\Sigma_{a1} - \Sigma_{a2}$ with a moderate positive correlation ($0.4 \leqslant |\sigma_{xy}| < 0.6$). Comparing the results for a case

with and without control rods, it is seen that some correlations increase significantly, these are 1) $\Sigma_{a1} - \Sigma_{12}$, 2) $\Sigma_{a1} - D_{f1}$ and 3) $\Sigma_{a1} - \nu\Sigma_{f1}$. In these cases, correlations become stronger, towards the positive or the negative side. Almost all other correlations are weak ($0.2 \leqslant |\sigma_{xy}| < 0.4$) or very weak ($|\sigma_{xy}| < 0.2$).

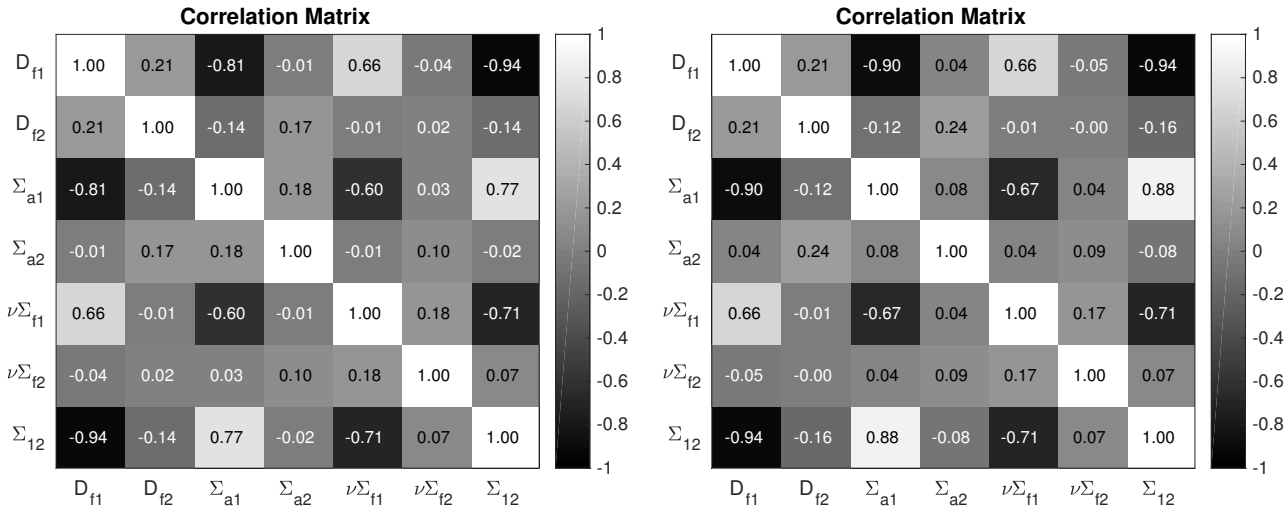

Fig. 6.1 – Correlation matrix among output parameters, typical results without (left) and with control rods (right) for segment 14.

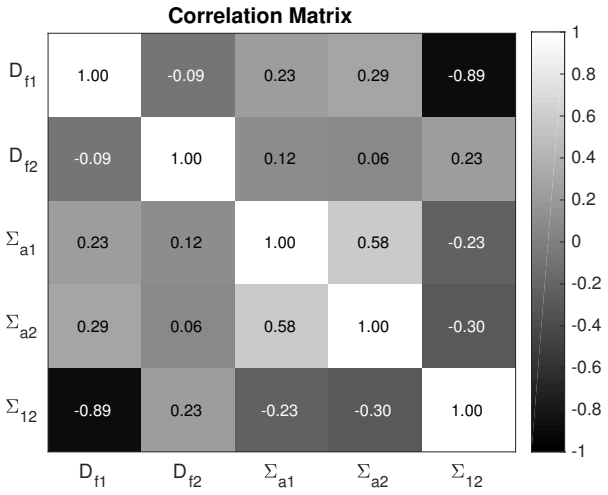

Fig. 6.2 – Correlation matrix among output parameters for segment 2.

The obtained uncertainty information for the scattering cross section is presented in Fig. 6.3 (histogram) and Fig. 6.4 (scatter plots -left- and moving averages -right-). The same data for other cross sections is seen in Table 6.1 (histograms), Table 6.2 (scatter plots) and Table 6.3 (moving averages). The histograms are useful to assign a distribution to parameters, for example normality. A Shapiro-Wilk test for normality is performed for the homogenized cross sections and its p-value[1] can be seen in Table 6.4. The hypothesis of

[1] A small p-value (typically < 0.05) indicates strong evidence to reject the null hypothesis (normality). A larger p-value indicates weak evidence against the null hypothesis, meaning that the test failed to reject the null hypothesis

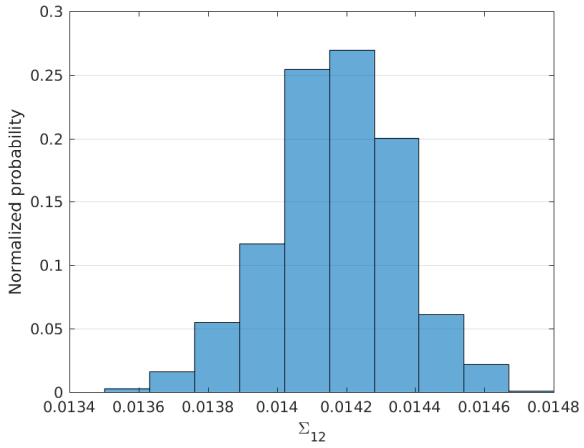

Fig. 6.3 – Histogram for scattering cross section for segment 14.

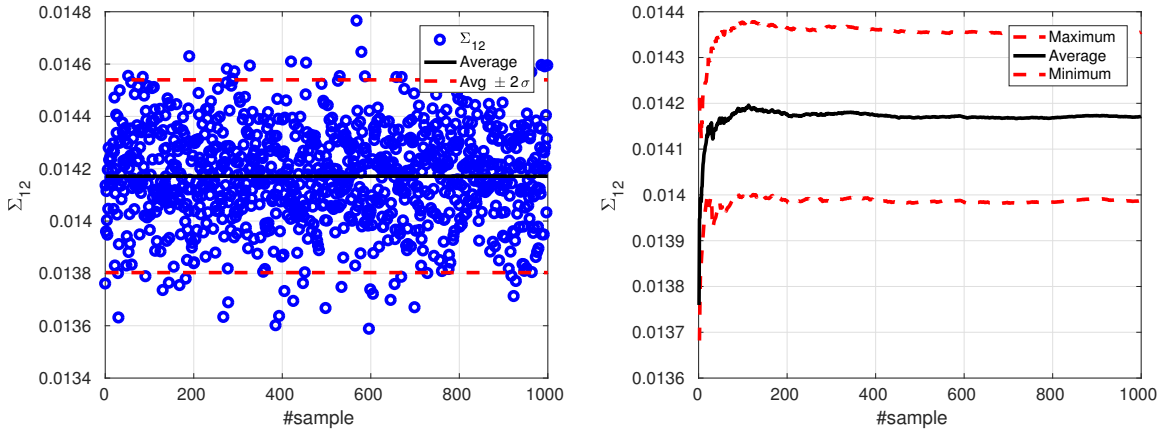

Fig. 6.4 – Data for scattering cross section for segment 14, scatter plot (left) and moving average (right).

normality for D_{f2}, Σ_{a1}, $\nu\Sigma_{f1}$ and $\nu\Sigma_{f2}$ cannot be rejected at a significance level of 5%. Scatter plots are good to visualize the point clouds distribution resulting from all samples and determine how many samples are outside the 2σ boundaries. Finally, the moving averages can be used to determine the parameter convergence, the higher the number of samples, the higher the convergence. It is seen that the moving averages converge, roughly, at 200 samples.

To obtain these results using branches and two homogenized regions in SCALE, the workaround shown in Fig. 5.5 is used. As an example, the resulting output parameter averages and standard deviations can be seen in Table 6.5 and Table 6.6 respectively. Data is shown for segment 14 without control rods, different moderator densities and fuel temperature constant to 879.5 K. Extensive uncertainty information obtained at lattice level is given in Appendix C.

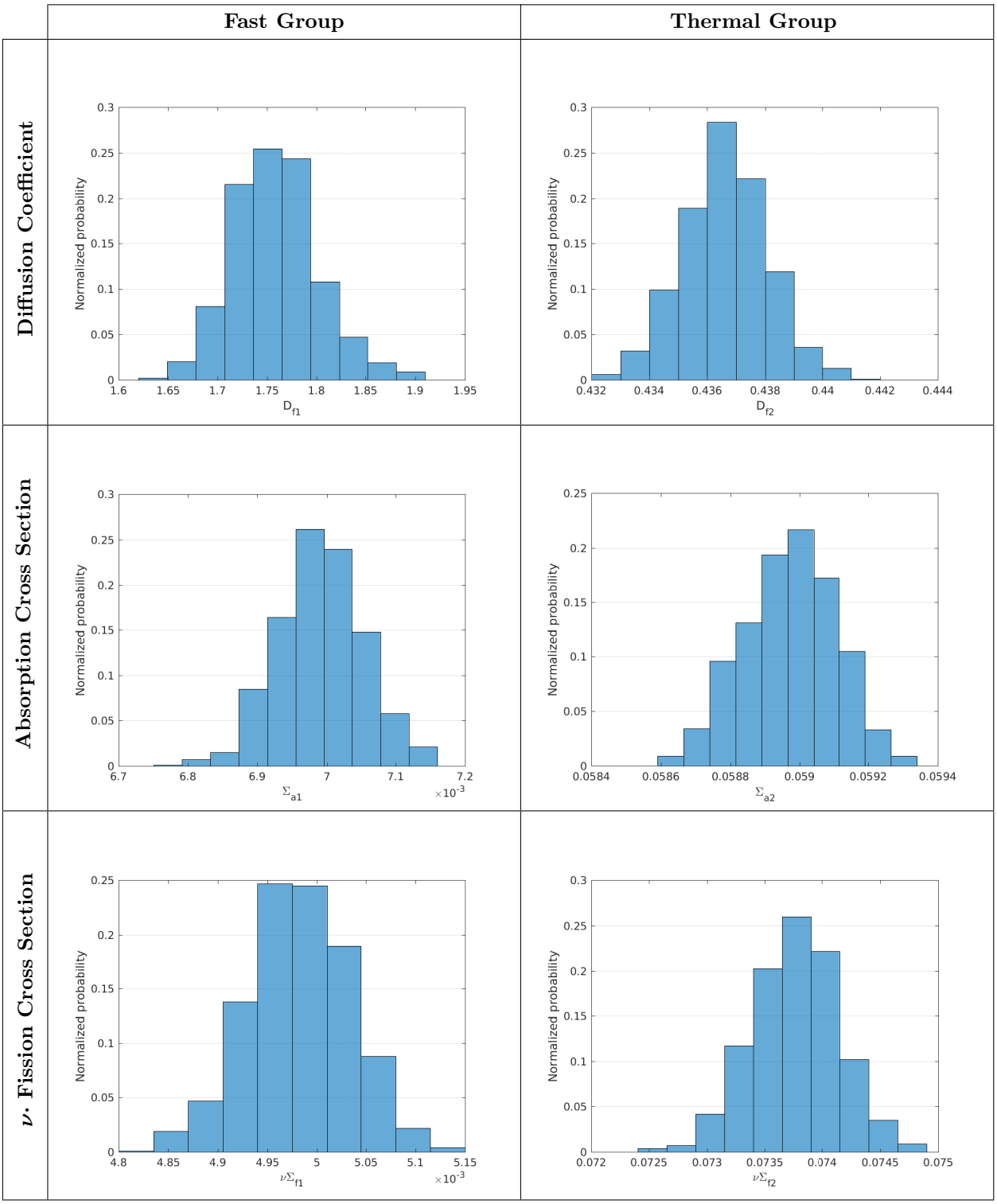

Table 6.1 – Histograms for output parameters for segment 14.

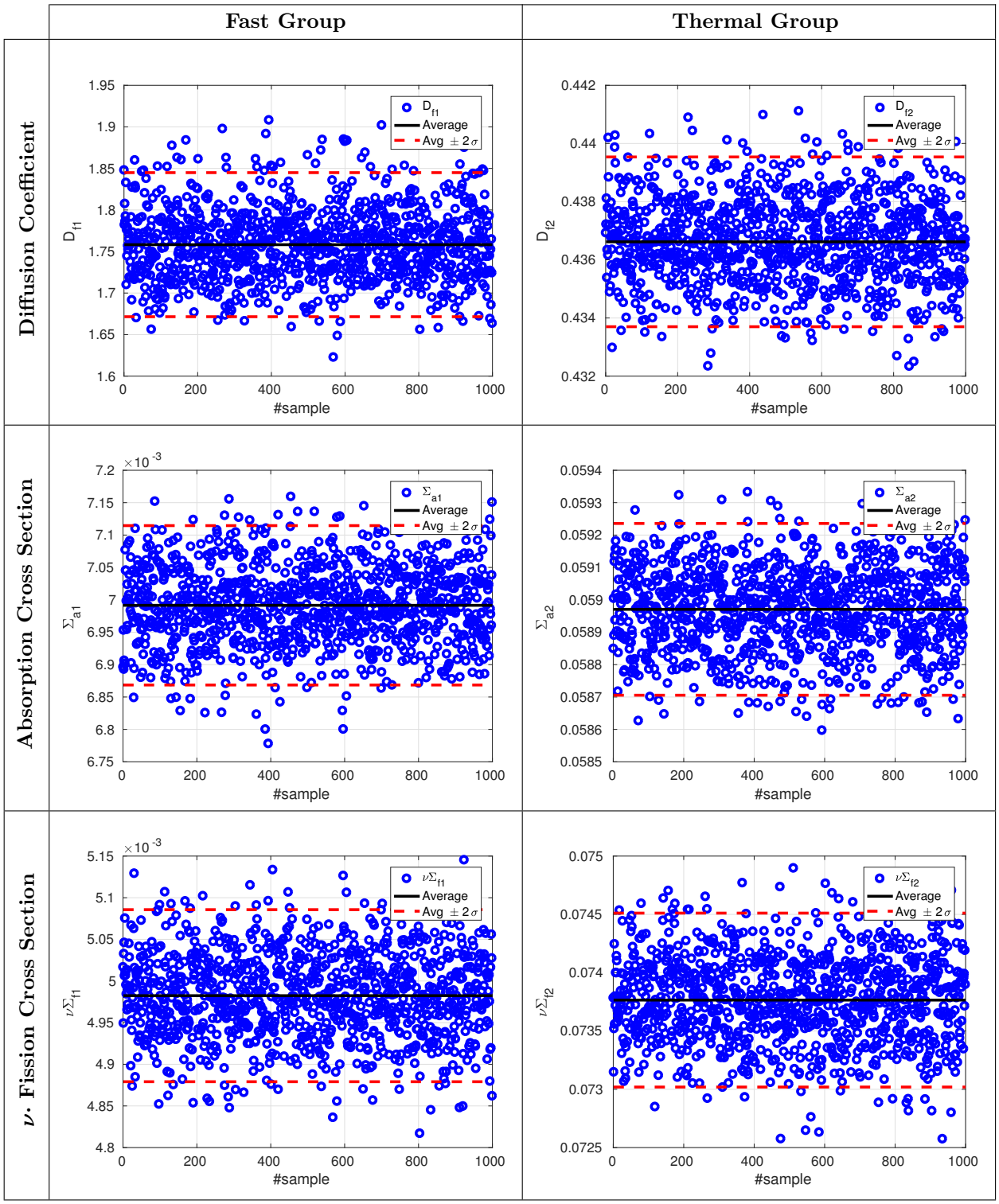

Table 6.2 – Scatter plots for output parameters for segment 14.

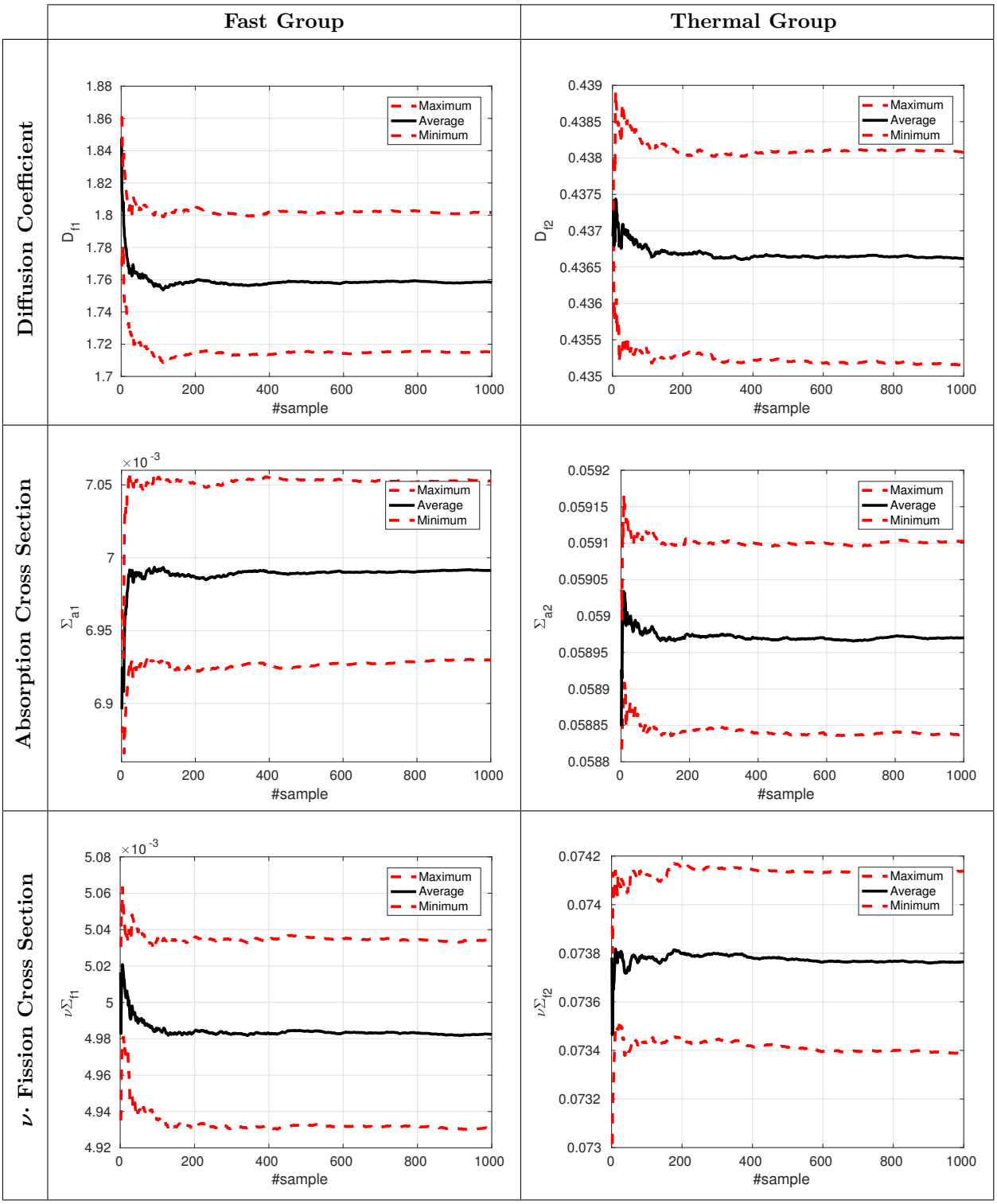

Table 6.3 – Moving averages for output parameters for segment 14.

Parameter	p-value
D_{f1}	0.00001
D_{f2}	0.78192
Σ_{a1}	0.60075
Σ_{a2}	0.01798
$\nu\Sigma_{f1}$	0.88551
$\nu\Sigma_{f1}$	0.78020
Σ_{12}	0.03710

Table 6.4 – Shapiro-Wilks test for normality p-value for neutronic parameters, segment 14.

$\mathbf{D_{moderator}}$ $\mathbf{(kg/m^3)}$	$\boldsymbol{D_{f1}}$	$\boldsymbol{D_{f2}}$	$\boldsymbol{\Sigma_{a1}}$	$\boldsymbol{\Sigma_{a2}}$	$\boldsymbol{\nu\Sigma_{f1}}$	$\boldsymbol{\nu\Sigma_{f2}}$	$\boldsymbol{\Sigma_{12}}$
38.14	1.393	2.772E-1	7.692E-3	7.219E-2	5.395E-3	9.147E-2	2.505E-2
177.53	1.423	2.950E-1	7.641E-3	6.811E-2	5.368E-3	8.535E-2	2.397E-2
456.32	1.481	3.227E-1	7.541E-3	6.417E-2	5.308E-3	7.981E-2	2.193E-2
735.11	1.548	3.516E-1	7.423E-3	6.157E-2	5.237E-3	7.640E-2	1.982E-2
840.34	1.758	4.366E-1	6.992E-3	5.897E-2	4.982E-3	7.376E-2	1.417E-2
942.81	2.039	5.701E-1	6.207E-3	5.593E-2	4.553E-3	7.021E-2	8.709E-3
998.29	2.219	6.670E-1	5.472E-3	5.429E-2	4.176E-3	6.799E-2	6.176E-3

Table 6.5 – Average output parameters as a function of moderator density for segment 14.

$\mathbf{D_{moderator}}$ $\mathbf{(kg/m^3)}$	$\boldsymbol{D_{f1}}$	$\boldsymbol{D_{f2}}$	$\boldsymbol{\Sigma_{a1}}$	$\boldsymbol{\Sigma_{a2}}$	$\boldsymbol{\nu\Sigma_{f1}}$	$\boldsymbol{\nu\Sigma_{f2}}$	$\boldsymbol{\Sigma_{12}}$
38.14	3.248E-2	7.294E-4	6.614E-5	1.675E-4	5.526E-5	4.579E-4	3.121E-4
177.53	3.335E-2	7.957E-4	6.593E-5	1.597E-4	5.488E-5	4.291E-4	2.995E-4
456.32	3.506E-2	9.076E-4	6.542E-5	1.505E-4	5.418E-5	4.027E-4	2.756E-4
735.11	3.702E-2	1.033E-3	6.472E-5	1.438E-4	5.345E-5	3.863E-4	2.508E-4
840.34	4.336E-2	1.459E-3	6.151E-5	1.326E-4	5.165E-5	3.729E-4	1.842E-4
942.81	5.179E-2	2.332E-3	5.361E-5	1.257E-4	5.066E-5	3.559E-4	1.176E-4
998.29	5.680E-2	3.144E-3	4.487E-5	1.269E-4	5.285E-5	3.454E-4	8.496E-5

Table 6.6 – Standard deviations for output parameters as a function of moderator density for segment 14.

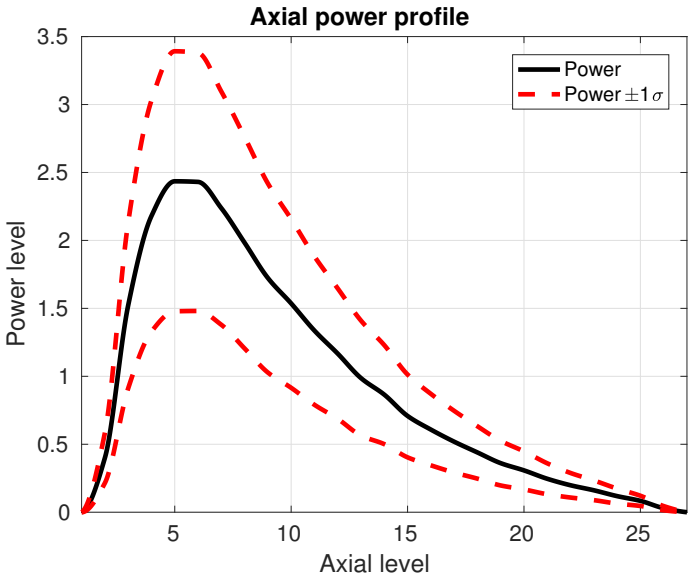

Fig. 6.5 – Normalized axial power profile with its $\pm\sigma$ zone.

6.1.2 Propagation through PARCSv3.2

Cross section uncertainty is propagated through PARCS with DAKOTA statistical tool. The BWR core described in Section 4.3 and 3D radial maps as thermohydraulic boundary conditions are used -between 600 and 1200 K for the fuel temperature and moderator density between 100 and 800 kg/m^3-. Table 6.7 contains different statistical information for the responses, i.e. multiplication factor -k_{eff}-, axial power peak -P_z- and peak node location -N_z-. The average and standard deviations are shown with their confidence interval at 95% level. It is seen that the peak node location has its average value at almost 6 and a standard deviation of about 1.5. Hence, there is a big change for the power peak to be located between nodes 4 and 7 -as its histogram shows-. This explains why the standard deviation of the axial power profile, Fig. 6.5, is so wide around the power peak (dashed-red lines). Response skewness and kurtosis are also shown, being zero the kurtosis of a normal distribution and the skewness of a symmetric distribution. Fig. 6.6 represents the average normalized radial power profile (left) and its standard deviation (right).

Table 6.8 shows the histograms and their *Cumulative Distribution Functions* (CDFs) compared with the standard normal CDF -obtained using the same average and standard deviation-. The CDF for the N_z response is not shown because it is a discrete function. A Shapiro-Wilk test for normality shows that k_{eff} comes from a standard normal distribution with a p-value of 0.96. While P_z and N_z do not come from a standard normal distribution with a p-value almost zero. Table 6.9 shows the scatter plots and the PRCCs for each response.

	Average	**Standard Deviation**	**Skewness**	**Kurtosis**
$\mathbf{k_{eff}}$	1.00205 ± 3.907E-5	6.297E-4 ± 2.888E-5	-0.0096	0.0375
$\mathbf{P_z}$	3.39000 ± 0.03204	0.51632 ± 0.02368	0.6508	0.4898
$\mathbf{N_z}$	5.930 ± 0.093	1.500 ± 0.069	0.5917	0.2044

Table 6.7 – Uncertainty information.

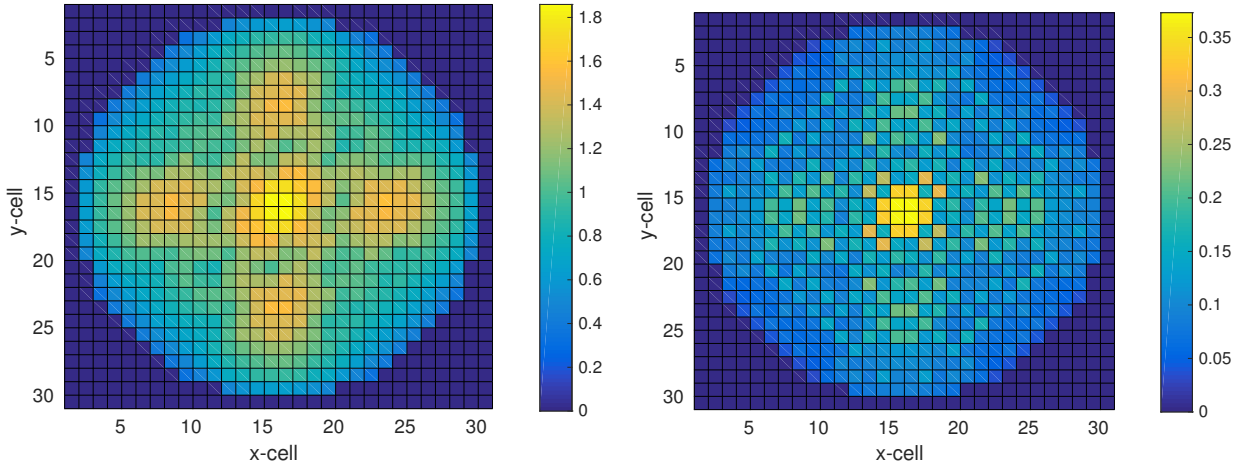

Fig. 6.6 – Normalized and collapsed radial power profile, average (left) and standard deviation (right).

The *Sensitivity Analysis* (SA) shows that the most sensitive parameters are $\nu\Sigma_{f2}$ and Σ_{a1}, see *Partial Rank Correlation Coefficient* (PRCC) plots in Table 6.9. Nonetheless, the PRCC must be studied with caution, especially if there is a big number of input parameters. PRCC is the sensitivity fraction apportioned by an input parameter to an output parameter. Therefore, if one group of input parameters is highly sensitive, the sensitivity fraction apportioned by other input parameters is partially hidden. In this case, the sensitivity apportioned by the homogenized cross sections in neutronic composition 28 and up to composition 33 is high, thus the significance of homogenized cross sections in other neutronic compositions is relatively low. This can be seen in Fig. 6.7, where the cumulative PRCC is shown for each segment (left). The cumulative PRCC is calculated as the normalized sum of all homogenized cross section PRCC belonging to a specific segment. Thus, the result is the sensitivity fraction apportioned by homogenized cross section in each segment. The cumulative PRCC for each homogenized cross section -in all segments- is also shown on the right plot. From Fig. 6.7, the conclusions are that the most sensitive homogenized cross section -for the three considered responses- are those belonging to segment 14 (neutronic compositions from 27 to 49). Information in Fig. 4.15 shows that segment 14 comprises the central nodes in fuel type 8 (from node 3 to 25). Looking at Fig. 4.24 (right radial mapping), it is easy to understand why the responses are so sensitive to segment 14. Fuel type 8 is used over a great fraction of the radial mapping in this BWR reactor. The second most sensitive segment is segment 13 (left plot in Fig. 6.7), while reflector segments (1, 2 and 3) and extreme fuel segments (10 and 15) have the lowest sensitivity towards all responses. The most sensitive homogenized cross sections -according to the right plot of Fig. 6.7- for all responses is $\nu\Sigma_{f2}$. This is followed by Σ_{a1} for the k_{eff} response and $\nu\Sigma_{f1}$ for responses P_z and N_z. The diffusion coefficient -both energy groups- has the lowest sensitivity towards the k_{eff}. The other homogenized cross sections have similar sensitivity for responses P_z and N_z.

	Histogram	CDF
$\mathbf{k_{eff}}$	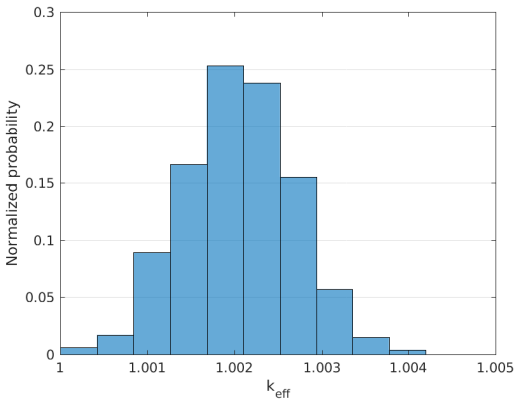	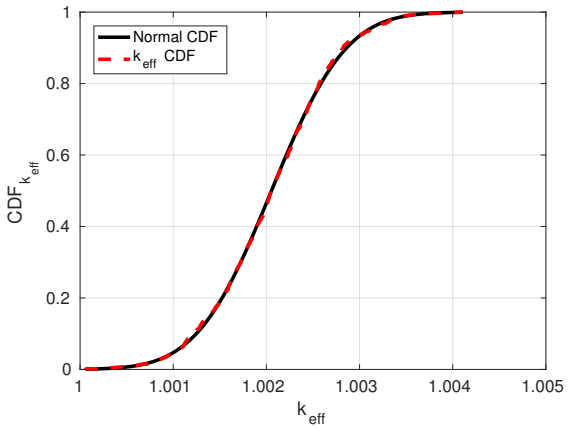
$\mathbf{P_z}$	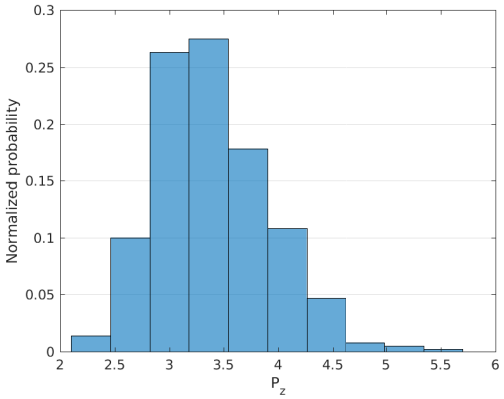	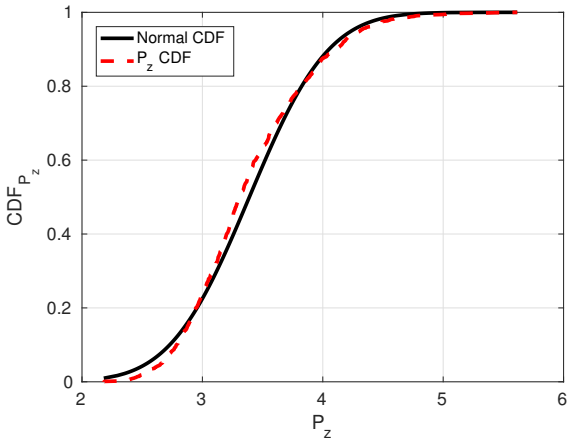
$\mathbf{N_z}$	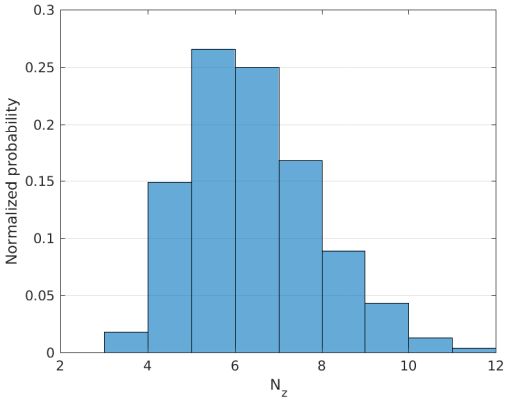	CDF not shown for discrete functions.

Table 6.8 – Cumulative distribution functions and histograms.

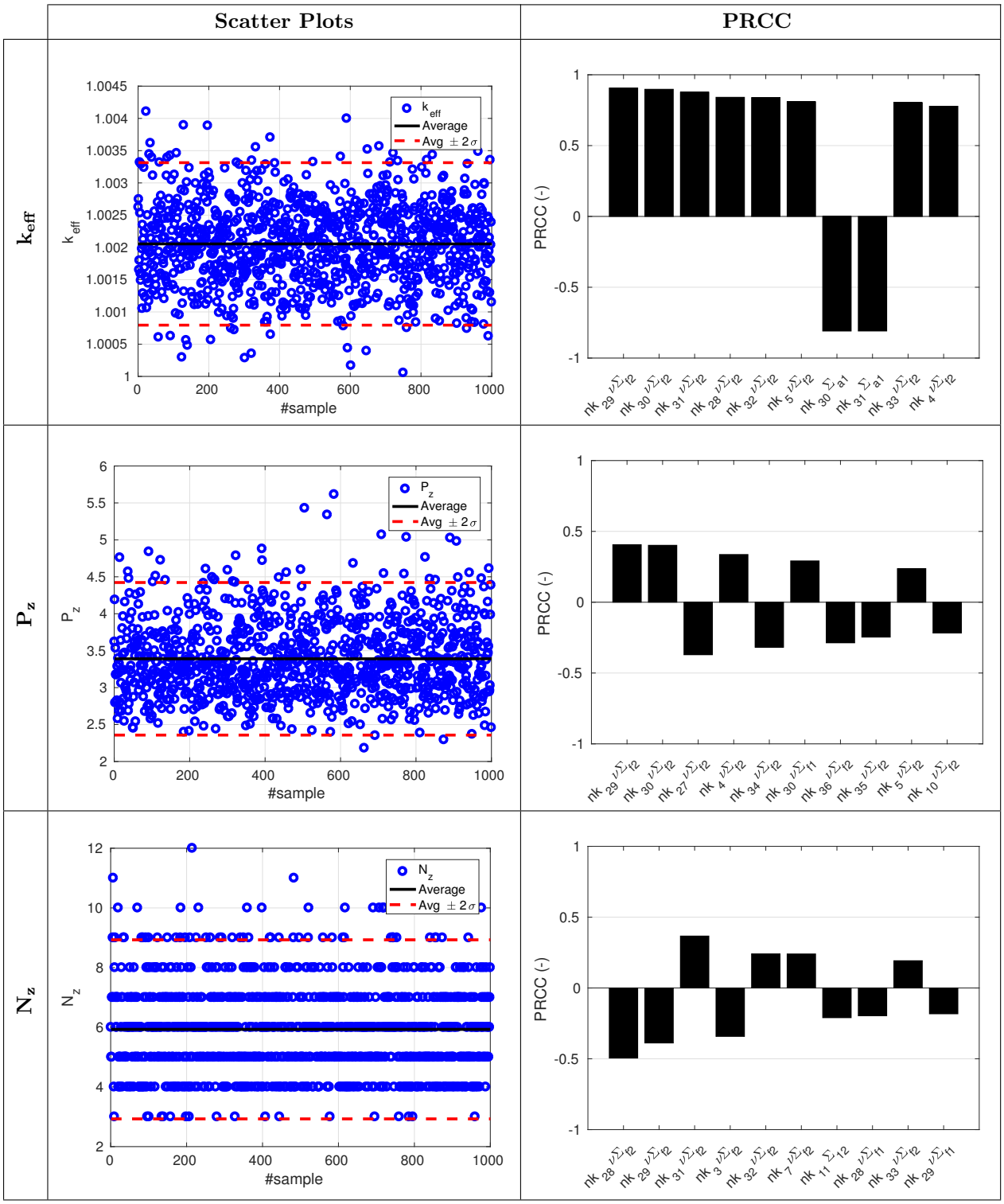

Table 6.9 – Scatter plots and partial rank correlation coefficients.

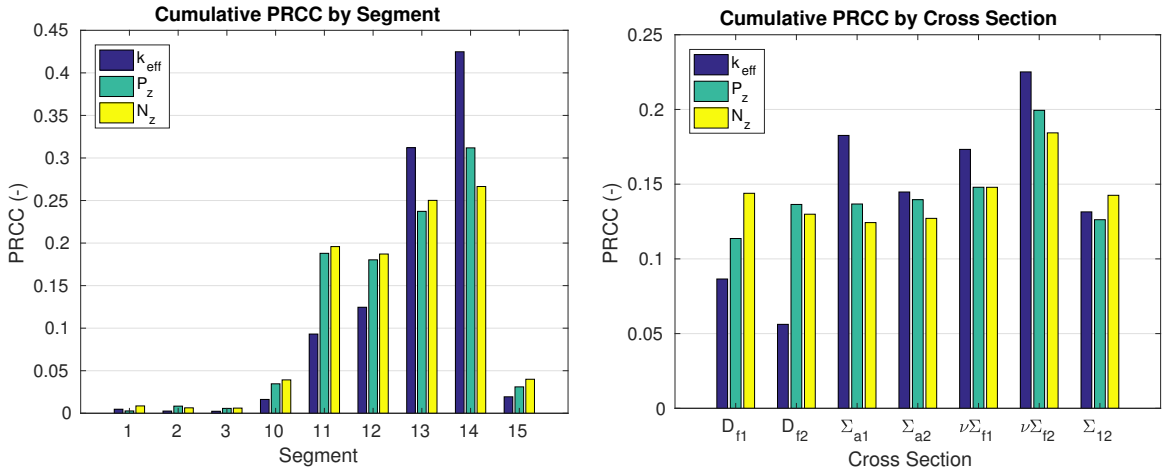

Fig. 6.7 – Cumulative PRCC by segment (left) and by homogenized cross section (right).

6.1.2.1 Analysis by segment

In order to distinguish the most sensitive homogenized cross sections for other segments, the U&S analysis is also performed by segments. Therefore, for each U&S analysis, only the homogenized cross sections belonging to a specific segment are considered as input parameters. Same responses are considered. The results for segment 13 are shown in Fig. 6.8. This is the second most sensitive segment towards the main responses (see left plot in Fig. 6.7). It is seen that the most sensitive homogenized cross section is, again, $\nu\Sigma_{f2}$. However, now its sensitivity towards P_z and N_z is considerably increased. This is followed by Σ_{a1} for the k_{eff} response and $\nu\Sigma_{f1}$ for responses P_z and N_z. Regarding the other homogenized cross sections, the same conclusions found in the global SA can be applied here. Extensive sensitivity information for both analysis (global SA and SA by segment) is given in Appendix D.

Table 6.10 shows the main statistics when only neutronic parameters in segment 13 are perturbed. Comparing the statistics with the ones obtained in the global SA, Table 6.7, it is seen that the standard deviations and their confidence intervals are reduced. In case of the k_{eff} and P_z, the reduction is almost one half. The same is observed with the average confidence interval. The skewness is reduced but the kurtosis is not. A Shapiro-Wilk test for normality shows that k_{eff} and P_z come from a standard normal distribution with a p-value of 0.78 and 0.42 respectively, see Fig. 6.9. While N_z does not come from a standard normal distribution with a p-value almost zero.

In order to see the sensitivity of reflector zones, another SA is performed where only homogenized cross sections of reflector compositions are perturbed. In Fig. 6.10 the most sensitive homogenized cross sections are seen for k_{eff} (left) and P_z. The most sensitive reflector composition -for both responses- is composition 103 (radial reflector), followed by composition 101 (bottom reflector). The homogenized cross sections in the reflector compositions are almost insensitive towards the node peak location. The cumulative PRCC by homogenized cross section for reflector compositions is seen in Fig. 6.11. Cross section $\nu\Sigma_f$ is not shown because it does not have a physical meaning in the reflector zone. The most sensitive homogenized cross section is D_{f1} followed by Σ_{a2}.

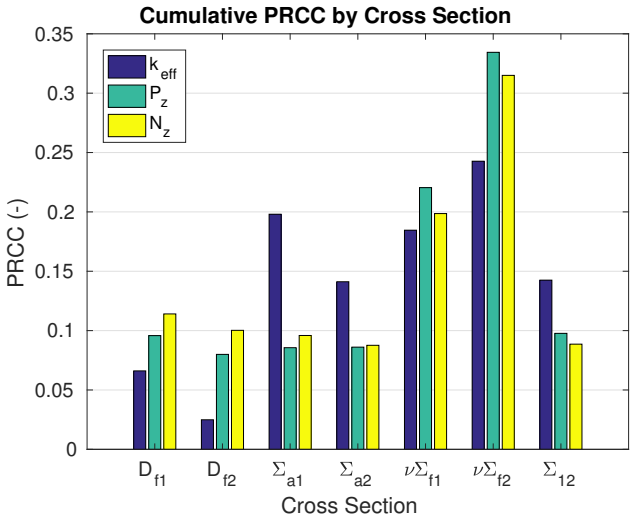

Fig. 6.8 – Cumulative PRCC by homogenized cross section when only neutronic parameters in segment 13 are perturbed.

	Average	Standard Deviation	Skewness	Kurtosis
$\mathbf{k_{eff}}$	1.00204 ± 1.980E-5	3.190E-4 ± 1.463E-5	0.0179	-0.1934
$\mathbf{P_z}$	2.93066 ± 0.01800	0.29009 ± 0.01330	0.0631	-0.1583
$\mathbf{N_z}$	5.760 ± 0.069	1.107 ± 0.051	0.5377	0.0760

Table 6.10 – Uncertainty information when only neutronic parameters in segment 13 are perturbed.

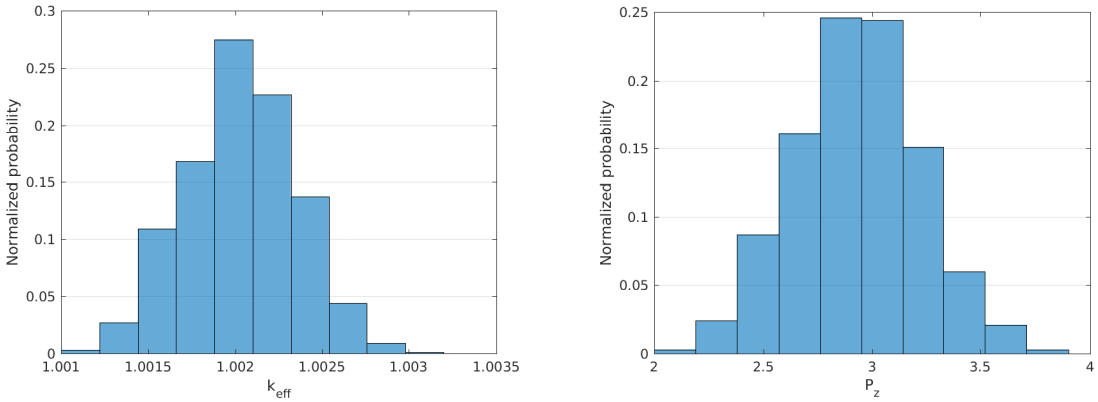

Fig. 6.9 – Histogram for k_{eff} (left) and P_z (right) when only neutronic parameters in segment 13 are perturbed.

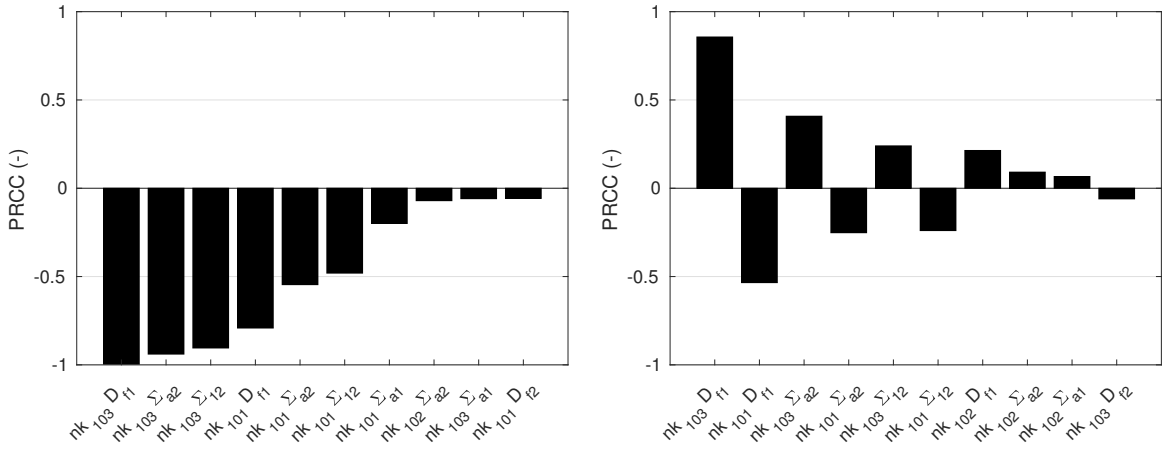

Fig. 6.10 – PRCC towards k_{eff} (left) and P_z (right) when only neutronic parameters in reflector segments are perturbed.

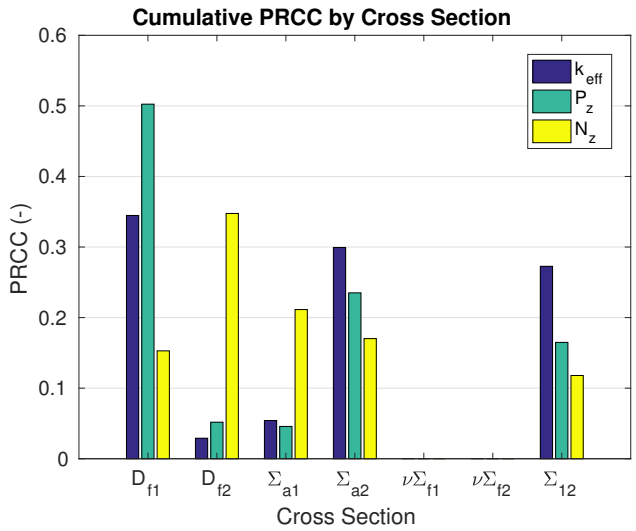

Fig. 6.11 – Cumulative PRCC by homogenized cross section when only neutronic parameters in reflector segments are perturbed.

6.2 Thermohydraulic parameter propagation

In this scenario, the PWR core described in Section 4.3 is used, the thermohydraulic boundary conditions are given by the thermohydraulic code TRACE5.0P3. Two different approximations are used to propagate the uncertainty. The *maximum response approach* calculates the U&S analysis only at time step where the maximum absolute response is found. The *index dependent approach* calculates the U&S analysis for each time step (whole simulation). The latter approximation gives a wider sensitivity view. The difference, between both approximations, lies in that different maximum responses are found -probably- at different time steps. Extensive sensitivity information for the maximum response approach is given in Appendix E.

6.2.1 Maximum response approach

Table 6.11 and Table 6.12 show the average, standard deviation (with the 95% confidence interval), skewness and kurtosis for the output parameters (enthalpy, power and reactivity) for both sampling methods. Their histograms and scatter plots are seen in Table 6.13 and Table 6.14 respectively. Besides, the SA is shown in Table 6.15, it contains the most sensitive input parameters for each output parameter. Input parameter abbreviations and definitions can be found in Table 5.2 and Table 5.3. As shown in Eq 2.12, an input parameter is considered to be sensitive enough if its PRCC > 0.1628. In this table, the sampling methods *Latin Hypercube Sampling* (LHS) and *Simple Random Sampling* (SRS) are compared (left and right columns respectively). The most sensitive input parameters, for both sampling methods, are tabulated in Table 6.16.

The fuel-clad gap size in assembly type 3 is always the most sensitive input parameter towards all output parameters and both sampling methods. The gap of sensitivity between the two most sensitive input parameters is significant in all cases. The gap size has a positive PRCC for the enthalpy and negative PRCC value for the power and reactivity. On one hand, if the gap size is increased, the fuel temperature is also increased and thus, the enthalpy increases. On the other hand, due to the increase of fuel temperature and the Doppler effect, the absorption cross section is also increased and thus, the power and reactivity decreases. Regarding the power and reactivity, even though the order is different, the top four most sensitive input parameters are the same (regardless of the sampling method used). However, these are in disagreement with the most sensitive input parameters for the enthalpy. Moreover, there are further disagreements with the less sensitive input parameters. Sensitivity coefficients are expressed as the fraction of sensitivity apportioned by each input parameter. Thus, the top sensitive input parameters make the biggest contribution to the uncertainty in output parameters. Therefore, other input parameters have little contribution and a little change -due to the sampling method used- could change the sensitivity ranking.

	Average	Standard Deviation	Skewness	Kurtosis
Enthalpy (J/kg)	2.628E+2 ± 8.274E-1	5.059E+0 ± 6.576E-1	0.2465	-1.2330
Power (W)	9.122E-1 ± 6.192E-5	3.785E-4 ± 4.921E-5	-0.4419	-1.0260
Reactivity ($)	-7.986E-2 ± 6.005E-5	3.671E-4 ± 4.773E-5	-0.5037	-1.0901

Table 6.11 – Statistics for output parameters using the SRS sampling method.

	Average	Standard Deviation	Skewness	Kurtosis
Enthalpy (J/kg)	2.636E+2 ± 8.173E-1	4.996E+0 ± 6.496E-1	0.0327	-1.1776
Power (W)	9.121E-1 ± 6.241E-5	3.816E-4 ± 4.960E-5	-0.2538	-1.1091
Reactivity ($)	-7.991E-2 ± 6.015E-5	3.677E-4 ± 4.781E-5	-0.3014	-1.1741

Table 6.12 – Statistics for output parameters using the LHS sampling method.

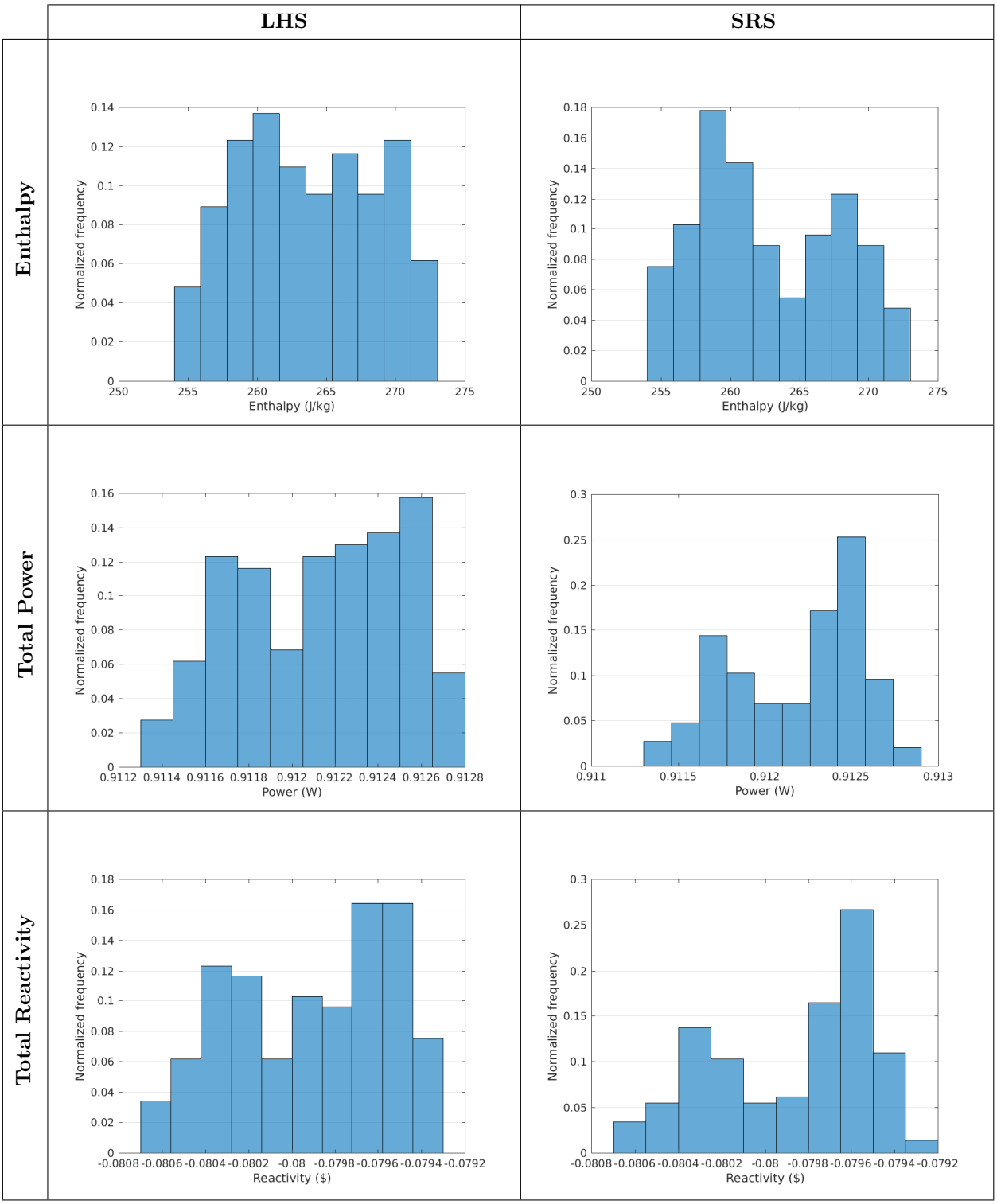

Table 6.13 – Histograms for output parameters.

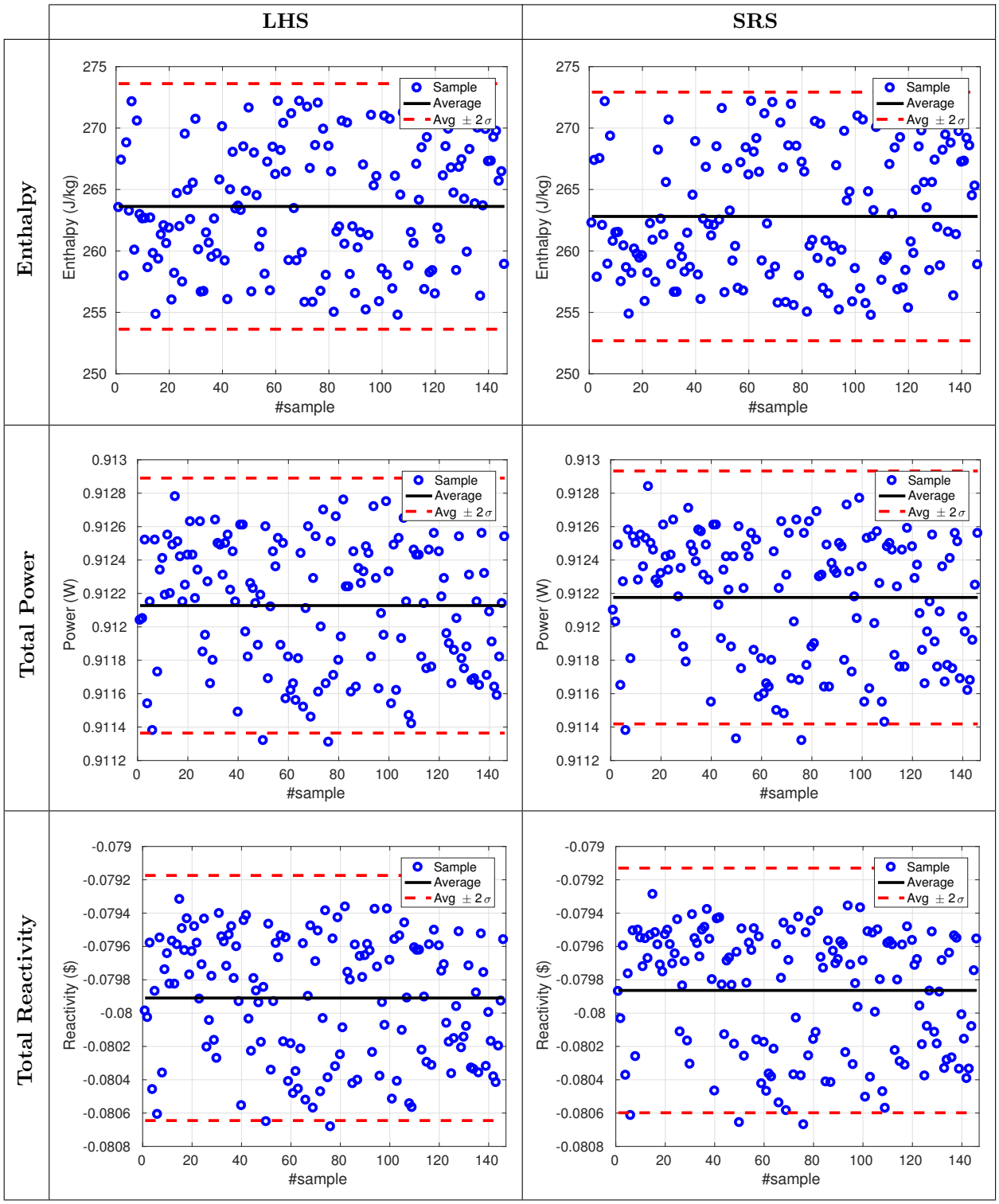

Table 6.14 – Scatter plots for output parameters.

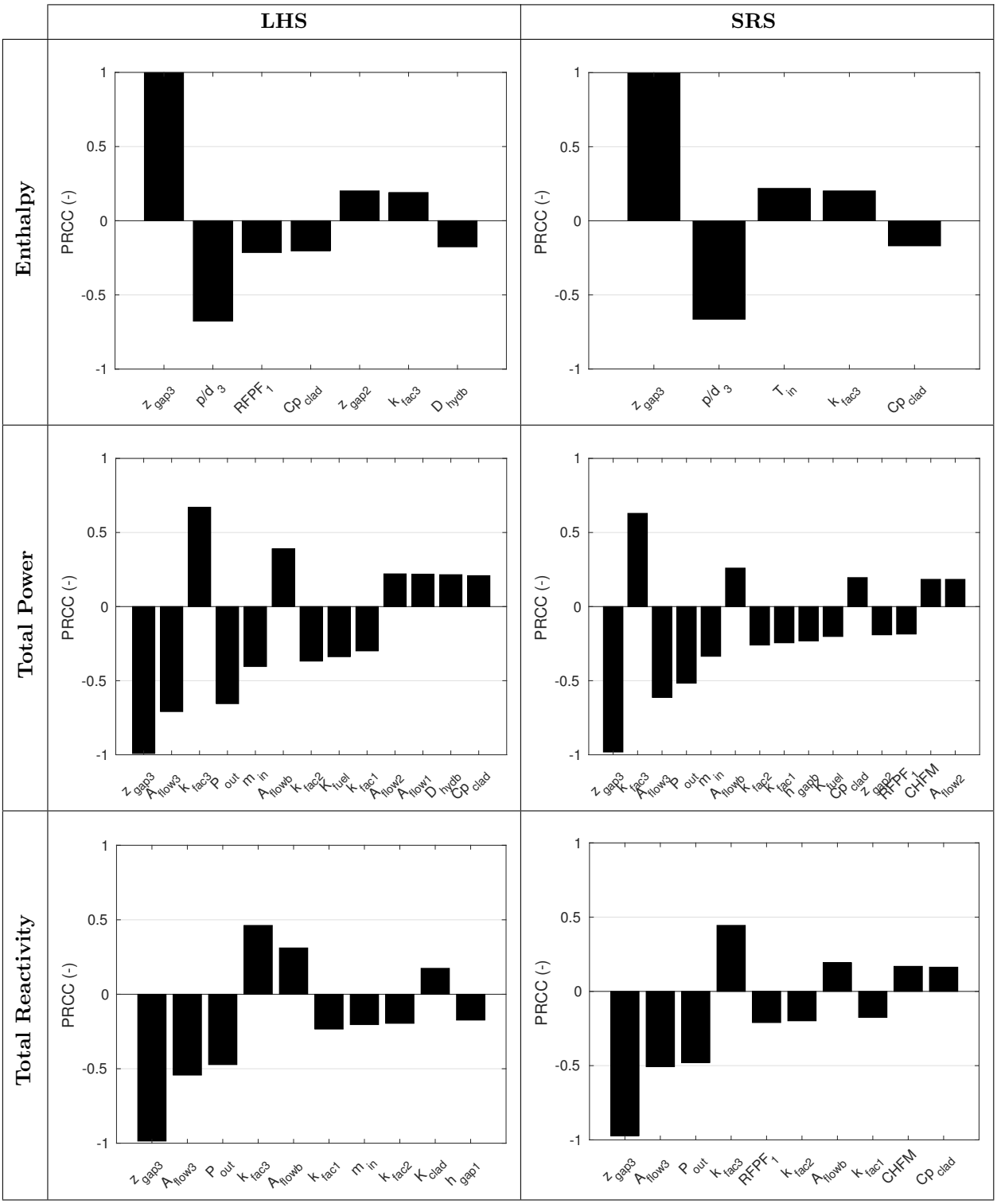

Table 6.15 – PRCC for most sensitive input parameters.

Enthalpy		**Power**		**Reactivity**	
LHS	SRS	LHS	SRS	LHS	SRS
z_{gap3}	z_{gap3}	z_{gap3}	z_{gap3}	z_{gap3}	z_{gap3}
p/d_3	p/d_3	A_{flow3}	k_{fac3}	A_{flow3}	A_{flow3}
T_{in}	T_{in}	k_{fac3}	A_{flow3}	P_{out}	P_{out}
RFPF_1	k_{fac3}	P_{out}	P_{out}	k_{fac3}	k_{fac3}
Cp_{clad}	Cp_{clad}	m_{in}	m_{in}	A_{flow0}	RFPF_1
z_{gap2}		A_{flow0}	A_{flow0}	k_{fac1}	k_{fac2}
k_{fac3}		k_{fac2}	k_{fac2}	m_{in}	A_{flow0}
D_{hyd0}		K_{fuel}	k_{fac1}	k_{fac2}	k_{fac1}
		k_{fac1}	h_{gap0}	K_{clad}	CHFM
		A_{flow2}	K_{fuel}	h_{gap1}	Cp_{clad}
		A_{flow1}	Cp_{clad}		
		D_{hyd0}	z_{gap2}		
		Cp_{clad}	RFPF_1		
			CHFM		
			A_{flow2}		

Table 6.16 – Most sensitive input parameters.

For both sampling methods, the assembly type 3 is always the assembly with more sensitive input parameters. Then assembly 2 and 1 are, roughly, equally sensitive, finally the bypass is the less sensitive. The great importance of input parameters belonging to assembly type 3 can be assessed using Fig. 4.24 (left plot). A great fraction of the core is represented using this assembly type (number 17 in that figure). Thus, a slight change in its definition affects the output parameters significantly. Mainly, the bypass does not have a great effect on the output parameters studied. The exception is the bypass flow area, which is significant enough, it greatly affects the core flow and thus the power and reactivity. The most sensitive boundary condition, for this case, is the outlet pressure for the power and reactivity followed by the inlet mass flow. Regarding the enthalpy, the most sensitive boundary condition is the liquid inlet temperature.

6.2.2 Index dependent approach

Table 6.17 shows the average output parameters (solid black line), the lower and upper 95% confidence interval (dashed-red lines) and the maximum/minimum response value (dash-dot blue lines) for each output parameter as a function of time. The total power response is normalized to one. Again, the left column shows the results for the LHS sampling method, whereas the right column shows the results for the SRS sampling method. A null transient of 50 seconds is run prior to the control rod drop transient for all results. It can be concluded that the most uncertain output parameter is the enthalpy, its uncertainty is almost 2%. The uncertainty for the power and reactivity is 0.05% and 0.6% respectively. Table 6.18 shows the standard deviations and their confidence intervals.

Regarding the sensitivity analysis, Table 6.19 shows the PRCC values as a function of time for all three output parameters and both sampling methods. A maximum of 14 most sensitive input parameters are shown. The results show that the most sensitive input parameters experience a great change in sensitivity when the *Anticipated Operational Occurrence* (AOO) occurs (50 seconds). It must be said that it is difficult to describe which are the most sensitive input parameters because PRCC values cross each other in time, hence the sensitivity ranking changes accordingly. It is clear that the most sensitive input parameter is, again, the gap size for the assembly type 3. For the enthalpy, the gap size is sensitive all the time, whereas,

for the power and reactivity, the sensitivity experience a sign change when the rod is dropped. The top three most sensitive parameters are the same for the power and reactivity, but different for the enthalpy. Nevertheless, from Table 6.19, it is not clear the trend for the most sensitive boundary conditions. It seems that the outlet pressure is the most sensitive boundary condition for the LHS sampling method and that the inlet liquid temperature is the most sensitive for the SRS sampling method. Again, in general, little difference is shown between LHS and SRS sampling methods for the most sensitive input parameters.

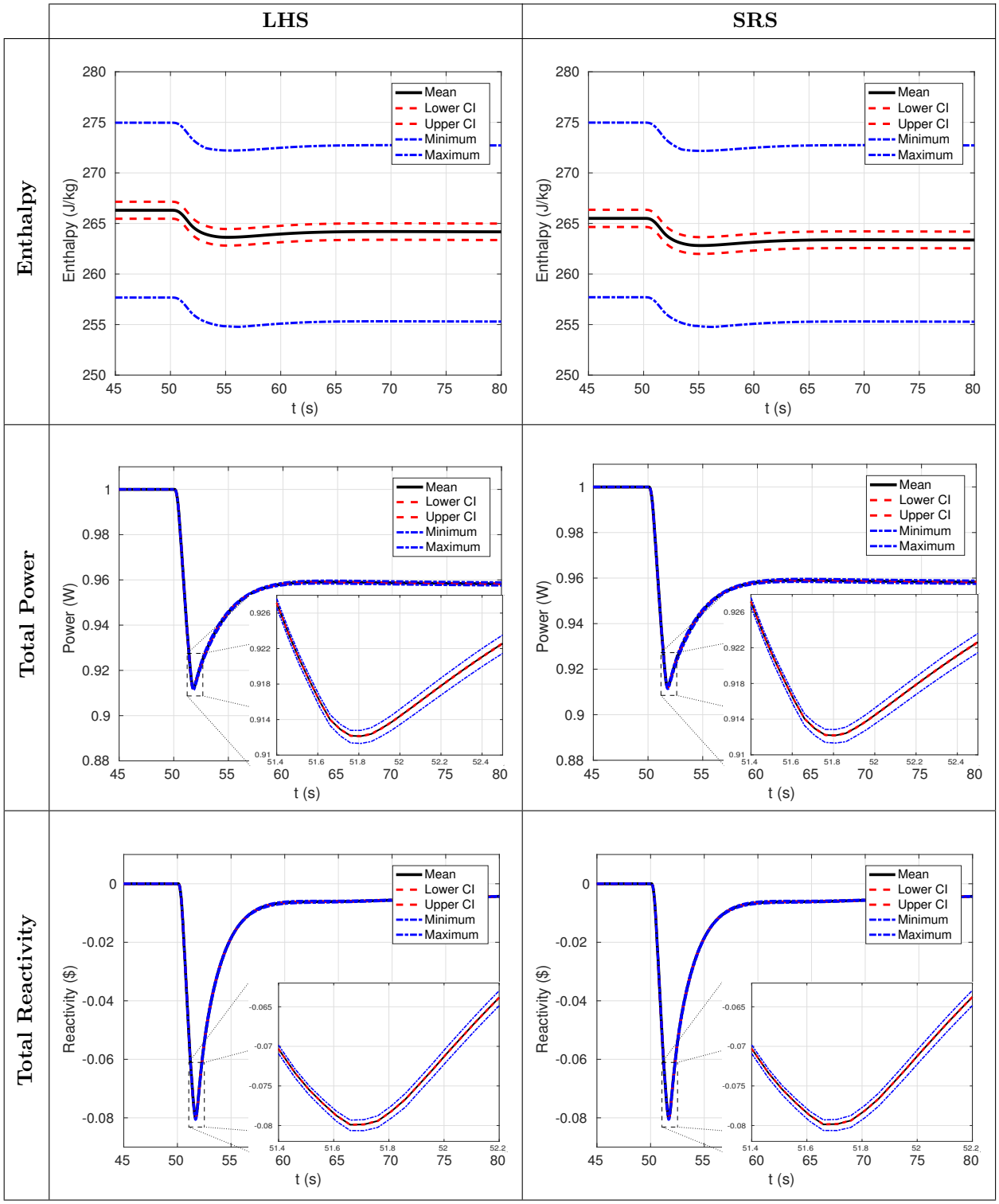

Table 6.17 – Average data (black line), confidence intervals (dashed-red lines) and maximum/minimum response values (dash-dot blue lines) for output parameters.

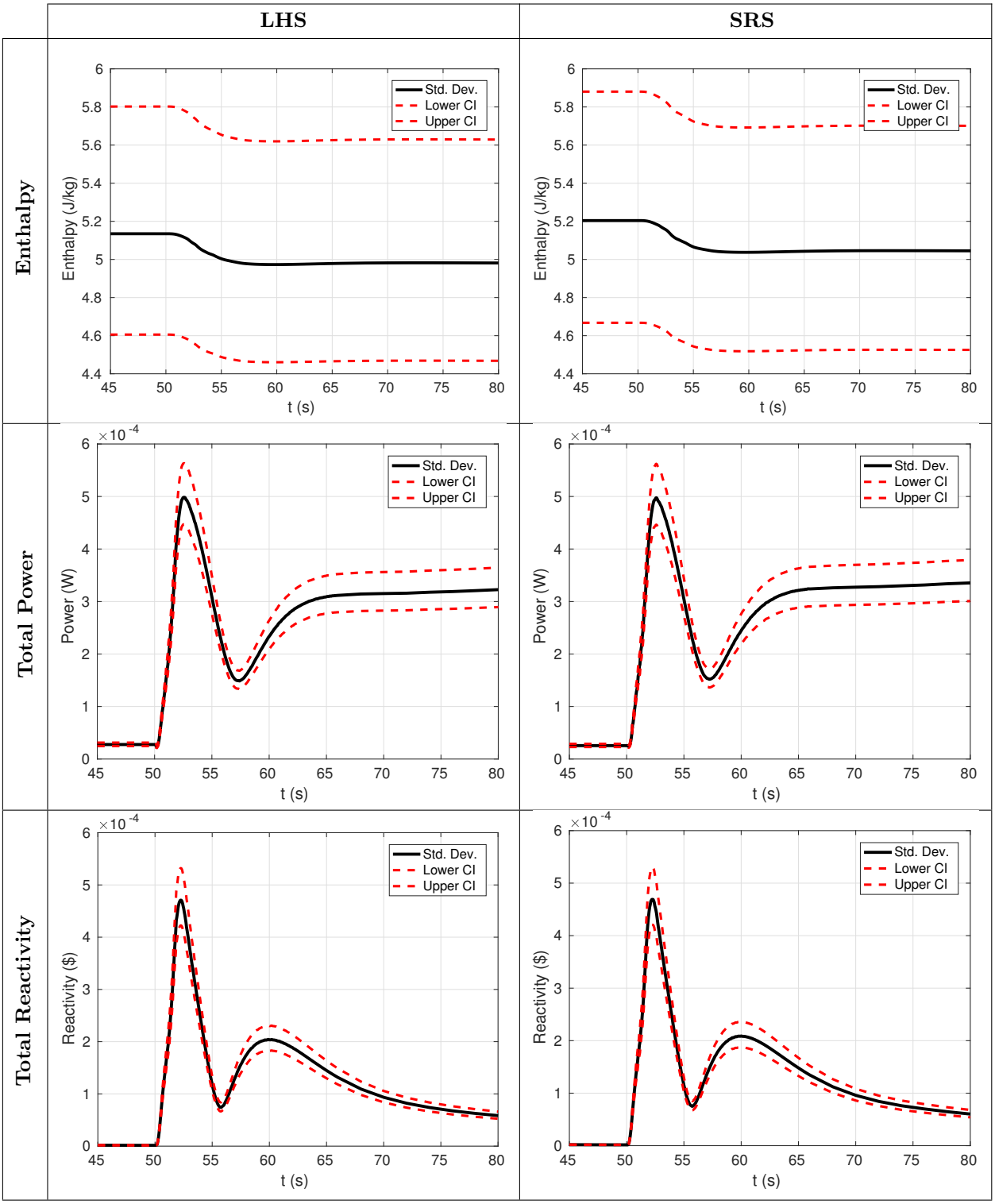

Table 6.18 – Standard deviations (black line) and confidence intervals (dashed-red lines) for output parameters.

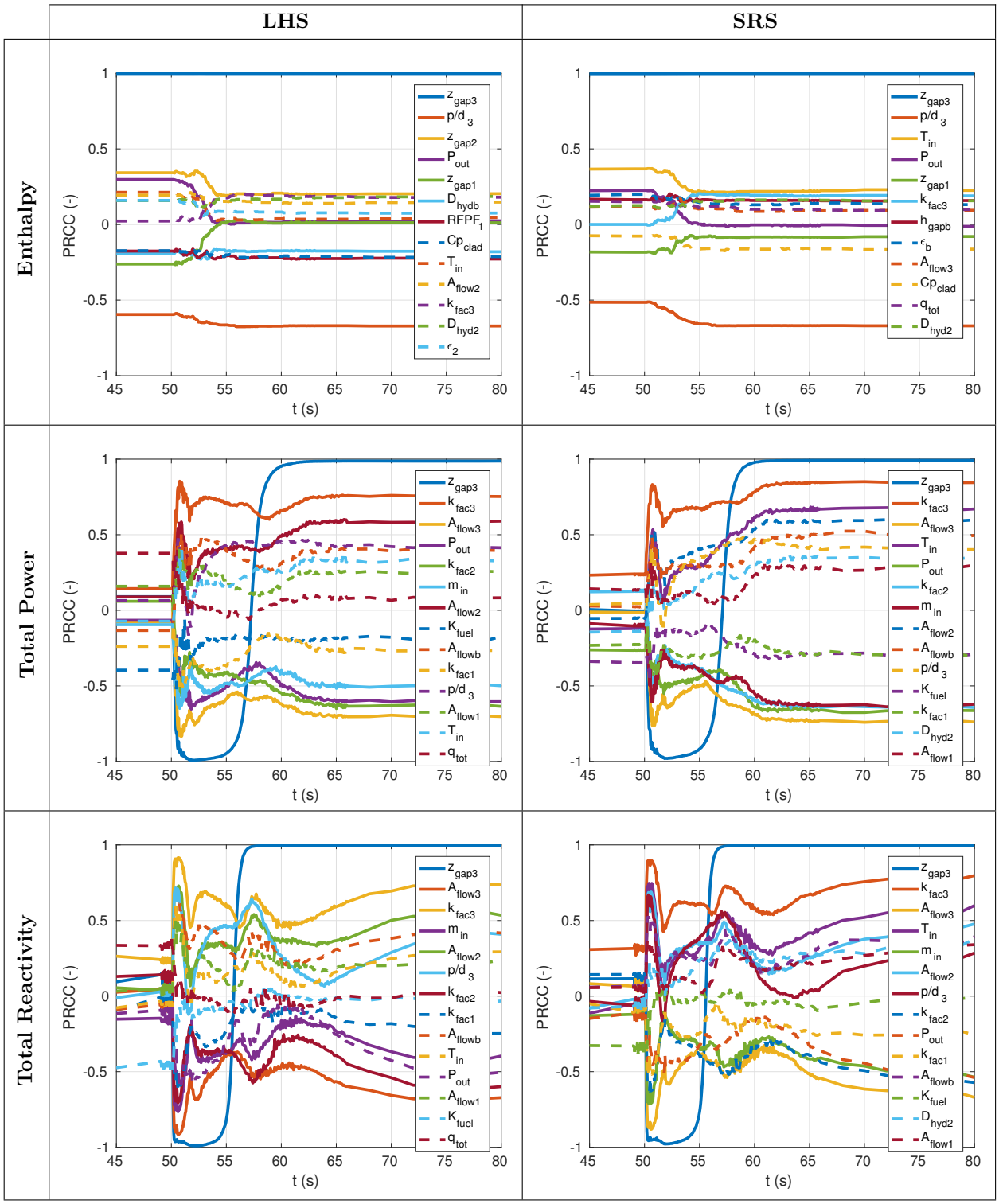

Table 6.19 – PRCC for most sensitive input parameters.

Chapter 7

Conclusions

. . . the outcome of this thesis summarized in a few pages.

A methodology to propagate the uncertainty in cross sections and other neutronic parameters is developed and explained in this PhD thesis using a BWR core. It comprises all phases involving computational simulations, from lattice neutronic phase (including collapse and homogenization) to the neutronic library generation and further use in a core simulator. All kind of information regarding an U&S analysis is obtained following a stochastic and nonparametric sampling. The methodology is not limited to neutronic parameters or any kind of reactor. The same methodology is used to propagate thermohydraulic parameters in a PWR core. It is important to mention that the whole process is automated with MATLAB, this feature provides a great advantage to perform massive studies for benchmarks and/or own executions. In this chapter, some final conclusions and future works are mentioned, these could be useful to clarify or lead to new ideas for future studies.

7.1 Conclusions

The main conclusions extracted in this PhD thesis are summarized below.

1. Propagation of neutronic parameters.
   - It is possible to extract uncertainty information for neutronic parameters at lattice and core level. Their accuracy depends on the number of samples (perturbations). In this PhD thesis, the maximum number of samples allowed by SAMPLER (1000) is used, although it is seen that output variables converge at around 200 samples. The same number is kept for PARCS propagation.
   - SCALE predictions are in concordance with a code-to-code comparison with CASMO. However, as seen in Fig. 4.26 and Fig. 4.27, some discrepancies are seen for the fast diffusion coefficient. This is not a problem for the purpose of this PhD thesis: test the U&S for neutronic parameters through the whole process (lattice and core codes) only in steady state and normal operation conditions. Nevertheless, in a future study it must be assessed how important these discrepancies are in a transient thermohydraulic-neutronic simulation.
   - The *Sensitivity Analysis* (SA) for the BWR core considered shows that the most sensitive homogenized cross section is $\nu\Sigma_{f2}$. Depending on the neutronic parameter studied, it is followed by Σ_{a1} or $\nu\Sigma_{f1}$. It is also possible to determine which is the most sensitive segment in the core. This could lead to define what could be the next steps to update the current "low-fidelity" covariance libraries or what segment model should be simulated in more detail.

  - If one segment is highly sensitive, homogenized cross sections belonging to other segments are partially hidden in the global SA. To disclose the sensitivity of homogenized cross sections belonging to less sensitive segments, another SA performed over a specific segment can be done. This could lead to know what segment should be modeled with less uncertainty.

2. Propagation of thermohydraulic parameters.

  - The SA for the PWR core considered shows that the fuel-clad gap size is the most sensitive input parameter towards the thermohydraulic parameters studied in this PhD thesis, for both sampling methods: SRS and LHS. The sensitivity ranking follows with the assembly flow area, friction factors and pitch to diameter ratio. It is possible to know what is the most sensitive fuel type and therefore, the uncertainty of the model can be strongly reduced if the uncertainty of this particular fuel type is reduced.
  - With the exception of the bypass flow area, parameters modeling the bypass are not especially sensitive. Its flow area mainly affects the power and the total reactivity (positive correlation).
  - Especial care must be taken when assigning uncertainty information to the boundary conditions. The convergence of the simulation is greatly affected by its boundaries.
  - The use of expert judgment to assign uncertainty information should be avoided. Nonetheless, sometimes it is necessary due to the lack of uncertainty information.
  - Discrepancies between LHS and SRS sampling methods are almost negligible (as Strydom 2013 also shows). However, these can change the sensitivity ranking for medium and low sensitive input parameters.

7.2 Remarks

Hereafter, some ideas are given to improve the cross section generation methodology.

- Interpolation method. Linear interpolation method is used in this thesis. There are other interpolation approximations built in MATLAB based on different linear, piecewise or spline schemes. However, a preliminary study showed that the interpolation approximation does not produce significant changes.
- Code-to-code comparison. The main disadvantage with a code-to-code comparison with CASMO is that it is a black box code (only the results were available). Then, if differences arise, it is difficult to assess the reasons. Therefore, it may be beneficial if a third lattice physics code could be used in the future, for example SERPENT code.
- Exposure studies. Even though the capability to generate neutronic libraries for cores with a certain exposure is available, future studies must assess the degree of accuracy of this capability.

It is thought that it is important to give a sense of the computational time employed in the different steps of the methodology. The approximate computational time for the different steps are summarized in Table 7.1. Undoubtedly, SCALE/SAMPLER calculations constitute the bottleneck, especially because of the number of samples. The conditions for this thesis are simplified: only 9 segments and simulation at beginning of cycle (fresh fuel). Computational time could increase dramatically if real conditions are to be simulated. If the simulations were performed with a certain exposure, the number of segments -and neutronic compositions- would increase drastically. Moreover, time in Table 7.1 is true provided that a powerful server[1] is used and

[1] Rigel server is composed by 72 nodes (Fujitsu BX920S3), each of them has two processors Intel Xeon E5-2450 8c/16T and 64 GB/RAM DDR3. There are 11 disks with 600 Gb (15krpm) and 23 disks with 3Tb (7,2krpm). The server has a computational capacity of up to 20,6 TeraFLOPS (LINPACK test).

an expert user performs the calculations. Otherwise, the computational time could experience a twofold increase. Besides, the whole process becomes prohibitive if big computational resources are not available. The computational time is expected to increase (approximately) linearly with the number of segments and the number of samples[2]. Here are some ideas to reduce the computational time needed to execute SCALE simulations.

- Use of Polaris. This is a new module in SCALE6.2 that provides 2D lattice physics analysis with depletion capability for LWR. It processes collapsed and homogenized cross sections and outputs the results in a formatted file `xfile016`. Polaris also provides an easy-to-use input format to allow users to setup lattice models with minimal lines of input. Unfortunately, control rods for BWR simulations are still not available in SCALE6.2.1. Preliminary results show that Polaris can reduce the calculation time -roughly- by a factor of 9 in a simple PWR model (Labarile et al. 2015). The average error is around 5% (and up to 14%) with respect to NEWT. It is expected that this error could be reduced even further in future studies.

- Reduce the branches in TRITON model. Nonetheless, this reduces the number of points available to the core physics code to interpolate the neutronic parameters and increases the prediction errors (especially if the neutronic parameters behavior is not linear). If the thermohydraulic conditions to be simulated in the core physics code are known in advance, it is possible to reduce the range (and the points) defined by the branches while keeping the distance between points. However, this limits the use of the generated neutronic library (limited by the thermohydraulic conditions to be simulated in the core simulator).

- Reduce the number of samples. This increases the output parameter uncertainty and therefore, it is limited by the regulatory body. In this thesis, 1000 samples are taken, which is the maximum number of samples allowed by SAMPLER. It is thought that the generated statistics are accurate enough for a general purpose.

- Increase server power or computational resources. SCALE calculations need high computational resources, its output files are big. Luckily, cross section data is stored in smaller files (`txtfile16`) and only a few output files are kept. Fig. 7.1 shows the computational resources employed by SCALE6.2, memory (left) and space (right), for a typical case with a high resource consumption. It shows that memory used has peaks of almost 30 GB (for cross section processing module WORKER) and 23 GB of space (space can be greatly reduced after simulation). This is a concern when there are thousands of simulations[3] with 62 branches each.

As seen in this PhD thesis, if there is a high number of input parameters (in the order of several hundreds), another issue arise when the PRCC is used to assess the sensitivity. As seen in Section 6.1.2, it is difficult to see what are the main sensitivity trends when several dozens of input parameters are highly sensitive. Several solutions are given here, the expert analyzer should decide what is -or are- the best approximation.

- Split the U&S in smaller analyses grouped by input parameters with common properties. In this thesis, these are grouped by segments (Section 6.1.2.1), then new U&S are performed with the resulting smaller input domains.

- Lump input parameters. Although this solution could worsen the study definition (due to the average process), it drastically reduces the U&S analysis time. For example, it would be possible to lump energy groups -at lattice level- and create new input parameters averaged over the energy domain.

[2] The computational time is also inversely proportional to the number of users. The server is based on a queue system to execute the jobs. In this thesis, 10 different users are used to accelerate the process.

[3] Approximately, there are 135 jobs running at the same time consuming 142 Gb of memory.

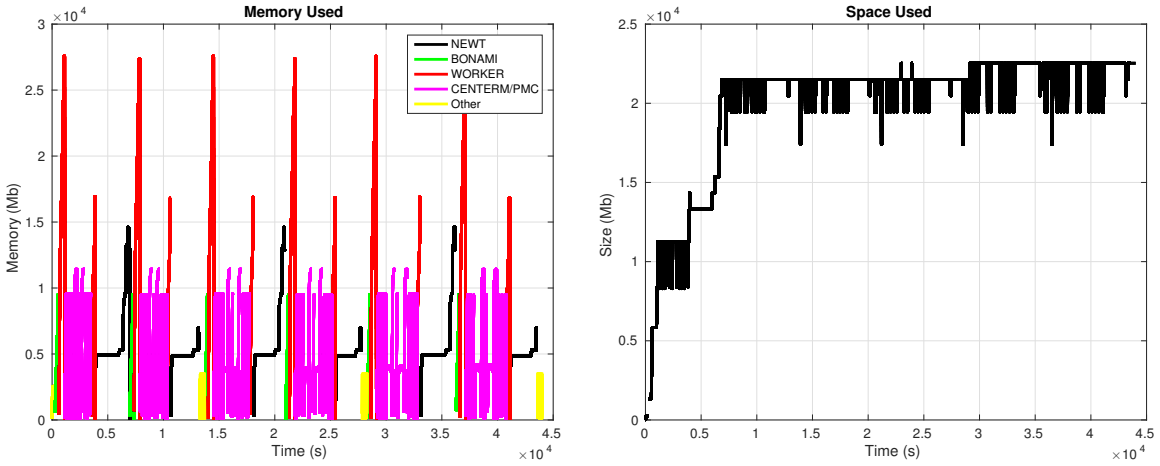

Fig. 7.1 – Computational resources employed by SCALE6.2 version.

Scenario	Task	Time	Processors
Nuclear data propagation	MCDancoff calculations	1 day	1
	SCALE/SAMPLER calculations (1000 repetitions)	22 days	∼150
	Post-process SAMPLER data	2 days	1
	PARCS calculations SSA (global SA or SA by segment)	60 min	1
	DAKOTA calculations (PARCS) and process data	2 min	1
Thermohydraulic variable propagation	TRACE/PARCS (SSA+CSS+CTR)	5 days	5
	DAKOTA calculations (TRACE/PARCS) and process data	30 min	1

Table 7.1 – Computational time summary.

The disadvantage of this solution is that some uncertainty information is lost when new statistics are calculated for the lumped parameters.

– Perform a SA prior to the *Uncertainty Quantification* (UQ). This analysis isolates the most sensitive input parameters and thus, non-sensitive input parameters can be discarded assuming a risk by the expert analyzer. In this thesis the *Gesellschaft für Anlagen und Reaktorsicherheit* (GRS) methodology is chosen because its simplicity of use, other methodologies could be difficult to implement or perform.

Another current concern is the uncertainty propagation for the fraction of delayed neutron precursors (β_i) and their decay constants (λ_i) through the lattice and core physics codes. As explained in Mesado et al. 2012, it is known that the fraction of delayed neutron precursors (and their decay constants) play an important role in the output variable variance. Especially, for assemblies near the end of cycle, delayed neutrons play an important role in the time evolution of the neutron flux, and so the uncertainty in β_i and λ_i will have a greater effect on the output parameters. An alternative method for β_i uncertainty propagation is given in Kodeli 2013. Moreover, Wang et al. 2013 shows some discrepancies for β_i calculations using several lattice

codes. In this thesis, due to the lack of information in the "low-fidelity[4]" covariance library, the uncertainties of these kinetic parameters have not been included a priori. In any case, the uncertainty of these parameters does not influence the steady state results.

7.3 Future work

To conclude this PhD thesis and after all the experience gained while developing this work, some interesting ideas are presented as future work to further develop the main purpose of this thesis.

- In Section 5.1.1, a procedure to create an in-house perturbation library is presented. However, due to format changes across different SCALE versions, it could not be implemented in this thesis. It will be interesting if a future work could reproduce -and update- this procedure. Then, results can be compared using different *Probability Distribution Functions* (PDFs) and/or sampling methods to generate the perturbation library.
- Perform SA at lattice level with SAMPLER, not yet supported in SCALE6.2.1.
- DAKOTA can be used to supply SA at lattice level, but only after the in-house perturbation library process is updated.
- Perform U&S with TSUNAMI (lattice level) and compare with SAMPLER and DAKOTA.
- Perturb kinetic parameters (yields and decay data). However, current "low-fidelity" covariance libraries contain poor uncertainty information for these parameters.
- U&S analysis in transient state. For example a turbine trip or an accident involving a control rod.
- Obtain neutronic libraries with an extra lattice physics code, SERPENT or HELIOS for example. Compare results with CASMO and SCALE.
- Compare thermohydraulic U&S with another thermohydraulic code, RELAP for example, and include more variables.
- Compare the 3D thermohydraulic model and the traditional 1D model with a severe asymmetric phenomenon.
- Keep the participation in the Benchmark for Uncertainty Analysis in Modelling (UAM) for the Design, Operation and Safety Analysis of LWRs. This PhD thesis has proved to be valuable to perform U&S at different code levels and several types of input parameters, as required for this benchmark. Following exercises need further development.

[4]Several methods are used to approximate the nuclide uncertainties not available in the *Nuclear Data Libraries* (NDLs). Thus, covariance libraries are often qualified as "low-fidelity". That is why covariance libraries are not generally included in the official NDLs, but distributed with the main U&S analysis codes.

Appendix A

List of MT reactions

A list of the most important MT nuclear interaction numbers is shown hereafter. Besides the MT number, the notation for the specific reaction and a brief description is given. In the notation, z stands for any of the particles: n, p, d, t, ^{3}He, α, or γ. Extensive information can be found in Herman and Trkov 2005.

MT	Reaction	Description
1	(n, total)	Neutron total cross section.
2	(z, z_0)	Elastic scattering cross section for incident particles.
3	$(z, \text{nonelas})$	Nonelastic cross section.
4	(z, n)	Production of one neutron in the exit channel.
11	$(z, 2nd)$	Production of two neutrons and a deuteron, plus a residual.
16	$(z, 2n)$	Production of two neutrons, plus a residual.
17	$(z, 3n)$	Production of three neutrons, plus a residual.
18	$(z, \text{fission})$	Total fission.
19	(z, f)	First-chance fission.
20	(z, nf)	Second-chance fission.
21	$(z, 2nf)$	Third-chance fission.
22	$(z, n\alpha)$	Production of a neutron and alpha particle, plus a residual.
27	(z, abs)	Absorption.
28	(z, np)	Production of a neutron and a proton, plus a residual.
50	(z, n_0)	Production of a neutron, leaving the residual nucleus in the ground state.
51	(z, n_1)	Production of a neutron, leaving the residual nucleus in the first excited state.
52	(z, n_2)	Production of a neutron, leaving the residual nucleus in the second excited state.
101	(z, disap)	Disappearance.
102	(z, γ)	Radiative capture.
103	(z, p)	Production of a proton, plus a residual.
104	(z, d)	Production of a deuteron, plus a residual.
105	(z, t)	Production of a triton, plus a residual.
106	$(z, ^3\text{He})$	Production of a He particles, plus a residual.
107	(z, α)	Production of an alpha particle, plus a residual.

Table A.1 – List of most important MT nuclear interaction numbers.

Appendix B

NEMTAB format

Data in NEMTAB libraries is divided in sections for different neutronic compositions. Each neutronic composition contains its cross section data tabulated as a function of feedback parameters (fuel temperature and moderator density) and the collapsed energy group. Neutronic data without control is stored in *nemtab* file, while controled neutronic data is kept within a second file *nemtabr*.

In NEMTAB files, lines starting by an apostrophe (*) are comments, nonetheless, these lines cannot be omitted. The library starts with a brief description of feedback parameters, five different feedback parameters are shown in line 4. Nevertheless, NEMTAB libraries only take into account fuel temperature, moderator density and control rod state Boron concentration feedback can also be included creating several NEMTAB libraries for different boron concentrations. The actual number of fuel temperature and moderator density feedback points is indicated in line 5, the first and second values, respectively, are used. Other data in this line is ignored. Then, the data for each neutronic composition is repeated sequentially, the number for the first neutronic composition is shown in line 8. Hereafter, the first few line for a NEMTAB library, with 6 fuel temperature and moderator density feedback points, are shown.

```
1 *
2 *  NEM-Cross Section Table Input
3 *
4 *    T Fuel         Press.         Boron ppm.    T Mod.         Void
5                6              6              0             0             0
6 *
7 *******           X-Section set #         1
8     1
9 *
```

For each neutronic composition, data is tabulated according to the collapsed energy group and neutronic parameter. Tables have, typically, 5 columns. The table for the first neutronic parameter, first collapsed energy group and first neutronic parameter must start in line 14. The first numbers in each table are the fuel temperature feedback points (length is indicated by first number in line 5), T_f. Immediately, the moderator density feedback points follow (length denoted by second number in line 5), ρ_m. The table continues with the neutronic data. A specific order is followed. First neutronic data corresponds to the first fuel temperature point and first moderator density point, $\Sigma(T_{f1}, \rho_{m1})$. Second neutronic data corresponds to the second fuel temperature point and first moderator density point, $\Sigma(T_{f2}, \rho_{m1})$. Data continues up to the last fuel temperature point, $\Sigma(T_{f6}, \rho_{m1})$. Then, the sequence is repeated for the second moderator density point, $\Sigma(T_{f1}, \rho_{m2}) \ldots \Sigma(T_{f6}, \rho_{m2})$, the third, $\Sigma(T_{f1}, \rho_{m3}) \ldots \Sigma(T_{f6}, \rho_{m3})$, etc. The table ends when the last fuel temperature and moderator density point is reached, $\Sigma(T_{f6}, \rho_{m6})$. Hereafter, a table with diffusion coefficient

data is shown as an example.

```
***************  Diffusion Coefficient Table
*
  .5470000E+03  .6179000E+03  .8000000E+03  .9000000E+03  .1000000E+04
  .1200000E+04  .3000000E+03  .4500000E+03  .6250000E+03  .7000000E+03
  .7500000E+03  .8000000E+03  .1906230E+01  .1914520E+01  .1930920E+01
  .1938190E+01  .1939600E+01  .1942220E+01  .1712220E+01  .1716180E+01
  .1724210E+01  .1727850E+01  .1729060E+01  .1731330E+01  .1519270E+01
  .1520360E+01  .1522820E+01  .1524030E+01  .1525040E+01  .1526940E+01
  .1446170E+01  .1446820E+01  .1448410E+01  .1449230E+01  .1450180E+01
  .1451930E+01  .1401290E+01  .1401910E+01  .1403420E+01  .1404210E+01
  .1405110E+01  .1406770E+01  .1359160E+01  .1359740E+01  .1361190E+01
  .1361940E+01  .1362790E+01  .1364380E+01
*
```

In each neutronic composition, 19 tables are specified. Each table contains data for a different neutronic parameter according to the following list.

1. Diffusion coefficient for the fast energy group, D_{f1}.
2. Absorption cross section for the fast energy group, Σ_{a1}.
3. Fission cross section for the fast energy group, Σ_{f1}.
4. Fission cross section for the fast energy group times the average number of neutrons produced per fission, $\nu\Sigma_{f1}$.
5. Scattering cross section from fast to thermal energy group, Σ_{12}.
6. Adjoint discontinuity factor for the west boundary in the assembly and fast energy group, ADF_{W1}.
7. Adjoint discontinuity factor for the south boundary in the assembly and fast energy group, ADF_{S1}.
8. Detector data for the fast flux, table is filled with zeros if no detector is used.
9. Detector data for the fast fission events, table is filled with zeros if no detector is used.
10. Diffusion coefficient for the thermal energy group, D_{f2}.
11. Absorption cross section for the thermal energy group, Σ_{a2}.
12. Fission cross section for the thermal energy group, Σ_{f2}.
13. Fission cross section for the thermal energy group times the average number of neutrons produced per fission, $\nu\Sigma_{f2}$.
14. Xenon macroscopic cross section, Σ_{Xe}.
15. Xenon microscopic cross section, σ_{Xe}.
16. Adjoint discontinuity factor for the west boundary in the assembly and thermal energy group, ADF_{W2}.
17. Adjoint discontinuity factor for the south boundary in the assembly and thermal energy group, ADF_{S2}.
18. Detector data for the thermal flux, table is filled with zeros if no detector is used.
19. Detector data for the thermal fission events, table is filled with zeros if no detector is used.

A final comment related with feedback parameters must be made. Feedback parameter values must be in increasing order and can be different from table to table. However, all tables must have the same number of points for each feedback parameter.

At the end of each neutronic composition, three extra neutronic parameters must be included. These are the effective delayed neutron yield (β), decay constants for delayed neutron groups (λ) and the inverse neutron velocity ($1/v_n$). The first two parameters must be discretized using 6 groups, the third uses only 2 groups. Hereafter, an example is shown.

```
262 ***************  Effective Delayed Neutron Yield in 6 Groups
263 *
264   .2069000E-03  .1277400E-02  .1155500E-02  .2484000E-02  .8998300E-03  .2179300E-03
265 *
266 ***************  Decay Constants for Delayed Neutron Groups
267 *
268   .1277200E-01  .3167600E-01  .1212400E+00  .3214200E+00  .1400700E+01  .3877600E+01
269 *
270 ***************  Inv. Neutron Velocities
271 *
272   .5550700E-07  .2379000E-05
273 *
274 *
```

Neutronic compositions representing reflector segments are simplified since the following neutronic parameters are always zero: Σ_f, $\nu\Sigma_f$, Σ_{Xe}, σ_{Xe}, β and λ. Typically, neutronic compositions representing reflector segments are included as the last neutronic compositions, but this is not mandatory.

With all these information for each neutronic composition, a core physics code is able to solve the diffusion equation. Next, a piece of a NEMTAB library is included as an example. It is long enough to cover the first neutronic composition entirely.

```
1  *
2  *  NEM-Cross Section Table Input
3  *
4  *    T Fuel         Press.         Boron ppm.    T Mod.         Void
5                 6              6              0              0              0
6  *
7  *******            X-Section set #        1
8      1
9  *
10 *       Group No.  1
11 *
12 ***************  Diffusion Coefficient Table
13 *
14   .5470000E+03  .6179000E+03  .8000000E+03  .9000000E+03  .1000000E+04
15   .1200000E+04  .3000000E+03  .4500000E+03  .6250000E+03  .7000000E+03
16   .7500000E+03  .8000000E+03  .1906230E+01  .1914520E+01  .1930920E+01
17   .1938190E+01  .1939600E+01  .1942220E+01  .1712220E+01  .1716180E+01
18   .1724210E+01  .1727850E+01  .1729060E+01  .1731330E+01  .1519270E+01
19   .1520360E+01  .1522820E+01  .1524030E+01  .1525040E+01  .1526940E+01
20   .1446170E+01  .1446820E+01  .1448410E+01  .1449230E+01  .1450180E+01
21   .1451930E+01  .1401290E+01  .1401910E+01  .1403420E+01  .1404210E+01
22   .1405110E+01  .1406770E+01  .1359160E+01  .1359740E+01  .1361190E+01
23   .1361940E+01  .1362790E+01  .1364380E+01
24 *
25 ***************  Absorption X-Section Table
26 *
```

```
  .5470000E+03  .6179000E+03  .8000000E+03  .9000000E+03  .1000000E+04
  .1200000E+04  .3000000E+03  .4500000E+03  .6250000E+03  .7000000E+03
  .7500000E+03  .8000000E+03  .8935381E-02  .8958090E-02  .9015140E-02
  .9045021E-02  .9080840E-02  .9147471E-02  .9736530E-02  .9769561E-02
  .9848291E-02  .9888250E-02  .9929181E-02  .1000531E-01  .1040643E-01
  .1044772E-01  .1054412E-01  .1059241E-01  .1063828E-01  .1072360E-01
  .1064401E-01  .1068747E-01  .1078866E-01  .1083928E-01  .1088689E-01
  .1097546E-01  .1078888E-01  .1083329E-01  .1093672E-01  .1098845E-01
  .1103711E-01  .1112761E-01  .1092879E-01  .1097414E-01  .1107976E-01
  .1113260E-01  .1118238E-01  .1127494E-01
*
***************  Fission X-Section Table
*
  .5470000E+03  .6179000E+03  .8000000E+03  .9000000E+03  .1000000E+04
  .1200000E+04  .3000000E+03  .4500000E+03  .6250000E+03  .7000000E+03
  .7500000E+03  .8000000E+03  .2068246E-02  .2044644E-02  .1998309E-02
  .1977904E-02  .1974608E-02  .1968469E-02  .2168381E-02  .2157034E-02
  .2134142E-02  .2123824E-02  .2120641E-02  .2114714E-02  .2249287E-02
  .2245972E-02  .2238437E-02  .2234738E-02  .2231624E-02  .2225833E-02
  .2283704E-02  .2281536E-02  .2276217E-02  .2273463E-02  .2270351E-02
  .2264571E-02  .2307510E-02  .2305359E-02  .2300042E-02  .2297305E-02
  .2294188E-02  .2288408E-02  .2331503E-02  .2329342E-02  .2324050E-02
  .2321299E-02  .2318185E-02  .2312378E-02
*
***************  Nu-Fission X-Section Table
*
  .5470000E+03  .6179000E+03  .8000000E+03  .9000000E+03  .1000000E+04
  .1200000E+04  .3000000E+03  .4500000E+03  .6250000E+03  .7000000E+03
  .7500000E+03  .8000000E+03  .5436510E-02  .5376860E-02  .5259590E-02
  .5207860E-02  .5199380E-02  .5183610E-02  .5702300E-02  .5673690E-02
  .5615911E-02  .5589840E-02  .5581760E-02  .5566710E-02  .5911890E-02
  .5903561E-02  .5884651E-02  .5875350E-02  .5867520E-02  .5852961E-02
  .5996710E-02  .5991290E-02  .5977960E-02  .5971070E-02  .5963280E-02
  .5948801E-02  .6053590E-02  .6048200E-02  .6034920E-02  .6028060E-02
  .6020270E-02  .6005791E-02  .6108490E-02  .6103110E-02  .6089870E-02
  .6083011E-02  .6075220E-02  .6060720E-02
*
***************  Scattering X-Section Table
*
****   From group 1 to 2
  .5470000E+03  .6179000E+03  .8000000E+03  .9000000E+03  .1000000E+04
  .1200000E+04  .3000000E+03  .4500000E+03  .6250000E+03  .7000000E+03
  .7500000E+03  .8000000E+03  .5211500E-02  .5158500E-02  .5050700E-02
  .5001700E-02  .4984300E-02  .4952000E-02  .8711000E-02  .8674799E-02
  .8596799E-02  .8559899E-02  .8536700E-02  .8493700E-02  .1302510E-01
  .1299840E-01  .1293650E-01  .1290570E-01  .1287720E-01  .1282420E-01
  .1494310E-01  .1491680E-01  .1485500E-01  .1482380E-01  .1479350E-01
  .1473710E-01  .1622360E-01  .1619640E-01  .1613230E-01  .1610010E-01
  .1606870E-01  .1601030E-01  .1752560E-01  .1749740E-01  .1743130E-01
  .1739800E-01  .1736560E-01  .1730520E-01
*
***************  Assembly Disc. Factor Table - W
*
  .5470000E+03  .6179000E+03  .8000000E+03  .9000000E+03  .1000000E+04
  .1200000E+04  .3000000E+03  .4500000E+03  .6250000E+03  .7000000E+03
  .7500000E+03  .8000000E+03  .9968500E+00  .9968500E+00  .9968500E+00
  .9968500E+00  .9968500E+00  .9968500E+00  .9945900E+00  .9945900E+00
  .9945900E+00  .9945900E+00  .9945900E+00  .9945900E+00  .9914400E+00
  .9914400E+00  .9914400E+00  .9914400E+00  .9914400E+00  .9914400E+00
  .9901600E+00  .9901600E+00  .9901600E+00  .9901600E+00  .9901600E+00
  .9901600E+00  .9894300E+00  .9894300E+00  .9894300E+00  .9894300E+00
```

```
  .9894300E+00  .9894300E+00  .9887900E+00  .9887900E+00  .9887900E+00
  .9887900E+00  .9887900E+00  .9887900E+00
*
***************  Assembly Disc. Factor Table - S
*
  .5470000E+03  .6179000E+03  .8000000E+03  .9000000E+03  .1000000E+04
  .1200000E+04  .3000000E+03  .4500000E+03  .6250000E+03  .7000000E+03
  .7500000E+03  .8000000E+03  .9968500E+00  .9968500E+00  .9968500E+00
  .9968500E+00  .9968500E+00  .9968500E+00  .9945900E+00  .9945900E+00
  .9945900E+00  .9945900E+00  .9945900E+00  .9945900E+00  .9914400E+00
  .9914400E+00  .9914400E+00  .9914400E+00  .9914400E+00  .9914400E+00
  .9901600E+00  .9901600E+00  .9901600E+00  .9901600E+00  .9901600E+00
  .9901600E+00  .9894300E+00  .9894300E+00  .9894300E+00  .9894300E+00
  .9894300E+00  .9894300E+00  .9887900E+00  .9887900E+00  .9887900E+00
  .9887900E+00  .9887900E+00  .9887900E+00
*
***************  Detector Flux Ratio Table
*
  .5470000E+03  .6179000E+03  .8000000E+03  .9000000E+03  .1000000E+04
  .1200000E+04  .3000000E+03  .4500000E+03  .6250000E+03  .7000000E+03
  .7500000E+03  .8000000E+03  .0000000E+00  .0000000E+00  .0000000E+00
  .0000000E+00  .0000000E+00  .0000000E+00  .0000000E+00  .0000000E+00
  .0000000E+00  .0000000E+00  .0000000E+00  .0000000E+00  .0000000E+00
  .0000000E+00  .0000000E+00  .0000000E+00  .0000000E+00  .0000000E+00
  .0000000E+00  .0000000E+00  .0000000E+00  .0000000E+00  .0000000E+00
  .0000000E+00  .0000000E+00  .0000000E+00  .0000000E+00  .0000000E+00
  .0000000E+00  .0000000E+00  .0000000E+00  .0000000E+00  .0000000E+00
  .0000000E+00  .0000000E+00  .0000000E+00
*
***************  Detector Microscopic X-Section Table
*
  .5470000E+03  .6179000E+03  .8000000E+03  .9000000E+03  .1000000E+04
  .1200000E+04  .3000000E+03  .4500000E+03  .6250000E+03  .7000000E+03
  .7500000E+03  .8000000E+03  .0000000E+00  .0000000E+00  .0000000E+00
  .0000000E+00  .0000000E+00  .0000000E+00  .0000000E+00  .0000000E+00
  .0000000E+00  .0000000E+00  .0000000E+00  .0000000E+00  .0000000E+00
  .0000000E+00  .0000000E+00  .0000000E+00  .0000000E+00  .0000000E+00
  .0000000E+00  .0000000E+00  .0000000E+00  .0000000E+00  .0000000E+00
  .0000000E+00  .0000000E+00  .0000000E+00  .0000000E+00  .0000000E+00
  .0000000E+00  .0000000E+00  .0000000E+00
*
*      Group No.  2
*
***************  Diffusion Coefficient Table
*
  .5470000E+03  .6179000E+03  .8000000E+03  .9000000E+03  .1000000E+04
  .1200000E+04  .3000000E+03  .4500000E+03  .6250000E+03  .7000000E+03
  .7500000E+03  .8000000E+03  .6987230E+00  .7009380E+00  .7053290E+00
  .7072780E+00  .7076850E+00  .7084410E+00  .5379320E+00  .5389770E+00
  .5410970E+00  .5420570E+00  .5423800E+00  .5429800E+00  .4184190E+00
  .4186880E+00  .4192960E+00  .4195940E+00  .4198430E+00  .4203050E+00
  .3795180E+00  .3796670E+00  .3800380E+00  .3802320E+00  .3804570E+00
  .3808760E+00  .3565970E+00  .3567380E+00  .3570890E+00  .3572720E+00
  .3574850E+00  .3578820E+00  .3348800E+00  .3350160E+00  .3353520E+00
  .3355270E+00  .3357320E+00  .3361120E+00
*
***************  Absorption X-Section Table
*
  .5470000E+03  .6179000E+03  .8000000E+03  .9000000E+03  .1000000E+04
  .1200000E+04  .3000000E+03  .4500000E+03  .6250000E+03  .7000000E+03
```

```
  .7500000E+03  .8000000E+03  .1010111E+00  .1002692E+00  .9881020E-01
  .9816660E-01  .9806059E-01  .9786340E-01  .1049915E+00  .1046372E+00
  .1039237E+00  .1036026E+00  .1035080E+00  .1033321E+00  .1098291E+00
  .1097274E+00  .1094973E+00  .1093842E+00  .1092898E+00  .1091144E+00
  .1125125E+00  .1124446E+00  .1122771E+00  .1121903E+00  .1120911E+00
  .1119065E+00  .1146448E+00  .1145738E+00  .1143983E+00  .1143073E+00
  .1142028E+00  .1140083E+00  .1173012E+00  .1172249E+00  .1170364E+00
  .1169385E+00  .1168259E+00  .1166165E+00
*
***************  Fission X-Section Table
*
  .5470000E+03  .6179000E+03  .8000000E+03  .9000000E+03  .1000000E+04
  .1200000E+04  .3000000E+03  .4500000E+03  .6250000E+03  .7000000E+03
  .7500000E+03  .8000000E+03  .5556513E-01  .5512356E-01  .5425604E-01
  .5387384E-01  .5381083E-01  .5369343E-01  .5616599E-01  .5595680E-01
  .5553575E-01  .5534634E-01  .5529001E-01  .5518529E-01  .5662308E-01
  .5656319E-01  .5642719E-01  .5636050E-01  .5630473E-01  .5620096E-01
  .5703561E-01  .5699519E-01  .5689601E-01  .5684456E-01  .5678610E-01
  .5667753E-01  .5744769E-01  .5740575E-01  .5730188E-01  .5724829E-01
  .5718704E-01  .5707347E-01  .5805315E-01  .5800821E-01  .5789782E-01
  .5784035E-01  .5777485E-01  .5765279E-01
*
***************  Nu-Fission X-Section Table
*
  .5470000E+03  .6179000E+03  .8000000E+03  .9000000E+03  .1000000E+04
  .1200000E+04  .3000000E+03  .4500000E+03  .6250000E+03  .7000000E+03
  .7500000E+03  .8000000E+03  .1460563E+00  .1449601E+00  .1428030E+00
  .1418509E+00  .1416904E+00  .1413920E+00  .1477025E+00  .1471843E+00
  .1461401E+00  .1456699E+00  .1455294E+00  .1452681E+00  .1488247E+00
  .1486769E+00  .1483420E+00  .1481774E+00  .1480398E+00  .1477838E+00
  .1497681E+00  .1496688E+00  .1494243E+00  .1492977E+00  .1491538E+00
  .1488862E+00  .1507100E+00  .1506063E+00  .1503504E+00  .1502178E+00
  .1500668E+00  .1497859E+00  .1520981E+00  .1519873E+00  .1517137E+00
  .1515718E+00  .1514094E+00  .1511074E+00
*
no corrected***  Xe Macroscopic X-Section Table
*
  .5470000E+03  .6179000E+03  .8000000E+03  .9000000E+03  .1000000E+04
  .1200000E+04  .3000000E+03  .4500000E+03  .6250000E+03  .7000000E+03
  .7500000E+03  .8000000E+03  .3980107E-02  .3941708E-02  .3866921E-02
  .3833998E-02  .3830500E-02  .3823819E-02  .3747968E-02  .3731605E-02
  .3699233E-02  .3684832E-02  .3681584E-02  .3675411E-02  .3622131E-02
  .3618425E-02  .3610075E-02  .3606116E-02  .3602795E-02  .3596779E-02
  .3616340E-02  .3614224E-02  .3608936E-02  .3606149E-02  .3602744E-02
  .3596467E-02  .3629854E-02  .3627607E-02  .3622066E-02  .3619208E-02
  .3615722E-02  .3609263E-02  .3662156E-02  .3659824E-02  .3654032E-02
  .3650988E-02  .3647308E-02  .3640603E-02
*
***************  Xe Microscopic X-Section Table
*
  .5470000E+03  .6179000E+03  .8000000E+03  .9000000E+03  .1000000E+04
  .1200000E+04  .3000000E+03  .4500000E+03  .6250000E+03  .7000000E+03
  .7500000E+03  .8000000E+03  .1085030E+07  .1071000E+07  .1043450E+07
  .1031310E+07  .1029400E+07  .1025840E+07  .1175280E+07  .1168610E+07
  .1155180E+07  .1149140E+07  .1147340E+07  .1143990E+07  .1250520E+07
  .1248680E+07  .1244510E+07  .1242460E+07  .1240760E+07  .1237580E+07
  .1296040E+07  .1294910E+07  .1292090E+07  .1290630E+07  .1288950E+07
  .1285830E+07  .1334260E+07  .1333140E+07  .1330370E+07  .1328930E+07
  .1327260E+07  .1324160E+07  .1383930E+07  .1382840E+07  .1380130E+07
  .1378720E+07  .1377070E+07  .1374020E+07
*
```

```
**************  Assembly Disc. Factor Table - W
*
  .5470000E+03  .6179000E+03  .8000000E+03  .9000000E+03  .1000000E+04
  .1200000E+04  .3000000E+03  .4500000E+03  .6250000E+03  .7000000E+03
  .7500000E+03  .8000000E+03  .1062000E+01  .1062000E+01  .1062000E+01
  .1062000E+01  .1062000E+01  .1062000E+01  .1068090E+01  .1068090E+01
  .1068090E+01  .1068090E+01  .1068090E+01  .1068090E+01  .1072500E+01
  .1072500E+01  .1072500E+01  .1072500E+01  .1072500E+01  .1072500E+01
  .1071700E+01  .1071700E+01  .1071700E+01  .1071700E+01  .1071700E+01
  .1071700E+01  .1070510E+01  .1070510E+01  .1070510E+01  .1070510E+01
  .1070510E+01  .1070510E+01  .1068410E+01  .1068410E+01  .1068410E+01
  .1068410E+01  .1068410E+01  .1068410E+01
*
**************  Assembly Disc. Factor Table - S
*
  .5470000E+03  .6179000E+03  .8000000E+03  .9000000E+03  .1000000E+04
  .1200000E+04  .3000000E+03  .4500000E+03  .6250000E+03  .7000000E+03
  .7500000E+03  .8000000E+03  .1062000E+01  .1062000E+01  .1062000E+01
  .1062000E+01  .1062000E+01  .1062000E+01  .1068090E+01  .1068090E+01
  .1068090E+01  .1068090E+01  .1068090E+01  .1068090E+01  .1072500E+01
  .1072500E+01  .1072500E+01  .1072500E+01  .1072500E+01  .1072500E+01
  .1071700E+01  .1071700E+01  .1071700E+01  .1071700E+01  .1071700E+01
  .1071700E+01  .1070510E+01  .1070510E+01  .1070510E+01  .1070510E+01
  .1070510E+01  .1070510E+01  .1068410E+01  .1068410E+01  .1068410E+01
  .1068410E+01  .1068410E+01  .1068410E+01
*
**************  Detector Flux Ratio Table
*
  .5470000E+03  .6179000E+03  .8000000E+03  .9000000E+03  .1000000E+04
  .1200000E+04  .3000000E+03  .4500000E+03  .6250000E+03  .7000000E+03
  .7500000E+03  .8000000E+03  .0000000E+00  .0000000E+00  .0000000E+00
  .0000000E+00  .0000000E+00  .0000000E+00  .0000000E+00  .0000000E+00
  .0000000E+00  .0000000E+00  .0000000E+00  .0000000E+00  .0000000E+00
  .0000000E+00  .0000000E+00  .0000000E+00  .0000000E+00  .0000000E+00
  .0000000E+00  .0000000E+00  .0000000E+00  .0000000E+00  .0000000E+00
  .0000000E+00  .0000000E+00  .0000000E+00  .0000000E+00  .0000000E+00
  .0000000E+00  .0000000E+00  .0000000E+00  .0000000E+00  .0000000E+00
  .0000000E+00  .0000000E+00  .0000000E+00
*
**************  Detector Microscopic X-Section Table
*
  .5470000E+03  .6179000E+03  .8000000E+03  .9000000E+03  .1000000E+04
  .1200000E+04  .3000000E+03  .4500000E+03  .6250000E+03  .7000000E+03
  .7500000E+03  .8000000E+03  .0000000E+00  .0000000E+00  .0000000E+00
  .0000000E+00  .0000000E+00  .0000000E+00  .0000000E+00  .0000000E+00
  .0000000E+00  .0000000E+00  .0000000E+00  .0000000E+00  .0000000E+00
  .0000000E+00  .0000000E+00  .0000000E+00  .0000000E+00  .0000000E+00
  .0000000E+00  .0000000E+00  .0000000E+00  .0000000E+00  .0000000E+00
  .0000000E+00  .0000000E+00  .0000000E+00  .0000000E+00  .0000000E+00
  .0000000E+00  .0000000E+00  .0000000E+00
*
**************  Effective Delayed Neutron Yield in 6 Groups
*
  .2069000E-03  .1277400E-02  .1155500E-02  .2484000E-02  .8998300E-03  .2179300E-03
*
**************  Decay Constants for Delayed Neutron Groups
*
  .1277200E-01  .3167600E-01  .1212400E+00  .3214200E+00  .1400700E+01  .3877600E+01
*
**************  Inv. Neutron Velocities
```

```
*
  .5550700E-07  .2379000E-05
*
*
*******           X-Section set #        2
    2
*
*      Group No.  1
*
***************  Diffusion Coefficient Table
*
  .5470000E+03  .6179000E+03  .8000000E+03  .9000000E+03  .1000000E+04
  .1200000E+04  .3000000E+03  .4500000E+03  .6250000E+03  .7000000E+03
  .7500000E+03  .8000000E+03  .1905690E+01  .1913880E+01  .1930090E+01
  .1937290E+01  .1938770E+01  .1941530E+01  .1712700E+01  .1716620E+01
  .1724580E+01  .1728200E+01  .1729450E+01  .1731770E+01  .1520180E+01
  .1521260E+01  .1523740E+01  .1524950E+01  .1525980E+01  .1527880E+01
  .1447140E+01  .1447800E+01  .1449410E+01  .1450240E+01  .1451190E+01
  .1452950E+01  .1402290E+01  .1402910E+01  .1404440E+01  .1405240E+01
  .1406140E+01  .1407820E+01  .1360140E+01  .1360740E+01  .1362200E+01
  .1362950E+01  .1363810E+01  .1365410E+01
*
***************  Absorption X-Section Table
*
  .5470000E+03  .6179000E+03  .8000000E+03  .9000000E+03  .1000000E+04
  .1200000E+04  .3000000E+03  .4500000E+03  .6250000E+03  .7000000E+03
  .7500000E+03  .8000000E+03  .9063771E-02  .9098311E-02  .9179250E-02
  .9219901E-02  .9259071E-02  .9331911E-02  .9921911E-02  .9960520E-02
  .1005072E-01  .1009593E-01  .1013899E-01  .1021908E-01  .1063514E-01
  .1067808E-01  .1077823E-01  .1082837E-01  .1087582E-01  .1096406E-01
  .1088441E-01  .1092905E-01  .1103312E-01  .1108523E-01  .1113450E-01
  .1122612E-01  .1103505E-01  .1108074E-01  .1118727E-01  .1124061E-01
  .1129106E-01  .1138489E-01  .1118104E-01  .1122774E-01  .1133668E-01
  .1139123E-01  .1144291E-01  .1153902E-01
*
***************  Fission X-Section Table
*
  .5470000E+03  .6179000E+03  .8000000E+03  .9000000E+03  .1000000E+04
  .1200000E+04  .3000000E+03  .4500000E+03  .6250000E+03  .7000000E+03
  .7500000E+03  .8000000E+03  .1875682E-02  .1853210E-02  .1809055E-02
  .1789591E-02  .1786351E-02  .1780327E-02  .1968901E-02  .1958099E-02
  .1936287E-02  .1926444E-02  .1923370E-02  .1917646E-02  .2045337E-02
  .2042162E-02  .2034961E-02  .2031417E-02  .2028434E-02  .2022882E-02
  .2077797E-02  .2075714E-02  .2070593E-02  .2067942E-02  .2064959E-02
  .2059409E-02  .2100294E-02  .2098211E-02  .2093095E-02  .2090449E-02
  .2087446E-02  .2081877E-02  .2122954E-02  .2120871E-02  .2115734E-02
  .2113083E-02  .2110075E-02  .2104478E-02
*
```

Appendix C

Uncertainty of output parameters

The average and standard deviation values are displayed in this appendix for the lattice physics code responses (collapsed and homogenized cross sections). The output parameters are shown for all feedback parameter combinations. The information in this appendix is summarized in Table C.1.

Segment	C. Rods	Average	Std. Deviation
1	0	Table C.2	Table C.17
2	0	Table C.3	Table C.18
3	0	Table C.4	Table C.19
10	0	Table C.5	Table C.20
	1	Table C.6	Table C.21
11	0	Table C.7	Table C.22
	1	Table C.8	Table C.23
12	0	Table C.9	Table C.24
	1	Table C.10	Table C.25
13	0	Table C.11	Table C.26
	1	Table C.12	Table C.27
14	0	Table C.13	Table C.28
	1	Table C.14	Table C.29
15	0	Table C.15	Table C.30
	1	Table C.16	Table C.31

Table C.1 – Summary table.

	$\mathbf{D_{mod}}$	$\mathbf{T_{fuel}}$ **(K)**						
	(kg/m^3)	293.0	660.8	853.5	1028.6	1396.5	1764.3	2132.2
	0.0381			1.951	1.951	1.951	1.951	1.951
	0.1775			1.946	1.946	1.946	1.947	1.947
	0.4563			1.937	1.937	1.937	1.938	1.938
D_{f1}	0.7351	1.926	1.927	1.927	1.927	1.927	1.928	1.928
	0.8403	1.891	1.892	1.892				
	0.9428	1.847	1.848	1.848				
	0.9983	1.813	1.814	1.814				
	0.0381			2.603E-1	2.603E-1	2.603E-1	2.603E-1	2.603E-1
	0.1775			2.604E-1	2.604E-1	2.604E-1	2.604E-1	2.604E-1
	0.4563			2.604E-1	2.604E-1	2.604E-1	2.604E-1	2.604E-1
D_{f2}	0.7351	2.605E-1	2.605E-1	2.605E-1	2.605E-1	2.605E-1	2.605E-1	2.605E-1
	0.8403	2.606E-1	2.606E-1	2.606E-1				
	0.9428	2.608E-1	2.608E-1	2.608E-1				
	0.9983	2.608E-1	2.608E-1	2.608E-1				
	0.0381			3.880E-4	3.879E-4	3.877E-4	3.876E-4	3.875E-4
	0.1775			3.877E-4	3.876E-4	3.874E-4	3.873E-4	3.872E-4
	0.4563			3.870E-4	3.868E-4	3.867E-4	3.865E-4	3.864E-4
Σ_{a1}	0.7351	3.865E-4	3.861E-4	3.860E-4	3.859E-4	3.857E-4	3.855E-4	3.854E-4
	0.8403	3.823E-4	3.819E-4	3.817E-4				
	0.9428	3.759E-4	3.754E-4	3.752E-4				
	0.9983	3.702E-4	3.696E-4	3.695E-4				
	0.0381			1.024E-2	1.024E-2	1.024E-2	1.024E-2	1.024E-2
	0.1775			1.024E-2	1.024E-2	1.024E-2	1.024E-2	1.024E-2
	0.4563			1.023E-2	1.023E-2	1.023E-2	1.023E-2	1.023E-2
Σ_{a2}	0.7351	1.023E-2	1.023E-2	1.023E-2	1.023E-2	1.023E-2	1.023E-2	1.023E-2
	0.8403	1.023E-2	1.023E-2	1.023E-2				
	0.9428	1.022E-2	1.022E-2	1.022E-2				
	0.9983	1.022E-2	1.022E-2	1.022E-2				
	0.0381			4.473E-2	4.470E-2	4.467E-2	4.465E-2	4.463E-2
	0.1775			4.478E-2	4.476E-2	4.473E-2	4.470E-2	4.468E-2
	0.4563			4.486E-2	4.483E-2	4.480E-2	4.477E-2	4.475E-2
Σ_{12}	0.7351	4.501E-2	4.494E-2	4.492E-2	4.489E-2	4.486E-2	4.483E-2	4.480E-2
	0.8403	4.507E-2	4.498E-2	4.496E-2				
	0.9428	4.490E-2	4.480E-2	4.477E-2				
	0.9983	4.462E-2	4.453E-2	4.450E-2				

Table C.2 – Average statistics for segment 1 and control rods withdrawn.

	$\mathbf{D_{mod}}$	$\mathbf{T_{fuel}}$ **(K)**						
	(kg/m^3)	293.0	660.8	853.5	1028.6	1396.5	1764.3	2132.2
$\boldsymbol{D_{f1}}$	0.0381			2.046	2.046	2.046	2.046	2.046
	0.1775			2.043	2.043	2.044	2.044	2.044
	0.4563			2.038	2.038	2.039	2.039	2.039
	0.7351	2.032	2.033	2.033	2.033	2.033	2.034	2.034
	0.8403	2.014	2.014	2.014				
	0.9428	1.989	1.990	1.990				
	0.9983	1.971	1.971	1.972				
$\boldsymbol{D_{f2}}$	0.0381			4.685E-1	4.685E-1	4.685E-1	4.685E-1	4.685E-1
	0.1775			4.687E-1	4.687E-1	4.687E-1	4.687E-1	4.687E-1
	0.4563			4.689E-1	4.689E-1	4.689E-1	4.689E-1	4.689E-1
	0.7351	4.691E-1	4.690E-1	4.690E-1	4.690E-1	4.690E-1	4.690E-1	4.690E-1
	0.8403	4.691E-1	4.690E-1	4.690E-1				
	0.9428	4.690E-1	4.689E-1	4.689E-1				
	0.9983	4.688E-1	4.688E-1	4.688E-1				
$\boldsymbol{\Sigma_{a1}}$	0.0381			1.112E-3	1.112E-3	1.112E-3	1.112E-3	1.112E-3
	0.1775			1.111E-3	1.111E-3	1.111E-3	1.111E-3	1.111E-3
	0.4563			1.109E-3	1.108E-3	1.108E-3	1.108E-3	1.108E-3
	0.7351	1.106E-3	1.106E-3	1.106E-3	1.106E-3	1.105E-3	1.105E-3	1.105E-3
	0.8403	1.095E-3	1.094E-3	1.094E-3				
	0.9428	1.080E-3	1.079E-3	1.079E-3				
	0.9983	1.068E-3	1.067E-3	1.067E-3				
$\boldsymbol{\Sigma_{a2}}$	0.0381			1.332E-2	1.332E-2	1.332E-2	1.332E-2	1.332E-2
	0.1775			1.330E-2	1.330E-2	1.330E-2	1.330E-2	1.330E-2
	0.4563			1.329E-2	1.330E-2	1.330E-2	1.330E-2	1.330E-2
	0.7351	1.330E-2	1.330E-2	1.330E-2	1.331E-2	1.331E-2	1.331E-2	1.331E-2
	0.8403	1.339E-2	1.339E-2	1.339E-2				
	0.9428	1.349E-2	1.350E-2	1.350E-2				
	0.9983	1.357E-2	1.357E-2	1.357E-2				
$\boldsymbol{\Sigma_{12}}$	0.0381			2.286E-2	2.285E-2	2.283E-2	2.282E-2	2.281E-2
	0.1775			2.287E-2	2.286E-2	2.285E-2	2.283E-2	2.282E-2
	0.4563			2.289E-2	2.288E-2	2.286E-2	2.285E-2	2.283E-2
	0.7351	2.294E-2	2.290E-2	2.289E-2	2.288E-2	2.286E-2	2.285E-2	2.284E-2
	0.8403	2.288E-2	2.284E-2	2.282E-2				
	0.9428	2.267E-2	2.262E-2	2.261E-2				
	0.9983	2.244E-2	2.239E-2	2.238E-2				

Table C.3 – Average statistics for segment 2 and control rods withdrawn.

	$\mathbf{D_{mod}}$	$\mathbf{T_{fuel}}$ **(K)**						
	(kg/m^3)	293.0	660.8	853.5	1028.6	1396.5	1764.3	2132.2
	0.0381			1.397	1.397	1.397	1.397	1.397
	0.1775			1.394	1.394	1.394	1.394	1.395
	0.4563			1.389	1.389	1.389	1.389	1.389
D_{f1}	0.7351	1.382	1.383	1.383	1.383	1.383	1.383	1.383
	0.8403	1.361	1.361	1.362				
	0.9428	1.335	1.335	1.335				
	0.9983	1.315	1.316	1.316				
	0.0381			3.068E-1	3.068E-1	3.068E-1	3.068E-1	3.068E-1
	0.1775			3.070E-1	3.070E-1	3.070E-1	3.070E-1	3.069E-1
	0.4563			3.071E-1	3.071E-1	3.071E-1	3.071E-1	3.071E-1
D_{f2}	0.7351	3.072E-1	3.071E-1	3.071E-1	3.071E-1	3.071E-1	3.071E-1	3.071E-1
	0.8403	3.067E-1	3.066E-1	3.066E-1				
	0.9428	3.059E-1	3.059E-1	3.059E-1				
	0.9983	3.053E-1	3.052E-1	3.052E-1				
	0.0381			1.817E-3	1.816E-3	1.816E-3	1.815E-3	1.814E-3
	0.1775			1.819E-3	1.818E-3	1.817E-3	1.817E-3	1.816E-3
	0.4563			1.822E-3	1.821E-3	1.820E-3	1.820E-3	1.819E-3
Σ_{a1}	0.7351	1.827E-3	1.825E-3	1.825E-3	1.824E-3	1.823E-3	1.823E-3	1.822E-3
	0.8403	1.835E-3	1.833E-3	1.832E-3				
	0.9428	1.837E-3	1.834E-3	1.833E-3				
	0.9983	1.832E-3	1.829E-3	1.828E-3				
	0.0381			3.792E-2	3.792E-2	3.792E-2	3.792E-2	3.792E-2
	0.1775			3.791E-2	3.791E-2	3.791E-2	3.791E-2	3.791E-2
	0.4563			3.792E-2	3.792E-2	3.792E-2	3.792E-2	3.792E-2
Σ_{a2}	0.7351	3.794E-2	3.794E-2	3.795E-2	3.795E-2	3.795E-2	3.795E-2	3.795E-2
	0.8403	3.812E-2	3.812E-2	3.812E-2				
	0.9428	3.832E-2	3.833E-2	3.833E-2				
	0.9983	3.847E-2	3.848E-2	3.848E-2				
	0.0381			2.970E-2	2.969E-2	2.966E-2	2.964E-2	2.963E-2
	0.1775			2.973E-2	2.972E-2	2.969E-2	2.967E-2	2.965E-2
	0.4563			2.977E-2	2.976E-2	2.973E-2	2.971E-2	2.969E-2
Σ_{12}	0.7351	2.987E-2	2.982E-2	2.980E-2	2.978E-2	2.976E-2	2.974E-2	2.972E-2
	0.8403	2.987E-2	2.980E-2	2.979E-2				
	0.9428	2.966E-2	2.959E-2	2.957E-2				
	0.9983	2.939E-2	2.931E-2	2.929E-2				

Table C.4 – Average statistics for segment 3 and control rods withdrawn.

	$\mathbf{D_{mod}}$			$\mathbf{T_{fuel}}$ **(K)**				
	(kg/m^3)	293.0	660.8	853.5	1028.6	1396.5	1764.3	2132.2
	0.0381			1.396	1.396	1.396	1.396	1.397
	0.1775			1.426	1.426	1.426	1.426	1.427
	0.4563			1.485	1.485	1.485	1.485	1.486
D_{f1}	0.7351	1.550	1.551	1.551	1.551	1.552	1.552	1.552
	0.8403	1.761	1.762	1.762				
	0.9428	2.042	2.043	2.043				
	0.9983	2.220	2.220	2.220				
	0.0381			2.694E-1	2.697E-1	2.705E-1	2.712E-1	2.720E-1
	0.1775			2.922E-1	2.925E-1	2.931E-1	2.938E-1	2.945E-1
	0.4563			3.252E-1	3.254E-1	3.261E-1	3.267E-1	3.274E-1
D_{f2}	0.7351	3.577E-1	3.584E-1	3.588E-1	3.591E-1	3.598E-1	3.604E-1	3.611E-1
	0.8403	4.545E-1	4.557E-1	4.563E-1				
	0.9428	6.202E-1	6.226E-1	6.239E-1				
	0.9983	7.557E-1	7.603E-1	7.626E-1				
	0.0381			6.049E-3	6.111E-3	6.238E-3	6.353E-3	6.458E-3
	0.1775			6.005E-3	6.066E-3	6.192E-3	6.306E-3	6.409E-3
	0.4563			5.923E-3	5.983E-3	6.105E-3	6.216E-3	6.317E-3
Σ_{a1}	0.7351	5.544E-3	5.741E-3	5.827E-3	5.886E-3	6.004E-3	6.112E-3	6.210E-3
	0.8403	5.232E-3	5.411E-3	5.489E-3				
	0.9428	4.665E-3	4.812E-3	4.874E-3				
	0.9983	4.118E-3	4.238E-3	4.288E-3				
	0.0381			3.594E-2	3.582E-2	3.555E-2	3.530E-2	3.505E-2
	0.1775			3.246E-2	3.237E-2	3.217E-2	3.197E-2	3.178E-2
	0.4563			2.937E-2	2.930E-2	2.913E-2	2.897E-2	2.882E-2
Σ_{a2}	0.7351	2.767E-2	2.749E-2	2.740E-2	2.734E-2	2.719E-2	2.705E-2	2.691E-2
	0.8403	2.577E-2	2.557E-2	2.547E-2				
	0.9428	2.365E-2	2.341E-2	2.328E-2				
	0.9983	2.234E-2	2.205E-2	2.190E-2				
	0.0381			2.770E-3	2.770E-3	2.769E-3	2.769E-3	2.769E-3
	0.1775			2.748E-3	2.748E-3	2.748E-3	2.747E-3	2.747E-3
	0.4563			2.704E-3	2.704E-3	2.704E-3	2.704E-3	2.704E-3
$\nu\Sigma_{f1}$	0.7351	2.656E-3	2.656E-3	2.656E-3	2.655E-3	2.655E-3	2.655E-3	2.655E-3
	0.8403	2.497E-3	2.496E-3	2.496E-3				
	0.9428	2.256E-3	2.256E-3	2.255E-3				
	0.9983	2.064E-3	2.062E-3	2.062E-3				
	0.0381			3.399E-2	3.385E-2	3.351E-2	3.319E-2	3.289E-2
	0.1775			3.067E-2	3.056E-2	3.030E-2	3.006E-2	2.982E-2
	0.4563			2.799E-2	2.791E-2	2.770E-2	2.750E-2	2.731E-2
$\nu\Sigma_{f2}$	0.7351	2.683E-2	2.660E-2	2.649E-2	2.641E-2	2.623E-2	2.605E-2	2.588E-2
	0.8403	2.640E-2	2.615E-2	2.602E-2				
	0.9428	2.564E-2	2.533E-2	2.517E-2				
	0.9983	2.490E-2	2.452E-2	2.433E-2				
	0.0381			2.628E-2	2.624E-2	2.618E-2	2.613E-2	2.609E-2
	0.1775			2.519E-2	2.516E-2	2.511E-2	2.506E-2	2.503E-2
	0.4563			2.315E-2	2.312E-2	2.307E-2	2.303E-2	2.301E-2
Σ_{12}	0.7351	2.117E-2	2.107E-2	2.103E-2	2.100E-2	2.096E-2	2.093E-2	2.091E-2
	0.8403	1.540E-2	1.531E-2	1.528E-2				
	0.9428	9.731E-3	9.668E-3	9.647E-3				
	0.9983	7.025E-3	6.983E-3	6.971E-3				

Table C.5 – Average statistics for segment 10 and control rods withdrawn.

	$\mathbf{D_{mod}}$	$\mathbf{T_{fuel}}$ **(K)**						
	(kg/m^3)	293.0	660.8	853.5	1028.6	1396.5	1764.3	2132.2
	0.0381			1.371	1.371	1.371	1.371	1.371
	0.1775			1.399	1.399	1.400	1.400	1.400
	0.4563			1.456	1.456	1.456	1.457	1.457
D_{f1}	0.7351	1.518	1.519	1.519	1.519	1.520	1.520	1.520
	0.8403	1.718	1.718	1.718				
	0.9428	1.979	1.980	1.980				
	0.9983	2.143	2.143	2.143				
	0.0381			2.691E-1	2.694E-1	2.702E-1	2.710E-1	2.718E-1
	0.1775			2.928E-1	2.931E-1	2.938E-1	2.945E-1	2.951E-1
	0.4563			3.271E-1	3.273E-1	3.280E-1	3.286E-1	3.293E-1
D_{f2}	0.7351	3.610E-1	3.617E-1	3.621E-1	3.624E-1	3.630E-1	3.637E-1	3.643E-1
	0.8403	4.626E-1	4.636E-1	4.642E-1				
	0.9428	6.307E-1	6.327E-1	6.338E-1				
	0.9983	7.576E-1	7.612E-1	7.630E-1				
	0.0381			8.532E-3	8.591E-3	8.711E-3	8.820E-3	8.919E-3
	0.1775			8.491E-3	8.549E-3	8.667E-3	8.775E-3	8.872E-3
	0.4563			8.417E-3	8.473E-3	8.588E-3	8.692E-3	8.786E-3
Σ_{a1}	0.7351	8.061E-3	8.245E-3	8.325E-3	8.380E-3	8.490E-3	8.590E-3	8.681E-3
	0.8403	7.710E-3	7.872E-3	7.941E-3				
	0.9428	6.914E-3	7.037E-3	7.089E-3				
	0.9983	6.086E-3	6.180E-3	6.218E-3				
	0.0381			4.502E-2	4.490E-2	4.461E-2	4.434E-2	4.408E-2
	0.1775			4.149E-2	4.140E-2	4.118E-2	4.097E-2	4.077E-2
	0.4563			3.844E-2	3.837E-2	3.819E-2	3.803E-2	3.787E-2
Σ_{a2}	0.7351	3.688E-2	3.669E-2	3.659E-2	3.653E-2	3.637E-2	3.623E-2	3.608E-2
	0.8403	3.541E-2	3.520E-2	3.510E-2				
	0.9428	3.404E-2	3.381E-2	3.369E-2				
	0.9983	3.355E-2	3.330E-2	3.317E-2				
	0.0381			2.746E-3	2.745E-3	2.745E-3	2.745E-3	2.744E-3
	0.1775			2.721E-3	2.721E-3	2.721E-3	2.720E-3	2.720E-3
	0.4563			2.672E-3	2.672E-3	2.672E-3	2.671E-3	2.671E-3
$\nu\Sigma_{f1}$	0.7351	2.617E-3	2.617E-3	2.617E-3	2.617E-3	2.616E-3	2.616E-3	2.616E-3
	0.8403	2.434E-3	2.433E-3	2.433E-3				
	0.9428	2.144E-3	2.143E-3	2.142E-3				
	0.9983	1.900E-3	1.898E-3	1.897E-3				
	0.0381			3.561E-2	3.546E-2	3.510E-2	3.477E-2	3.445E-2
	0.1775			3.205E-2	3.194E-2	3.167E-2	3.141E-2	3.116E-2
	0.4563			2.912E-2	2.903E-2	2.882E-2	2.861E-2	2.841E-2
$\nu\Sigma_{f2}$	0.7351	2.777E-2	2.754E-2	2.742E-2	2.734E-2	2.715E-2	2.697E-2	2.679E-2
	0.8403	2.682E-2	2.657E-2	2.644E-2				
	0.9428	2.522E-2	2.492E-2	2.477E-2				
	0.9983	2.391E-2	2.357E-2	2.339E-2				
	0.0381			2.345E-2	2.342E-2	2.336E-2	2.331E-2	2.327E-2
	0.1775			2.235E-2	2.232E-2	2.227E-2	2.222E-2	2.218E-2
	0.4563			2.026E-2	2.024E-2	2.019E-2	2.015E-2	2.012E-2
Σ_{12}	0.7351	1.824E-2	1.815E-2	1.811E-2	1.808E-2	1.804E-2	1.801E-2	1.798E-2
	0.8403	1.244E-2	1.237E-2	1.234E-2				
	0.9428	6.916E-3	6.865E-3	6.847E-3				
	0.9983	4.428E-3	4.397E-3	4.387E-3				

Table C.6 – Average statistics for segment 10 and control rods inserted.

	$\mathbf{D_{mod}}$	$\mathbf{T_{fuel}}$ **(K)**						
	(kg/m^3)	293.0	660.8	853.5	1028.6	1396.5	1764.3	2132.2
	0.0381			1.402	1.402	1.402	1.402	1.403
	0.1775			1.432	1.432	1.432	1.433	1.433
	0.4563			1.491	1.491	1.492	1.492	1.492
D_{f1}	0.7351	1.558	1.558	1.558	1.558	1.559	1.559	1.559
	0.8403	1.771	1.771	1.772				
	0.9428	2.056	2.057	2.057				
	0.9983	2.239	2.239	2.239				
	0.0381			2.771E-1	2.773E-1	2.776E-1	2.780E-1	2.784E-1
	0.1775			2.955E-1	2.956E-1	2.960E-1	2.963E-1	2.967E-1
	0.4563			3.238E-1	3.239E-1	3.242E-1	3.246E-1	3.249E-1
D_{f2}	0.7351	3.527E-1	3.530E-1	3.532E-1	3.534E-1	3.537E-1	3.541E-1	3.544E-1
	0.8403	4.391E-1	4.396E-1	4.399E-1				
	0.9428	5.764E-1	5.773E-1	5.778E-1				
	0.9983	6.775E-1	6.790E-1	6.798E-1				
	0.0381			7.439E-3	7.499E-3	7.623E-3	7.735E-3	7.835E-3
	0.1775			7.390E-3	7.450E-3	7.572E-3	7.682E-3	7.781E-3
	0.4563			7.294E-3	7.352E-3	7.471E-3	7.578E-3	7.675E-3
Σ_{a1}	0.7351	6.900E-3	7.096E-3	7.181E-3	7.237E-3	7.352E-3	7.456E-3	7.550E-3
	0.8403	6.514E-3	6.691E-3	6.767E-3				
	0.9428	5.808E-3	5.951E-3	6.011E-3				
	0.9983	5.136E-3	5.252E-3	5.300E-3				
	0.0381			6.732E-2	6.719E-2	6.688E-2	6.658E-2	6.629E-2
	0.1775			6.320E-2	6.309E-2	6.284E-2	6.259E-2	6.235E-2
	0.4563			5.927E-2	5.919E-2	5.897E-2	5.876E-2	5.856E-2
Σ_{a2}	0.7351	5.707E-2	5.684E-2	5.672E-2	5.664E-2	5.644E-2	5.625E-2	5.606E-2
	0.8403	5.460E-2	5.437E-2	5.424E-2				
	0.9428	5.180E-2	5.155E-2	5.142E-2				
	0.9983	5.029E-2	5.003E-2	4.989E-2				
	0.0381			5.071E-3	5.070E-3	5.069E-3	5.067E-3	5.065E-3
	0.1775			5.046E-3	5.045E-3	5.043E-3	5.041E-3	5.039E-3
	0.4563			4.990E-3	4.989E-3	4.987E-3	4.985E-3	4.983E-3
$\nu\Sigma_{f1}$	0.7351	4.926E-3	4.926E-3	4.925E-3	4.924E-3	4.922E-3	4.919E-3	4.917E-3
	0.8403	4.692E-3	4.690E-3	4.688E-3				
	0.9428	4.297E-3	4.293E-3	4.290E-3				
	0.9983	3.950E-3	3.944E-3	3.941E-3				
	0.0381			8.668E-2	8.645E-2	8.592E-2	8.540E-2	8.490E-2
	0.1775			8.060E-2	8.042E-2	7.998E-2	7.956E-2	7.915E-2
	0.4563			7.521E-2	7.506E-2	7.470E-2	7.434E-2	7.400E-2
$\nu\Sigma_{f2}$	0.7351	7.255E-2	7.216E-2	7.196E-2	7.182E-2	7.150E-2	7.118E-2	7.086E-2
	0.8403	7.042E-2	7.002E-2	6.981E-2				
	0.9428	6.744E-2	6.703E-2	6.681E-2				
	0.9983	6.547E-2	6.505E-2	6.483E-2				
	0.0381			2.519E-2	2.516E-2	2.510E-2	2.504E-2	2.500E-2
	0.1775			2.412E-2	2.408E-2	2.402E-2	2.397E-2	2.393E-2
	0.4563			2.208E-2	2.205E-2	2.199E-2	2.194E-2	2.190E-2
Σ_{12}	0.7351	2.012E-2	2.001E-2	1.997E-2	1.994E-2	1.988E-2	1.984E-2	1.981E-2
	0.8403	1.443E-2	1.434E-2	1.430E-2				
	0.9428	8.909E-3	8.842E-3	8.818E-3				
	0.9983	6.328E-3	6.281E-3	6.265E-3				

Table C.7 – Average statistics for segment 11 and control rods withdrawn.

	$\mathbf{D_{mod}}$	$\mathbf{T_{fuel}}$ **(K)**						
	(kg/m^3)	293.0	660.8	853.5	1028.6	1396.5	1764.3	2132.2
	0.0381			1.377	1.377	1.377	1.377	1.377
	0.1775			1.405	1.406	1.406	1.406	1.406
	0.4563			1.462	1.462	1.463	1.463	1.463
D_{f1}	0.7351	1.525	1.526	1.526	1.526	1.527	1.527	1.527
	0.8403	1.727	1.728	1.728				
	0.9428	1.993	1.994	1.994				
	0.9983	2.162	2.162	2.162				
	0.0381			2.767E-1	2.768E-1	2.772E-1	2.775E-1	2.779E-1
	0.1775			2.957E-1	2.958E-1	2.962E-1	2.965E-1	2.969E-1
	0.4563			3.252E-1	3.253E-1	3.256E-1	3.259E-1	3.263E-1
D_{f2}	0.7351	3.554E-1	3.557E-1	3.559E-1	3.560E-1	3.564E-1	3.567E-1	3.571E-1
	0.8403	4.461E-1	4.465E-1	4.467E-1				
	0.9428	5.838E-1	5.845E-1	5.849E-1				
	0.9983	6.759E-1	6.772E-1	6.778E-1				
	0.0381			9.834E-3	9.892E-3	1.001E-2	1.011E-2	1.021E-2
	0.1775			9.786E-3	9.842E-3	9.957E-3	1.006E-2	1.015E-2
	0.4563			9.690E-3	9.745E-3	9.856E-3	9.957E-3	1.005E-2
Σ_{a1}	0.7351	9.309E-3	9.491E-3	9.570E-3	9.622E-3	9.729E-3	9.825E-3	9.912E-3
	0.8403	8.835E-3	8.994E-3	9.062E-3				
	0.9428	7.806E-3	7.925E-3	7.974E-3				
	0.9983	6.782E-3	6.871E-3	6.908E-3				
	0.0381			8.138E-2	8.124E-2	8.090E-2	8.057E-2	8.025E-2
	0.1775			7.688E-2	7.676E-2	7.648E-2	7.621E-2	7.594E-2
	0.4563			7.255E-2	7.245E-2	7.222E-2	7.198E-2	7.176E-2
Σ_{a2}	0.7351	7.006E-2	6.980E-2	6.967E-2	6.958E-2	6.936E-2	6.915E-2	6.894E-2
	0.8403	6.670E-2	6.644E-2	6.630E-2				
	0.9428	6.234E-2	6.208E-2	6.193E-2				
	0.9983	6.004E-2	5.978E-2	5.964E-2				
	0.0381			5.024E-3	5.023E-3	5.021E-3	5.019E-3	5.017E-3
	0.1775			4.992E-3	4.991E-3	4.989E-3	4.987E-3	4.984E-3
	0.4563			4.922E-3	4.921E-3	4.918E-3	4.916E-3	4.914E-3
$\nu\Sigma_{f1}$	0.7351	4.842E-3	4.841E-3	4.840E-3	4.838E-3	4.836E-3	4.833E-3	4.831E-3
	0.8403	4.543E-3	4.540E-3	4.538E-3				
	0.9428	4.016E-3	4.010E-3	4.007E-3				
	0.9983	3.537E-3	3.530E-3	3.527E-3				
	0.0381			9.340E-2	9.316E-2	9.259E-2	9.204E-2	9.151E-2
	0.1775			8.668E-2	8.648E-2	8.602E-2	8.557E-2	8.513E-2
	0.4563			8.052E-2	8.036E-2	7.997E-2	7.960E-2	7.923E-2
$\nu\Sigma_{f2}$	0.7351	7.723E-2	7.681E-2	7.660E-2	7.646E-2	7.611E-2	7.577E-2	7.544E-2
	0.8403	7.333E-2	7.291E-2	7.270E-2				
	0.9428	6.782E-2	6.741E-2	6.720E-2				
	0.9983	6.444E-2	6.404E-2	6.383E-2				
	0.0381			2.246E-2	2.243E-2	2.237E-2	2.232E-2	2.227E-2
	0.1775			2.136E-2	2.133E-2	2.128E-2	2.123E-2	2.118E-2
	0.4563			1.929E-2	1.926E-2	1.921E-2	1.917E-2	1.913E-2
Σ_{12}	0.7351	1.730E-2	1.720E-2	1.716E-2	1.713E-2	1.708E-2	1.704E-2	1.700E-2
	0.8403	1.162E-2	1.154E-2	1.151E-2				
	0.9428	6.318E-3	6.265E-3	6.245E-3				
	0.9983	4.008E-3	3.976E-3	3.964E-3				

Table C.8 – Average statistics for segment 11 and control rods inserted.

	$\mathbf{D_{mod}}$	$\mathbf{T_{fuel}}$ (K)						
	(kg/m^3)	293.0	660.8	853.5	1028.6	1396.5	1764.3	2132.2
	0.0381			1.402	1.402	1.403	1.403	1.403
	0.1775			1.432	1.432	1.433	1.433	1.433
	0.4563			1.492	1.492	1.492	1.492	1.493
D_{f1}	0.7351	1.558	1.559	1.559	1.559	1.559	1.560	1.560
	0.8403	1.772	1.772	1.773				
	0.9428	2.058	2.058	2.058				
	0.9983	2.241	2.241	2.241				
	0.0381			2.775E-1	2.776E-1	2.779E-1	2.782E-1	2.786E-1
	0.1775			2.954E-1	2.955E-1	2.958E-1	2.961E-1	2.964E-1
	0.4563			3.232E-1	3.233E-1	3.236E-1	3.239E-1	3.242E-1
D_{f2}	0.7351	3.518E-1	3.521E-1	3.523E-1	3.524E-1	3.527E-1	3.530E-1	3.533E-1
	0.8403	4.372E-1	4.376E-1	4.378E-1				
	0.9428	5.714E-1	5.722E-1	5.726E-1				
	0.9983	6.689E-1	6.702E-1	6.708E-1				
	0.0381			7.597E-3	7.658E-3	7.782E-3	7.893E-3	7.994E-3
	0.1775			7.547E-3	7.607E-3	7.729E-3	7.839E-3	7.938E-3
	0.4563			7.448E-3	7.506E-3	7.625E-3	7.732E-3	7.829E-3
Σ_{a1}	0.7351	7.050E-3	7.246E-3	7.331E-3	7.388E-3	7.503E-3	7.606E-3	7.699E-3
	0.8403	6.653E-3	6.830E-3	6.905E-3				
	0.9428	5.927E-3	6.071E-3	6.131E-3				
	0.9983	5.240E-3	5.356E-3	5.403E-3				
	0.0381			7.156E-2	7.143E-2	7.113E-2	7.084E-2	7.056E-2
	0.1775			6.750E-2	6.739E-2	6.715E-2	6.690E-2	6.666E-2
	0.4563			6.358E-2	6.349E-2	6.328E-2	6.307E-2	6.286E-2
Σ_{a2}	0.7351	6.134E-2	6.111E-2	6.099E-2	6.091E-2	6.072E-2	6.052E-2	6.033E-2
	0.8403	5.878E-2	5.855E-2	5.843E-2				
	0.9428	5.579E-2	5.555E-2	5.541E-2				
	0.9983	5.417E-2	5.392E-2	5.378E-2				
	0.0381			5.304E-3	5.303E-3	5.302E-3	5.300E-3	5.298E-3
	0.1775			5.278E-3	5.277E-3	5.275E-3	5.273E-3	5.271E-3
	0.4563			5.219E-3	5.218E-3	5.216E-3	5.214E-3	5.211E-3
$\nu\Sigma_{f1}$	0.7351	5.151E-3	5.151E-3	5.150E-3	5.149E-3	5.147E-3	5.145E-3	5.142E-3
	0.8403	4.905E-3	4.903E-3	4.901E-3				
	0.9428	4.489E-3	4.484E-3	4.482E-3				
	0.9983	4.122E-3	4.116E-3	4.113E-3				
	0.0381			9.033E-2	9.011E-2	8.958E-2	8.907E-2	8.858E-2
	0.1775			8.424E-2	8.406E-2	8.363E-2	8.321E-2	8.280E-2
	0.4563			7.875E-2	7.860E-2	7.824E-2	7.789E-2	7.755E-2
$\nu\Sigma_{f2}$	0.7351	7.597E-2	7.558E-2	7.537E-2	7.524E-2	7.492E-2	7.460E-2	7.428E-2
	0.8403	7.340E-2	7.300E-2	7.280E-2				
	0.9428	6.991E-2	6.952E-2	6.931E-2				
	0.9983	6.772E-2	6.732E-2	6.711E-2				
	0.0381			2.508E-2	2.504E-2	2.498E-2	2.492E-2	2.488E-2
	0.1775			2.400E-2	2.396E-2	2.390E-2	2.385E-2	2.381E-2
	0.4563			2.196E-2	2.193E-2	2.187E-2	2.182E-2	2.178E-2
Σ_{12}	0.7351	2.000E-2	1.989E-2	1.985E-2	1.982E-2	1.977E-2	1.972E-2	1.969E-2
	0.8403	1.433E-2	1.423E-2	1.420E-2				
	0.9428	8.822E-3	8.755E-3	8.730E-3				
	0.9983	6.256E-3	6.209E-3	6.193E-3				

Table C.9 – Average statistics for segment 12 and control rods withdrawn.

	$\mathbf{D_{mod}}$	$\mathbf{T_{fuel}}$ **(K)**						
	(kg/m^3)	293.0	660.8	853.5	1028.6	1396.5	1764.3	2132.2
	0.0381			1.376	1.376	1.376	1.377	1.377
	0.1775			1.405	1.405	1.405	1.406	1.406
	0.4563			1.462	1.462	1.462	1.463	1.463
D_{f1}	0.7351	1.525	1.526	1.526	1.526	1.526	1.527	1.527
	0.8403	1.727	1.728	1.728				
	0.9428	1.994	1.995	1.995				
	0.9983	2.163	2.163	2.164				
	0.0381			2.769E-1	2.770E-1	2.773E-1	2.777E-1	2.780E-1
	0.1775			2.955E-1	2.956E-1	2.959E-1	2.962E-1	2.965E-1
	0.4563			3.245E-1	3.246E-1	3.249E-1	3.252E-1	3.255E-1
D_{f2}	0.7351	3.544E-1	3.547E-1	3.548E-1	3.549E-1	3.552E-1	3.555E-1	3.558E-1
	0.8403	4.439E-1	4.442E-1	4.444E-1				
	0.9428	5.774E-1	5.779E-1	5.783E-1				
	0.9983	6.642E-1	6.652E-1	6.657E-1				
	0.0381			1.005E-2	1.011E-2	1.023E-2	1.033E-2	1.043E-2
	0.1775			9.997E-3	1.005E-2	1.017E-2	1.027E-2	1.037E-2
	0.4563			9.889E-3	9.943E-3	1.005E-2	1.015E-2	1.024E-2
Σ_{a1}	0.7351	9.492E-3	9.675E-3	9.753E-3	9.806E-3	9.913E-3	1.001E-2	1.009E-2
	0.8403	8.978E-3	9.137E-3	9.205E-3				
	0.9428	7.907E-3	8.026E-3	8.075E-3				
	0.9983	6.859E-3	6.948E-3	6.984E-3				
	0.0381			8.754E-2	8.740E-2	8.708E-2	8.676E-2	8.646E-2
	0.1775			8.314E-2	8.303E-2	8.276E-2	8.249E-2	8.224E-2
	0.4563			7.879E-2	7.869E-2	7.846E-2	7.824E-2	7.802E-2
Σ_{a2}	0.7351	7.620E-2	7.595E-2	7.582E-2	7.573E-2	7.552E-2	7.531E-2	7.511E-2
	0.8403	7.254E-2	7.229E-2	7.216E-2				
	0.9428	6.773E-2	6.748E-2	6.735E-2				
	0.9983	6.516E-2	6.492E-2	6.478E-2				
	0.0381			5.252E-3	5.251E-3	5.249E-3	5.247E-3	5.244E-3
	0.1775			5.218E-3	5.217E-3	5.215E-3	5.212E-3	5.210E-3
	0.4563			5.143E-3	5.142E-3	5.140E-3	5.138E-3	5.135E-3
$\nu\Sigma_{f1}$	0.7351	5.058E-3	5.057E-3	5.057E-3	5.055E-3	5.053E-3	5.050E-3	5.047E-3
	0.8403	4.744E-3	4.741E-3	4.739E-3				
	0.9428	4.189E-3	4.183E-3	4.180E-3				
	0.9983	3.685E-3	3.678E-3	3.674E-3				
	0.0381			9.724E-2	9.700E-2	9.644E-2	9.590E-2	9.538E-2
	0.1775			9.049E-2	9.029E-2	8.983E-2	8.939E-2	8.896E-2
	0.4563			8.415E-2	8.399E-2	8.360E-2	8.323E-2	8.287E-2
$\nu\Sigma_{f2}$	0.7351	8.062E-2	8.021E-2	8.000E-2	7.986E-2	7.951E-2	7.918E-2	7.885E-2
	0.8403	7.588E-2	7.548E-2	7.527E-2				
	0.9428	6.938E-2	6.899E-2	6.879E-2				
	0.9983	6.556E-2	6.520E-2	6.501E-2				
	0.0381			2.227E-2	2.224E-2	2.218E-2	2.213E-2	2.208E-2
	0.1775			2.118E-2	2.115E-2	2.109E-2	2.104E-2	2.100E-2
	0.4563			1.912E-2	1.909E-2	1.903E-2	1.899E-2	1.895E-2
Σ_{12}	0.7351	1.713E-2	1.703E-2	1.699E-2	1.697E-2	1.691E-2	1.687E-2	1.684E-2
	0.8403	1.150E-2	1.142E-2	1.138E-2				
	0.9428	6.240E-3	6.187E-3	6.167E-3				
	0.9983	3.957E-3	3.924E-3	3.913E-3				

Table C.10 – Average statistics for segment 12 and control rods inserted.

	$\mathbf{D_{mod}}$	$\mathbf{T_{fuel}}$ **(K)**						
	(kg/m^3)	293.0	660.8	853.5	1028.6	1396.5	1764.3	2132.2
	0.0381			1.393	1.393	1.393	1.393	1.393
	0.1775			1.422	1.422	1.423	1.423	1.423
	0.4563			1.481	1.481	1.481	1.482	1.482
D_{f1}	0.7351	1.546	1.547	1.547	1.547	1.547	1.548	1.548
	0.8403	1.756	1.757	1.757				
	0.9428	2.037	2.037	2.038				
	0.9983	2.217	2.217	2.217				
	0.0381			2.769E-1	2.770E-1	2.774E-1	2.778E-1	2.781E-1
	0.1775			2.951E-1	2.953E-1	2.956E-1	2.960E-1	2.963E-1
	0.4563			3.232E-1	3.234E-1	3.237E-1	3.241E-1	3.244E-1
D_{f2}	0.7351	3.520E-1	3.524E-1	3.525E-1	3.527E-1	3.530E-1	3.534E-1	3.537E-1
	0.8403	4.379E-1	4.384E-1	4.386E-1				
	0.9428	5.740E-1	5.749E-1	5.753E-1				
	0.9983	6.738E-1	6.753E-1	6.760E-1				
	0.0381			7.531E-3	7.601E-3	7.726E-3	7.838E-3	7.940E-3
	0.1775			7.482E-3	7.551E-3	7.674E-3	7.785E-3	7.885E-3
	0.4563			7.385E-3	7.452E-3	7.572E-3	7.680E-3	7.777E-3
Σ_{a1}	0.7351	6.996E-3	7.193E-3	7.270E-3	7.336E-3	7.452E-3	7.556E-3	7.650E-3
	0.8403	6.604E-3	6.783E-3	6.851E-3				
	0.9428	5.887E-3	6.032E-3	6.086E-3				
	0.9983	5.206E-3	5.324E-3	5.367E-3				
	0.0381			6.794E-2	6.778E-2	6.747E-2	6.717E-2	6.687E-2
	0.1775			6.380E-2	6.367E-2	6.341E-2	6.316E-2	6.292E-2
	0.4563			5.986E-2	5.975E-2	5.953E-2	5.931E-2	5.910E-2
Σ_{a2}	0.7351	5.763E-2	5.739E-2	5.728E-2	5.718E-2	5.698E-2	5.679E-2	5.659E-2
	0.8403	5.513E-2	5.489E-2	5.477E-2				
	0.9428	5.229E-2	5.203E-2	5.191E-2				
	0.9983	5.077E-2	5.050E-2	5.037E-2				
	0.0381			5.158E-3	5.157E-3	5.156E-3	5.154E-3	5.152E-3
	0.1775			5.132E-3	5.131E-3	5.130E-3	5.128E-3	5.125E-3
	0.4563			5.075E-3	5.074E-3	5.072E-3	5.070E-3	5.067E-3
$\nu\Sigma_{f1}$	0.7351	5.010E-3	5.009E-3	5.008E-3	5.007E-3	5.005E-3	5.003E-3	5.000E-3
	0.8403	4.770E-3	4.767E-3	4.766E-3				
	0.9428	4.365E-3	4.360E-3	4.358E-3				
	0.9983	4.010E-3	4.004E-3	4.001E-3				
	0.0381			8.780E-2	8.752E-2	8.698E-2	8.645E-2	8.595E-2
	0.1775			8.168E-2	8.146E-2	8.101E-2	8.058E-2	8.016E-2
	0.4563			7.624E-2	7.606E-2	7.569E-2	7.533E-2	7.498E-2
$\nu\Sigma_{f2}$	0.7351	7.354E-2	7.314E-2	7.296E-2	7.279E-2	7.246E-2	7.213E-2	7.181E-2
	0.8403	7.135E-2	7.094E-2	7.076E-2				
	0.9428	6.832E-2	6.790E-2	6.771E-2				
	0.9983	6.632E-2	6.590E-2	6.570E-2				
	0.0381			2.517E-2	2.513E-2	2.507E-2	2.502E-2	2.497E-2
	0.1775			2.409E-2	2.406E-2	2.400E-2	2.394E-2	2.390E-2
	0.4563			2.205E-2	2.202E-2	2.196E-2	2.191E-2	2.188E-2
Σ_{12}	0.7351	2.009E-2	1.998E-2	1.994E-2	1.991E-2	1.986E-2	1.981E-2	1.978E-2
	0.8403	1.441E-2	1.431E-2	1.428E-2				
	0.9428	8.888E-3	8.821E-3	8.798E-3				
	0.9983	6.311E-3	6.264E-3	6.249E-3				

Table C.11 – Average statistics for segment 13 and control rods withdrawn.

	$\mathbf{D_{mod}}$	$\mathbf{T_{fuel}}$ **(K)**						
	(kg/m^3)	293.0	660.8	853.5	1028.6	1396.5	1764.3	2132.2
	0.0381			1.368	1.368	1.368	1.368	1.369
	0.1775			1.396	1.396	1.397	1.397	1.397
	0.4563			1.452	1.452	1.453	1.453	1.453
D_{f1}	0.7351	1.515	1.515	1.515	1.516	1.516	1.516	1.516
	0.8403	1.714	1.714	1.714				
	0.9428	1.975	1.976	1.976				
	0.9983	2.141	2.141	2.141				
	0.0381			2.764E-1	2.765E-1	2.769E-1	2.773E-1	2.776E-1
	0.1775			2.953E-1	2.954E-1	2.958E-1	2.961E-1	2.965E-1
	0.4563			3.246E-1	3.247E-1	3.251E-1	3.254E-1	3.257E-1
D_{f2}	0.7351	3.547E-1	3.550E-1	3.552E-1	3.553E-1	3.556E-1	3.560E-1	3.563E-1
	0.8403	4.448E-1	4.452E-1	4.454E-1				
	0.9428	5.812E-1	5.820E-1	5.823E-1				
	0.9983	6.722E-1	6.734E-1	6.739E-1				
	0.0381			9.924E-3	9.991E-3	1.011E-2	1.022E-2	1.031E-2
	0.1775			9.875E-3	9.940E-3	1.006E-2	1.016E-2	1.026E-2
	0.4563			9.778E-3	9.841E-3	9.954E-3	1.005E-2	1.015E-2
Σ_{a1}	0.7351	9.400E-3	9.584E-3	9.656E-3	9.717E-3	9.824E-3	9.921E-3	1.001E-2
	0.8403	8.919E-3	9.080E-3	9.141E-3				
	0.9428	7.877E-3	7.997E-3	8.042E-3				
	0.9983	6.842E-3	6.932E-3	6.965E-3				
	0.0381			8.209E-2	8.191E-2	8.157E-2	8.123E-2	8.091E-2
	0.1775			7.756E-2	7.742E-2	7.713E-2	7.685E-2	7.658E-2
	0.4563			7.321E-2	7.309E-2	7.284E-2	7.261E-2	7.238E-2
Σ_{a2}	0.7351	7.068E-2	7.042E-2	7.030E-2	7.019E-2	6.997E-2	6.975E-2	6.954E-2
	0.8403	6.727E-2	6.700E-2	6.687E-2				
	0.9428	6.283E-2	6.256E-2	6.243E-2				
	0.9983	6.049E-2	6.022E-2	6.009E-2				
	0.0381			5.110E-3	5.109E-3	5.108E-3	5.105E-3	5.103E-3
	0.1775			5.077E-3	5.076E-3	5.075E-3	5.072E-3	5.070E-3
	0.4563			5.006E-3	5.005E-3	5.003E-3	5.000E-3	4.997E-3
$\nu\Sigma_{f1}$	0.7351	4.924E-3	4.923E-3	4.922E-3	4.921E-3	4.918E-3	4.915E-3	4.913E-3
	0.8403	4.619E-3	4.616E-3	4.614E-3				
	0.9428	4.080E-3	4.074E-3	4.071E-3				
	0.9983	3.592E-3	3.585E-3	3.582E-3				
	0.0381			9.463E-2	9.434E-2	9.375E-2	9.320E-2	9.265E-2
	0.1775			8.785E-2	8.762E-2	8.715E-2	8.669E-2	8.624E-2
	0.4563			8.164E-2	8.145E-2	8.105E-2	8.067E-2	8.029E-2
$\nu\Sigma_{f2}$	0.7351	7.830E-2	7.787E-2	7.768E-2	7.751E-2	7.715E-2	7.681E-2	7.647E-2
	0.8403	7.432E-2	7.389E-2	7.370E-2				
	0.9428	6.871E-2	6.830E-2	6.811E-2				
	0.9983	6.530E-2	6.489E-2	6.470E-2				
	0.0381			2.244E-2	2.241E-2	2.235E-2	2.229E-2	2.225E-2
	0.1775			2.134E-2	2.131E-2	2.125E-2	2.120E-2	2.116E-2
	0.4563			1.927E-2	1.924E-2	1.919E-2	1.914E-2	1.910E-2
Σ_{12}	0.7351	1.727E-2	1.717E-2	1.714E-2	1.711E-2	1.706E-2	1.702E-2	1.698E-2
	0.8403	1.160E-2	1.152E-2	1.149E-2				
	0.9428	6.304E-3	6.251E-3	6.233E-3				
	0.9983	4.000E-3	3.967E-3	3.957E-3				

Table C.12 – Average statistics for segment 13 and control rods inserted.

	$\mathbf{D_{mod}}$	$\mathbf{T_{fuel}}$ (K)						
	(kg/m^3)	293.0	660.8	853.5	1028.6	1396.5	1764.3	2132.2
	0.0381			1.393	1.393	1.393	1.394	1.394
	0.1775			1.423	1.423	1.423	1.423	1.423
	0.4563			1.481	1.482	1.482	1.482	1.482
D_{f1}	0.7351	1.547	1.547	1.548	1.548	1.548	1.548	1.548
	0.8403	1.757	1.758	1.758				
	0.9428	2.039	2.039	2.039				
	0.9983	2.219	2.219	2.219				
	0.0381			2.772E-1	2.773E-1	2.777E-1	2.780E-1	2.783E-1
	0.1775			2.950E-1	2.952E-1	2.955E-1	2.958E-1	2.961E-1
	0.4563			3.227E-1	3.228E-1	3.231E-1	3.234E-1	3.237E-1
D_{f2}	0.7351	3.511E-1	3.514E-1	3.516E-1	3.517E-1	3.520E-1	3.523E-1	3.526E-1
	0.8403	4.360E-1	4.364E-1	4.366E-1				
	0.9428	5.690E-1	5.698E-1	5.701E-1				
	0.9983	6.652E-1	6.664E-1	6.670E-1				
	0.0381			7.692E-3	7.762E-3	7.887E-3	7.999E-3	8.100E-3
	0.1775			7.641E-3	7.711E-3	7.834E-3	7.944E-3	8.044E-3
	0.4563			7.541E-3	7.609E-3	7.728E-3	7.836E-3	7.933E-3
Σ_{a1}	0.7351	7.148E-3	7.346E-3	7.423E-3	7.488E-3	7.604E-3	7.708E-3	7.802E-3
	0.8403	6.744E-3	6.923E-3	6.992E-3				
	0.9428	6.008E-3	6.153E-3	6.207E-3				
	0.9983	5.311E-3	5.429E-3	5.472E-3				
	0.0381			7.219E-2	7.204E-2	7.173E-2	7.144E-2	7.115E-2
	0.1775			6.811E-2	6.799E-2	6.773E-2	6.749E-2	6.724E-2
	0.4563			6.417E-2	6.407E-2	6.385E-2	6.363E-2	6.343E-2
Σ_{a2}	0.7351	6.191E-2	6.168E-2	6.157E-2	6.147E-2	6.127E-2	6.108E-2	6.088E-2
	0.8403	5.932E-2	5.908E-2	5.897E-2				
	0.9428	5.629E-2	5.605E-2	5.593E-2				
	0.9983	5.466E-2	5.441E-2	5.429E-2				
	0.0381			5.395E-3	5.394E-3	5.393E-3	5.391E-3	5.388E-3
	0.1775			5.368E-3	5.367E-3	5.365E-3	5.363E-3	5.361E-3
	0.4563			5.308E-3	5.306E-3	5.305E-3	5.302E-3	5.300E-3
$\nu\Sigma_{f1}$	0.7351	5.238E-3	5.238E-3	5.237E-3	5.236E-3	5.234E-3	5.232E-3	5.229E-3
	0.8403	4.986E-3	4.984E-3	4.982E-3				
	0.9428	4.560E-3	4.555E-3	4.553E-3				
	0.9983	4.184E-3	4.178E-3	4.176E-3				
	0.0381			9.147E-2	9.120E-2	9.066E-2	9.015E-2	8.965E-2
	0.1775			8.535E-2	8.513E-2	8.469E-2	8.426E-2	8.385E-2
	0.4563			7.981E-2	7.963E-2	7.926E-2	7.890E-2	7.855E-2
$\nu\Sigma_{f2}$	0.7351	7.698E-2	7.658E-2	7.640E-2	7.623E-2	7.590E-2	7.558E-2	7.526E-2
	0.8403	7.435E-2	7.395E-2	7.376E-2				
	0.9428	7.080E-2	7.040E-2	7.021E-2				
	0.9983	6.858E-2	6.818E-2	6.799E-2				
	0.0381			2.505E-2	2.501E-2	2.495E-2	2.490E-2	2.485E-2
	0.1775			2.397E-2	2.394E-2	2.387E-2	2.382E-2	2.378E-2
	0.4563			2.193E-2	2.190E-2	2.184E-2	2.179E-2	2.175E-2
Σ_{12}	0.7351	1.997E-2	1.986E-2	1.982E-2	1.979E-2	1.974E-2	1.969E-2	1.966E-2
	0.8403	1.430E-2	1.420E-2	1.417E-2				
	0.9428	8.800E-3	8.732E-3	8.709E-3				
	0.9983	6.239E-3	6.191E-3	6.176E-3				

Table C.13 – Average statistics for segment 14 and control rods withdrawn.

	$\mathbf{D_{mod}}$	$\mathbf{T_{fuel}}$ (K)						
	(kg/m^3)	293.0	660.8	853.5	1028.6	1396.5	1764.3	2132.2
	0.0381			1.367	1.367	1.367	1.368	1.368
	0.1775			1.396	1.396	1.396	1.396	1.397
	0.4563			1.452	1.452	1.452	1.453	1.453
D_{f1}	0.7351	1.514	1.515	1.515	1.515	1.516	1.516	1.516
	0.8403	1.714	1.714	1.715				
	0.9428	1.976	1.977	1.977				
	0.9983	2.142	2.142	2.142				
	0.0381			2.766E-1	2.767E-1	2.771E-1	2.774E-1	2.777E-1
	0.1775			2.951E-1	2.952E-1	2.955E-1	2.958E-1	2.961E-1
	0.4563			3.239E-1	3.240E-1	3.243E-1	3.246E-1	3.249E-1
D_{f2}	0.7351	3.536E-1	3.539E-1	3.541E-1	3.542E-1	3.545E-1	3.548E-1	3.551E-1
	0.8403	4.426E-1	4.429E-1	4.431E-1				
	0.9428	5.748E-1	5.754E-1	5.756E-1				
	0.9983	6.605E-1	6.614E-1	6.619E-1				
	0.0381			1.014E-2	1.021E-2	1.033E-2	1.043E-2	1.053E-2
	0.1775			1.009E-2	1.015E-2	1.027E-2	1.037E-2	1.047E-2
	0.4563			9.979E-3	1.004E-2	1.015E-2	1.026E-2	1.035E-2
Σ_{a1}	0.7351	9.586E-3	9.770E-3	9.842E-3	9.903E-3	1.001E-2	1.011E-2	1.019E-2
	0.8403	9.064E-3	9.225E-3	9.286E-3				
	0.9428	7.979E-3	8.099E-3	8.144E-3				
	0.9983	6.920E-3	7.009E-3	7.042E-3				
	0.0381			8.826E-2	8.809E-2	8.776E-2	8.744E-2	8.713E-2
	0.1775			8.384E-2	8.370E-2	8.342E-2	8.315E-2	8.289E-2
	0.4563			7.946E-2	7.934E-2	7.911E-2	7.887E-2	7.865E-2
Σ_{a2}	0.7351	7.683E-2	7.658E-2	7.646E-2	7.636E-2	7.614E-2	7.593E-2	7.572E-2
	0.8403	7.312E-2	7.286E-2	7.274E-2				
	0.9428	6.823E-2	6.798E-2	6.786E-2				
	0.9983	6.562E-2	6.537E-2	6.525E-2				
	0.0381			5.342E-3	5.341E-3	5.339E-3	5.337E-3	5.334E-3
	0.1775			5.307E-3	5.306E-3	5.304E-3	5.302E-3	5.299E-3
	0.4563			5.231E-3	5.230E-3	5.228E-3	5.225E-3	5.222E-3
$\nu\Sigma_{f1}$	0.7351	5.144E-3	5.143E-3	5.142E-3	5.141E-3	5.138E-3	5.136E-3	5.133E-3
	0.8403	4.822E-3	4.819E-3	4.817E-3				
	0.9428	4.256E-3	4.249E-3	4.246E-3				
	0.9983	3.742E-3	3.734E-3	3.731E-3				
	0.0381			9.849E-2	9.820E-2	9.763E-2	9.708E-2	9.655E-2
	0.1775			9.169E-2	9.146E-2	9.099E-2	9.054E-2	9.010E-2
	0.4563			8.529E-2	8.510E-2	8.471E-2	8.433E-2	8.396E-2
$\nu\Sigma_{f2}$	0.7351	8.172E-2	8.129E-2	8.110E-2	8.093E-2	8.058E-2	8.024E-2	7.990E-2
	0.8403	7.689E-2	7.648E-2	7.629E-2				
	0.9428	7.028E-2	6.989E-2	6.970E-2				
	0.9983	6.642E-2	6.605E-2	6.587E-2				
	0.0381			2.225E-2	2.221E-2	2.215E-2	2.210E-2	2.206E-2
	0.1775			2.116E-2	2.112E-2	2.106E-2	2.101E-2	2.097E-2
	0.4563			1.909E-2	1.906E-2	1.901E-2	1.896E-2	1.892E-2
Σ_{12}	0.7351	1.711E-2	1.701E-2	1.697E-2	1.694E-2	1.689E-2	1.685E-2	1.681E-2
	0.8403	1.148E-2	1.139E-2	1.136E-2				
	0.9428	6.225E-3	6.172E-3	6.154E-3				
	0.9983	3.948E-3	3.915E-3	3.905E-3				

Table C.14 – Average statistics for segment 14 and control rods inserted.

	$\mathbf{D_{mod}}$	$\mathbf{T_{fuel}}$ (K)						
	(kg/m^3)	293.0	660.8	853.5	1028.6	1396.5	1764.3	2132.2
	0.0381			1.386	1.387	1.387	1.387	1.387
	0.1775			1.416	1.416	1.416	1.417	1.417
	0.4563			1.474	1.474	1.475	1.475	1.475
D_{f1}	0.7351	1.539	1.540	1.540	1.540	1.540	1.540	1.541
	0.8403	1.747	1.747	1.748				
	0.9428	2.023	2.023	2.024				
	0.9983	2.198	2.198	2.198				
	0.0381			2.691E-1	2.695E-1	2.703E-1	2.710E-1	2.718E-1
	0.1775			2.918E-1	2.921E-1	2.928E-1	2.935E-1	2.942E-1
	0.4563			3.246E-1	3.249E-1	3.256E-1	3.262E-1	3.269E-1
D_{f2}	0.7351	3.570E-1	3.578E-1	3.581E-1	3.584E-1	3.591E-1	3.598E-1	3.605E-1
	0.8403	4.534E-1	4.545E-1	4.551E-1				
	0.9428	6.178E-1	6.202E-1	6.214E-1				
	0.9983	7.520E-1	7.565E-1	7.586E-1				
	0.0381			6.119E-3	6.190E-3	6.318E-3	6.434E-3	6.539E-3
	0.1775			6.074E-3	6.145E-3	6.271E-3	6.386E-3	6.490E-3
	0.4563			5.991E-3	6.060E-3	6.183E-3	6.295E-3	6.397E-3
Σ_{a1}	0.7351	5.618E-3	5.817E-3	5.895E-3	5.962E-3	6.082E-3	6.190E-3	6.289E-3
	0.8403	5.302E-3	5.483E-3	5.554E-3				
	0.9428	4.728E-3	4.877E-3	4.933E-3				
	0.9983	4.176E-3	4.297E-3	4.343E-3				
	0.0381			3.633E-2	3.619E-2	3.591E-2	3.565E-2	3.540E-2
	0.1775			3.283E-2	3.272E-2	3.251E-2	3.231E-2	3.211E-2
	0.4563			2.971E-2	2.962E-2	2.946E-2	2.929E-2	2.913E-2
Σ_{a2}	0.7351	2.799E-2	2.781E-2	2.773E-2	2.766E-2	2.751E-2	2.736E-2	2.722E-2
	0.8403	2.609E-2	2.589E-2	2.579E-2				
	0.9428	2.395E-2	2.370E-2	2.359E-2				
	0.9983	2.263E-2	2.234E-2	2.220E-2				
	0.0381			2.816E-3	2.816E-3	2.816E-3	2.815E-3	2.815E-3
	0.1775			2.794E-3	2.794E-3	2.793E-3	2.793E-3	2.793E-3
	0.4563			2.749E-3	2.749E-3	2.749E-3	2.749E-3	2.749E-3
$\nu\Sigma_{f1}$	0.7351	2.700E-3	2.700E-3	2.699E-3	2.699E-3	2.699E-3	2.699E-3	2.699E-3
	0.8403	2.537E-3	2.537E-3	2.537E-3				
	0.9428	2.292E-3	2.291E-3	2.291E-3				
	0.9983	2.095E-3	2.093E-3	2.093E-3				
	0.0381			3.450E-2	3.432E-2	3.398E-2	3.365E-2	3.334E-2
	0.1775			3.114E-2	3.101E-2	3.074E-2	3.049E-2	3.025E-2
	0.4563			2.843E-2	2.832E-2	2.811E-2	2.791E-2	2.771E-2
$\nu\Sigma_{f2}$	0.7351	2.724E-2	2.701E-2	2.690E-2	2.681E-2	2.662E-2	2.644E-2	2.626E-2
	0.8403	2.680E-2	2.654E-2	2.642E-2				
	0.9428	2.602E-2	2.570E-2	2.555E-2				
	0.9983	2.526E-2	2.488E-2	2.470E-2				
	0.0381			2.627E-2	2.623E-2	2.617E-2	2.612E-2	2.608E-2
	0.1775			2.519E-2	2.515E-2	2.510E-2	2.505E-2	2.502E-2
	0.4563			2.314E-2	2.311E-2	2.306E-2	2.302E-2	2.300E-2
Σ_{12}	0.7351	2.116E-2	2.106E-2	2.102E-2	2.099E-2	2.095E-2	2.092E-2	2.090E-2
	0.8403	1.539E-2	1.530E-2	1.527E-2				
	0.9428	9.719E-3	9.657E-3	9.637E-3				
	0.9983	7.015E-3	6.973E-3	6.962E-3				

Table C.15 – Average statistics for segment 15 and control rods withdrawn.

	$\mathbf{D_{mod}}$	$\mathbf{T_{fuel}}$ **(K)**						
	(kg/m^3)	293.0	660.8	853.5	1028.6	1396.5	1764.3	2132.2
	0.0381			1.362	1.362	1.362	1.362	1.362
	0.1775			1.390	1.390	1.390	1.391	1.391
	0.4563			1.446	1.446	1.446	1.446	1.447
D_{f1}	0.7351	1.507	1.508	1.508	1.508	1.509	1.509	1.509
	0.8403	1.704	1.705	1.705				
	0.9428	1.961	1.962	1.962				
	0.9983	2.122	2.122	2.122				
	0.0381			2.688E-1	2.692E-1	2.700E-1	2.708E-1	2.716E-1
	0.1775			2.924E-1	2.927E-1	2.934E-1	2.941E-1	2.948E-1
	0.4563			3.265E-1	3.268E-1	3.274E-1	3.281E-1	3.287E-1
D_{f2}	0.7351	3.603E-1	3.610E-1	3.614E-1	3.617E-1	3.623E-1	3.630E-1	3.636E-1
	0.8403	4.614E-1	4.624E-1	4.629E-1				
	0.9428	6.282E-1	6.302E-1	6.311E-1				
	0.9983	7.538E-1	7.573E-1	7.589E-1				
	0.0381			8.600E-3	8.668E-3	8.789E-3	8.899E-3	8.998E-3
	0.1775			8.558E-3	8.625E-3	8.744E-3	8.853E-3	8.951E-3
	0.4563			8.483E-3	8.548E-3	8.664E-3	8.769E-3	8.864E-3
Σ_{a1}	0.7351	8.132E-3	8.318E-3	8.391E-3	8.454E-3	8.565E-3	8.666E-3	8.757E-3
	0.8403	7.776E-3	7.940E-3	8.003E-3				
	0.9428	6.971E-3	7.096E-3	7.143E-3				
	0.9983	6.135E-3	6.230E-3	6.266E-3				
	0.0381			4.544E-2	4.529E-2	4.500E-2	4.472E-2	4.445E-2
	0.1775			4.189E-2	4.177E-2	4.155E-2	4.133E-2	4.113E-2
	0.4563			3.881E-2	3.872E-2	3.854E-2	3.837E-2	3.820E-2
Σ_{a2}	0.7351	3.722E-2	3.703E-2	3.694E-2	3.686E-2	3.670E-2	3.655E-2	3.640E-2
	0.8403	3.573E-2	3.552E-2	3.543E-2				
	0.9428	3.432E-2	3.409E-2	3.398E-2				
	0.9983	3.380E-2	3.354E-2	3.342E-2				
	0.0381			2.792E-3	2.791E-3	2.791E-3	2.791E-3	2.790E-3
	0.1775			2.767E-3	2.767E-3	2.766E-3	2.766E-3	2.766E-3
	0.4563			2.716E-3	2.716E-3	2.716E-3	2.716E-3	2.716E-3
$\nu\Sigma_{f1}$	0.7351	2.661E-3	2.660E-3	2.660E-3	2.660E-3	2.660E-3	2.659E-3	2.659E-3
	0.8403	2.473E-3	2.473E-3	2.472E-3				
	0.9428	2.177E-3	2.176E-3	2.176E-3				
	0.9983	1.929E-3	1.927E-3	1.926E-3				
	0.0381			3.615E-2	3.596E-2	3.560E-2	3.526E-2	3.493E-2
	0.1775			3.255E-2	3.241E-2	3.213E-2	3.187E-2	3.161E-2
	0.4563			2.958E-2	2.947E-2	2.925E-2	2.904E-2	2.883E-2
$\nu\Sigma_{f2}$	0.7351	2.820E-2	2.796E-2	2.785E-2	2.776E-2	2.756E-2	2.738E-2	2.719E-2
	0.8403	2.723E-2	2.697E-2	2.685E-2				
	0.9428	2.560E-2	2.529E-2	2.515E-2				
	0.9983	2.426E-2	2.391E-2	2.375E-2				
	0.0381			2.345E-2	2.341E-2	2.336E-2	2.331E-2	2.327E-2
	0.1775			2.235E-2	2.231E-2	2.226E-2	2.221E-2	2.218E-2
	0.4563			2.026E-2	2.023E-2	2.018E-2	2.014E-2	2.011E-2
Σ_{12}	0.7351	1.823E-2	1.814E-2	1.810E-2	1.807E-2	1.803E-2	1.800E-2	1.798E-2
	0.8403	1.244E-2	1.236E-2	1.233E-2				
	0.9428	6.910E-3	6.859E-3	6.842E-3				
	0.9983	4.424E-3	4.393E-3	4.384E-3				

Table C.16 – Average statistics for segment 15 and control rods inserted.

	$\mathbf{D_{mod}}$	$\mathbf{T_{fuel}}$ **(K)**						
	(kg/m^3)	293.0	660.8	853.5	1028.6	1396.5	1764.3	2132.2
$\boldsymbol{D_{f1}}$	0.0381			4.067E-2	4.066E-2	4.065E-2	4.065E-2	4.064E-2
	0.1775			4.056E-2	4.056E-2	4.055E-2	4.054E-2	4.053E-2
	0.4563			4.036E-2	4.035E-2	4.034E-2	4.033E-2	4.032E-2
	0.7351	4.015E-2	4.014E-2	4.013E-2	4.012E-2	4.011E-2	4.011E-2	4.010E-2
	0.8403	3.946E-2	3.945E-2	3.944E-2				
	0.9428	3.902E-2	3.903E-2	3.904E-2				
	0.9983	4.030E-2	4.051E-2	4.058E-2				
$\boldsymbol{D_{f2}}$	0.0381			5.179E-4	5.179E-4	5.179E-4	5.179E-4	5.179E-4
	0.1775			5.180E-4	5.180E-4	5.179E-4	5.180E-4	5.180E-4
	0.4563			5.181E-4	5.181E-4	5.181E-4	5.181E-4	5.181E-4
	0.7351	5.182E-4	5.182E-4	5.182E-4	5.182E-4	5.182E-4	5.181E-4	5.181E-4
	0.8403	5.182E-4	5.181E-4	5.181E-4				
	0.9428	5.181E-4	5.181E-4	5.181E-4				
	0.9983	5.181E-4	5.180E-4	5.180E-4				
$\boldsymbol{\Sigma_{a1}}$	0.0381			7.486E-6	7.486E-6	7.485E-6	7.484E-6	7.483E-6
	0.1775			7.446E-6	7.445E-6	7.444E-6	7.443E-6	7.442E-6
	0.4563			7.367E-6	7.366E-6	7.365E-6	7.364E-6	7.363E-6
	0.7351	7.282E-6	7.281E-6	7.280E-6	7.279E-6	7.278E-6	7.277E-6	7.276E-6
	0.8403	6.995E-6	6.992E-6	6.991E-6				
	0.9428	6.683E-6	6.682E-6	6.682E-6				
	0.9983	6.646E-6	6.673E-6	6.681E-6				
$\boldsymbol{\Sigma_{a2}}$	0.0381			1.076E-4	1.076E-4	1.076E-4	1.076E-4	1.076E-4
	0.1775			1.076E-4	1.076E-4	1.076E-4	1.076E-4	1.076E-4
	0.4563			1.076E-4	1.076E-4	1.076E-4	1.076E-4	1.076E-4
	0.7351	1.076E-4	1.076E-4	1.076E-4	1.076E-4	1.075E-4	1.075E-4	1.075E-4
	0.8403	1.075E-4	1.075E-4	1.075E-4				
	0.9428	1.074E-4	1.074E-4	1.074E-4				
	0.9983	1.074E-4	1.074E-4	1.074E-4				
$\boldsymbol{\Sigma_{12}}$	0.0381			6.835E-4	6.828E-4	6.819E-4	6.811E-4	6.804E-4
	0.1775			6.848E-4	6.841E-4	6.831E-4	6.822E-4	6.814E-4
	0.4563			6.861E-4	6.853E-4	6.842E-4	6.833E-4	6.825E-4
	0.7351	6.895E-4	6.873E-4	6.866E-4	6.858E-4	6.847E-4	6.837E-4	6.829E-4
	0.8403	6.877E-4	6.850E-4	6.842E-4				
	0.9428	6.810E-4	6.782E-4	6.773E-4				
	0.9983	6.832E-4	6.823E-4	6.821E-4				

Table C.17 – Standard deviation statistics for segment 1 and control rods withdrawn.

	$\mathbf{D_{mod}}$	$\mathbf{T_{fuel}}$ **(K)**						
	(kg/m³)	293.0	660.8	853.5	1028.6	1396.5	1764.3	2132.2
	0.0381			2.450E-2	2.450E-2	2.449E-2	2.449E-2	2.448E-2
	0.1775			2.451E-2	2.450E-2	2.450E-2	2.449E-2	2.448E-2
	0.4563			2.452E-2	2.452E-2	2.451E-2	2.451E-2	2.450E-2
D_{f1}	0.7351	2.457E-2	2.456E-2	2.455E-2	2.455E-2	2.454E-2	2.454E-2	2.453E-2
	0.8403	2.475E-2	2.474E-2	2.473E-2				
	0.9428	2.515E-2	2.515E-2	2.515E-2				
	0.9983	2.611E-2	2.619E-2	2.622E-2				
	0.0381			1.374E-3	1.374E-3	1.374E-3	1.374E-3	1.374E-3
	0.1775			1.375E-3	1.375E-3	1.374E-3	1.374E-3	1.374E-3
	0.4563			1.377E-3	1.377E-3	1.376E-3	1.376E-3	1.376E-3
D_{f2}	0.7351	1.379E-3	1.379E-3	1.379E-3	1.379E-3	1.379E-3	1.379E-3	1.379E-3
	0.8403	1.386E-3	1.386E-3	1.386E-3				
	0.9428	1.395E-3	1.394E-3	1.394E-3				
	0.9983	1.402E-3	1.402E-3	1.402E-3				
	0.0381			2.312E-5	2.312E-5	2.312E-5	2.312E-5	2.312E-5
	0.1775			2.308E-5	2.308E-5	2.308E-5	2.308E-5	2.308E-5
	0.4563			2.300E-5	2.300E-5	2.300E-5	2.300E-5	2.300E-5
Σ_{a1}	0.7351	2.291E-5	2.291E-5	2.291E-5	2.291E-5	2.291E-5	2.291E-5	2.291E-5
	0.8403	2.258E-5	2.257E-5	2.257E-5				
	0.9428	2.220E-5	2.220E-5	2.220E-5				
	0.9983	2.206E-5	2.207E-5	2.208E-5				
	0.0381			1.836E-4	1.837E-4	1.837E-4	1.837E-4	1.837E-4
	0.1775			1.835E-4	1.835E-4	1.835E-4	1.835E-4	1.835E-4
	0.4563			1.833E-4	1.833E-4	1.833E-4	1.834E-4	1.834E-4
Σ_{a2}	0.7351	1.832E-4	1.833E-4	1.833E-4	1.833E-4	1.833E-4	1.833E-4	1.833E-4
	0.8403	1.837E-4	1.837E-4	1.837E-4				
	0.9428	1.844E-4	1.844E-4	1.844E-4				
	0.9983	1.853E-4	1.854E-4	1.854E-4				
	0.0381			2.828E-4	2.825E-4	2.820E-4	2.816E-4	2.812E-4
	0.1775			2.837E-4	2.833E-4	2.828E-4	2.824E-4	2.820E-4
	0.4563			2.848E-4	2.845E-4	2.839E-4	2.835E-4	2.831E-4
Σ_{12}	0.7351	2.871E-4	2.860E-4	2.857E-4	2.853E-4	2.848E-4	2.843E-4	2.839E-4
	0.8403	2.884E-4	2.871E-4	2.867E-4				
	0.9428	2.864E-4	2.850E-4	2.845E-4				
	0.9983	2.855E-4	2.846E-4	2.844E-4				

Table C.18 – Standard deviation statistics for segment 2 and control rods withdrawn.

	$\mathbf{D_{mod}}$	$\mathbf{T_{fuel}}$ **(K)**						
	(kg/m^3)	293.0	660.8	853.5	1028.6	1396.5	1764.3	2132.2
D_{f1}	0.0381			2.164E-2	2.163E-2	2.163E-2	2.163E-2	2.162E-2
	0.1775			2.162E-2	2.162E-2	2.161E-2	2.161E-2	2.161E-2
	0.4563			2.159E-2	2.158E-2	2.158E-2	2.158E-2	2.157E-2
	0.7351	2.156E-2	2.156E-2	2.155E-2	2.155E-2	2.155E-2	2.155E-2	2.154E-2
	0.8403	2.151E-2	2.151E-2	2.151E-2				
	0.9428	2.163E-2	2.163E-2	2.163E-2				
	0.9983	2.222E-2	2.229E-2	2.231E-2				
D_{f2}	0.0381			1.653E-3	1.652E-3	1.652E-3	1.652E-3	1.652E-3
	0.1775			1.653E-3	1.653E-3	1.653E-3	1.653E-3	1.653E-3
	0.4563			1.656E-3	1.656E-3	1.656E-3	1.656E-3	1.655E-3
	0.7351	1.659E-3	1.659E-3	1.659E-3	1.659E-3	1.659E-3	1.658E-3	1.658E-3
	0.8403	1.667E-3	1.667E-3	1.667E-3				
	0.9428	1.673E-3	1.673E-3	1.673E-3				
	0.9983	1.676E-3	1.675E-3	1.675E-3				
Σ_{a1}	0.0381			6.195E-5	6.193E-5	6.189E-5	6.186E-5	6.183E-5
	0.1775			6.208E-5	6.205E-5	6.201E-5	6.198E-5	6.195E-5
	0.4563			6.230E-5	6.227E-5	6.223E-5	6.219E-5	6.216E-5
	0.7351	6.263E-5	6.255E-5	6.252E-5	6.249E-5	6.244E-5	6.240E-5	6.237E-5
	0.8403	6.325E-5	6.314E-5	6.310E-5				
	0.9428	6.359E-5	6.346E-5	6.342E-5				
	0.9983	6.350E-5	6.337E-5	6.333E-5				
Σ_{a2}	0.0381			8.263E-4	8.264E-4	8.264E-4	8.264E-4	8.264E-4
	0.1775			8.259E-4	8.259E-4	8.259E-4	8.260E-4	8.260E-4
	0.4563			8.264E-4	8.264E-4	8.265E-4	8.265E-4	8.265E-4
	0.7351	8.275E-4	8.276E-4	8.277E-4	8.277E-4	8.278E-4	8.278E-4	8.278E-4
	0.8403	8.345E-4	8.347E-4	8.347E-4				
	0.9428	8.428E-4	8.429E-4	8.429E-4				
	0.9983	8.484E-4	8.485E-4	8.485E-4				
Σ_{12}	0.0381			3.932E-4	3.927E-4	3.921E-4	3.915E-4	3.910E-4
	0.1775			3.941E-4	3.937E-4	3.930E-4	3.925E-4	3.920E-4
	0.4563			3.954E-4	3.949E-4	3.942E-4	3.936E-4	3.930E-4
	0.7351	3.980E-4	3.966E-4	3.962E-4	3.956E-4	3.949E-4	3.942E-4	3.937E-4
	0.8403	3.980E-4	3.962E-4	3.957E-4				
	0.9428	3.921E-4	3.903E-4	3.897E-4				
	0.9983	3.876E-4	3.866E-4	3.863E-4				

Table C.19 – Standard deviation statistics for segment 3 and control rods withdrawn.

	$\mathbf{D_{mod}}$	$\mathbf{T_{fuel}}$ (K)						
	($\mathbf{kg/m^3}$)	293.0	660.8	853.5	1028.6	1396.5	1764.3	2132.2
	0.0381			3.265E-2	3.266E-2	3.269E-2	3.271E-2	3.272E-2
	0.1775			3.352E-2	3.353E-2	3.356E-2	3.358E-2	3.360E-2
	0.4563			3.525E-2	3.526E-2	3.529E-2	3.532E-2	3.534E-2
D_{f1}	0.7351	3.713E-2	3.719E-2	3.722E-2	3.723E-2	3.727E-2	3.729E-2	3.732E-2
	0.8403	4.346E-2	4.356E-2	4.360E-2				
	0.9428	5.177E-2	5.194E-2	5.201E-2				
	0.9983	5.739E-2	5.777E-2	5.792E-2				
	0.0381			6.826E-4	6.801E-4	6.743E-4	6.689E-4	6.640E-4
	0.1775			7.718E-4	7.697E-4	7.647E-4	7.598E-4	7.552E-4
	0.4563			9.076E-4	9.056E-4	9.010E-4	8.967E-4	8.927E-4
D_{f2}	0.7351	1.063E-3	1.058E-3	1.055E-3	1.053E-3	1.048E-3	1.044E-3	1.040E-3
	0.8403	1.532E-3	1.525E-3	1.521E-3				
	0.9428	2.566E-3	2.556E-3	2.551E-3				
	0.9983	3.643E-3	3.631E-3	3.625E-3				
	0.0381			5.147E-5	5.237E-5	5.418E-5	5.581E-5	5.728E-5
	0.1775			5.126E-5	5.215E-5	5.395E-5	5.556E-5	5.702E-5
	0.4563			5.085E-5	5.173E-5	5.350E-5	5.508E-5	5.650E-5
Σ_{a1}	0.7351	4.596E-5	4.900E-5	5.030E-5	5.116E-5	5.290E-5	5.444E-5	5.583E-5
	0.8403	4.377E-5	4.660E-5	4.780E-5				
	0.9428	3.812E-5	4.052E-5	4.152E-5				
	0.9983	3.185E-5	3.385E-5	3.467E-5				
	0.0381			1.824E-4	1.823E-4	1.819E-4	1.818E-4	1.816E-4
	0.1775			1.704E-4	1.702E-4	1.698E-4	1.695E-4	1.692E-4
	0.4563			1.580E-4	1.579E-4	1.575E-4	1.571E-4	1.568E-4
Σ_{a2}	0.7351	1.503E-4	1.498E-4	1.496E-4	1.494E-4	1.490E-4	1.487E-4	1.484E-4
	0.8403	1.407E-4	1.401E-4	1.399E-4				
	0.9428	1.303E-4	1.298E-4	1.296E-4				
	0.9983	1.237E-4	1.232E-4	1.230E-4				
	0.0381			7.677E-5	7.680E-5	7.685E-5	7.690E-5	7.694E-5
	0.1775			7.633E-5	7.635E-5	7.641E-5	7.645E-5	7.649E-5
	0.4563			7.551E-5	7.554E-5	7.560E-5	7.564E-5	7.568E-5
$\nu\Sigma_{f1}$	0.7351	7.449E-5	7.461E-5	7.466E-5	7.470E-5	7.476E-5	7.481E-5	7.485E-5
	0.8403	7.230E-5	7.248E-5	7.255E-5				
	0.9428	7.082E-5	7.120E-5	7.136E-5				
	0.9983	7.752E-5	7.885E-5	7.938E-5				
	0.0381			1.806E-4	1.799E-4	1.784E-4	1.771E-4	1.760E-4
	0.1775			1.627E-4	1.621E-4	1.609E-4	1.598E-4	1.589E-4
	0.4563			1.484E-4	1.479E-4	1.469E-4	1.460E-4	1.452E-4
$\nu\Sigma_{f2}$	0.7351	1.424E-4	1.411E-4	1.404E-4	1.400E-4	1.391E-4	1.382E-4	1.375E-4
	0.8403	1.403E-4	1.388E-4	1.381E-4				
	0.9428	1.368E-4	1.350E-4	1.340E-4				
	0.9983	1.333E-4	1.309E-4	1.298E-4				
	0.0381			3.233E-4	3.230E-4	3.226E-4	3.222E-4	3.220E-4
	0.1775			3.107E-4	3.105E-4	3.102E-4	3.099E-4	3.098E-4
	0.4563			2.872E-4	2.870E-4	2.867E-4	2.866E-4	2.866E-4
Σ_{12}	0.7351	2.637E-4	2.630E-4	2.627E-4	2.626E-4	2.625E-4	2.624E-4	2.626E-4
	0.8403	1.968E-4	1.963E-4	1.961E-4				
	0.9428	1.288E-4	1.286E-4	1.285E-4				
	0.9983	9.655E-5	9.690E-5	9.711E-5				

Table C.20 – Standard deviation statistics for segment 10 and control rods withdrawn.

	$\mathbf{D_{mod}}$	$\mathbf{T_{fuel}}$ (K)						
	($\mathbf{kg/m^3}$)	293.0	660.8	853.5	1028.6	1396.5	1764.3	2132.2
	0.0381			3.109E-2	3.110E-2	3.113E-2	3.114E-2	3.116E-2
	0.1775			3.188E-2	3.189E-2	3.191E-2	3.193E-2	3.195E-2
	0.4563			3.342E-2	3.344E-2	3.346E-2	3.348E-2	3.350E-2
D_{f1}	0.7351	3.509E-2	3.515E-2	3.517E-2	3.519E-2	3.522E-2	3.524E-2	3.526E-2
	0.8403	4.062E-2	4.071E-2	4.075E-2				
	0.9428	4.765E-2	4.781E-2	4.787E-2				
	0.9983	5.217E-2	5.250E-2	5.263E-2				
	0.0381			6.906E-4	6.881E-4	6.818E-4	6.760E-4	6.705E-4
	0.1775			7.820E-4	7.798E-4	7.745E-4	7.695E-4	7.649E-4
	0.4563			9.222E-4	9.202E-4	9.154E-4	9.109E-4	9.066E-4
D_{f2}	0.7351	1.082E-3	1.077E-3	1.074E-3	1.072E-3	1.067E-3	1.063E-3	1.059E-3
	0.8403	1.571E-3	1.565E-3	1.561E-3				
	0.9428	2.625E-3	2.616E-3	2.611E-3				
	0.9983	3.654E-3	3.641E-3	3.634E-3				
	0.0381			6.755E-5	6.843E-5	7.023E-5	7.185E-5	7.331E-5
	0.1775			6.776E-5	6.863E-5	7.042E-5	7.202E-5	7.345E-5
	0.4563			6.830E-5	6.916E-5	7.090E-5	7.247E-5	7.387E-5
Σ_{a1}	0.7351	6.463E-5	6.758E-5	6.884E-5	6.968E-5	7.137E-5	7.289E-5	7.425E-5
	0.8403	6.542E-5	6.810E-5	6.924E-5				
	0.9428	6.054E-5	6.274E-5	6.365E-5				
	0.9983	5.176E-5	5.364E-5	5.441E-5				
	0.0381			1.986E-4	1.985E-4	1.983E-4	1.984E-4	1.984E-4
	0.1775			1.852E-4	1.851E-4	1.848E-4	1.847E-4	1.846E-4
	0.4563			1.713E-4	1.712E-4	1.709E-4	1.707E-4	1.706E-4
Σ_{a2}	0.7351	1.620E-4	1.617E-4	1.616E-4	1.615E-4	1.612E-4	1.610E-4	1.609E-4
	0.8403	1.494E-4	1.491E-4	1.490E-4				
	0.9428	1.350E-4	1.350E-4	1.350E-4				
	0.9983	1.271E-4	1.274E-4	1.276E-4				
	0.0381			7.599E-5	7.602E-5	7.607E-5	7.612E-5	7.615E-5
	0.1775			7.550E-5	7.553E-5	7.558E-5	7.563E-5	7.567E-5
	0.4563			7.461E-5	7.464E-5	7.470E-5	7.475E-5	7.479E-5
$\nu\Sigma_{f1}$	0.7351	7.351E-5	7.363E-5	7.368E-5	7.371E-5	7.377E-5	7.383E-5	7.387E-5
	0.8403	7.103E-5	7.121E-5	7.128E-5				
	0.9428	6.919E-5	6.955E-5	6.970E-5				
	0.9983	7.517E-5	7.642E-5	7.692E-5				
	0.0381			1.888E-4	1.881E-4	1.865E-4	1.850E-4	1.838E-4
	0.1775			1.698E-4	1.692E-4	1.679E-4	1.667E-4	1.657E-4
	0.4563			1.543E-4	1.538E-4	1.527E-4	1.517E-4	1.508E-4
$\nu\Sigma_{f2}$	0.7351	1.474E-4	1.460E-4	1.453E-4	1.449E-4	1.439E-4	1.430E-4	1.421E-4
	0.8403	1.426E-4	1.410E-4	1.403E-4				
	0.9428	1.347E-4	1.328E-4	1.319E-4				
	0.9983	1.280E-4	1.257E-4	1.246E-4				
	0.0381			3.004E-4	3.001E-4	2.997E-4	2.994E-4	2.992E-4
	0.1775			2.872E-4	2.870E-4	2.866E-4	2.864E-4	2.862E-4
	0.4563			2.621E-4	2.619E-4	2.617E-4	2.615E-4	2.614E-4
Σ_{12}	0.7351	2.370E-4	2.363E-4	2.360E-4	2.359E-4	2.357E-4	2.356E-4	2.356E-4
	0.8403	1.658E-4	1.652E-4	1.651E-4				
	0.9428	9.512E-5	9.487E-5	9.481E-5				
	0.9983	6.290E-5	6.304E-5	6.314E-5				

Table C.21 – Standard deviation statistics for segment 10 and control rods inserted.

	$\mathbf{D_{mod}}$	$\mathbf{T_{fuel}}$ **(K)**						
	(kg/m^3)	293.0	660.8	853.5	1028.6	1396.5	1764.3	2132.2
	0.0381			3.255E-2	3.256E-2	3.259E-2	3.261E-2	3.262E-2
	0.1775			3.342E-2	3.343E-2	3.346E-2	3.348E-2	3.350E-2
	0.4563			3.514E-2	3.516E-2	3.518E-2	3.521E-2	3.523E-2
D_{f1}	0.7351	3.702E-2	3.708E-2	3.711E-2	3.712E-2	3.715E-2	3.718E-2	3.720E-2
	0.8403	4.336E-2	4.345E-2	4.349E-2				
	0.9428	5.178E-2	5.194E-2	5.200E-2				
	0.9983	5.676E-2	5.701E-2	5.710E-2				
	0.0381			7.258E-4	7.247E-4	7.218E-4	7.190E-4	7.162E-4
	0.1775			7.944E-4	7.933E-4	7.908E-4	7.883E-4	7.858E-4
	0.4563			9.090E-4	9.080E-4	9.056E-4	9.032E-4	9.009E-4
D_{f2}	0.7351	1.041E-3	1.039E-3	1.037E-3	1.036E-3	1.034E-3	1.032E-3	1.029E-3
	0.8403	1.474E-3	1.470E-3	1.469E-3				
	0.9428	2.369E-3	2.364E-3	2.361E-3				
	0.9983	3.214E-3	3.208E-3	3.204E-3				
	0.0381			6.355E-5	6.444E-5	6.624E-5	6.786E-5	6.930E-5
	0.1775			6.336E-5	6.424E-5	6.603E-5	6.762E-5	6.905E-5
	0.4563			6.290E-5	6.376E-5	6.552E-5	6.708E-5	6.848E-5
Σ_{a1}	0.7351	5.796E-5	6.098E-5	6.226E-5	6.310E-5	6.481E-5	6.633E-5	6.770E-5
	0.8403	5.525E-5	5.804E-5	5.921E-5				
	0.9428	4.832E-5	5.065E-5	5.161E-5				
	0.9983	4.049E-5	4.240E-5	4.317E-5				
	0.0381			1.680E-4	1.681E-4	1.686E-4	1.692E-4	1.699E-4
	0.1775			1.596E-4	1.597E-4	1.600E-4	1.604E-4	1.608E-4
	0.4563			1.496E-4	1.496E-4	1.499E-4	1.502E-4	1.505E-4
Σ_{a2}	0.7351	1.419E-4	1.420E-4	1.421E-4	1.421E-4	1.423E-4	1.426E-4	1.429E-4
	0.8403	1.291E-4	1.294E-4	1.296E-4				
	0.9428	1.191E-4	1.197E-4	1.201E-4				
	0.9983	1.175E-4	1.181E-4	1.186E-4				
	0.0381			5.612E-5	5.615E-5	5.620E-5	5.625E-5	5.629E-5
	0.1775			5.572E-5	5.574E-5	5.579E-5	5.584E-5	5.589E-5
	0.4563			5.498E-5	5.501E-5	5.507E-5	5.512E-5	5.517E-5
$\nu\Sigma_{f1}$	0.7351	5.408E-5	5.418E-5	5.422E-5	5.425E-5	5.431E-5	5.437E-5	5.442E-5
	0.8403	5.212E-5	5.226E-5	5.233E-5				
	0.9428	5.082E-5	5.108E-5	5.118E-5				
	0.9983	5.260E-5	5.315E-5	5.338E-5				
	0.0381			4.354E-4	4.345E-4	4.324E-4	4.306E-4	4.290E-4
	0.1775			4.066E-4	4.058E-4	4.041E-4	4.026E-4	4.011E-4
	0.4563			3.808E-4	3.802E-4	3.787E-4	3.774E-4	3.761E-4
$\nu\Sigma_{f2}$	0.7351	3.678E-4	3.660E-4	3.651E-4	3.645E-4	3.632E-4	3.620E-4	3.609E-4
	0.8403	3.567E-4	3.549E-4	3.540E-4				
	0.9428	3.419E-4	3.403E-4	3.394E-4				
	0.9983	3.327E-4	3.309E-4	3.299E-4				
	0.0381			3.128E-4	3.125E-4	3.121E-4	3.117E-4	3.114E-4
	0.1775			3.002E-4	3.000E-4	2.995E-4	2.992E-4	2.989E-4
	0.4563			2.763E-4	2.761E-4	2.757E-4	2.754E-4	2.751E-4
Σ_{12}	0.7351	2.528E-4	2.519E-4	2.516E-4	2.514E-4	2.511E-4	2.508E-4	2.506E-4
	0.8403	1.859E-4	1.852E-4	1.850E-4				
	0.9428	1.189E-4	1.185E-4	1.183E-4				
	0.9983	8.582E-5	8.569E-5	8.567E-5				

Table C.22 – Standard deviation statistics for segment 11 and control rods withdrawn.

	$\mathbf{D_{mod}}$	$\mathbf{T_{fuel}}$ (K)						
	($\mathbf{kg/m^3}$)	293.0	660.8	853.5	1028.6	1396.5	1764.3	2132.2
	0.0381			3.101E-2	3.102E-2	3.104E-2	3.106E-2	3.108E-2
	0.1775			3.180E-2	3.181E-2	3.183E-2	3.185E-2	3.187E-2
	0.4563			3.334E-2	3.335E-2	3.338E-2	3.340E-2	3.342E-2
D_{f1}	0.7351	3.500E-2	3.506E-2	3.508E-2	3.510E-2	3.513E-2	3.515E-2	3.518E-2
	0.8403	4.055E-2	4.064E-2	4.067E-2				
	0.9428	4.766E-2	4.779E-2	4.785E-2				
	0.9983	5.158E-2	5.179E-2	5.187E-2				
	0.0381			7.312E-4	7.300E-4	7.271E-4	7.241E-4	7.212E-4
	0.1775			8.012E-4	8.002E-4	7.975E-4	7.949E-4	7.923E-4
	0.4563			9.188E-4	9.177E-4	9.153E-4	9.128E-4	9.105E-4
D_{f2}	0.7351	1.055E-3	1.052E-3	1.050E-3	1.049E-3	1.047E-3	1.045E-3	1.042E-3
	0.8403	1.500E-3	1.497E-3	1.495E-3				
	0.9428	2.389E-3	2.385E-3	2.382E-3				
	0.9983	3.169E-3	3.162E-3	3.158E-3				
	0.0381			8.096E-5	8.182E-5	8.356E-5	8.512E-5	8.651E-5
	0.1775			8.124E-5	8.209E-5	8.381E-5	8.535E-5	8.673E-5
	0.4563			8.183E-5	8.266E-5	8.434E-5	8.584E-5	8.718E-5
Σ_{a1}	0.7351	7.826E-5	8.111E-5	8.232E-5	8.312E-5	8.474E-5	8.619E-5	8.749E-5
	0.8403	7.832E-5	8.088E-5	8.196E-5				
	0.9428	7.126E-5	7.331E-5	7.415E-5				
	0.9983	5.982E-5	6.144E-5	6.209E-5				
	0.0381			1.852E-4	1.856E-4	1.865E-4	1.875E-4	1.886E-4
	0.1775			1.763E-4	1.766E-4	1.773E-4	1.780E-4	1.788E-4
	0.4563			1.652E-4	1.654E-4	1.660E-4	1.666E-4	1.672E-4
Σ_{a2}	0.7351	1.559E-4	1.564E-4	1.566E-4	1.568E-4	1.573E-4	1.578E-4	1.584E-4
	0.8403	1.404E-4	1.410E-4	1.413E-4				
	0.9428	1.281E-4	1.291E-4	1.296E-4				
	0.9983	1.259E-4	1.270E-4	1.277E-4				
	0.0381			5.541E-5	5.544E-5	5.549E-5	5.554E-5	5.558E-5
	0.1775			5.501E-5	5.503E-5	5.508E-5	5.513E-5	5.518E-5
	0.4563			5.427E-5	5.430E-5	5.435E-5	5.441E-5	5.445E-5
$\nu\Sigma_{f1}$	0.7351	5.337E-5	5.347E-5	5.351E-5	5.354E-5	5.360E-5	5.366E-5	5.371E-5
	0.8403	5.145E-5	5.159E-5	5.165E-5				
	0.9428	5.047E-5	5.074E-5	5.085E-5				
	0.9983	5.274E-5	5.328E-5	5.350E-5				
	0.0381			4.684E-4	4.674E-4	4.652E-4	4.632E-4	4.614E-4
	0.1775			4.367E-4	4.359E-4	4.340E-4	4.323E-4	4.308E-4
	0.4563			4.074E-4	4.068E-4	4.052E-4	4.037E-4	4.023E-4
$\nu\Sigma_{f2}$	0.7351	3.915E-4	3.895E-4	3.886E-4	3.879E-4	3.865E-4	3.851E-4	3.838E-4
	0.8403	3.716E-4	3.696E-4	3.687E-4				
	0.9428	3.438E-4	3.421E-4	3.412E-4				
	0.9983	3.274E-4	3.256E-4	3.246E-4				
	0.0381			2.912E-4	2.910E-4	2.906E-4	2.902E-4	2.899E-4
	0.1775			2.779E-4	2.777E-4	2.772E-4	2.769E-4	2.766E-4
	0.4563			2.525E-4	2.522E-4	2.519E-4	2.515E-4	2.513E-4
Σ_{12}	0.7351	2.271E-4	2.264E-4	2.261E-4	2.259E-4	2.255E-4	2.252E-4	2.251E-4
	0.8403	1.562E-4	1.556E-4	1.553E-4				
	0.9428	8.749E-5	8.710E-5	8.697E-5				
	0.9983	5.617E-5	5.602E-5	5.598E-5				

Table C.23 – Standard deviation statistics for segment 11 and control rods inserted.

	$\mathbf{D_{mod}}$	$\mathbf{T_{fuel}}$ **(K)**						
	(kg/m^3)	293.0	660.8	853.5	1028.6	1396.5	1764.3	2132.2
	0.0381			3.253E-2	3.254E-2	3.256E-2	3.258E-2	3.260E-2
	0.1775			3.340E-2	3.341E-2	3.343E-2	3.345E-2	3.347E-2
	0.4563			3.512E-2	3.513E-2	3.516E-2	3.518E-2	3.520E-2
D_{f1}	0.7351	3.699E-2	3.705E-2	3.708E-2	3.710E-2	3.713E-2	3.715E-2	3.718E-2
	0.8403	4.333E-2	4.343E-2	4.347E-2				
	0.9428	5.177E-2	5.193E-2	5.199E-2				
	0.9983	5.675E-2	5.699E-2	5.709E-2				
	0.0381			7.283E-4	7.273E-4	7.247E-4	7.221E-4	7.196E-4
	0.1775			7.949E-4	7.939E-4	7.915E-4	7.892E-4	7.870E-4
	0.4563			9.071E-4	9.063E-4	9.040E-4	9.019E-4	8.998E-4
D_{f2}	0.7351	1.037E-3	1.035E-3	1.034E-3	1.033E-3	1.030E-3	1.028E-3	1.026E-3
	0.8403	1.466E-3	1.463E-3	1.461E-3				
	0.9428	2.348E-3	2.344E-3	2.341E-3				
	0.9983	3.172E-3	3.167E-3	3.163E-3				
	0.0381			6.529E-5	6.618E-5	6.799E-5	6.960E-5	7.104E-5
	0.1775			6.508E-5	6.596E-5	6.774E-5	6.933E-5	7.076E-5
	0.4563			6.456E-5	6.542E-5	6.718E-5	6.873E-5	7.013E-5
Σ_{a1}	0.7351	5.957E-5	6.258E-5	6.386E-5	6.470E-5	6.640E-5	6.792E-5	6.928E-5
	0.8403	5.672E-5	5.949E-5	6.066E-5				
	0.9428	4.960E-5	5.192E-5	5.288E-5				
	0.9983	4.161E-5	4.351E-5	4.428E-5				
	0.0381			1.668E-4	1.670E-4	1.675E-4	1.681E-4	1.688E-4
	0.1775			1.589E-4	1.590E-4	1.594E-4	1.598E-4	1.603E-4
	0.4563			1.497E-4	1.498E-4	1.501E-4	1.504E-4	1.508E-4
Σ_{a2}	0.7351	1.427E-4	1.429E-4	1.430E-4	1.431E-4	1.434E-4	1.438E-4	1.442E-4
	0.8403	1.312E-4	1.316E-4	1.319E-4				
	0.9428	1.240E-4	1.247E-4	1.251E-4				
	0.9983	1.250E-4	1.258E-4	1.263E-4				
	0.0381			5.426E-5	5.428E-5	5.433E-5	5.438E-5	5.442E-5
	0.1775			5.388E-5	5.390E-5	5.395E-5	5.400E-5	5.404E-5
	0.4563			5.318E-5	5.321E-5	5.326E-5	5.332E-5	5.336E-5
$\nu\Sigma_{f1}$	0.7351	5.233E-5	5.242E-5	5.246E-5	5.249E-5	5.255E-5	5.261E-5	5.266E-5
	0.8403	5.046E-5	5.060E-5	5.066E-5				
	0.9428	4.924E-5	4.950E-5	4.960E-5				
	0.9983	5.096E-5	5.147E-5	5.168E-5				
	0.0381			4.523E-4	4.514E-4	4.494E-4	4.476E-4	4.459E-4
	0.1775			4.236E-4	4.229E-4	4.212E-4	4.196E-4	4.182E-4
	0.4563			3.975E-4	3.969E-4	3.954E-4	3.941E-4	3.929E-4
$\nu\Sigma_{f2}$	0.7351	3.839E-4	3.821E-4	3.813E-4	3.807E-4	3.794E-4	3.782E-4	3.770E-4
	0.8403	3.707E-4	3.690E-4	3.681E-4				
	0.9428	3.537E-4	3.522E-4	3.514E-4				
	0.9983	3.436E-4	3.419E-4	3.410E-4				
	0.0381			3.113E-4	3.111E-4	3.106E-4	3.102E-4	3.099E-4
	0.1775			2.987E-4	2.984E-4	2.980E-4	2.976E-4	2.973E-4
	0.4563			2.748E-4	2.746E-4	2.742E-4	2.738E-4	2.736E-4
Σ_{12}	0.7351	2.512E-4	2.504E-4	2.501E-4	2.498E-4	2.495E-4	2.492E-4	2.490E-4
	0.8403	1.845E-4	1.838E-4	1.835E-4				
	0.9428	1.177E-4	1.173E-4	1.172E-4				
	0.9983	8.484E-5	8.469E-5	8.468E-5				

Table C.24 – Standard deviation statistics for segment 12 and control rods withdrawn.

	$\mathbf{D_{mod}}$	$\mathbf{T_{fuel}}$ (K)						
	($\mathbf{kg/m^3}$)	293.0	660.8	853.5	1028.6	1396.5	1764.3	2132.2
	0.0381			3.095E-2	3.096E-2	3.098E-2	3.100E-2	3.102E-2
	0.1775			3.173E-2	3.175E-2	3.177E-2	3.179E-2	3.180E-2
	0.4563			3.328E-2	3.329E-2	3.331E-2	3.334E-2	3.335E-2
D_{f1}	0.7351	3.494E-2	3.500E-2	3.502E-2	3.503E-2	3.506E-2	3.509E-2	3.511E-2
	0.8403	4.048E-2	4.057E-2	4.060E-2				
	0.9428	4.760E-2	4.774E-2	4.780E-2				
	0.9983	5.153E-2	5.173E-2	5.181E-2				
	0.0381			7.344E-4	7.333E-4	7.307E-4	7.279E-4	7.254E-4
	0.1775			8.020E-4	8.010E-4	7.986E-4	7.962E-4	7.939E-4
	0.4563			9.167E-4	9.158E-4	9.136E-4	9.114E-4	9.092E-4
D_{f2}	0.7351	1.050E-3	1.047E-3	1.046E-3	1.045E-3	1.043E-3	1.041E-3	1.039E-3
	0.8403	1.490E-3	1.487E-3	1.486E-3				
	0.9428	2.362E-3	2.358E-3	2.356E-3				
	0.9983	3.114E-3	3.108E-3	3.105E-3				
	0.0381			8.517E-5	8.602E-5	8.777E-5	8.932E-5	9.071E-5
	0.1775			8.533E-5	8.618E-5	8.789E-5	8.942E-5	9.079E-5
	0.4563			8.557E-5	8.639E-5	8.806E-5	8.955E-5	9.088E-5
Σ_{a1}	0.7351	8.161E-5	8.445E-5	8.566E-5	8.646E-5	8.807E-5	8.951E-5	9.081E-5
	0.8403	8.060E-5	8.316E-5	8.424E-5				
	0.9428	7.264E-5	7.468E-5	7.552E-5				
	0.9983	6.079E-5	6.241E-5	6.305E-5				
	0.0381			1.801E-4	1.804E-4	1.813E-4	1.822E-4	1.832E-4
	0.1775			1.723E-4	1.725E-4	1.732E-4	1.739E-4	1.747E-4
	0.4563			1.633E-4	1.635E-4	1.641E-4	1.647E-4	1.654E-4
Σ_{a2}	0.7351	1.561E-4	1.566E-4	1.569E-4	1.571E-4	1.576E-4	1.582E-4	1.589E-4
	0.8403	1.440E-4	1.447E-4	1.450E-4				
	0.9428	1.362E-4	1.372E-4	1.378E-4				
	0.9983	1.372E-4	1.384E-4	1.391E-4				
	0.0381			5.356E-5	5.359E-5	5.363E-5	5.368E-5	5.372E-5
	0.1775			5.318E-5	5.321E-5	5.326E-5	5.331E-5	5.335E-5
	0.4563			5.250E-5	5.253E-5	5.259E-5	5.264E-5	5.269E-5
$\nu\Sigma_{f1}$	0.7351	5.167E-5	5.176E-5	5.179E-5	5.183E-5	5.189E-5	5.194E-5	5.200E-5
	0.8403	4.986E-5	5.000E-5	5.006E-5				
	0.9428	4.901E-5	4.927E-5	4.938E-5				
	0.9983	5.128E-5	5.179E-5	5.200E-5				
	0.0381			4.862E-4	4.852E-4	4.830E-4	4.810E-4	4.792E-4
	0.1775			4.546E-4	4.538E-4	4.519E-4	4.502E-4	4.486E-4
	0.4563			4.246E-4	4.239E-4	4.222E-4	4.208E-4	4.194E-4
$\nu\Sigma_{f2}$	0.7351	4.076E-4	4.056E-4	4.047E-4	4.040E-4	4.026E-4	4.012E-4	4.000E-4
	0.8403	3.837E-4	3.819E-4	3.810E-4				
	0.9428	3.515E-4	3.500E-4	3.492E-4				
	0.9983	3.333E-4	3.317E-4	3.308E-4				
	0.0381			2.867E-4	2.865E-4	2.860E-4	2.856E-4	2.853E-4
	0.1775			2.734E-4	2.732E-4	2.727E-4	2.724E-4	2.721E-4
	0.4563			2.483E-4	2.480E-4	2.476E-4	2.473E-4	2.470E-4
Σ_{12}	0.7351	2.233E-4	2.225E-4	2.222E-4	2.220E-4	2.217E-4	2.214E-4	2.212E-4
	0.8403	1.536E-4	1.529E-4	1.527E-4				
	0.9428	8.612E-5	8.573E-5	8.559E-5				
	0.9983	5.532E-5	5.516E-5	5.511E-5				

Table C.25 – Standard deviation statistics for segment 12 and control rods inserted.

	$\mathbf{D_{mod}}$	$\mathbf{T_{fuel}}$ (K)						
	$\mathbf{(kg/m^3)}$	293.0	660.8	853.5	1028.6	1396.5	1764.3	2132.2
	0.0381			3.251E-2	3.252E-2	3.255E-2	3.257E-2	3.258E-2
	0.1775			3.337E-2	3.339E-2	3.341E-2	3.343E-2	3.345E-2
	0.4563			3.509E-2	3.510E-2	3.513E-2	3.516E-2	3.518E-2
D_{f1}	0.7351	3.696E-2	3.702E-2	3.704E-2	3.706E-2	3.709E-2	3.712E-2	3.714E-2
	0.8403	4.325E-2	4.334E-2	4.338E-2				
	0.9428	5.158E-2	5.174E-2	5.180E-2				
	0.9983	5.648E-2	5.673E-2	5.681E-2				
	0.0381			7.270E-4	7.256E-4	7.228E-4	7.200E-4	7.174E-4
	0.1775			7.953E-4	7.940E-4	7.915E-4	7.890E-4	7.865E-4
	0.4563			9.097E-4	9.085E-4	9.061E-4	9.037E-4	9.014E-4
D_{f2}	0.7351	1.041E-3	1.039E-3	1.037E-3	1.036E-3	1.034E-3	1.032E-3	1.029E-3
	0.8403	1.472E-3	1.469E-3	1.467E-3				
	0.9428	2.361E-3	2.356E-3	2.353E-3				
	0.9983	3.195E-3	3.189E-3	3.185E-3				
	0.0381			6.437E-5	6.540E-5	6.723E-5	6.886E-5	7.032E-5
	0.1775			6.418E-5	6.520E-5	6.701E-5	6.862E-5	7.007E-5
	0.4563			6.372E-5	6.473E-5	6.650E-5	6.808E-5	6.950E-5
Σ_{a1}	0.7351	5.886E-5	6.192E-5	6.309E-5	6.407E-5	6.580E-5	6.734E-5	6.872E-5
	0.8403	5.612E-5	5.895E-5	6.002E-5				
	0.9428	4.908E-5	5.143E-5	5.231E-5				
	0.9983	4.109E-5	4.303E-5	4.374E-5				
	0.0381			1.687E-4	1.689E-4	1.694E-4	1.700E-4	1.707E-4
	0.1775			1.604E-4	1.605E-4	1.609E-4	1.612E-4	1.617E-4
	0.4563			1.504E-4	1.505E-4	1.507E-4	1.510E-4	1.514E-4
Σ_{a2}	0.7351	1.427E-4	1.428E-4	1.429E-4	1.430E-4	1.432E-4	1.435E-4	1.438E-4
	0.8403	1.299E-4	1.302E-4	1.304E-4				
	0.9428	1.198E-4	1.205E-4	1.208E-4				
	0.9983	1.182E-4	1.189E-4	1.193E-4				
	0.0381			5.717E-5	5.720E-5	5.725E-5	5.730E-5	5.734E-5
	0.1775			5.676E-5	5.679E-5	5.684E-5	5.689E-5	5.694E-5
	0.4563			5.601E-5	5.605E-5	5.610E-5	5.616E-5	5.621E-5
$\nu\Sigma_{f1}$	0.7351	5.511E-5	5.521E-5	5.525E-5	5.528E-5	5.535E-5	5.540E-5	5.546E-5
	0.8403	5.315E-5	5.330E-5	5.335E-5				
	0.9428	5.191E-5	5.219E-5	5.229E-5				
	0.9983	5.381E-5	5.438E-5	5.459E-5				
	0.0381			4.409E-4	4.397E-4	4.377E-4	4.359E-4	4.343E-4
	0.1775			4.119E-4	4.110E-4	4.092E-4	4.077E-4	4.062E-4
	0.4563			3.860E-4	3.852E-4	3.837E-4	3.823E-4	3.811E-4
$\nu\Sigma_{f2}$	0.7351	3.727E-4	3.708E-4	3.700E-4	3.693E-4	3.680E-4	3.668E-4	3.656E-4
	0.8403	3.613E-4	3.595E-4	3.587E-4				
	0.9428	3.462E-4	3.446E-4	3.438E-4				
	0.9983	3.370E-4	3.351E-4	3.342E-4				
	0.0381			3.136E-4	3.133E-4	3.128E-4	3.124E-4	3.121E-4
	0.1775			3.010E-4	3.007E-4	3.003E-4	2.999E-4	2.996E-4
	0.4563			2.771E-4	2.768E-4	2.764E-4	2.761E-4	2.759E-4
Σ_{12}	0.7351	2.535E-4	2.527E-4	2.524E-4	2.522E-4	2.518E-4	2.516E-4	2.514E-4
	0.8403	1.865E-4	1.858E-4	1.856E-4				
	0.9428	1.193E-4	1.189E-4	1.188E-4				
	0.9983	8.609E-5	8.597E-5	8.596E-5				

Table C.26 – Standard deviation statistics for segment 13 and control rods withdrawn.

	$\mathbf{D_{mod}}$	$\mathbf{T_{fuel}}$ (K)						
	($\mathbf{kg/m^3}$)	293.0	660.8	853.5	1028.6	1396.5	1764.3	2132.2
	0.0381			3.098E-2	3.100E-2	3.102E-2	3.104E-2	3.105E-2
	0.1775			3.176E-2	3.178E-2	3.180E-2	3.182E-2	3.184E-2
	0.4563			3.330E-2	3.332E-2	3.334E-2	3.337E-2	3.339E-2
D_{f1}	0.7351	3.496E-2	3.502E-2	3.504E-2	3.506E-2	3.509E-2	3.511E-2	3.514E-2
	0.8403	4.047E-2	4.056E-2	4.059E-2				
	0.9428	4.750E-2	4.764E-2	4.769E-2				
	0.9983	5.136E-2	5.157E-2	5.164E-2				
	0.0381			7.324E-4	7.310E-4	7.280E-4	7.251E-4	7.223E-4
	0.1775			8.021E-4	8.008E-4	7.982E-4	7.956E-4	7.930E-4
	0.4563			9.194E-4	9.181E-4	9.157E-4	9.132E-4	9.109E-4
D_{f2}	0.7351	1.055E-3	1.052E-3	1.051E-3	1.049E-3	1.047E-3	1.045E-3	1.042E-3
	0.8403	1.498E-3	1.495E-3	1.493E-3				
	0.9428	2.381E-3	2.376E-3	2.374E-3				
	0.9983	3.150E-3	3.143E-3	3.140E-3				
	0.0381			8.181E-5	8.280E-5	8.456E-5	8.614E-5	8.755E-5
	0.1775			8.211E-5	8.309E-5	8.483E-5	8.639E-5	8.778E-5
	0.4563			8.270E-5	8.366E-5	8.536E-5	8.687E-5	8.823E-5
Σ_{a1}	0.7351	7.920E-5	8.209E-5	8.320E-5	8.414E-5	8.578E-5	8.724E-5	8.856E-5
	0.8403	7.925E-5	8.186E-5	8.285E-5				
	0.9428	7.207E-5	7.415E-5	7.493E-5				
	0.9983	6.045E-5	6.208E-5	6.269E-5				
	0.0381			1.861E-4	1.866E-4	1.876E-4	1.886E-4	1.897E-4
	0.1775			1.773E-4	1.776E-4	1.783E-4	1.791E-4	1.799E-4
	0.4563			1.662E-4	1.665E-4	1.671E-4	1.677E-4	1.683E-4
Σ_{a2}	0.7351	1.569E-4	1.574E-4	1.576E-4	1.578E-4	1.583E-4	1.589E-4	1.595E-4
	0.8403	1.413E-4	1.419E-4	1.422E-4				
	0.9428	1.289E-4	1.299E-4	1.304E-4				
	0.9983	1.266E-4	1.278E-4	1.284E-4				
	0.0381			5.645E-5	5.647E-5	5.653E-5	5.657E-5	5.662E-5
	0.1775			5.603E-5	5.606E-5	5.611E-5	5.616E-5	5.621E-5
	0.4563			5.529E-5	5.532E-5	5.538E-5	5.543E-5	5.548E-5
$\nu\Sigma_{f1}$	0.7351	5.438E-5	5.448E-5	5.452E-5	5.456E-5	5.462E-5	5.468E-5	5.474E-5
	0.8403	5.247E-5	5.261E-5	5.267E-5				
	0.9428	5.156E-5	5.184E-5	5.194E-5				
	0.9983	5.394E-5	5.451E-5	5.471E-5				
	0.0381			4.744E-4	4.732E-4	4.710E-4	4.690E-4	4.671E-4
	0.1775			4.425E-4	4.415E-4	4.396E-4	4.379E-4	4.363E-4
	0.4563			4.130E-4	4.121E-4	4.105E-4	4.090E-4	4.076E-4
$\nu\Sigma_{f2}$	0.7351	3.968E-4	3.948E-4	3.939E-4	3.931E-4	3.916E-4	3.902E-4	3.890E-4
	0.8403	3.764E-4	3.745E-4	3.736E-4				
	0.9428	3.482E-4	3.465E-4	3.457E-4				
	0.9983	3.317E-4	3.298E-4	3.289E-4				
	0.0381			2.921E-4	2.918E-4	2.913E-4	2.910E-4	2.907E-4
	0.1775			2.787E-4	2.784E-4	2.780E-4	2.777E-4	2.774E-4
	0.4563			2.533E-4	2.530E-4	2.526E-4	2.523E-4	2.521E-4
Σ_{12}	0.7351	2.279E-4	2.271E-4	2.268E-4	2.266E-4	2.263E-4	2.260E-4	2.258E-4
	0.8403	1.568E-4	1.562E-4	1.559E-4				
	0.9428	8.784E-5	8.745E-5	8.733E-5				
	0.9983	5.642E-5	5.626E-5	5.623E-5				

Table C.27 – Standard deviation statistics for segment 13 and control rods inserted.

	$\mathbf{D_{mod}}$	$\mathbf{T_{fuel}}$ **(K)**						
	(kg/m^3)	293.0	660.8	853.5	1028.6	1396.5	1764.3	2132.2
	0.0381			3.248E-2	3.250E-2	3.252E-2	3.254E-2	3.256E-2
	0.1775			3.335E-2	3.336E-2	3.339E-2	3.341E-2	3.343E-2
	0.4563			3.506E-2	3.508E-2	3.511E-2	3.513E-2	3.515E-2
D_{f1}	0.7351	3.693E-2	3.699E-2	3.702E-2	3.704E-2	3.707E-2	3.709E-2	3.712E-2
	0.8403	4.323E-2	4.332E-2	4.336E-2				
	0.9428	5.157E-2	5.173E-2	5.179E-2				
	0.9983	5.647E-2	5.671E-2	5.680E-2				
	0.0381			7.294E-4	7.282E-4	7.256E-4	7.229E-4	7.205E-4
	0.1775			7.957E-4	7.945E-4	7.922E-4	7.899E-4	7.876E-4
	0.4563			9.076E-4	9.065E-4	9.044E-4	9.022E-4	9.001E-4
D_{f2}	0.7351	1.037E-3	1.035E-3	1.033E-3	1.032E-3	1.030E-3	1.028E-3	1.026E-3
	0.8403	1.464E-3	1.461E-3	1.459E-3				
	0.9428	2.339E-3	2.335E-3	2.332E-3				
	0.9983	3.153E-3	3.147E-3	3.144E-3				
	0.0381			6.614E-5	6.718E-5	6.900E-5	7.063E-5	7.209E-5
	0.1775			6.593E-5	6.696E-5	6.876E-5	7.037E-5	7.181E-5
	0.4563			6.542E-5	6.642E-5	6.819E-5	6.976E-5	7.118E-5
Σ_{a1}	0.7351	6.050E-5	6.356E-5	6.472E-5	6.570E-5	6.743E-5	6.896E-5	7.033E-5
	0.8403	5.762E-5	6.044E-5	6.151E-5				
	0.9428	5.039E-5	5.274E-5	5.361E-5				
	0.9983	4.225E-5	4.417E-5	4.487E-5				
	0.0381			1.675E-4	1.678E-4	1.683E-4	1.690E-4	1.697E-4
	0.1775			1.597E-4	1.598E-4	1.602E-4	1.607E-4	1.612E-4
	0.4563			1.505E-4	1.506E-4	1.509E-4	1.513E-4	1.517E-4
Σ_{a2}	0.7351	1.434E-4	1.436E-4	1.438E-4	1.439E-4	1.442E-4	1.446E-4	1.450E-4
	0.8403	1.320E-4	1.324E-4	1.326E-4				
	0.9428	1.246E-4	1.254E-4	1.257E-4				
	0.9983	1.257E-4	1.265E-4	1.269E-4				
	0.0381			5.526E-5	5.529E-5	5.534E-5	5.539E-5	5.543E-5
	0.1775			5.488E-5	5.490E-5	5.495E-5	5.500E-5	5.505E-5
	0.4563			5.418E-5	5.421E-5	5.426E-5	5.432E-5	5.437E-5
$\nu\Sigma_{f1}$	0.7351	5.332E-5	5.341E-5	5.345E-5	5.349E-5	5.355E-5	5.360E-5	5.366E-5
	0.8403	5.145E-5	5.159E-5	5.165E-5				
	0.9428	5.029E-5	5.056E-5	5.066E-5				
	0.9983	5.212E-5	5.266E-5	5.285E-5				
	0.0381			4.579E-4	4.568E-4	4.547E-4	4.529E-4	4.513E-4
	0.1775			4.291E-4	4.281E-4	4.264E-4	4.248E-4	4.234E-4
	0.4563			4.027E-4	4.019E-4	4.005E-4	3.991E-4	3.979E-4
$\nu\Sigma_{f2}$	0.7351	3.889E-4	3.871E-4	3.863E-4	3.856E-4	3.843E-4	3.830E-4	3.819E-4
	0.8403	3.754E-4	3.736E-4	3.729E-4				
	0.9428	3.581E-4	3.566E-4	3.559E-4				
	0.9983	3.479E-4	3.462E-4	3.454E-4				
	0.0381			3.121E-4	3.118E-4	3.113E-4	3.109E-4	3.106E-4
	0.1775			2.995E-4	2.992E-4	2.987E-4	2.983E-4	2.980E-4
	0.4563			2.756E-4	2.753E-4	2.749E-4	2.745E-4	2.743E-4
Σ_{12}	0.7351	2.520E-4	2.511E-4	2.508E-4	2.506E-4	2.502E-4	2.499E-4	2.497E-4
	0.8403	1.851E-4	1.844E-4	1.842E-4				
	0.9428	1.182E-4	1.177E-4	1.176E-4				
	0.9983	8.519E-5	8.499E-5	8.496E-5				

Table C.28 – Standard deviation statistics for segment 14 and control rods withdrawn.

	$\mathbf{D_{mod}}$	$\mathbf{T_{fuel}}$ (K)						
	($\mathbf{kg/m^3}$)	293.0	660.8	853.5	1028.6	1396.5	1764.3	2132.2
	0.0381			3.092E-2	3.094E-2	3.096E-2	3.098E-2	3.099E-2
	0.1775			3.170E-2	3.172E-2	3.174E-2	3.176E-2	3.178E-2
	0.4563			3.324E-2	3.325E-2	3.328E-2	3.330E-2	3.332E-2
D_{f1}	0.7351	3.490E-2	3.495E-2	3.498E-2	3.499E-2	3.502E-2	3.505E-2	3.507E-2
	0.8403	4.041E-2	4.049E-2	4.053E-2				
	0.9428	4.745E-2	4.759E-2	4.764E-2				
	0.9983	5.131E-2	5.151E-2	5.158E-2				
	0.0381			7.354E-4	7.341E-4	7.314E-4	7.288E-4	7.263E-4
	0.1775			8.027E-4	8.016E-4	7.991E-4	7.968E-4	7.944E-4
	0.4563			9.172E-4	9.161E-4	9.138E-4	9.116E-4	9.095E-4
D_{f2}	0.7351	1.050E-3	1.047E-3	1.046E-3	1.045E-3	1.043E-3	1.041E-3	1.039E-3
	0.8403	1.488E-3	1.485E-3	1.484E-3				
	0.9428	2.353E-3	2.349E-3	2.347E-3				
	0.9983	3.094E-3	3.088E-3	3.085E-3				
	0.0381			8.606E-5	8.705E-5	8.881E-5	9.038E-5	9.179E-5
	0.1775			8.623E-5	8.722E-5	8.895E-5	9.050E-5	9.189E-5
	0.4563			8.648E-5	8.744E-5	8.913E-5	9.064E-5	9.199E-5
Σ_{a1}	0.7351	8.259E-5	8.548E-5	8.658E-5	8.751E-5	8.915E-5	9.060E-5	9.191E-5
	0.8403	8.158E-5	8.418E-5	8.517E-5				
	0.9428	7.348E-5	7.555E-5	7.632E-5				
	0.9983	6.144E-5	6.308E-5	6.368E-5				
	0.0381			1.810E-4	1.814E-4	1.823E-4	1.832E-4	1.842E-4
	0.1775			1.732E-4	1.735E-4	1.742E-4	1.749E-4	1.757E-4
	0.4563			1.642E-4	1.645E-4	1.651E-4	1.657E-4	1.664E-4
Σ_{a2}	0.7351	1.570E-4	1.575E-4	1.577E-4	1.580E-4	1.586E-4	1.592E-4	1.598E-4
	0.8403	1.448E-4	1.455E-4	1.458E-4				
	0.9428	1.369E-4	1.379E-4	1.384E-4				
	0.9983	1.378E-4	1.390E-4	1.397E-4				
	0.0381			5.455E-5	5.458E-5	5.463E-5	5.468E-5	5.472E-5
	0.1775			5.417E-5	5.420E-5	5.425E-5	5.430E-5	5.435E-5
	0.4563			5.348E-5	5.351E-5	5.357E-5	5.362E-5	5.367E-5
$\nu\Sigma_{f1}$	0.7351	5.264E-5	5.273E-5	5.277E-5	5.281E-5	5.287E-5	5.293E-5	5.298E-5
	0.8403	5.084E-5	5.098E-5	5.104E-5				
	0.9428	5.007E-5	5.034E-5	5.044E-5				
	0.9983	5.245E-5	5.298E-5	5.317E-5				
	0.0381			4.923E-4	4.911E-4	4.888E-4	4.868E-4	4.850E-4
	0.1775			4.605E-4	4.595E-4	4.576E-4	4.558E-4	4.542E-4
	0.4563			4.302E-4	4.294E-4	4.277E-4	4.262E-4	4.248E-4
$\nu\Sigma_{f2}$	0.7351	4.130E-4	4.110E-4	4.101E-4	4.094E-4	4.079E-4	4.065E-4	4.052E-4
	0.8403	3.886E-4	3.868E-4	3.860E-4				
	0.9428	3.560E-4	3.544E-4	3.537E-4				
	0.9983	3.375E-4	3.359E-4	3.351E-4				
	0.0381			2.875E-4	2.872E-4	2.867E-4	2.863E-4	2.860E-4
	0.1775			2.742E-4	2.739E-4	2.735E-4	2.731E-4	2.728E-4
	0.4563			2.490E-4	2.488E-4	2.484E-4	2.480E-4	2.478E-4
Σ_{12}	0.7351	2.240E-4	2.232E-4	2.230E-4	2.227E-4	2.224E-4	2.221E-4	2.219E-4
	0.8403	1.541E-4	1.535E-4	1.533E-4				
	0.9428	8.645E-5	8.605E-5	8.593E-5				
	0.9983	5.556E-5	5.538E-5	5.535E-5				

Table C.29 – Standard deviation statistics for segment 14 and control rods inserted.

	$\mathbf{D_{mod}}$	$\mathbf{T_{fuel}}$ **(K)**						
	(kg/m^3)	293.0	660.8	853.5	1028.6	1396.5	1764.3	2132.2
	0.0381			3.261E-2	3.263E-2	3.265E-2	3.267E-2	3.269E-2
	0.1775			3.348E-2	3.349E-2	3.352E-2	3.354E-2	3.356E-2
	0.4563			3.520E-2	3.522E-2	3.524E-2	3.527E-2	3.529E-2
D_{f1}	0.7351	3.707E-2	3.713E-2	3.716E-2	3.718E-2	3.721E-2	3.724E-2	3.726E-2
	0.8403	4.335E-2	4.345E-2	4.349E-2				
	0.9428	5.156E-2	5.174E-2	5.181E-2				
	0.9983	5.709E-2	5.747E-2	5.761E-2				
	0.0381			6.846E-4	6.818E-4	6.759E-4	6.704E-4	6.654E-4
	0.1775			7.735E-4	7.710E-4	7.660E-4	7.613E-4	7.567E-4
	0.4563			9.092E-4	9.070E-4	9.023E-4	8.980E-4	8.940E-4
D_{f2}	0.7351	1.064E-3	1.059E-3	1.056E-3	1.054E-3	1.049E-3	1.045E-3	1.041E-3
	0.8403	1.532E-3	1.526E-3	1.522E-3				
	0.9428	2.562E-3	2.553E-3	2.548E-3				
	0.9983	3.631E-3	3.619E-3	3.614E-3				
	0.0381			5.204E-5	5.309E-5	5.492E-5	5.657E-5	5.805E-5
	0.1775			5.184E-5	5.287E-5	5.470E-5	5.633E-5	5.780E-5
	0.4563			5.143E-5	5.244E-5	5.424E-5	5.584E-5	5.728E-5
Σ_{a1}	0.7351	4.661E-5	4.970E-5	5.089E-5	5.188E-5	5.364E-5	5.521E-5	5.661E-5
	0.8403	4.439E-5	4.727E-5	4.836E-5				
	0.9428	3.866E-5	4.110E-5	4.201E-5				
	0.9983	3.228E-5	3.431E-5	3.506E-5				
	0.0381			1.837E-4	1.835E-4	1.832E-4	1.831E-4	1.829E-4
	0.1775			1.717E-4	1.715E-4	1.711E-4	1.708E-4	1.705E-4
	0.4563			1.594E-4	1.592E-4	1.588E-4	1.584E-4	1.581E-4
Σ_{a2}	0.7351	1.517E-4	1.511E-4	1.509E-4	1.507E-4	1.503E-4	1.500E-4	1.497E-4
	0.8403	1.420E-4	1.414E-4	1.412E-4				
	0.9428	1.315E-4	1.311E-4	1.308E-4				
	0.9983	1.250E-4	1.244E-4	1.242E-4				
	0.0381			7.827E-5	7.830E-5	7.835E-5	7.840E-5	7.844E-5
	0.1775			7.782E-5	7.785E-5	7.791E-5	7.795E-5	7.799E-5
	0.4563			7.700E-5	7.704E-5	7.710E-5	7.715E-5	7.719E-5
$\nu\Sigma_{f1}$	0.7351	7.598E-5	7.611E-5	7.616E-5	7.620E-5	7.626E-5	7.632E-5	7.636E-5
	0.8403	7.381E-5	7.399E-5	7.406E-5				
	0.9428	7.242E-5	7.281E-5	7.295E-5				
	0.9983	7.933E-5	8.069E-5	8.118E-5				
	0.0381			1.834E-4	1.825E-4	1.810E-4	1.796E-4	1.785E-4
	0.1775			1.652E-4	1.645E-4	1.633E-4	1.622E-4	1.612E-4
	0.4563			1.507E-4	1.502E-4	1.491E-4	1.482E-4	1.474E-4
$\nu\Sigma_{f2}$	0.7351	1.446E-4	1.432E-4	1.426E-4	1.421E-4	1.412E-4	1.403E-4	1.395E-4
	0.8403	1.425E-4	1.409E-4	1.403E-4				
	0.9428	1.389E-4	1.370E-4	1.361E-4				
	0.9983	1.353E-4	1.328E-4	1.318E-4				
	0.0381			3.243E-4	3.240E-4	3.236E-4	3.233E-4	3.231E-4
	0.1775			3.119E-4	3.116E-4	3.112E-4	3.110E-4	3.109E-4
	0.4563			2.882E-4	2.880E-4	2.877E-4	2.876E-4	2.876E-4
Σ_{12}	0.7351	2.647E-4	2.640E-4	2.638E-4	2.636E-4	2.634E-4	2.635E-4	2.636E-4
	0.8403	1.977E-4	1.971E-4	1.970E-4				
	0.9428	1.294E-4	1.292E-4	1.292E-4				
	0.9983	9.696E-5	9.732E-5	9.750E-5				

Table C.30 – Standard deviation statistics for segment 15 and control rods withdrawn.

	$\mathbf{D_{mod}}$	$\mathbf{T_{fuel}}$ (K)						
	($\mathbf{kg/m^3}$)	293.0	660.8	853.5	1028.6	1396.5	1764.3	2132.2
	0.0381			3.107E-2	3.108E-2	3.110E-2	3.112E-2	3.114E-2
	0.1775			3.185E-2	3.186E-2	3.189E-2	3.191E-2	3.192E-2
	0.4563			3.339E-2	3.341E-2	3.343E-2	3.345E-2	3.347E-2
D_{f1}	0.7351	3.505E-2	3.511E-2	3.513E-2	3.515E-2	3.518E-2	3.520E-2	3.523E-2
	0.8403	4.055E-2	4.064E-2	4.067E-2				
	0.9428	4.749E-2	4.765E-2	4.771E-2				
	0.9983	5.194E-2	5.227E-2	5.239E-2				
	0.0381			6.927E-4	6.896E-4	6.834E-4	6.776E-4	6.722E-4
	0.1775			7.839E-4	7.813E-4	7.760E-4	7.709E-4	7.662E-4
	0.4563			9.239E-4	9.216E-4	9.168E-4	9.123E-4	9.081E-4
D_{f2}	0.7351	1.083E-3	1.078E-3	1.075E-3	1.073E-3	1.068E-3	1.064E-3	1.060E-3
	0.8403	1.572E-3	1.565E-3	1.562E-3				
	0.9428	2.620E-3	2.611E-3	2.607E-3				
	0.9983	3.640E-3	3.627E-3	3.622E-3				
	0.0381			6.814E-5	6.917E-5	7.099E-5	7.262E-5	7.409E-5
	0.1775			6.836E-5	6.938E-5	7.118E-5	7.279E-5	7.425E-5
	0.4563			6.890E-5	6.990E-5	7.167E-5	7.325E-5	7.467E-5
Σ_{a1}	0.7351	6.531E-5	6.829E-5	6.945E-5	7.042E-5	7.214E-5	7.367E-5	7.505E-5
	0.8403	6.610E-5	6.882E-5	6.986E-5				
	0.9428	6.112E-5	6.335E-5	6.419E-5				
	0.9983	5.221E-5	5.411E-5	5.481E-5				
	0.0381			2.001E-4	2.000E-4	1.998E-4	1.999E-4	1.999E-4
	0.1775			1.867E-4	1.866E-4	1.864E-4	1.862E-4	1.861E-4
	0.4563			1.728E-4	1.727E-4	1.725E-4	1.723E-4	1.721E-4
Σ_{a2}	0.7351	1.636E-4	1.632E-4	1.631E-4	1.630E-4	1.627E-4	1.625E-4	1.624E-4
	0.8403	1.508E-4	1.505E-4	1.504E-4				
	0.9428	1.363E-4	1.363E-4	1.363E-4				
	0.9983	1.283E-4	1.286E-4	1.287E-4				
	0.0381			7.748E-5	7.751E-5	7.756E-5	7.761E-5	7.765E-5
	0.1775			7.699E-5	7.702E-5	7.708E-5	7.712E-5	7.716E-5
	0.4563			7.609E-5	7.612E-5	7.618E-5	7.624E-5	7.628E-5
$\nu\Sigma_{f1}$	0.7351	7.498E-5	7.511E-5	7.516E-5	7.520E-5	7.526E-5	7.532E-5	7.536E-5
	0.8403	7.252E-5	7.270E-5	7.277E-5				
	0.9428	7.075E-5	7.113E-5	7.127E-5				
	0.9983	7.692E-5	7.821E-5	7.867E-5				
	0.0381			1.918E-4	1.909E-4	1.892E-4	1.877E-4	1.865E-4
	0.1775			1.724E-4	1.717E-4	1.704E-4	1.692E-4	1.681E-4
	0.4563			1.567E-4	1.561E-4	1.550E-4	1.540E-4	1.531E-4
$\nu\Sigma_{f2}$	0.7351	1.497E-4	1.482E-4	1.476E-4	1.471E-4	1.461E-4	1.451E-4	1.443E-4
	0.8403	1.448E-4	1.432E-4	1.426E-4				
	0.9428	1.367E-4	1.348E-4	1.340E-4				
	0.9983	1.300E-4	1.276E-4	1.266E-4				
	0.0381			3.015E-4	3.013E-4	3.009E-4	3.006E-4	3.004E-4
	0.1775			2.884E-4	2.881E-4	2.878E-4	2.875E-4	2.874E-4
	0.4563			2.632E-4	2.630E-4	2.627E-4	2.626E-4	2.625E-4
Σ_{12}	0.7351	2.380E-4	2.373E-4	2.371E-4	2.369E-4	2.367E-4	2.367E-4	2.367E-4
	0.8403	1.666E-4	1.661E-4	1.659E-4				
	0.9428	9.562E-5	9.536E-5	9.530E-5				
	0.9983	6.325E-5	6.338E-5	6.346E-5				

Table C.31 – Standard deviation statistics for segment 15 and control rods inserted.

Appendix D

Sensitivity of neutronic parameters

Sensitivity of input parameters at core level is displayed in this appendix. The input parameters are classified according to the homogenized and collapsed cross section and neutronic composition. Sensitivity, expressed as the PRCC, is shown for the most/less sensitive input parameters in a tabulated form. Table D.1 summaries the information in this appendix.

Analysis	**Output parameter**	**Table**
Global	k_{eff}	Table D.2
	P_z	Table D.3
	N_z	Table D.4
Segment 13	k_{eff}	Table D.5
	P_z	Table D.6
	N_z	Table D.7
Reflectors	k_{eff}	Table D.8
	P_z	Table D.9
	N_z	Table D.10

Table D.1 – Summary table.

Index	Cross section	NK comp.	PRCC
1	$\nu\Sigma_{f2}$	29	9.065E-01
2	$\nu\Sigma_{f2}$	30	8.974E-01
3	$\nu\Sigma_{f2}$	31	8.771E-01
4	$\nu\Sigma_{f2}$	28	8.409E-01
5	$\nu\Sigma_{f2}$	32	8.389E-01
6	$\nu\Sigma_{f2}$	5	8.095E-01
7	Σ_{a1}	30	-8.091E-01
8	Σ_{a1}	31	-8.089E-01
9	$\nu\Sigma_{f2}$	33	8.036E-01
10	$\nu\Sigma_{f2}$	4	7.777E-01
11	$\nu\Sigma_{f1}$	30	7.605E-01
12	Σ_{a1}	29	-7.511E-01
13	$\nu\Sigma_{f2}$	6	7.471E-01
14	Σ_{a1}	32	-7.447E-01
15	$\nu\Sigma_{f1}$	31	7.272E-01
16	Σ_{a1}	33	-7.213E-01
17	$\nu\Sigma_{f1}$	32	6.963E-01
18	$\nu\Sigma_{f1}$	29	6.696E-01
19	Σ_{a1}	5	-6.648E-01
20	$\nu\Sigma_{f2}$	34	6.610E-01
21	$\nu\Sigma_{f2}$	3	6.598E-01
22	$\nu\Sigma_{f2}$	7	6.535E-01
23	Σ_{a2}	29	-6.530E-01
24	Σ_{12}	29	6.491E-01
25	Σ_{a1}	28	-6.432E-01
26	Σ_{a2}	30	-6.407E-01
27	Σ_{a1}	6	-6.308E-01
28	Σ_{a1}	34	-6.242E-01
29	$\nu\Sigma_{f2}$	35	6.209E-01
30	$\nu\Sigma_{f1}$	33	6.075E-01
31	Σ_{12}	30	6.049E-01
32	Σ_{a1}	4	-6.027E-01
33	$\nu\Sigma_{f1}$	34	6.013E-01
34	Σ_{a2}	31	-5.994E-01
35	Σ_{a2}	32	-5.897E-01
36	$\nu\Sigma_{f1}$	28	5.806E-01
37	$\nu\Sigma_{f2}$	8	5.799E-01
38	Σ_{a1}	7	-5.799E-01
39	Σ_{12}	31	5.672E-01
40	Σ_{a1}	35	-5.666E-01

Index	Cross section	NK comp.	PRCC
676	Σ_{a1}	97	-4.588E-03
677	Σ_{a2}	70	4.533E-03
678	$\nu\Sigma_{f2}$	17	-4.455E-03
679	D_{f1}	65	-4.313E-03
680	Σ_{12}	23	-4.233E-03
681	Σ_{12}	83	-4.225E-03
682	Σ_{a2}	20	-4.224E-03
683	Σ_{a2}	73	-4.210E-03
684	D_{f1}	23	-4.143E-03
685	Σ_{12}	26	-4.061E-03
686	D_{f1}	83	-3.874E-03
687	$\nu\Sigma_{f2}$	19	-3.829E-03
688	Σ_{a1}	23	-3.478E-03
689	Σ_{a1}	24	3.347E-03
690	Σ_{a1}	64	3.202E-03
691	D_{f2}	88	3.082E-03
692	$\nu\Sigma_{f1}$	66	-2.898E-03
693	Σ_{a2}	102	-2.799E-03
694	Σ_{a1}	89	-2.706E-03
695	Σ_{a1}	72	2.679E-03
696	Σ_{12}	96	-2.526E-03
697	Σ_{a1}	91	2.501E-03
698	Σ_{12}	91	2.329E-03
699	Σ_{a2}	64	2.297E-03
700	Σ_{a2}	17	2.022E-03
701	$\nu\Sigma_{f1}$	44	1.992E-03
702	Σ_{a2}	93	1.963E-03
703	D_{f2}	17	-1.831E-03
704	D_{f2}	32	1.744E-03
705	D_{f2}	71	1.633E-03
706	D_{f2}	72	-1.524E-03
707	D_{f1}	99	1.484E-03
708	Σ_{12}	15	1.354E-03
709	Σ_{12}	19	1.025E-03
710	Σ_{12}	52	-8.423E-04
711	$\nu\Sigma_{f1}$	51	-7.047E-04
712	Σ_{a1}	68	-7.042E-04
713	$\nu\Sigma_{f1}$	78	-3.346E-04
714	$\nu\Sigma_{f2}$	77	-2.256E-04
715	D_{f2}	33	1.136E-04

Table D.2 – Higher (left) and lower (right) PRCC list for k_{eff}.

Index	Cross section	NK comp.	PRCC
1	$\nu\Sigma_{f2}$	29	4.060E-01
2	$\nu\Sigma_{f2}$	30	4.017E-01
3	$\nu\Sigma_{f2}$	27	-3.710E-01
4	$\nu\Sigma_{f2}$	4	3.367E-01
5	$\nu\Sigma_{f2}$	34	-3.181E-01
6	$\nu\Sigma_{f1}$	30	2.916E-01
7	$\nu\Sigma_{f2}$	36	-2.868E-01
8	$\nu\Sigma_{f2}$	35	-2.464E-01
9	$\nu\Sigma_{f2}$	5	2.369E-01
10	$\nu\Sigma_{f2}$	10	-2.176E-01
11	$\nu\Sigma_{f2}$	38	-2.025E-01
12	$\nu\Sigma_{f2}$	37	-1.988E-01
13	$\nu\Sigma_{f2}$	33	-1.884E-01
14	$\nu\Sigma_{f1}$	27	-1.845E-01
15	D_{f2}	86	1.843E-01
16	$\nu\Sigma_{f2}$	47	-1.798E-01
17	D_{f2}	57	-1.763E-01
18	$\nu\Sigma_{f2}$	31	1.737E-01
19	$\nu\Sigma_{f1}$	29	1.706E-01
20	Σ_{a1}	44	-1.602E-01
21	Σ_{12}	67	-1.590E-01
22	$\nu\Sigma_{f1}$	36	-1.570E-01
23	Σ_{a2}	43	-1.563E-01
24	D_{f2}	42	1.492E-01
25	$\nu\Sigma_{f1}$	38	-1.488E-01
26	$\nu\Sigma_{f1}$	37	-1.469E-01
27	$\nu\Sigma_{f1}$	6	1.463E-01
28	Σ_{a1}	94	-1.455E-01
29	D_{f2}	28	-1.446E-01
30	$\nu\Sigma_{f2}$	64	1.445E-01
31	$\nu\Sigma_{f2}$	11	-1.408E-01
32	Σ_{a2}	61	1.405E-01
33	Σ_{a2}	100	1.401E-01
34	Σ_{a1}	69	1.396E-01
35	$\nu\Sigma_{f1}$	35	-1.390E-01
36	Σ_{a2}	15	1.376E-01
37	$\nu\Sigma_{f2}$	62	-1.373E-01
38	D_{f1}	50	-1.363E-01
39	Σ_{a1}	75	1.359E-01
40	Σ_{12}	36	1.350E-01

Index	Cross section	NK comp.	PRCC
676	$\nu\Sigma_{f2}$	60	-5.591E-03
677	Σ_{a2}	97	5.535E-03
678	Σ_{12}	1	-5.489E-03
679	$\nu\Sigma_{f2}$	40	-5.433E-03
680	$\nu\Sigma_{f2}$	65	5.394E-03
681	Σ_{a2}	71	-5.342E-03
682	D_{f1}	80	5.246E-03
683	D_{f1}	70	-5.168E-03
684	$\nu\Sigma_{f2}$	84	5.134E-03
685	Σ_{a1}	3	-5.033E-03
686	D_{f1}	4	5.021E-03
687	D_{f1}	75	-4.998E-03
688	D_{f2}	100	4.944E-03
689	$\nu\Sigma_{f2}$	73	4.725E-03
690	$\nu\Sigma_{f2}$	98	4.163E-03
691	Σ_{12}	2	-4.010E-03
692	Σ_{a1}	53	-3.867E-03
693	Σ_{12}	56	-3.745E-03
694	Σ_{12}	11	-3.489E-03
695	$\nu\Sigma_{f1}$	2	-3.437E-03
696	D_{f2}	66	3.361E-03
697	$\nu\Sigma_{f1}$	70	-3.101E-03
698	Σ_{a1}	43	2.371E-03
699	D_{f1}	96	-2.327E-03
700	D_{f1}	71	-2.251E-03
701	Σ_{12}	60	-2.105E-03
702	Σ_{a1}	85	-1.924E-03
703	Σ_{a1}	7	-1.844E-03
704	Σ_{a1}	68	-1.788E-03
705	D_{f1}	37	-1.629E-03
706	$\nu\Sigma_{f2}$	41	-1.523E-03
707	Σ_{12}	39	-1.414E-03
708	$\nu\Sigma_{f1}$	61	1.121E-03
709	Σ_{12}	68	-1.049E-03
710	$\nu\Sigma_{f2}$	24	-9.887E-04
711	D_{f1}	32	9.140E-04
712	$\nu\Sigma_{f2}$	70	-8.571E-04
713	Σ_{a1}	51	-4.271E-04
714	$\nu\Sigma_{f2}$	99	9.603E-05
715	$\nu\Sigma_{f1}$	81	3.868E-05

Table D.3 – Higher (left) and lower (right) PRCC list for P_z.

Index	Cross section	NK comp.	PRCC
1	$\nu\Sigma_{f2}$	28	-4.948E-01
2	$\nu\Sigma_{f2}$	29	-3.882E-01
3	$\nu\Sigma_{f2}$	31	3.666E-01
4	$\nu\Sigma_{f2}$	3	-3.418E-01
5	$\nu\Sigma_{f2}$	32	2.409E-01
6	$\nu\Sigma_{f2}$	7	2.404E-01
7	Σ_{12}	11	-2.098E-01
8	$\nu\Sigma_{f1}$	28	-1.963E-01
9	$\nu\Sigma_{f2}$	33	1.925E-01
10	$\nu\Sigma_{f1}$	29	-1.823E-01
11	$\nu\Sigma_{f2}$	4	-1.778E-01
12	$\nu\Sigma_{f1}$	1	-1.732E-01
13	Σ_{a2}	26	1.681E-01
14	Σ_{a1}	76	-1.593E-01
15	$\nu\Sigma_{f2}$	6	1.535E-01
16	Σ_{12}	14	1.447E-01
17	$\nu\Sigma_{f1}$	31	1.443E-01
18	D_{f1}	79	1.437E-01
19	Σ_{12}	75	1.432E-01
20	$\nu\Sigma_{f1}$	6	1.429E-01
21	$\nu\Sigma_{f1}$	3	-1.421E-01
22	D_{f1}	59	1.373E-01
23	Σ_{12}	81	-1.359E-01
24	D_{f2}	39	1.347E-01
25	$\nu\Sigma_{f1}$	22	1.333E-01
26	D_{f1}	35	1.310E-01
27	D_{f1}	62	1.306E-01
28	$\nu\Sigma_{f1}$	4	-1.304E-01
29	Σ_{12}	85	-1.290E-01
30	$\nu\Sigma_{f1}$	82	1.286E-01
31	D_{f2}	100	1.277E-01
32	$\nu\Sigma_{f2}$	42	1.259E-01
33	$\nu\Sigma_{f1}$	64	1.239E-01
34	$\nu\Sigma_{f1}$	70	-1.236E-01
35	Σ_{a1}	12	-1.226E-01
36	D_{f1}	78	-1.197E-01
37	Σ_{a1}	22	1.182E-01
38	Σ_{a1}	95	1.176E-01
39	$\nu\Sigma_{f1}$	27	-1.170E-01
40	$\nu\Sigma_{f2}$	14	1.149E-01

Index	Cross section	NK comp.	PRCC
676	Σ_{a2}	8	4.800E-03
677	D_{f1}	52	-4.660E-03
678	Σ_{a1}	96	4.656E-03
679	D_{f1}	89	-4.650E-03
680	Σ_{12}	94	4.439E-03
681	Σ_{12}	62	4.360E-03
682	D_{f2}	84	4.330E-03
683	$\nu\Sigma_{f1}$	32	-4.327E-03
684	$\nu\Sigma_{f1}$	15	4.185E-03
685	Σ_{a1}	48	-4.106E-03
686	$\nu\Sigma_{f1}$	77	-3.649E-03
687	D_{f2}	89	-3.592E-03
688	D_{f1}	37	-3.361E-03
689	D_{f2}	8	-3.218E-03
690	Σ_{a1}	8	3.083E-03
691	D_{f1}	23	3.058E-03
692	Σ_{12}	60	-2.575E-03
693	Σ_{a1}	98	2.564E-03
694	Σ_{a1}	61	-2.419E-03
695	Σ_{a2}	78	2.137E-03
696	Σ_{a2}	92	2.116E-03
697	Σ_{a2}	77	-2.106E-03
698	$\nu\Sigma_{f1}$	42	1.953E-03
699	D_{f1}	40	-1.876E-03
700	$\nu\Sigma_{f2}$	91	-1.868E-03
701	D_{f2}	58	1.754E-03
702	$\nu\Sigma_{f2}$	49	-1.503E-03
703	$\nu\Sigma_{f2}$	89	-1.484E-03
704	Σ_{a2}	82	-1.481E-03
705	Σ_{12}	57	1.241E-03
706	Σ_{a1}	37	1.157E-03
707	Σ_{a1}	93	-7.842E-04
708	Σ_{a2}	49	7.461E-04
709	$\nu\Sigma_{f1}$	69	6.719E-04
710	Σ_{a1}	42	5.536E-04
711	$\nu\Sigma_{f2}$	95	-3.492E-04
712	D_{f2}	96	3.420E-04
713	$\nu\Sigma_{f2}$	76	-3.395E-04
714	Σ_{12}	26	-1.438E-04
715	$\nu\Sigma_{f1}$	13	9.956E-05

Table D.4 – Higher (left) and lower (right) PRCC list for N_z.

Index	Cross section	NK comp.	PRCC
1	$\nu\Sigma_{f2}$	5	8.610E-01
2	$\nu\Sigma_{f2}$	4	8.577E-01
3	$\nu\Sigma_{f2}$	6	8.413E-01
4	$\nu\Sigma_{f2}$	7	7.728E-01
5	$\nu\Sigma_{f2}$	3	7.502E-01
6	Σ_{a1}	5	-7.397E-01
7	Σ_{a1}	6	-7.204E-01
8	Σ_{a1}	4	-6.948E-01
9	$\nu\Sigma_{f2}$	8	6.839E-01
10	Σ_{a1}	7	-6.549E-01
11	$\nu\Sigma_{f1}$	5	6.499E-01
12	$\nu\Sigma_{f1}$	6	6.424E-01
13	$\nu\Sigma_{f1}$	7	6.321E-01
14	Σ_{a2}	5	-6.254E-01
15	$\nu\Sigma_{f1}$	4	6.224E-01
16	$\nu\Sigma_{f2}$	9	6.065E-01
17	Σ_{12}	5	5.831E-01
18	Σ_{a1}	8	-5.811E-01
19	Σ_{a2}	4	-5.650E-01
20	Σ_{12}	4	5.632E-01
21	Σ_{a2}	6	-5.622E-01
22	Σ_{12}	6	5.533E-01
23	$\nu\Sigma_{f1}$	8	5.419E-01
24	Σ_{a1}	3	-5.282E-01
25	$\nu\Sigma_{f2}$	2	5.261E-01
26	Σ_{a2}	3	-5.038E-01
27	Σ_{a1}	9	-5.032E-01
28	$\nu\Sigma_{f1}$	3	5.027E-01
29	$\nu\Sigma_{f2}$	10	5.027E-01
30	Σ_{12}	7	4.962E-01
31	Σ_{12}	3	4.938E-01
32	Σ_{a2}	7	-4.654E-01
33	Σ_{a1}	10	-4.575E-01
34	$\nu\Sigma_{f1}$	9	4.378E-01
35	Σ_{a2}	8	-4.266E-01
36	Σ_{12}	8	4.241E-01
37	$\nu\Sigma_{f1}$	10	4.166E-01
38	$\nu\Sigma_{f2}$	11	4.015E-01
39	$\nu\Sigma_{f2}$	12	3.660E-01
40	Σ_{a1}	11	-3.519E-01

Index	Cross section	NK comp.	PRCC
122	D_{f2}	12	-2.243E-02
123	Σ_{12}	24	-2.223E-02
124	$\nu\Sigma_{f2}$	18	2.219E-02
125	D_{f1}	24	2.070E-02
126	D_{f2}	21	-1.891E-02
127	D_{f1}	19	1.788E-02
128	Σ_{12}	18	-1.721E-02
129	D_{f2}	13	-1.650E-02
130	D_{f2}	16	-1.635E-02
131	Σ_{a1}	21	-1.633E-02
132	Σ_{a1}	19	-1.611E-02
133	$\nu\Sigma_{f2}$	22	1.487E-02
134	Σ_{a2}	24	-1.477E-02
135	$\nu\Sigma_{f2}$	21	-1.473E-02
136	$\nu\Sigma_{f2}$	19	-1.394E-02
137	D_{f2}	11	-1.388E-02
138	Σ_{a2}	18	1.370E-02
139	$\nu\Sigma_{f1}$	22	1.280E-02
140	D_{f1}	21	1.254E-02
141	Σ_{12}	19	-1.093E-02
142	$\nu\Sigma_{f1}$	21	-1.077E-02
143	Σ_{a2}	23	1.068E-02
144	Σ_{a2}	20	9.793E-03
145	D_{f1}	23	-9.407E-03
146	D_{f1}	22	-9.126E-03
147	Σ_{a2}	17	-8.753E-03
148	$\nu\Sigma_{f2}$	20	8.740E-03
149	D_{f2}	20	-8.058E-03
150	Σ_{a2}	22	-7.196E-03
151	$\nu\Sigma_{f1}$	24	6.689E-03
152	D_{f1}	15	-5.834E-03
153	Σ_{12}	20	5.304E-03
154	Σ_{a1}	20	-4.703E-03
155	D_{f2}	4	-3.002E-03
156	Σ_{a2}	21	-2.605E-03
157	$\nu\Sigma_{f1}$	16	-1.767E-03
158	Σ_{12}	14	-1.250E-03
159	Σ_{12}	22	7.629E-04
160	Σ_{a1}	22	1.010E-04
161	D_{f2}	8	4.298E-05

Table D.5 – Higher (left) and lower (right) PRCC list for k_{eff}, only segment 13 is perturbed.

Index	Cross section	NK comp.	PRCC
1	$\nu\Sigma_{f2}$	4	4.256E-01
2	$\nu\Sigma_{f2}$	5	3.972E-01
3	$\nu\Sigma_{f2}$	8	-2.133E-01
4	$\nu\Sigma_{f1}$	4	2.075E-01
5	$\nu\Sigma_{f1}$	5	1.996E-01
6	$\nu\Sigma_{f1}$	9	-1.641E-01
7	$\nu\Sigma_{f2}$	2	-1.541E-01
8	$\nu\Sigma_{f2}$	7	-1.406E-01
9	$\nu\Sigma_{f1}$	11	-1.276E-01
10	$\nu\Sigma_{f1}$	8	-1.241E-01
11	$\nu\Sigma_{f2}$	10	-1.184E-01
12	$\nu\Sigma_{f2}$	11	-1.183E-01
13	$\nu\Sigma_{f2}$	12	-1.163E-01
14	$\nu\Sigma_{f2}$	9	-1.109E-01
15	$\nu\Sigma_{f2}$	13	-1.052E-01
16	$\nu\Sigma_{f2}$	6	9.976E-02
17	Σ_{a2}	4	-9.599E-02
18	D_{f2}	20	8.559E-02
19	D_{f1}	16	8.526E-02
20	$\nu\Sigma_{f1}$	14	-8.288E-02
21	$\nu\Sigma_{f1}$	24	8.281E-02
22	$\nu\Sigma_{f1}$	10	-8.149E-02
23	Σ_{a2}	19	-7.998E-02
24	Σ_{a1}	17	7.892E-02
25	Σ_{12}	22	-7.830E-02
26	$\nu\Sigma_{f1}$	7	-7.514E-02
27	Σ_{12}	18	-7.201E-02
28	D_{f1}	21	6.840E-02
29	D_{f1}	17	-6.704E-02
30	$\nu\Sigma_{f2}$	24	6.594E-02
31	$\nu\Sigma_{f2}$	23	6.543E-02
32	Σ_{a1}	12	6.283E-02
33	$\nu\Sigma_{f1}$	12	-6.198E-02
34	$\nu\Sigma_{f2}$	22	-6.086E-02
35	Σ_{a1}	19	5.982E-02
36	D_{f2}	18	5.764E-02
37	$\nu\Sigma_{f1}$	20	5.618E-02
38	$\nu\Sigma_{f1}$	16	-5.591E-02
39	D_{f2}	19	5.539E-02
40	Σ_{a1}	23	-5.519E-02

Index	Cross section	NK comp.	PRCC
122	Σ_{a2}	5	-1.280E-02
123	D_{f1}	8	1.207E-02
124	D_{f2}	5	1.157E-02
125	D_{f2}	24	1.152E-02
126	$\nu\Sigma_{f1}$	21	-1.109E-02
127	$\nu\Sigma_{f2}$	15	1.056E-02
128	D_{f2}	17	-1.010E-02
129	D_{f1}	10	9.920E-03
130	Σ_{12}	21	9.842E-03
131	Σ_{a2}	15	-9.586E-03
132	Σ_{a1}	10	-9.289E-03
133	D_{f2}	8	-9.085E-03
134	D_{f1}	19	-8.929E-03
135	D_{f2}	10	-8.758E-03
136	Σ_{a1}	20	8.720E-03
137	Σ_{a2}	13	8.060E-03
138	Σ_{a2}	21	7.933E-03
139	Σ_{a2}	22	7.316E-03
140	Σ_{a2}	16	7.024E-03
141	$\nu\Sigma_{f2}$	21	-6.937E-03
142	D_{f1}	14	6.677E-03
143	Σ_{a2}	20	6.514E-03
144	D_{f2}	4	-6.188E-03
145	Σ_{a1}	6	6.124E-03
146	Σ_{a1}	18	6.099E-03
147	D_{f1}	2	-5.465E-03
148	D_{f1}	18	-5.019E-03
149	D_{f2}	11	-4.996E-03
150	Σ_{a1}	14	-4.665E-03
151	D_{f2}	2	-2.873E-03
152	Σ_{a1}	11	2.552E-03
153	Σ_{12}	2	-2.297E-03
154	Σ_{a1}	13	1.550E-03
155	D_{f2}	16	-1.508E-03
156	Σ_{a2}	8	-1.365E-03
157	D_{f2}	21	1.049E-03
158	$\nu\Sigma_{f1}$	22	1.049E-03
159	$\nu\Sigma_{f2}$	19	-7.235E-04
160	Σ_{12}	20	-5.953E-04
161	Σ_{a1}	4	4.469E-05

Table D.6 – Higher (left) and lower (right) PRCC list for P_z, only segment 13 is perturbed.

Index	Cross section	NK comp.	PRCC
1	$\nu\Sigma_{f2}$	4	-4.484E-01
2	$\nu\Sigma_{f2}$	6	3.508E-01
3	$\nu\Sigma_{f2}$	3	-2.846E-01
4	$\nu\Sigma_{f1}$	4	-1.828E-01
5	$\nu\Sigma_{f1}$	3	-1.754E-01
6	$\nu\Sigma_{f2}$	5	1.707E-01
7	$\nu\Sigma_{f2}$	7	1.486E-01
8	$\nu\Sigma_{f1}$	6	1.435E-01
9	Σ_{a1}	14	-9.844E-02
10	D_{f2}	11	8.539E-02
11	$\nu\Sigma_{f2}$	24	-8.383E-02
12	D_{f2}	2	7.703E-02
13	$\nu\Sigma_{f2}$	23	-7.564E-02
14	D_{f1}	18	-7.480E-02
15	$\nu\Sigma_{f1}$	7	7.421E-02
16	Σ_{12}	18	7.332E-02
17	Σ_{12}	2	7.168E-02
18	$\nu\Sigma_{f1}$	13	7.027E-02
19	D_{f1}	24	6.765E-02
20	Σ_{a1}	9	-6.629E-02
21	D_{f1}	12	6.501E-02
22	$\nu\Sigma_{f1}$	5	6.382E-02
23	D_{f1}	21	-5.759E-02
24	$\nu\Sigma_{f2}$	19	-5.726E-02
25	D_{f1}	20	-5.564E-02
26	Σ_{a1}	15	-5.323E-02
27	$\nu\Sigma_{f1}$	23	5.275E-02
28	D_{f2}	12	-5.234E-02
29	D_{f2}	21	5.225E-02
30	$\nu\Sigma_{f2}$	17	-5.218E-02
31	Σ_{a1}	21	5.182E-02
32	$\nu\Sigma_{f1}$	19	-5.075E-02
33	$\nu\Sigma_{f1}$	11	4.915E-02
34	Σ_{a2}	18	-4.801E-02
35	Σ_{12}	3	-4.673E-02
36	$\nu\Sigma_{f2}$	8	4.565E-02
37	Σ_{12}	11	4.558E-02
38	D_{f2}	4	4.459E-02
39	Σ_{a1}	12	4.436E-02
40	Σ_{a2}	16	4.409E-02

Index	Cross section	NK comp.	PRCC
122	D_{f2}	8	-1.308E-02
123	Σ_{a1}	17	-1.274E-02
124	Σ_{a2}	11	1.250E-02
125	Σ_{a2}	23	-1.230E-02
126	$\nu\Sigma_{f2}$	16	1.128E-02
127	Σ_{a2}	5	-1.100E-02
128	Σ_{a2}	3	-1.067E-02
129	Σ_{a1}	23	1.065E-02
130	Σ_{a1}	2	1.006E-02
131	$\nu\Sigma_{f2}$	18	9.902E-03
132	D_{f2}	17	-9.559E-03
133	D_{f2}	3	-8.082E-03
134	Σ_{12}	12	7.446E-03
135	Σ_{a1}	3	7.417E-03
136	D_{f1}	15	7.193E-03
137	D_{f1}	17	5.460E-03
138	D_{f2}	7	-4.885E-03
139	Σ_{12}	5	4.573E-03
140	$\nu\Sigma_{f2}$	13	4.268E-03
141	Σ_{12}	21	-4.267E-03
142	Σ_{a1}	13	3.985E-03
143	Σ_{12}	14	3.764E-03
144	D_{f2}	9	-3.760E-03
145	Σ_{12}	19	-3.451E-03
146	Σ_{a1}	11	-3.441E-03
147	D_{f2}	13	-3.412E-03
148	Σ_{a1}	20	-3.301E-03
149	D_{f1}	19	-3.170E-03
150	Σ_{a2}	6	-3.098E-03
151	Σ_{12}	4	2.661E-03
152	$\nu\Sigma_{f2}$	20	2.334E-03
153	Σ_{a2}	15	-2.310E-03
154	$\nu\Sigma_{f2}$	12	-2.153E-03
155	Σ_{12}	15	2.079E-03
156	$\nu\Sigma_{f1}$	15	2.055E-03
157	Σ_{a1}	8	-1.121E-03
158	D_{f2}	23	-9.268E-04
159	Σ_{12}	10	-7.530E-04
160	Σ_{a1}	18	4.814E-05
161	Σ_{a2}	8	-4.433E-05

Table D.7 – Higher (left) and lower (right) PRCC list for N_z, only segment 13 is perturbed.

Index	Cross section	NK comp.	PRCC
1	D_{f1}	103	-9.958E-01
2	Σ_{a2}	103	-9.391E-01
3	Σ_{12}	103	-9.044E-01
4	D_{f1}	101	-7.914E-01
5	Σ_{a2}	101	-5.458E-01
6	Σ_{12}	101	-4.805E-01
7	Σ_{a1}	101	-1.993E-01

Index	Cross section	NK comp.	PRCC
9	Σ_{a1}	103	-5.889E-02
10	D_{f2}	101	-5.748E-02
11	D_{f2}	102	-5.215E-02
12	D_{f2}	103	4.141E-02
13	Σ_{12}	102	-3.162E-02
14	Σ_{a1}	102	2.303E-02
15	D_{f1}	102	-3.461E-03

Table D.8 – Higher (left) and lower (right) PRCC list for k_{eff}, only reflector segments are perturbed.

Index	Cross section	NK comp.	PRCC
1	D_{f1}	103	8.565E-01
2	D_{f1}	101	-5.343E-01
3	Σ_{a2}	103	4.079E-01
4	Σ_{a2}	101	-2.517E-01
5	Σ_{12}	103	2.399E-01
6	Σ_{12}	101	-2.396E-01
7	D_{f1}	102	2.139E-01

Index	Cross section	NK comp.	PRCC
9	Σ_{a1}	102	6.656E-02
10	D_{f2}	103	-6.006E-02
11	D_{f2}	102	5.832E-02
12	D_{f2}	101	-4.701E-02
13	Σ_{12}	102	4.699E-02
14	Σ_{a1}	103	4.539E-02
15	Σ_{a1}	101	-3.429E-02

Table D.9 – Higher (left) and lower (right) PRCC list for P_z, only reflector segments are perturbed.

Index	Cross section	NK comp.	PRCC
1	D_{f2}	103	-9.150E-02
2	Σ_{a1}	101	-6.071E-02
3	Σ_{a2}	101	4.247E-02
4	Σ_{12}	102	-2.888E-02
5	D_{f2}	101	2.501E-02
6	D_{f1}	102	-2.320E-02
7	Σ_{a2}	103	-2.223E-02

Index	Cross section	NK comp.	PRCC
9	D_{f2}	102	-1.976E-02
10	Σ_{12}	103	1.668E-02
11	D_{f1}	103	1.505E-02
12	Σ_{a1}	103	-1.302E-02
13	Σ_{a1}	102	9.135E-03
14	Σ_{a2}	102	2.031E-03
15	Σ_{12}	101	-6.675E-04

Table D.10 – Higher (left) and lower (right) PRCC list for N_z, only reflector segments are perturbed.

Appendix E

Sensitivity of thermohydraulic parameters

Sensitivity of thermohydraulic parameters for the TRACE5.0P3/PARCSv3.2 coupled simulations is displayed in this appendix. There are 43 input parameters, these are represented as variables in the first column, the meaning of each variable is found in Table 5.2 and Table 5.3. The output parameters are the enthalpy, total power and total reactivity. Sensitivity is given as PRCC only for the maximum response approach and using two sampling methods: SRS and LHS.

	Enthalpy	**Power**	**Reactivity**
P_{out}	3.14559e-03	-5.16410e-01	-4.79186e-01
q_{tot}	1.15763e-01	-7.31966e-02	-9.15421e-02
m_{in}	-8.00178e-02	-3.35477e-01	-1.51881e-01
ϵ_b	1.42124e-01	4.04980e-02	4.61264e-02
ϵ_1	-8.02745e-02	-3.54257e-02	1.24703e-02
ϵ_2	3.77025e-02	-8.55942e-02	-1.26018e-02
ϵ_3	3.72281e-02	4.21584e-02	6.98897e-02
A_{flowb}	2.68028e-03	2.60011e-01	1.93169e-01
A_{flow1}	-4.28073e-03	9.62173e-02	6.21445e-02
A_{flow2}	-1.60432e-02	1.83816e-01	1.32877e-01
A_{flow3}	1.05276e-01	-6.12637e-01	-5.06907e-01
p/d_b	-1.86293e-02	1.29199e-01	1.17149e-01
p/d_1	-8.26580e-03	3.13686e-02	1.68337e-02
p/d_2	-2.67372e-02	1.54048e-01	1.46468e-01
p/d_3	-6.64416e-01	-1.04817e-01	-1.45146e-01
RFPF_0	1.40346e-01	-3.72477e-02	4.75956e-02
RFPF_1	-1.25384e-01	-1.85234e-01	-2.09952e-01
RFPF_2	-2.92555e-02	6.13752e-02	-7.24299e-02
RFPF_3	-7.67441e-03	-1.06074e-01	1.33437e-03
h_{gapb}	1.57794e-01	-2.31396e-01	-1.58808e-01
h_{gap1}	-1.54860e-01	-5.50976e-02	-1.57564e-01
h_{gap2}	-1.16605e-01	6.04164e-02	1.35900e-01
h_{gap3}	7.84668e-02	-1.36533e-02	-7.94683e-03
k_{facb}	-7.42928e-02	-6.00833e-02	-7.27946e-02
k_{fac1}	-8.89196e-02	-2.44275e-01	-1.75476e-01
k_{fac2}	-7.37741e-02	-2.59491e-01	-1.98157e-01
k_{fac3}	2.02036e-01	6.29205e-01	4.44641e-01
D_{hydb}	9.93241e-02	1.58620e-01	2.06643e-02
D_{hyd1}	7.21282e-02	4.32577e-03	4.53501e-02
D_{hyd2}	1.54700e-01	-9.94180e-03	6.91712e-02
D_{hyd3}	-3.52628e-02	-1.90289e-02	-7.37504e-02
Cp_{fuel}	-8.71656e-02	8.55271e-02	-2.33623e-02
Cp_{clad}	-1.68776e-01	1.95823e-01	1.63053e-01
K_{fuel}	-8.53943e-03	-2.01680e-01	4.13713e-02
K_{clad}	2.91915e-02	7.13808e-02	-3.30715e-03
T_{in}	2.18925e-01	1.17328e-01	5.86005e-02
z_{gapb}	-3.47777e-02	8.29038e-02	9.07120e-02
z_{gap1}	-7.92343e-02	1.01521e-01	5.27055e-02
z_{gap2}	8.61872e-03	-1.90414e-01	-1.06287e-01
z_{gap3}	9.97565e-01	-9.81367e-01	-9.72085e-01
CHFM	-3.43364e-02	1.84000e-01	1.68787e-01
$q_{\text{byp}}/q_{\text{tot}}$	-1.06088e-01	8.30711e-02	4.41004e-02
$q_{\text{mod}}/q_{\text{tot}}$	3.16627e-02	3.32047e-02	1.03787e-01

Table E.1 – PRCC list for thermohydraulic parameters, SRS sampling method.

	Enthalpy	**Power**	**Reactivity**
P_{out}	2.11735e-03	-6.55080e-01	-4.72294e-01
q_{tot}	1.04597e-01	4.05580e-02	3.32977e-03
m_{in}	5.09561e-02	-4.04393e-01	-2.03742e-01
ϵ_b	-5.73134e-02	5.34386e-02	1.18012e-01
ϵ_1	-9.02133e-02	8.46622e-02	-5.83471e-02
ϵ_2	8.48123e-02	-7.92265e-02	-1.40869e-01
ϵ_3	3.23120e-02	3.94651e-02	1.25350e-01
A_{flowb}	1.19047e-02	3.89733e-01	3.10984e-01
A_{flow1}	-2.80016e-04	2.19100e-01	1.27228e-01
A_{flow2}	1.53153e-01	2.20994e-01	1.00882e-01
A_{flow3}	-5.74727e-02	-7.08516e-01	-5.42780e-01
p/d_b	2.03620e-02	7.54767e-02	1.16038e-01
p/d_1	-1.21739e-01	1.93912e-02	-1.04955e-01
p/d_2	-3.99723e-03	1.43575e-01	1.37284e-01
p/d_3	-6.76702e-01	-6.55500e-02	-8.58731e-02
RFPF_0	-4.85159e-02	5.37916e-02	-5.43524e-02
RFPF_1	-2.14365e-01	-5.20320e-02	-6.40490e-03
RFPF_2	-5.43817e-02	6.06222e-03	3.40710e-02
RFPF_3	1.06776e-01	-5.94500e-02	3.51387e-03
h_{gapb}	5.02357e-02	-8.59615e-02	-1.27956e-01
h_{gap1}	1.10418e-01	-8.80925e-02	-1.73276e-01
h_{gap2}	2.98168e-02	-8.28422e-02	-1.09386e-01
h_{gap3}	-1.21389e-01	-5.21975e-02	-1.00027e-01
k_{facb}	-1.21381e-01	-8.96403e-02	-1.48630e-02
k_{fac1}	-4.35158e-02	-2.98853e-01	-2.33696e-01
k_{fac2}	-1.40564e-01	-3.67848e-01	-1.95091e-01
k_{fac3}	1.90362e-01	6.70658e-01	4.62193e-01
D_{hydb}	-1.75921e-01	2.15384e-01	4.01436e-02
D_{hyd1}	-4.26334e-02	4.69500e-02	-1.25610e-01
D_{hyd2}	1.62504e-01	3.28270e-02	-9.39231e-02
D_{hyd3}	1.32218e-02	-7.70542e-02	-6.67576e-02
Cp_{fuel}	1.15174e-02	-4.67932e-02	7.43399e-02
Cp_{clad}	-2.03457e-01	2.08961e-01	1.41701e-01
K_{fuel}	1.24217e-01	-3.38260e-01	-1.28368e-01
K_{clad}	-4.15533e-02	5.58759e-02	1.74225e-01
T_{in}	3.52802e-02	4.73908e-02	-1.89233e-02
z_{gapb}	-1.71755e-02	7.66513e-02	1.91738e-02
z_{gap1}	3.14562e-02	1.03942e-02	-1.15555e-01
z_{gap2}	2.01335e-01	-1.55625e-01	-4.64215e-02
z_{gap3}	9.97991e-01	-9.91157e-01	-9.85573e-01
CHFM	-5.21570e-02	6.18840e-02	1.55812e-01
$q_{\text{byp}}/q_{\text{tot}}$	-9.42766e-02	8.06444e-02	-8.25378e-02
$q_{\text{mod}}/q_{\text{tot}}$	1.48188e-01	-1.12479e-01	1.55223e-02

Table E.2 – PRCC list for thermohydraulic parameters, LHS sampling method.

Appendix F

List of publications

Published papers

M. Garcia-Fenoll, **C. Mesado**, T. Barrachina, R. Miró, G. Verdú, J.A. Bermejo, A. López, and A. Ortego. Validation of 3D neutronic-thermohydraulic coupled codes RELAP5/PARCSv2.7 and TRACEv5.0P3/PARCSv3.0 against a PWR control rod drop transient. *Journal of Nuclear Science and Technology*, 2017.

C. Mesado, A. Soler, T. Barrachina, R. Miró, J.C. García-Díaz, R. Macián-Juan, and G. Verdú. Uncertainty and Sensitivity of Neutron Kinetic Parameters in the Dynamic Response of a PWR Rod Ejection Accident Coupled Simulation. *Science and Technology of Nuclear Installations*, 2012. doi: 10.1155/2012/625878.

Papers in progress

C. Mesado, R. Miró, T. Barrachina, and G. Verdú. Cross Section Uncertainty Propagation through SCALE6.2.1 Lattice Physics Code. 2017a.

C. Mesado, R. Miró, T. Barrachina, and G. Verdú. Neutronic Parameter Uncertainty Propagation and Sensitivity Analysis through PARCSv3.2 Core Physics Code. 2017b.

Published books

C. Mesado, R. Miró, A. Labarile, and T. Barrachina. TXT2NTAB Code User's Guide. Generating NEMTAB cross-section libraries from txtfile16. Technical report, Universitat Politècnica de València (UPV), 2017c.

C. Mesado, R. Miró, T. Barrachina, and G. Verdú. Modeling 3D Cores for PWR Using Vessel Components in TRACE v5.0P3 (NUREG/IA-0460). Technical report, Universitat Politècnica de València (UPV), 2015a.

R. Miró, A. Jambrina, **C. Mesado**, T. Barrachina, and G. Verdú. TRAC-BF1 to TRACE Model Semi-Automatic Conversion. PBTT Example (NUREG/IA-0461). Technical report, Universitat Politècnica de València (UPV), 2015.

R. Miró, T. Barrachina, V. Faria, **C. Mesado**, and G. Verdú. *Uso del código SCALE 6.1 y secuencias aplicables, generación de datos cinéticos. Aplicación al código TRACE/PARCS, resolución de casos prácticos.* 2012. ISBN V-187-2013.

International conferences

A. Labarile, **C. Mesado**, T. Barrachina, R. Miró, and G. Verdú. TXT2NTAB. Generating NEMTAB cross-section libraries from SCALE. In *OECD Benchmark for Uncertainty Analysis in Best-Estimate Modelling (UAM) for Design, Operation and Safety Analysis of LWRs – Eleventh Workshop (UAM-11)*, 2017a.

A. Labarile, T. Barrachina, **C. Mesado**, R. Miró, and G. Verdú. Sensitivity and uncertainty analysis of nuclear data with SCALE6.2.1 code. Application to UAM-LWR assemblies. In *OECD Benchmark for Uncertainty Analysis in Best-Estimate Modelling (UAM) for Design, Operation and Safety Analysis of LWRs – Eleventh Workshop (UAM-11)*, 2017b.

C. Mesado, M. Garcia-Fenoll, J. Martorell, R. Miró, T. Barrachina, and G. Verdú. Transitorio de caida de barra en un PWR en SNAP/TRACE/PARCS con vasija cilíndrica y núcleo cartesiano. In *Spring CAMP Meeting, Valencia, Spain*, 2017d.

A. Labarile, T. Barrachina, **C. Mesado**, R. Miró, and G. Verdú. TSUNAMI-3D and SAMPLER/KENO comparison for sensitivity and uncertainty analysis in neutron multiplication factor for LWRs. In *International Conference on Mathematics and Computational Methods Applied to Nuclear Science and Engineering (M&C), Jeju, Korea*, 2017c.

A. Labarile, **C. Mesado**, R. Miró, T. Barrachina, and G. Verdú. Sensitivity and uncertainty analysis in nuclear data with SCALE 6.2 code. Application to LWRs assemblies. In *International Congress on Advances in Nuclear Power Plants (ICAPP), Fukui and Kyoto, Japan*, 2017d.

A. Labarile, R. Miró, **C. Mesado**, T. Barrachina, and G. Verdú. Participation in the OECD/NEA benchmarks for LWRs modelling using SCALE6.2 code. In *Unifying Theory and Experiments in the 21^{st} Century PHYSOR, Sun Valley (ID), USA*, 2016a.

C. Mesado, A. Labarile, R. Miró, and G. Verdú. Core Physics results. UPV contribution. In *OECD Benchmark for Uncertainty Analysis in Best-Estimate Modelling (UAM) for Design, Operation and Safety Analysis of LWRs – Tenth Workshop (UAM-10)*, 2016b.

A. Labarile, **C. Mesado**, R. Miró, and G. Verdú. Lattice Physics results. UPV contribution. In *OECD Benchmark for Uncertainty Analysis in Best-Estimate Modelling (UAM) for Design, Operation and Safety Analysis of LWRs – Tenth Workshop (UAM-10)*, 2016b.

A. Labarile, **C. Mesado**, R. Miró, and G. Verdú. Generating NEMTAB cross-sections with the SCALE code. In *OECD/NEA Oskarshamn-2 (O2) BWR Stability Benchmark for Coupled Code Calculations and Uncertainty Analysis in Modelling – Fifth Workshop (O2-5)*, 2016c.

A. Labarile, R. Miró, **C. Mesado**, T. Barrachina, and G. Verdú. Participation in OECD/NEA Oskarshamn-2 (O-2) BWR Stability Benchmark for Uncertainty Analysis in Modelling using TRITON for Transport Calculations and SAMPLER for Cross-Sections Error Propagation. In *24^{th} International Conference Nuclear Energy for New Europe (NENE)*, 2015a. ISBN 978-961-6207-38-6.

C. Mesado, M. Garcia-Fenoll, R. Miró, and G. Verdú. Control rod drop transient: uncertainty and sensitivity analysis of thermal-hydraulic variables using a 3D model with TRACE V5.0P3/PARCS 3.0. In *International Topical Meeting on Nuclear Reactor Thermal-hydraulics (NURETH-16), Chicago (IL), USA*, 2015b.

C. Mesado, D. Morera, R. Miró, T. Barrachina, G. Verdú, A. Concejal, A. Soler, and J. Melara. Comparison of depletion results for a boiling water reactor fuel element with CASMO and SCALE6.1 (TRITON/NEWT). In *Proceedings of the International Nuclear Atlantic Conference - INAC*, 2013a. ISBN 978-85-99141-05-2.

C. Mesado, R. Miró, T. Barrachina, and G. Verdú. PWR simulation using a 3D cartesian vessel with TRACE/PARCS. In *Spring CAMP Meeting, Pisa, Italy*, 2013b.

C. Mesado, A. Jambrina, T. Barrachina, R. Miró, and G. Verdú. PBTT model from TRAC-B to TRACE conversion. In *Proceedings of the International topical meeting on nuclear reactor thermal hydraulics (NURETH-15), Italy*, 2013c. ISBN 978-88-902391-2-0.

A. Jambrina, **C. Mesado**, T. Barrachina, R. Miró, G. Verdú, A. Concejal, and J. Melara. Peach Bottom Turbine Trip benchmark analysis with TRAC-BF1/PARCS and TRACE/PARCS coupled codes. In *Proceedings of the International topical meeting on nuclear reactor thermal hydraulics (NURETH-15), Italy*, 2013a. ISBN 978-88-902391-2-0.

C. Mesado, T. Barrachina, R. Miró, and G. Verdú. PWR Simulation using a 3D vessel with TRACE/-PARCS. In *Proceedings of the International topical meeting on nuclear reactor thermal hydraulics (NURETH-15), Italy*, 2013d. ISBN 978-88-902391-2-0.

National conferences

C. Mesado, F.J. Sabater, C. Casado, and J.F. Serrano. Actualización del Procedimiento Técnico de Diseño de ENUSA para el cálculo de calor residual con el código SCALE 6.1.2. In *Proceedings of the 43rd Spanish nuclear society annual meeting (SNE), Málaga, Spain*, 2017e.

C. Mesado, R. Miró, and G. Verdú. Uncertainty Quantification and Sensitivity Analysis for Cross Sections in Lattice and Core Physics Codes. In *Proceedings of the 43rd Spanish nuclear society annual meeting (SNE), Málaga, Spain*, 2017f.

J. Martorell, R. Miró, **C. Mesado**, and G. Verdú. Diseño de una herramienta gráfica interactiva bajo plataforma SNAP para el análisis de seguridad nuclear de transitorios termohidráulico-neutrónicos 3D en centrales PWR-KWU. In *Proceedings of the 42nd Spanish nuclear society annual meeting (SNE), Santander, Spain*, 2016.

A. Labarile, **C. Mesado**, R. Miró, and G. Verdú. Generación de librerias neutrónicas a partir SCALE y posterior análisis de un BWR con PARCS. In *Proceedings of the 42nd Spanish nuclear society annual meeting (SNE), Santander, Spain*, 2016d.

A. Labarile, R. Miró, **C. Mesado**, T. Barrachina, and G. Verdú. Participación en el "Oskarshamn-2 BWR Stability Benchmark" de la OECD/NEA. Cálculo del transporte y propagación de errores de secciones eficaces. In *Proceedings of the 41st Spanish nuclear society annual meeting (SNE), A Coruña, Spain*, 2015b.

C. Mesado, R. Miró, T. Barrachina, and G. Verdú. Propagación de incertidumbre y sensibilidad en librerías master de secciones eficaces con SCALE6.2-SAMPLER y DAKOTA. In *Proceedings of the 41st Spanish nuclear society annual meeting (SNE), A Coruña, Spain*, 2015c.

C. Mesado, R. Miró, T. Barrachina, and G. Verdú. Secciones eficaces obtenidas de un modelado BWR con el código de quemado SCALE 6.2 y comparación con CASMO. In *Proceedings of the 40th Spanish nuclear society annual meeting (SNE), Valencia, Spain*, 2014a.

C. Mesado, R. Miró, T. Barrachina, and G. Verdú. Principales características y posibilidades del nuevo módulo de SCALE 6.2 para cálculo de sensibilidad e incertidumbre por muestreo: SAMPLER. In *Proceedings of the 40th Spanish nuclear society annual meeting (SNE), Valencia, Spain*, 2014b.

C. Mesado, R. Miró, T. Barrachina, and G. Verdú. Ejecución del modelo Peach Bottom Turbine Trip en estado transitorio con TRACE V5.0P3/PARCS 3.0. In *Proceedings of the 40th Spanish nuclear society annual meeting (SNE), Valencia, Spain*, 2014c.

C. Mesado, M. Garcia-Fenoll, R. Miró, T. Barrachina, and G. Verdú. Modelado de un PWR mediante componentes 3D. In *Proceedings of the 39th Spanish nuclear society annual meeting (SNE), Reus, Spain*, 2013e.

A. Jambrina, **C. Mesado**, T. Barrachina, R. Miró, , and G. Verdú. Conversión del input de Peach Bottom de TRAC-BF1 a TRACE. In *Proceedings of the 39th Spanish nuclear society annual meeting (SNE), Reus, Spain*, 2013b.

T. Vayá, **C. Mesado**, R. Miró, and G. Verdú. Simulación de un PWR usando una vasija 3D mediante TRACE/PARCS. In *Proceedings of the 38th Spanish nuclear society annual meeting (SNE), Cáceres, Spain*, 2012.

C. Mesado, T. Barrachina, R. Miró, R. Macián, and G. Verdú. Análisis de sensibilidad e incertidumbres en la generación de los parámetros neutrónicos utilizados en la simulación de transitorios en reactores BWR y PWR con códigos acoplados. In *Proceedings of the 37th Spanish nuclear society annual meeting (SNE), Burgos, Spain*, 2011.

Acknowledgements

First, I would like to thank all Professors who, some way or another, contributed to lead this PhD adventure to safe harbor. My main advisor, Professor Rafael Miró, for his dedication to the work and all his students. Without his multidisciplinary skills I would have never achieved this PhD thesis. My PhD director and co-advisor, Professor Gumersindo Verdú, for the financial support (together with Professor Rafael Miró) and all the endless contract renewals. My American mentor, Professor Nam Dinh, who taught me about uncertainty and how hard can be something as simple as writing. Moreover, Professor Sergio Chiva, who gave me the opportunity to enter the world of CFDs, and IBERINCO (Iberdrola Ingeniería y Construcción, S. A.), for the shared data.

Furthermore, I would like to give recognition to the whole ISIRIM group, where I have been gladly working the last five years. Especially to Amparo Soler, Marina Garcia and Teresa Barrachina for their support, co-working and advice. I give a huge acknowledgment to all Rigel users who let me use their account to run my countless simulations in the server. These are Victor Faria, Agustín Abarca, Marina Garcia, Amparo Soler, Nicolás Olmo, Pablo Botas, Daniel Morera, Patricio Hidalga, Álvaro Bernal and Antonella Labarile. Of course, Rigel administrator, Francisco Rosich, must be included in the list for taking care of the server (which I overflowed a couple of times). I need to mention a few coworkers, whose company was essential to have a pleasant work environment, better meals (especially "carajillo"/coffee time) and parties: Carlos Peña, Álvaro Bernal, Nicolás Olmo and Sergio Morató. Also Victor Faria, a peculiar Brazilian, coworker, housemate and fellow traveler whom I could learn a philosophy of life. Other UPV coworkers are Consuelo Gómez, María Lorduy, Javier Martínez, José Ordoñez and Jara Turégano.

Before ending this PhD adventure, I would like to express my appreciation to *Cor Trobat* and all its members. Especially to Esther Bernat and her both sons: Juanan and Ximo; now, not-so-distant family. I thank all members for the rehearsal times, concerts and especially parties. Special thanks to Ampa and Bea, for their little help in this thesis and good moments in life. I share good memories with *Cor Trobat* and I am glad to be part of it.

I am grateful to all persons I met abroad and helped me one way or another. Dr. Juan Carlos Román (from Valladolid) now working at Rolls-Royce, Dr. Xiaoke Ku (from China) now working as a Professor in Zhejiang University, Dr. Saju Olaofe (from Nigeria) now working on one of the largest petrochemical companies in the world, Toni Martínez (from Valencia) now finishing his PhD in architecture and Rohan Joshi (from India) now working as structural analyst. Moreover, I am also thankful to a great friend I already knew before getting on this adventure, Dr. Jordi Ripollés, now working as a Professor at Universitat de les Illes Balears. I am looking forward to continuing our research path with little pain.

Last, but not least, I would like to express my gratitude to my parents for their unconditional support all this time, my grandmother for her wise stories and great meals, my brother for being always there and the rest of my family. Of course, also to Amanda, for waking me up even at 5 am to finish this PhD, to withstand my uncountable hours of work and dedication that I had to steal from her, and definitely for loving me so much. This would have not been the same without you.

To finish this PhD thesis, I would like to write a few words about my experience as a researcher. It is true that research is more valued abroad and better paid. That is obvious if we compare the Spanish investment in R&D (1.24% of its GDP with a downward trend) with the average European Union investment (2.02%) or other world powers, such as the USA with a solid 2.81% (2013 data). Nevertheless, there is a lot of talent in Spain. In the global ranking of published papers, in 2011 we were in the 10^{th} position, that means that Spanish production is around the 3% worldwide with an upwards trend. Not bad considering the severe cutbacks we had on R&D in the last few years. For me, it was possible to live out of research in Spain because I was lucky enough to be in a powerful research group, even though I had to apply once for the unemployment benefit. Of course, Spanish weather and food give extra points, but I perfectly understand people who is forced to look for a job in other countries. Anyway, any PhD is full of ups and downs and, as Einstein discovered, time becomes relative. This can be better explained with the following sentence: *If I knew how long it'll take, it wouldn't be called research.* That is why getting on a PhD experience is not something to take lightly and must be thought seriously. Some people think that working at the university is easy. Certainly, the great advantage is the flexibility in schedule. Still, this does not mean that we do not work enough. It is true that I usually go to work at -let's say- comfortable hours, but I have been uncountable hours at the university and closed the department late at night, even on weekends. Nonetheless, this experience made me discover that I can do anything I set my mind to, such as work in other countries, travel anywhere and meet amazing people abroad. As my advisor says: *Impossible is nothing.* I improved my MATLAB skills -of which I consider myself a fan- and discovered how addictive and frustrating programming can be. I had many different experiences, from learning Dutch while being at freezing temperatures in The Netherlands (-20 $^{\text{o}}$C) to enjoy awesome landscapes in a trip around the USA: The Grand Canyon, California, New York, Puerto Rico... I am also aware that working as a researcher implies a life full of uncertainty, at least until you become a full professor. It is funny if you think about it: my life became more uncertain by studying -physical- uncertainties. Where will I go next? Brazil? Spain?... Will I take some time to make up my mind?... Who knows.

Carles Mesado
Valencia, March 2016

After one year to redo and update most of the work and some bureaucratic problems, I am now near the end of this thesis -this time for real-. Since my contract with the university was terminated, and while looking for a new contract employer to continue my professional life, I dealt with several options before finding my actual job. The options in mind were, spending some time in Ecuador, a post-doc in Brazil or even in Germany. Luckily enough, while spending some time in Ecuador, I sent my CV to a nuclear related company with its headquarters in Madrid: ENUSA. They contacted me while I was still in Ecuador and we had an interview as soon as I went back to Spain. They offered me the vacancy in a week, which I gladly accepted.

Last, but not least, I dedicate this PhD thesis to my grandmother, because I know she would have liked to see how his grandson becomes a doctor.

Carles Mesado
Madrid, April 2017

Agraïments

Primerament, m'agradaria agrair a tots els professors que, d'una manera o altra, han contribuït a portar a bon terme aquest doctorat. El tutor principal, el professor Rafael Miró, per la seua dedicació al treball i a tots els seus estudiants. Sense el seu coneixement en diversos àmbits, no hauria pogut acabar aquesta tesi doctoral. El director del doctorat i tutor secundari, el professor Gumersindo Verdú, pel seu recolzament econòmic (conjuntament amb el professor Rafael Miró) i les múltiples renovacions de contracte. El mentor americà, el professor Nam Dinh, qui em va ensenyar sobre incerteses i com de difícil pot ser una cosa tan simple com escriure. Així mateix, el professor Sergio Chiva, qui em va donar l'oportunitat d'entrar en el món dels CFDs, i IBERINCO (Iberdrola Ingeniería y Construcción, S. A.), per les dades facilitades.

També agraïsc a tot el grup ISIRIM, on he estat feliçment treballant els últims cinc anys. Especialment a Amparo Soler, Marina Garcia i Teresa Barrachina pel seu recolzament, companyonia i consell. Un enorme agraïment a tots els usuaris de Rigel que em van deixar utilitzar el seu compte per llançar les incomptables simulacions en el servidor. Aquests són: Victor Faria, Agustín Abarca, Marina Garcia, Amparo Soler, Nicolás Olmo, Pablo Botas, Daniel Morera, Patricio Hidalga, Álvaro Bernal i Antonella Labarile. Per descomptat, també he d'incloure a l'administrador de Rigel, Francisco Rosich, per cuidar del servidor, el qual vaig excedir la memòria disponible un parell de vegades. Voldria mencionar que la companyia de certs companys ha sigut essencial per a tindre un bon ambient de treball, millors menjars (especialment rebentats o cafè) i festes. Carlos Peña, Álvaro Bernal, Nicolás Olmo i Sergio Morató. També Victor Faria, un brasiler peculiar, company de treball, de pis i de viatges de qui he pogut aprendre una filosofia de vida. Altres companys de la UPV són Consuelo Gómez, María Lorduy, Javier Martínez, José Ordoñez i Jara Turégano

Abans d'acabar aquesta aventura, m'agradaria expressar l'apreciació cap al *Cor Trobat* i tots els seus membres. Especialment a Esther Bernat i els seus fills: Juanan i Ximo, ara ja part de la família no tan llunyana. Agraïsc a tots els membres pels assajos, concerts i, especialment, festes. Agraïments especials per a Ampa i Bea, per la seua xicoteta ajuda a aquesta tesi i bons moments en la vida. Compartisc bons records amb *Cor Trobat* i estic content de formar part d'ell.

Vull agrair a totes les persones que he conegut a l'estranger i m'han ajudat d'una forma o altra. Dr. Juan Carlos Román (de Valladolid), ara treballant en Rolls Royce; Dr. Xiaoke Ku (de Xina), ara treballant como a professor a la Universitat de Zhejiang; Dr. Saju Olaofe (de Nigèria), ara treballant en una de las empreses petroquímiques més grans del món; Toni Martínez (de València), ara acabant el doctorat en arquitectura, i Rohan Joshi (de la Índia), ara treballant com a enginyer d'estructures. Igualment, estic agraït a un amic que ja coneixia abans d'embarcar-me en aquesta aventura, Dr. Jordi Ripollés, ara treballant com a professor a la Universitat de les Illes Balears. Espere que puguem continuar el nostre itinerari d'investigació sense molt de sofriment.

Per últim, però no menys important, m'agradaria mostrar la meua gratitud als meus pares per el seu recolzament incondicional tot aquest temps, a la meua àvia per les seues sàvies històries i bones menjades, al meu germà per estar sempre ací i a la resta de la família. Per descomptat, també a Amanda, per despertar-me, fins i tot a les cinc del matí, per a acabar aquesta tesi; per aguantar les innumerables hores de treball i dedicació que li he hagut de furtar, i en definitiva, per voler-me tant. Açò no haguera estat el mateix sense vosaltres.

Per a finalitzar aquesta tesi doctoral, m'agradaria escriure unes paraules sobre la meua experiència amb la investigació. És de veres que la investigació està més valorada a l'estranger i millor pagada. Açò és evident si comparem la inversió espanyola en R+D (1.24% del PIB amb una tendència a la baixa) amb la mitjana de la inversió de la Unió Europea (2.02%) o altres potències mundials, com els EUA amb un sòlid 2.81% (dades del 2013). Tanmateix, hi ha molt de talent a Espanya. En la classificació global d'articles publicats, en 2011 estàvem en la dècima posició, això significa que la producció espanyola es del voltant del 3% mundial amb una tendència a l'alça. No gens malament si considerem les severes retallades en R+D els darrers anys. Per a mi va ser possible viure de la investigació a Espanya perquè vaig tindre la sort d'entrar a un grup potent, encara així vaig haver de demanar la prestació per desocupació una volta. Per descomptat, el clima i el menjar espanyols donen punts extra, però entenc perfectament a les persones que es veuen forçades a buscar treball a altres països. De totes maneres, qualsevol doctorat està ple d'alts i baixos i, com va descobrir Einstein, el temps és relatiu. Açò pot explicar-se millor amb la següent frase: *Si sabés quant tardaré, no s'anomenaria investigació.* Aquesta és la raó per la qual la decisió de començar un doctorat no hauria de prendre's a la lleugera, sinó que s'ha de pensar seriosament. Algunes persones pensen que treballar a la universitat es fàcil. Definitivament, un avantatge important és la flexibilitat d'horaris. És de veres que normalment comence a treballar, més bé, a bones hores; però també he estat incomptables hores a la universitat i he tancat el departament per les nits, inclosos caps de setmana. Tanmateix, aquesta experiència m'ha fet descobrir que puc aconseguir qualsevol cosa que em propose. Com diu el meu tutor: *No hi ha res impossible.* He millorat les habilitats amb el MATLAB, del qual em considere fan, i he descobert com d'addictiu i frustrant pot ser programar. He tingut moltes experiències diferents, des d'aprendre holandès en gèlides condiciones a Holanda (-20 ºC) fins a disfrutar d'espectaculars paisatges en un viatge pels EUA: el Gran Canyó, Califòrnia, Nova York, Puerto Rico... També sóc conscient què treballar com a investigador implica una vida plena d'incerteses, almenys fins a ser professor titular. És divertit si ho penses: la meua vida és més incerta per estudiar incerteses (físiques). On aniré ara? Brasil? Espanya?... Prendré un temps per aclarir-me?... Qui sap.

Carles Mesado
València, Març 2016

Després d'un any per a refer i actualitzar gran part del traball i de certs problemes burocràtics, estic ara a prop d'acabar aquesta tesi, aquesta vegada de veritat. Des que el meu contracte amb la universitat va acabar, i mentre buscava un nou contracte per a continuar la meua vida professional, vaig estar barallant diverses opcions abans de trobar el meu traball actual. Les opcions en ment foren, pasar un temps a Equador, un posdoc a Brasil, i fins i tot, a Alemanya. Per coses del destí, mentre estava a Equador, vaig enviar el meu CV a una empresa relacionada amb el món nuclear amb seu a Madrid: ENUSA. Em contactaren mentre encara estava a Equador i vam tindre una entrevista tan prompte com vaig tornar a Espanya. M'oferiren la plaça en una setmana, la qual vaig acceptar gustosament.

Per últim, no por això menys important, dedique aquesta tesi doctoral a la meua àvia, porquè sé que li haguera agradat vore com el seu nèt es converteix en doctor.

Carles Mesado
Madrid, Abril 2017

Agradecimientos

Me gustaría agradecer a todos los profesores que, de un modo u otro, han contribuido a llevar este doctorado a buen puerto. Mi tutor principal, el profesor Rafael Miró, por su dedicación al trabajo y a todos sus estudiantes. Sin su conocimiento en diversos ámbitos no habría podido acabar esta tesis doctoral. Mi director de doctorado y tutor secundario, el profesor Gumersindo Verdú, por el apoyo financiero (conjuntamente con el profesor Rafael Miró) y las múltiples renovaciones de contrato. Mi mentor americano, profesor Nam Dinh, quien me enseñó acerca de incertidumbres y como puede ser de difícil algo tan simple como escribir. Asimismo, el profesor Sergio Chiva, quien me dio la oportunidad de entrar en el mundo de los CFDs, e IBERINCO (Iberdrola Ingeniería y Construcción, S. A.), por los datos facilitados.

También me gustaría agradecer a todo el grupo ISIRIM, donde he estado felizmente trabajando los últimos cinco años. Especialmente a Amparo Soler, Marina Garcia y Teresa Barrachina por su apoyo, compañerismo y consejo. Un enorme agradecimiento a todos los usuarios de Rigel que me dejaron usar su cuenta para lanzar mis innumerables simulaciones en el servidor. Estos son: Victor Faria, Agustín Abarca, Marina Garcia, Amparo Soler, Nicolás Olmo, Pablo Botas, Daniel Morera, Patricio Hidalga, Álvaro Bernal y Antonella Labarile. Por supuesto, también he de incluir al administrador de Rigel, Francisco Rosich, por cuidar del servidor, el cual excedí la memoria disponible un par de veces. Mencionar a unos compañeros cuya compañía ha sido esencial para tener un buen ambiente de trabajo, mejores comidas (especialmente carajillos o café) y fiestas. Carlos Peña, Álvaro Bernal, Nicolás Olmo y Sergio Morató. También Victor Faria, un brasileño peculiar, compañero de trabajo, de piso y de viajes de quien pude aprender una filosofía de vida. Otros compañeros de la UPV son Consuelo Gómez, María Lorduy, Javier Martínez, José Ordoñez y Jara Turégano

Antes de terminar esta aventura me gustaría expresar mi aprecio a *Cor Trobat* y todos sus miembros. Especialmente a Esther Bernat y sus hijos: Juanan y Ximo, ahora parte de la familia no tan lejana. Agradezco a todos los miembros por los ensayos, conciertos y especialmente fiestas. Agradecimientos especiales a Ampa y Bea, por su pequeña ayuda en esta tesis y buenos momentos en la vida. Comparto buenos recuerdos con *Cor Trobat* y estoy contento de formar parte de él.

Agradecer a todas las personas que he conocido en el extranjero y me ayudaron de una forma u otra. Dr. Juan Carlos Román (de Valladolid) ahora trabajando en Rolls Royce, Dr. Xiaoke Ku (de China) ahora trabajando como profesor en la Universidad de Zhejiang, Dr. Saju Olaofe (de Nigeria) ahora trabajando en una de las empresas petroquímicas más grandes del mundo, Toni Martínez (de Valencia) ahora acabando su doctorado en arquitectura y Rohan Joshi (de la India) ahora trabajando como ingeniero de estructuras. Igualmente estoy agradecido a un amigo que ya conocía antes de embarcarme en esta aventura, Dr. Jordi Ripollés, ahora trabajando como profesor en la Universitat de les Illes Balears. Espero que podamos continuar nuestro itinerario de investigación sin mucho sufrimiento.

Por último, pero no menos importante, me gustaría mostrar mi gratitud a mis padres por su apoyo incondicional todo este tiempo, a mi abuela por sus sabias historias y buenas comidas, a mi hermano por estar siempre ahí y a la familia restante. Por supuesto, también a Amanda, por despertarme incluso a las 5 de la mañana para terminar esta tesis; por aguantar mis inumerables horas de trabajo y dedicación que le he tenido que robar, y en definitiva, por quererme tanto. Esto no hubiese sido lo mismo sin vosotros.

Para finalizar esta tesis doctoral, me gustaría escribir unas palabras sobre mi experiencia en la investigación. Es verdad que la investigación está más valorada en el extranjero y mejor pagada. Esto es obvio si comparamos la inversión española de I+D (1.24% del PIB con una tendencia a la baja) con la media de la inversión de la Unión Europea (2.02%) u otras potencias mundiales, como EEUU con un sólido 2.81% (datos del 2013). Sin embargo, hay mucho talento en España. En la clasificación global de artículos publicados, en 2011 estuvimos en la décima posición, eso significa que la producción española es de alrededor del 3% mundial con una tendencia a la alza. Nada mal si consideramos los severos recortes en I+D en los pasados años. Para mí fue posible vivir de la investigación en España porque tuve la suerte de entrar en un grupo potente, aun así tuve que pedir la prestación de desempleo una vez. Por supuesto, el tiempo y la comida española dan puntos extra, pero entiendo perfectamente a las personas que se ven forzadas a buscar trabajo en otros países. De todos modos, cualquier doctorado está lleno de altibajos y, como descubrió Einstein, el tiempo es relativo. Esto puede explicarse mejor con la siguiente frase: *Si supiera cuanto voy a tardar, no se llamaría investigación.* Esta es la razón por la cual la decisión de empezar un doctorado no debería tomarse a la ligera, sino que se ha de pensar seriamente. Algunas personas creen que trabajar en la universitat es fácil. Definitivamente, una ventaja importante es la flexibilidad de horarios. Es verdad que normalmente voy a trabajar, más bien, a buenas horas; pero también he estado incontables horas en la universidad y he cerrado el departamento por las noches, incluso en fines de semana. Sin embargo, esta experiencia me ha hecho descubrir que puedo alcanzar cualquier cosa que me proponga, como trabajar en otros países, viajar a donde sea y conocer gente fantástica. Como dice mi tutor: *No hay nada imposible.* He mejorado mis habilidades con MATLAB, del cual me considero fan, y he descubierto lo adictivo y frustrante que puede ser programar. He tenido muchas experiencias distintas, desde aprender holandés en gélidas condiciones en Holanda (-20 ^{o}C) a disfrutar de espectaculares paisajes en un viaje por EEUU: el Gran Cañón, California, Nueva York, Puerto Rico... También soy consciente que trabajar como investigador implica una vida llena de incertidumbre, por lo menos hasta ser profesor titular. Es gracioso si piensas en ello: mi vida es más incierta por estudiar incertidumbres (físicas). ¿Dónde iré ahora? ¿Brasil? ¿España?... ¿Me tomaré un tiempo para aclararme?... Quién sabe.

Carles Mesado
Valencia, Marzo 2016

Después de un año para rehacer y actualizar gran parte del trabajo y de ciertos problemas burocráticos, estoy ahora cerca de terminar esta tesis, esta vez de verdad. Desde que mi contrato con la universidad terminó, y mientras buscaba un nuevo contrato para continuar mi vida profesional, estuve barajando diversas opciones antes de encontrar mi trabajo actual. Las opciones en mente fueron, pasar un tiempo trabajando en Ecuador, un posdoc en Brasil o incluso en Alemania. Por cosas del destino, mientras estaba en Ecuador, envié mi CV a una empresa relacionada con el mundo nuclear con sede en Madrid: ENUSA. Me contactaron mientras aún estaba en Ecuador y tuvimos una entrevista tan pronto como volví a España. Me ofrecieron la plaza en una semana, la cual acepté gustosamente.

Por último, no por ello menos importante, dedico esta tesis doctoral a mi abuela, porque sé que le hubiese gustado ver como su nieto se convierte en doctor.

Carles Mesado
Madrid, Abril 2017

Bibliography

Ade, B. (2012). SCALE/TRITON Primer: A Primer for Light Water Reactor Lattice Physics Calculations. Technical report, Oak Ridge National Laboratory (ORNL).

Adetula, B. and Bokov, P. (2012). Computational method for global sensitivity analysis of reactor neutronic parameters. *Science and Technology of Nuclear Installations*.

Aragonés, J. (2008). Basis for Coupled 3-D Neutronics and Thermal-Hydraulics. In *CSNI-NEAOCDE Seminar, Lecture*, volume 25.

Avramova, M., Ivanov, K., Krzykacz-Hausmann, B., Velkov, K., Pautz, A., and Perin, Y. (2009). Uncertainty analysis of COBRA-TF void distribution predictions for the OECD/NRC BFBT Benchmark. In *Proceedings of the International Conference on Advances in Mathematics, Computational Methods, and Reactor Physics (M&C'09)*.

Bajorek, S. et al. (2007). TRACE V5.435 User's Manual-Volume 1: Input Specification. Technical report, US Nuclear Regulatory Commission, Washington, DC,.

Bajorek, S. et al. (2011). TRACE V5.435 Theory Manual: Filed Equations, Solution Methods, and Physical Models. Technical report, US Nuclear Regulatory Commission, Washington, DC,.

Barrachina, T. et al. (2009). Rod Ejection Accident 3D-Dynamic Analysis in Almaraz NPP with RELAP5/PARCS v2.7 and Simtab Cross-Sections Tables. *Proceedings of Top Fuel*, pages 6–10.

Barrachina, T., Garcia, M., Anchel, F., Miró, R., Verdú, G., Ortego, A., and Martínez-Murillo, J. (2010a). Rod ejection accident 3D-dynamic analysis in Almaraz NPP with RELAP5/PARCS V2.7 coupled codes.

Barrachina, T., Garcia-Fenoll, M., Anchel, F., Miró, R., Verdú, G., Ortego, A., and Martínez-Murillo, J. (2010b). Analysis of the influence of the thermalhydraulic to neutronic mapping in the RIA analysis in Almaraz NPP. In *Proceedings of the 2010 International Congress on Advances in Nuclear Power Plants-ICAPP'10*.

Barrachina, T., Soler, A., Jambrina, A., Miró, R., Verdú, G., and Concejal, A. (2013). High order boron transport scheme in TRAC-BF1.

Borkowski, J., Wade, N., Giles, M., Rouhani, S., Shumway, R., Singer, G., Taylor, D., and Weaver, W. (1992). TRAC-BF1/MOD1: An advanced best-estimate computer program for BWR accident analysis, Model description. Technical report, Nuclear Regulatory Commission, Washington, DC (United States). Div. of Systems Research; Idaho National Engineering Lab., Idaho Falls, ID (United States).

Boyack, B., Duffey, R., Wilson, G., Griffith, P., Lellouche, G., Levy, S., Rohatgi, U., Wulff, W., and Zuber, N. (1989). Quantifying reactor safety margins: application of code scaling, applicability, and uncertainty evaluation methodology to a large-break, loss-of-coolant accident (NUREG/CR-5249). Technical report, Nuclear Regulatory Commission, Washington, DC (USA). Div. of Systems Research.

Briggs, L. et al. (2009). Uncertainty quantification approaches for advanced reactor analyses. Technical report, Argonne National Laboratory (ANL).

Canuti, E., Petruzzi, A., D'Auria, F., and Kozlowski, T. (2012). Sensitivity Studies for the Exercise I-1 of the OECD/UAM Benchmark. *Science and Technology of Nuclear Installations*.

Conover, W. (1999). *Practical nonparametric statistics, third edition*. John Wiley & Sons, Inc, third edition.

D'Auria, F. et al. (2004). Neutronics/thermal-hydraulics coupling in LWR technology: state-of-the-art report (REAC-SOAR). Technical report, CRISSUE-S–WP2, OCDE/NEA-5436.

D'Auria, F., Glaeser, H., Lee, S., Misák, J., Modro, M., and Schultz, R. (2008). Best Estimate Safety Analysis for Nuclear Power Plants: Uncertainty Evaluation. *IAEA Safety Report Series*, (52).

DeHart, M. (2005). NEWT: A new transport algorithm for two-dimensional discrete ordinates analysis in non-orthogonal geometries. Technical report, Oak Ridge National Laboratory (ORNL).

DeHart, M. and Bowman, S. (2011). Reactor physics methods and analysis capabilities in SCALE. *Nuclear Technology*, 174(2):196–213.

Denise, B., Andrew, J., and Garrett, E. (2014). MCNP6 user's manual. Code Version 6.1.1beta. Technical report, Los Alamos National Laboratory, Version.

Department of Energy, U. (1983). *General Design Criteria Manual, DOE 6430.1*.

Díez, C., Herrero, J., Cabellos, O., and Martínez, J. (2013). Propagation of cross-section uncertainties in criticality calculations in the framework of UAM-Phase I using MCNPX-2.7 e and SCALE-6.1. *Science and Technology of Nuclear Installations*.

DiGiovine, A., RHODES III, J., Smith, K., VERPLANCK, D., and Umbarger, J. (1995). SIMULATE-3 User's Manual. Technical report, Studsvik0SOA-95015, Studsvik of America, Inc.

Downar, T., Lee, D., Xu, Y., Kozlowski, T., and Staudenmier, J. (2004). PARCS v2. 6 US NRC Core Neutronics Simulator Theory Manual. Technical report.

Downar, T., Xu, Y., and Seker, V. (2010). PARCS v3. 0 US NRC Core Neutronics Simulator User Manual. Technical report, Department of Nuclear Engineering and Radiological Sciences — University of Michigan.

Duderstadt, J. and Hamilton, L. (1976). *Nuclear reactor analysis*. John Wiley and Sons, Inc., New York.

Edenius, M., Ekberg, K., Forssén, B., and Knott, D. (1995). CASMO-4, A Fuel Assembly Burnup Program, User's Manual. Technical report, Studsvik0SOA-9501, Studsvik of America, Inc.

Gajev, I. (2012). *Sensitivity and Uncertainty Analysis of Boiling Water Reactor Stability Simulations*. KTH Royal Institute of Technology.

Gauld, I., Radulescu, G., Ilas, G., Murphy, B., Williams, M., and Wiarda, D. (2011). Isotopic depletion and decay methods and analysis capabilities in SCALE. *Nuclear Technology*, 174(2):169–195.

Goluoglu, S., Hollenbach, D., Landers, N., Petrie, L., Bucholz, J., Weber, C., and Hopper, C. (2011). The material information processor for SCALE. Technical report, Oak Ridge National Laboratory (ORNL).

Guba, A., Makai, M., and Pál, L. (2003). Statistical aspects of best estimate method—I. *Reliability engineering & system safety*, 80(3):217–232.

Herman, M. and Trkov, A. (2005). ENDF-6 Formats Manual. Technical report, National Nuclear Data Centre, BNL, Upton, New York.

Hernández-Solís, A. (2012). *Uncertainty and sensitivity analysis applied to LWR neutronic and thermal-hydraulic calculations*. Chalmers University of Technology.

Hong, I. and Connolly, A. (2008). Generalized Tolerance Limit Evaluation Method to Determine Statistically Meaningful Minimum Code Simulations. In *16th International Conference on Nuclear Engineering*, pages 653–660. American Society of Mechanical Engineers.

Hong, I., Oh, D., and Kim, I. (2013). Generic Application of Wilks' Tolerance Limit Evaluation Approach to Nuclear Safety.

Hueso, C., Sánchez-Cervera Huerta, S., Herrero Carrascosa, J., García Herranz, N., and Ahnert Iglesias, C. (2011). Estudio de la funcionalización de secciones eficaces de celda en multigrupos para cálculos best-estimate 3D pin-by-pin de núcleos PWR.

Ilas, G., Gauld, I., and Radulescu, G. (2012). Validation of new depletion capabilities and ENDF/B-VII data libraries in SCALE. *Annals of Nuclear Energy*, 46:43–55.

Ivanov, B., Ivanov, K., and Stamm'ler, R. (2004). Helios, current coupling collision probability method, applied for solving the NEA C5G7 MOX benchmark. *Progress in Nuclear Energy*, 45(2):119–124.

Ivanov, K., Avramova, M., Kamerow, S., Kodeli, I., Sartori, E., Ivanov, E., and Cabellos, O. (2013). Benchmarks for Uncertainty Analysis in Modelling (UAM) for the Design, Operation and Safety Analysis of LWRs-Volume I: Specification and Support Data for Neutronics Cases (Phase I). Technical report, Organisation for Economic Co-Operation and Development, Nuclear Energy Agency-OECD/NEA.

Jatuff, F., Perret, G., Murphy, M., Giust, F., and Chawla, R. (2009). Void reactivity coefficient benchmark results for a 10× 10 BWR assembly in the full 0–100% void fraction range. *Annals of Nuclear Energy*, 36(6):853–858.

Jessee, M. and DeHart, M. (2011). TRITON: A multipurpose transport, depletion, and sensitivity and uncertainty analysis module. Technical report, Oak Ridge National Laboratory (ORNL).

Jevremovic, T. (2009). *Nuclear principles in engineering*. Springer.

Kodeli, I. (2013). Sensitivity and uncertainty in the effective delayed neutron fraction (β_{eff}). *Nuclear Instruments and Methods in Physics Research Section A: Accelerators, Spectrometers, Detectors and Associated Equipment*, 715:70 – 78.

Labarile, A., Miró, R., Barrachina, T., and Verdú, G. (2015). TRITON vs POLARIS. Comparison Between Two Modules for LWRs Modelling in SCALE6.2. In *Proceedings of the 24th International Conference Nuclear Energy for New Europe (NENE2015)*.

Leppänen, J. (2015). Serpent–A continuous-energy Monte Carlo reactor physics burnup calculation code. Technical report, VTT Technical Research Centre of Finland.

Macián-Juan, R., Tietsch, W., and Sassen, F. (2012). Proposal for the Development and Implementation of an Uncertainty and Sensitivity Analysis Module in SNAP. *US NRC NUREG/IA-0407, Washington (DC, USA) April*.

Martínez-Murillo, J., Novo, M., Miró, R., Barrachina, T., Verdú, G., and Almaraz-Trillo, A. (2011). Coupled RELAP/PARCS Full Plant Model – Assessment of a Cooling Transient in Trillo Nuclear Power Plant.

Massih, A. and Jernkvist, L. (2010). *Nuclear Fuel Behaviour under Reactivity-initiated Accident (RIA) Condition: State-of-the-art Report.* Nuclear Energy Agency, Organisation for Economic Co-operation and Development (OECD).

McKay, M. (1988). Sensitivity and uncertainty analysis using a statistical sample of input values. *Uncertainty analysis, Chapter 4*, pages 145–186.

Mesado, C., Miró, R., Barrachina, T., and Verdú, G. (2015). Modeling 3D Cores for PWR Using Vessel Components in TRACE v5.0P3 (NUREG/IA-0460). Technical report, Universitat Politècnica de València (UPV).

Mesado, C., Miró, R., Labarile, A., and Barrachina, T. (2017). TXT2NTAB Code User's Guide. Generating NEMTAB cross-section libraries from txtfile16. Technical report, Universitat Politècnica de València (UPV).

Mesado, C., Soler, A., Barrachina, T., Miró, R., García-Díaz, J., Macián-Juan, R., and Verdú, G. (2012). Uncertainty and Sensitivity of Neutron Kinetic Parameters in the Dynamic Response of a PWR Rod Ejection Accident Coupled Simulation. *Science and Technology of Nuclear Installations.*

Miró, R., Ginestar, D., Verdú, G., and Hennig, D. (2002). A nodal modal method for the neutron diffusion equation. Application to BWR instabilities analysis. *Annals of Nuclear Energy*, 29(10):1171–1194.

Miró, R., Jambrina, A., Mesado, C., Barrachina, T., and Verdú, G. (2015). TRAC-BF1 to TRACE Model Semi-Automatic Conversion. PBTT Example (NUREG/IA-0461). Technical report, Universitat Politècnica de València (UPV).

Miró, R., Maggini, F., Barrachina, T., Verdú, G., Gómez, A., Ortego, A., and Murillo, J. (2006a). Analysis of a rod withdrawal in a PWR core with the neutronic-thermalhydraulic coupled code RELAP/PARCS and RELAP/VALKIN. *Advances in Reactor Physics (PHYSOR).*

Miró, R., Verdú, G., Sanchez, A., Barrachina, T., and Gómez, A. (2006b). Analysis of a rod withdrawal accident in a BWR with the neutronic-thermalhydraulic coupled code TRAC-BF1/VALKIN and TRACE/-PARCS. Technical report, American Nuclear Society, 555 North Kensington Avenue, La Grange Park, IL 60526 (United States).

NEA (2004a). *Neutronics/Thermal-hydraulics Coupling in LWR Technology, CRISSUE-S WP1: Data Requirements and Databases Needed for Transient Simulations and Qualification. Vol. 1.* OECD, NEA No 4452.

Núñez-Carrera, A., François, J., and Espinosa-Paredes, G. (2004). Comparison between HELIOS critical-depletion calculations and a PWR thorium cell burnup benchmark. *Annals of Nuclear Energy*, 31(7):713–722.

Pal, L. and Makai, M. (2002). Remarks on statistical aspects of safety analysis of complex systems. *arXiv preprint physics/0308086.*

Petrie, L. and Rearden, B. (2011). MCDANCOFF Data guide. Technical report, Oak Ridge National Laboratory (ORNL).

Petruzzi, A. and D'Auria, F. (2008). Thermal-hydraulic system codes in nulcear reactor safety and qualification procedures. *Science and Technology of Nuclear Installations.*

Rachamin, R., Wemple, C., and Fridman, E. (2013). Neutronic analysis of SFR core with HELIOS-2, Serpent, and DYN3D codes. *Annals of Nuclear Energy*, 55:194–204.

Rearden, B. (2011). TSUNAMI-3D: Control Module for Three-Dimensional Cross-Section Sensitivity and Uncertainty Analysis for Criticality. Technical report, Oak Ridge National Laboratory (ORNL).

Rearden, B., Jessee, M., and Williams, M. (2011). TSUNAMI-1D: Control Module for one-dimensional Cross-section Sensitivity and Uncertainty. Technical report, Oak Ridge National Laboratory (ORNL).

Rhoades, W. and Childs, R. (1987). The TORT three-dimensional discrete ordinates neutron/photon transport code. Technical report, Oak Ridge National Lab., TN (USA).

Roselló, O. (2004). *Desarrollo de una metodología de generación de secciones eficaces para la simplificación del núcleo de reactores de agua ligera y aplicación en códigos acoplados neutrónicos termohidráulicos*. PhD thesis, Universitat Politècnica de València (UPV).

Schultz, R. (2003). RELAP5-3D© Code Manual Volume V: User's Guidelines. Technical report, INEEL-EXT-98-00084. Rev. 2.2, October.

Stacey, W. (2007). *Nuclear reactor physics*. John Wiley & Sons.

Strydom, G. (2013). Uncertainty and Sensitivity Analyses of a Pebble Bed HTGR Loss of Cooling Event. *Science and Technology of Nuclear Installations*.

Swiler, L. and Wyss, G. (2004). A User's Guide to Sandia's Latin Hypercube Sampling Software: LHS UNIX Library Standalone Version. Technical report, Sandia Technical Report SAND2004-2439.

Sánchez-Cervera, S., García-Herranz, N., J. Herrero, J., and Cuervo, D. (2014b). Effects of cross sections tables generation and optimization on rod ejection transient analyses. *Annals of Nuclear Energy*, 73:387 – 391.

US-NRC et al. (2007). Standard Review Plan for the Review of Safety Analysis Reports for Nuclear Power Plants: LWR Edition - Transient and Accident Analysis. *NUREG-0800*.

Vedovi, J., Yang, J., Klebanov, L., Vreeland, D., and Zino, J. (2012). Best-estimate plus uncertainty thermal-hydraulic stability analysis of BWRs using TRACG code. Technical report, American Nuclear Society, 555 North Kensington Avenue, La Grange Park, IL 60526 (United States).

Wang, D., Ade, B., and Ward, A. (2013). Cross Section Generation Guidelines for TRACE-PARCS. Technical report, Oak Ridge National Laboratory (ORNL).

Wemple, C., Gheorghiu, H., Stamm'ler, R., and Villarino, E. (2008). Recent advances in the HELIOS-2 lattice physics code. In *International Conference on the Physics of Reactors (PHYSOR-08), Interlaken, Switzerland*.

Wickett, T., D'Auria, F., Glaeser, H., Chojnacki, E., Lage, C., Sweet, D., Neil, A., Galassi, G., Belsito, S., Ingegneri, M., et al. (1998). Report of the Uncertainty Method Study. Technical report, Vol. I OECD/CSNI Report NEA/CSNI/R(97)35.

Wieselquist, W., Zhu, T., Vasiliev, A., and Ferroukhi, H. (2013). PSI methodologies for nuclear data uncertainty propagation with CASMO-5M and MCNPX: results for OECD/NEA UAM benchmark phase I. *Science and Technology of Nuclear Installations*.

Wilks, S. (1941). Determination of sample sizes for setting tolerance limits. *The Annals of Mathematical Statistics*, 12(1):91–96.

Wilks, S. (1942). Statistical prediction with special reference to the problem of tolerance limits. *The annals of mathematical statistics*, 13(4):400–409.

Williams, M., Havlůj, F., Wiarda, D., Gauld, I., Lefebvre, R., Dugan, K., Rearden, B., and Wieselquist, W. (2013a). SAMPLER: A module for statistical uncertainty analysis with SCALE sequences. Technical report, Oak Ridge National Laboratory (ORNL).

Williams, M., Ilas, G., Jessee, M., Rearden, B., Wiarda, D., Zwermann, W., Gallner, L., Klein, M., Krzykacz-Hausmann, B., and Pautz, A. (2013b). A statistical sampling method for uncertainty analysis with SCALE and XSUSA. *Nuclear Technology*, 183(3):515–526.

Xu, Y. and Downar, T. (2005). GenPMAXS code for generating the PARCS cross section interface file PMAXS. Technical report, Purdue University School Of Engineering.

Yankov, A., Collins, B., Klein, M., Jessee, M., Zwermann, W., Velkov, K., Pautz, A., and Downar, T. (2012). A Two-Step Approach to Uncertainty Quantification of Core Simulators. *Science and Technology of Nuclear Installations*.

Abbreviations

Adjoint Sensitivity Analysis Procedure (ASAP)
Analytic Nodal Method (ANM)
Anticipated Operational Occurrence (AOO)
Anticipated Transients Without Scram (ATWS)
Assembly Discontinuity Factor (ADF)
Atomic Energy Authority Winfrith (AEAW)

Best Estimate (BE)
Best Estimate And Uncertainty (BEAU)
Best Estimate Plus Uncertainty (BEPU)
Bi-Conjugate Gradient Stabilized (BiCGSTAB)
Boiling Water Reactor (BWR)

Canada Deuterium Uranium (CANDU)
Capability of Internal Assessment of Uncertainty (CIAU)
Chemical Volume Control System (CVCS)
Coarsh Mesh Finite Difference (CMFD)
Code Scaling, Applicability and Uncertainty (CSAU)
Cold Zero Power (CZP)
Continuous Energy (CE)
Conventional Perturbation Theory (CPT)
Coupled Steady State (CSS)
Coupled Transient (CTR)
Critical Heat Flux (CHF)
Critical Power Ratio (CPR)
Cumulative Distribution Function (CDF)

Departure from Nucleate Boiling Ratio (DNBR)
Design Basis Accident (DBA)
Deterministic Realistic Method (DRM)

Emergency Core Cooling System (ECCS)
Empresa Nacional del Uranio, SA (ENUSA)
Evaluated Nuclear Data File (ENDF)
Extended Step Characteristic (ESC)

Fine-Mesh Finite Difference (FMFD)
Finite Difference Method (FDM)
First-Order and Second-Order Reliability Methods (FORM-SORM)
Forward Sensitivity Analysis Procedure (FSAP)

General Design Criteria (GDC)
Generalized Perturbation Theory (GPT)
Generic Statistical Uncertainty Analysis Methodology (GSUAM)
Gesellschaft für Anlagen und Reaktorsicherheit (GRS)

Hot Zero Power (HZP)

Integral Test Facility (ITF)

Latin Hypercube Sampling (LHS)
Light Water Reactor (LWR)
Lose Of Coolant Accident (LOCA)

Message Passing Interface (MPI)
Minimum Critical Power Ratio (MCPR)
Monte Carlo (MC)

Nodal Expansion Method (NEM)
Nuclear Data Library (NDL)

Parallel Virtual Machine (PVM)
Partial Correlation Coefficient (PCC)
Partial Rank Correlation Coefficient (PRCC)
Peach Bottom Turbine Trip (PBTT)
Phenomena Identification and Ranking Table (PIRT)
Pressurized Water Reactor (PWR)
Probability Distribution Function (PDF)

Reactivity Initiated Accident (RIA)
Reactivity Insertion Limit (RIL)
Reactor Coolant System (RCS)
Rod Drop Accident (RDA)
Rod Ejection Accident (REA)

Sensitivity Analysis (SA)
Separate Effects Test Facilities (SETF)
Simple Correlation Coefficient (SCC)
Simple Random Sampling (SRS)
Simple Rank Correlation Coefficient (SRCC)
Stability-Enhancing Two-Step (SETS)
Steady State Alone (SSA)
Step Characteristic (SC)
Stochastic Finite Element Method (SFEM)

Three Mile Island (TMI)
Triangle-based Polynomial Expansion Method (TPEN)

U. S. Nuclear Regulatory Commission (NRC)
Uncertainty and Sensitivity (U&S)
Uncertainty Methodology based on Accuracy Extrapolation (UMAE)
Uncertainty Quantification (UQ)

Water-Water Energetic Reactor (VVER)